FINAL REPORT

VEHICLE IMPACT IN BOX GIRDER BRIDGES AND BRIDGE SUBSTRUCTURES

PHASE I
STRAIGHT BOX GIRDER BRIDGES

Research Report No. FL/DOT/RMC/0696-8677

Highway Planning and Research Program

HPR Project No. 0510696
State Project No. 99700-3538-119
FIU Project No. 49-80-57-18-195-00

Ton-Lo Wang
Dongzhou Huang

December 1994

Department of Civil and Environmental Engineering
College of Engineering and Design
Florida International University
Miami, Florida

Technical Report Documentation Page

1. Report No.	2. Government Accession No.	3. Recipient's Catalog No.
FL/DOT/RMC/0696-8677		

4. Title and Subtitle	5. Report Date
Vehicle Impact Analysis in Box Girder Bridges : Phase I, Straight Box Girder Bridges	December 1994
	6. Performing Organization Code

7. Author(s)	8. Performing Organization Report No.
Ton-Lo Wang and Dongzhou Huang	

9. Performing Organization Name and Address	10. Work Unit No.
Florida International University Department of Civil and Environmental Engineering University Park Miami, Florida 33199	11. Contract or Grant No. WPI 0510696, B-8677
	13. Type of Report and Period Covered Interim Report January 1994 - December 1994
12. Sponsoring Agency Name and Address Florida Department of Transportation Research Center, MS30 605 Suwannee Street Tallahassee, Florida 32399-0450	14. Sponsoring Agency Code 99700-3538-119

15. Supplementary Notes

Prepared in cooperation with the Federal Highway Administration

16. Abstract

This is the first part of the three-year project on vehicle impact in box girder bridges and bridge substructures. The objective of this investigation is to present a procedure for the study of the dynamic response of straight box girder bridges and to analyze their dynamic behavior due to vehicles passing over rough bridge decks.

In this study, the box girder bridge is divided into a number of finite thin-walled box girder elements. The nodal displacement parameters of the element are ten, including lateral and vertical translations and their first derivatives, torsional and distortional angles as well as their first and second derivatives. The element stiffness and mass matrices are given. Two examples studied by former investigators are used to validate the presented dynamic model and the computer program. Simply supported box girder bridges with and without diaphragms, continuous and cantilever bridges are designed according to AASHTO specifications. Their dynamic characteristics are studied. The effects of diaphragms, road surface roughness, vehicle speeds, hinges, and damping ratio are analyzed.

17. Key Words	18. Distribution Statement
Thin-walled Box Girder, Finite Element Method, Simple Bridges, Continuous Bridges, Cantilever Bridges, Dynamic Response, Impact.	This document is available to the public through the National Technical Information Service, Springfield, Virginia, 22161

19. Security Classify. (of this report)	20. Security Classify. (of this page)	21. No. of Pages	22. Price
Unclassified	Unclassified	254	

Form DoT F 1700.7 (g-

METRIC CONVERSIONS

inch x 25.40 = mm

foot x 0.3048 = m

lb (force) x 4.448 = N

kip (force) x 4.448 = kN

lb (mass) x 454 = g (mass)

kip (mass) x 454 = kg (mass)

kip/in x 0.175 = kN/mm

psi x 6.895 = kPa

ksi x 6.895 = MPa

mph x 1.609 = km/hr

DISCLAIMER

"The opinions, findings and conclusions expresses in this publication are those of the authors and not necessarily those of the Department of Transportation or the U.S. Department of Transportation.

Prepared in cooperation with the State of Florida Department of Transportation and the U.S. Department of Transportation."

ACKNOWLEDGMENTS

The authors wish to express their sincere appreciation to the Florida Department of Transportation (FDOT) for funding this research. Special thanks are also extended to Dr. Mohsen Shahawy, Chief Structural Analyst, Structures Research and Testing Center, FDOT for his valuable advice, suggestions, and comments during the course of this study.

Also, the authors would like to express their thanks to graduate student, research assistant, Mr. Kaizan Huang for his assistance in generating the Figures and Tables.

TABLE OF CONTENTS

LIST OF TABLES

LIST OF FIGURES

CHAPTER I

INTRODUCTION

Box girder bridges have received wide attention in the design office because of their desirable characteristics. More and more box girder bridges have been built in Florida and throughout the world. In particular, this type of bridge is very effective in resisting bending because of their wide bottom flanges. Because of the enclosed shape of the box girder, it offers substantial rigidity in resisting torsion of the bridge. The high torsional strength of box girder bridges makes their construction particularly suited to structures with significant curvature. The high torsional strength also permits the bridge to be designed as a unit without considering individual girders. In addition, the box can resist corrosion of steel box bridge more readily, as half of the steel surface is contained within the section. Along with these basic advantages, the box shape girder is an aesthetically pleasing structure.

For their distinguished merit of the characteristics, there are various types of box girder bridges which have been developed during the past decades. According to the different shapes of bridge alignments, box girder bridges can be divided into straight and curved girder bridges. Based on different cross-sections, the box girder bridges could be parted into single and multi-box girder bridges. According to the different kinds of structural systems, box girder bridges could be separated into continuous box girder, cantilever box girder, T-shaped frame box girder bridges, and so on. Box girder also can be divided into concrete and steel box girder bridges on the basis of materials of which the girders consist.

Because of the widespread use of box girder bridges and their particular mechanic characteristics, many investigations on the static and dynamic behaviors of box girder bridges have been conducted in America and other countries [1, 3, 8, 9, 10, 13, 14, 15, 16, 17, 18, 21, 23, 24, 25, 26, 27, 28, 29, 30, 31, 32, 33, 34, 35, 36, 37, 38, 39, 40, 42, 43, 46, 47, 48, 50, 51, 55]. Comparatively, the study of dynamic response of box girder bridges to vehicles is very little. This seems , on the surface, to be illogical since a bridge is the main structure built with the specific purpose of providing for dynamic loading, i.e., the design load magnitude and position is a function of time. However, the dynamic analysis of box girder bridges in general is a complex mathematical problem that has prevented extensive work in this area [4, 48]. Inhanathan and Wieland [241 studied the vibration of straight single box girder bridges due to vehicle moving, using planar bridge and vehicle modes. Jones and Chu [27] considered the response of a straight box girder beam of constant cross-section subjected to the movement of a mass supported by four springs with folded plate theory. Hutton and Cheng [23] used finite strip method and planar two-axle vehicle model to study the dynamic response of a single span straight box girder bridge. As the former investigators used a simple vehicle model and didn't consider the effect of road surface roughness, little applicable results for bridge design have been obtained. The current AASHTO specification provided designers with no specific guidance regarding the impact evaluation of straight box girder bridges.

Since 1960's, for aesthetic, economic, and construction considerations, curved box girder bridges have become increasingly popular and have been the interesting subject of research. Komatsu, Nakai, et al. [29, 30, 31, 321 presented several papers in the early 1970's on the free and forced dynamic response of horizontally curved box girder bridges and gave

differential equations for stress resultants and displacements. In 1975, Rabizadeh and Shore [42] presented a finite element method for the dynamic analysis of a curved box girder bridge. The roadway slab and flanges of the box girders are discretized by using cylindrical shell elements. The intermediate and end plate diaphragms in the curved box girder are discretized by rectangular plate elements. The strut or axial force member used in diaphragms has one degreeof-freedom at each of its two nodes. The research conducted by Rabizadeh and Shore forms the basis of the AASHTO provisions relative to the dynamic impact factors, for the design of horizontally curved composite box girder bridges. Schelling, et al. [46] treated a multi-box girder bridge as a planar grid and a vehicle as two constant forces with no, mass to study the impact factors of horizontally curved steel box girder bridges. Unfortunately, all previous research work on the dynamic investigation of box girder bridges have following main shortcomings:

(1) The vehicle loading was modeled as a set of moving constant forces without considering the effect of space loading and vehicle springs.

(2) One vehicle loading was considered and the mass of the moving vehicle was neglected in many investigations. However, recent studies have shown that the weight of vehicle is an important factor which affected the impact of bridges.

(3) Smooth bridge deck was assumed without considering the road surface roughness which is a very important factor for impact study of bridges.

(4) The effect of damping was neglected in the impact study of curved box girder bridges.

(5) The effect of the span length and transverse loading position have not fully studied, especially for concrete box girder as well as single and multi-cell box girder bridges.

(6) No comprehensive comparison between the experimental results and theoretical ones has been made, though several field tests reported high impact would occur in curved box-girder bridges [1, 28, 38].

Because of the above shortcomings, the previous obtained results have not completely reflected the real characteristics of box girder bridges. Their impact behaviors imperatively need to be further studied in order to avoid unnecessary waste of materials. Moreover, there are many box girder bridges in Florida. In order to insure their safety for the traveling public and to protect their initial investment, the evaluation of existing box girder bridges has become a very important problem. This also needs a reliable method for determining the dynamic response of box girder bridges due to moving vehicles.

The substructure of a bridge is one of its most significant components in regard to design and greatly influences its economy. Vehicle loading is a main design loading for the substructure. The impact loading of piers recommended by AASHTO specification has not accounted for the characteristics of piers itself and the interaction between superstructures and substructures. Vehicle braking on highway bridges is also a very important dynamic loading for bridge piers. The current AASHTO specifications stipulate that the effect of a longitudinal force of 5 percent of the live load in all lanes carrying traffic headed in the same direction should be considered in the design of substructure. Ontario, Highway Bridge Design code says that the braking force for a design lane shall be taken as an equivalent static force of either 160 kN or

10 % of the lane load, whichever is greater. The method for estimating vehicle braking loading needs to be further experimental and theoretical study. Moreover, the increasing weight of vehicles and the variation of the connecting way between superstructure and substructure also make the further investigations of vehicle loading for substructure design more inevitable.

The proposed research will preliminarily divided into three phases. In Phase I, the research will be focused in the study of dynamic loading of straight box girder bridges. The main objectives are: (1) the development of space multi-vehicle loading models; (2) the development of space straight models; (3) the study of dynamic response of simply supported straight box girder bridges; (4) the investigation of dynamic response of the cantilever box girder and continuous box girder bridges.

In Phase II, the research will be concentrated on the impact study of horizontally curved box girder bridges. The main tasks in this phase will be: (1) the development of space multivehicle loading models for curved box girder bridges; (2) the development of space curved box girder bridge models; (3) the study of maximum impact factors of simply supported curved box girder bridges; (4) the study of maximum impact factors of multi-span continuous box girder bridges; (5) the investigation of field tests and comparison between experimental and theoretical results.

In Phase III, the study of dynamic loading of bridge substructures and vehicle braking will be conducted. The specific objectives are: (1) the development of vehicle braking model, (2) the develop of interactive model between bridge and substructure, (3) the study of the

interaction between superstructure and substructure, (4)the study of the dynamic loading of bridge substructures and the braking force; (5) the study of influence of pier length and types; (6) the investigation of field testing and the comparison between theoretical and experimental results.

The mathematical model for thin-walled box girder bridges is described in Chapter 2. The stiffness and mass matrices of the finite thin-walled box girder element are presented first. Then, two box girder bridges studied by former investigators are examined again to validate the presented bridge model.

Chapter 3 is primarily about the dynamic analysis of simply supported box girder bridges. In this chapter, the whole analytical procedure for dynamic response exited by moving vehicles is briefly described, including vehicle model, road surface roughness, bridge/vehicle interaction equations, and numerical method. Then, the free and forced vibration characteristics of simply supported box girder bridges are discussed.

The dynamic behavior of continuous and cantilever box girder bridges is examined in Chapter 4. One continuous and two cantilever box girder bridges designed based on AASHTO specifications are given first. Then, the effect of loading models, vehicle speed, road roughness, hinges, etc. are studied. Also included in Chapter 4 are maximum impact factors of the bridges and their comparison with ASSHTO specifications.

The significant conclusions and recommendations are given in Chapter 5.

CHAPTER H

MODEL OF BOX GIRDER BRIDGES

2.1. Introduction

The usage of thin-walled box girders in highway bridge construction has been proven to be a very efficient structural solution for medium-and-long bridges for reason mentioned in Chapter 1. However, analytically, the box girder reveals a complex problem. For this reason, it has received a great deal of attention by the researchers over the past decades. A fundamental contribution to the general solution of the problem was given by Vlasov [63]. Since then, many papers on the static, stability, and vibration analysis of box girders have been published [6, 21, 35, 43, 44, 61]. Comparatively, papers on the dynamic response of thin-walled girders to moving vehicles are quite limited. Jones and Chu [27] considered the response of a box girder beam of constant cross-section subjected to the movement of a mass supported by four springs without considering road surface roughness. In their study, the bridge deck was accurately modeled using a number of strips in conjunction with folded plate theory. Hutton and Cheung [23] studied the effects of vehicle and bridge parameters upon the dynamic response of a box girder bridge based on finite strip method. In their investigation, the vehicle was modeled as a plane rigid body supported at two points by a suspension idealization. The road surface profile was assumed to deviate from the horizontal by a sine wave of wavelength A. In all foregoing investigations on dynamic response of box girder bridge to moving vehicles, the vehicle model and deck surface profile model need to be improved. Also, the folded plate and finite strip

element methods used in their studies have some shortcomings. For example, it is not easy to - isolate the effect of torsional and distortional warping on normal stresses from that of bending, to account for each type of structural action, to account for its relative significance in the overall behavior of the box, as well as to analyze the box girder bridges with variable depth of crosssection and complex boundary conditions.

The purpose of this Chapter is to present the basic theory of box girder and its formulae of finite element for evaluating the static and dynamic load of box girder bridges, as well as the validation of the theory.

2.2. Displacements of Thin-Walled Box Girders

It is, well-known that a box girder (Fig. 2-1) subjected to transversely nonuniform loading undergoes deformation of the cross section. This behavior gives rise to longitudinal stresses due to nonuniform warping and transverse flexural stresses due directly to deformation of the cross section. In order to account for this behavior, four displacements are taken into consideration in this study, i.e.

$$\{\delta\}=[u\ v\ \theta\ \theta]^T \qquad 2\text{-}1$$

where u is the lateral translation (see Fig. 2-2); v is the vertical translation (see Fig.2-3); 9 is the angle of twist about shear center which describe the rigid rotation of cross section (see Figs. 2-1 and 2-4), and ~ is the distortional angle [35] which is defined that the y and x axes rotate about distortion center (see Figs. 2-1 and 2-5) an angle 0 and v6, respectively. Based on the definition of ~, the distortion of the cross section can be expressed as

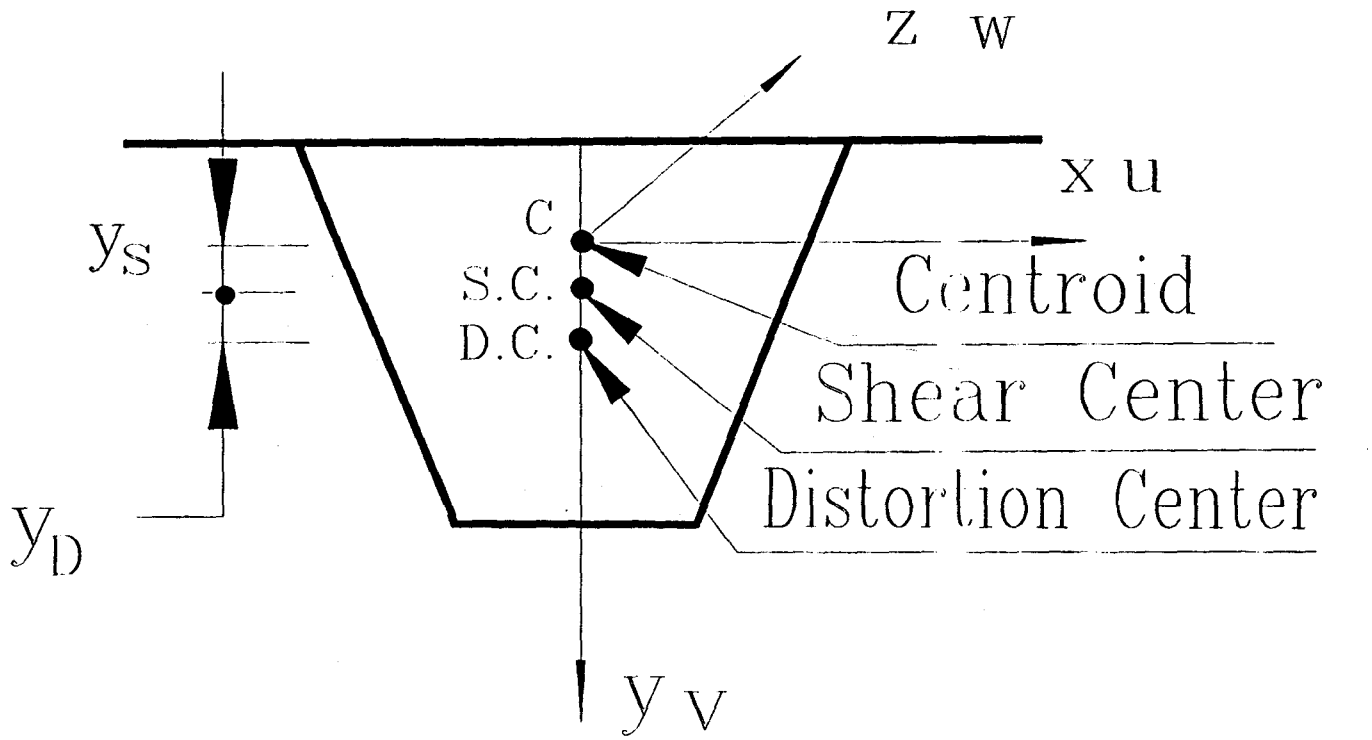

Fig. 2-1. Typical Cross-Section of Box Girder

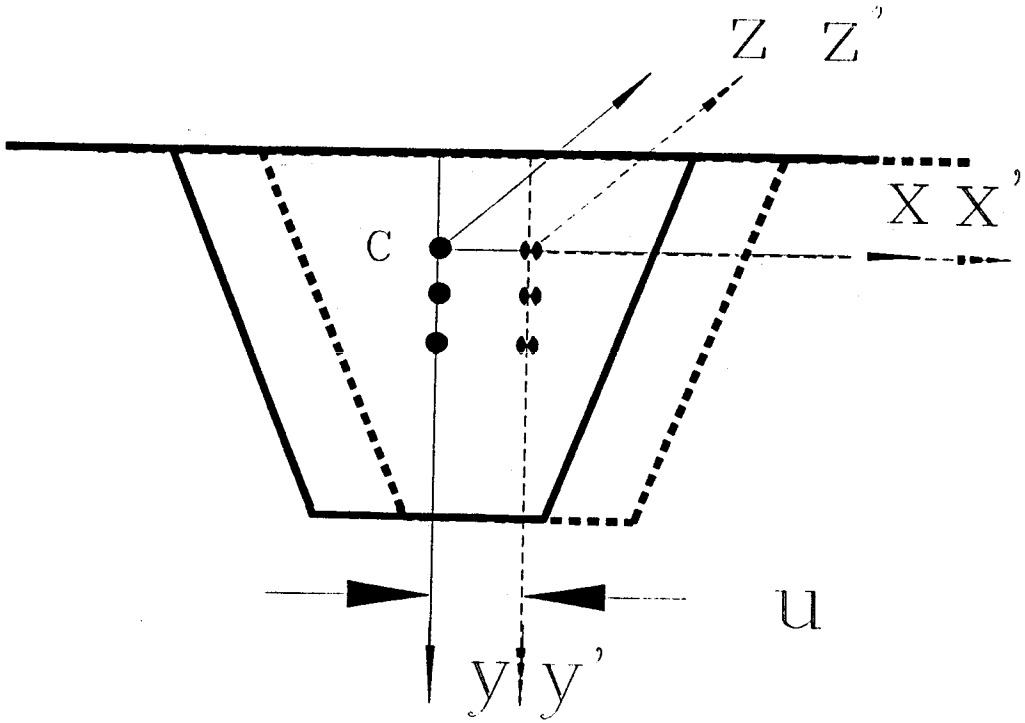

Fig. 2-2. Lateral Displacement of Box Girder

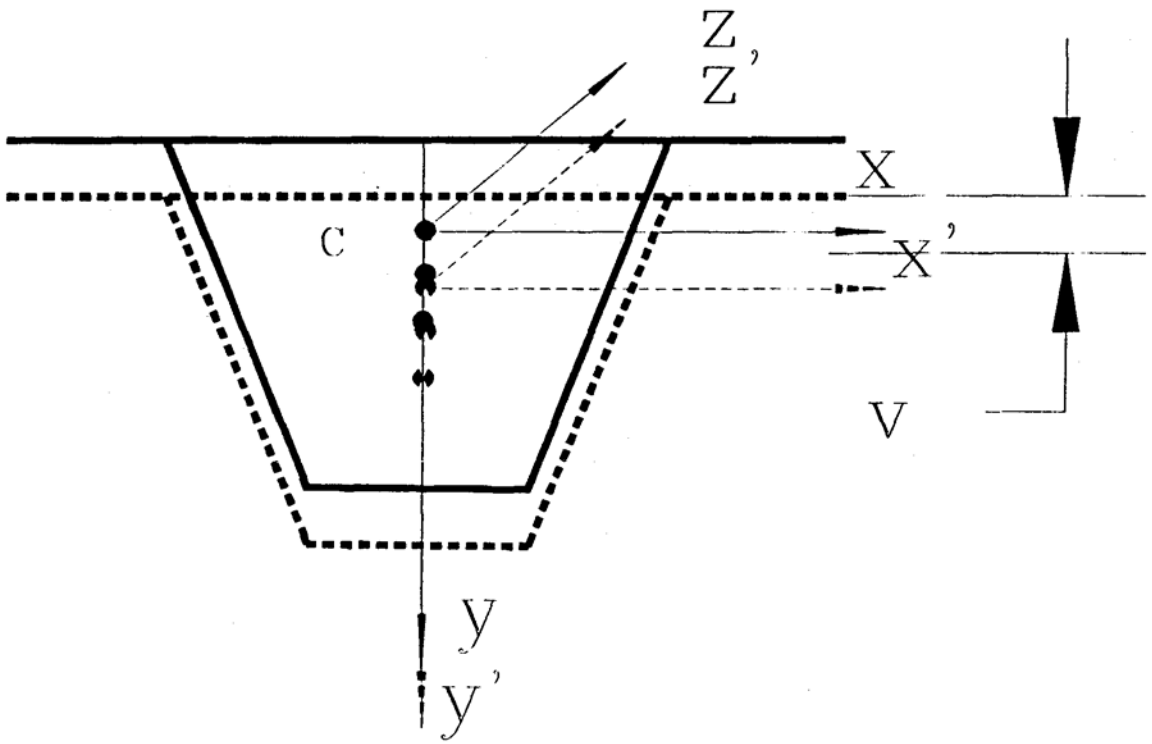

Fig. 2-3. Vertical Displacement of Box Girder

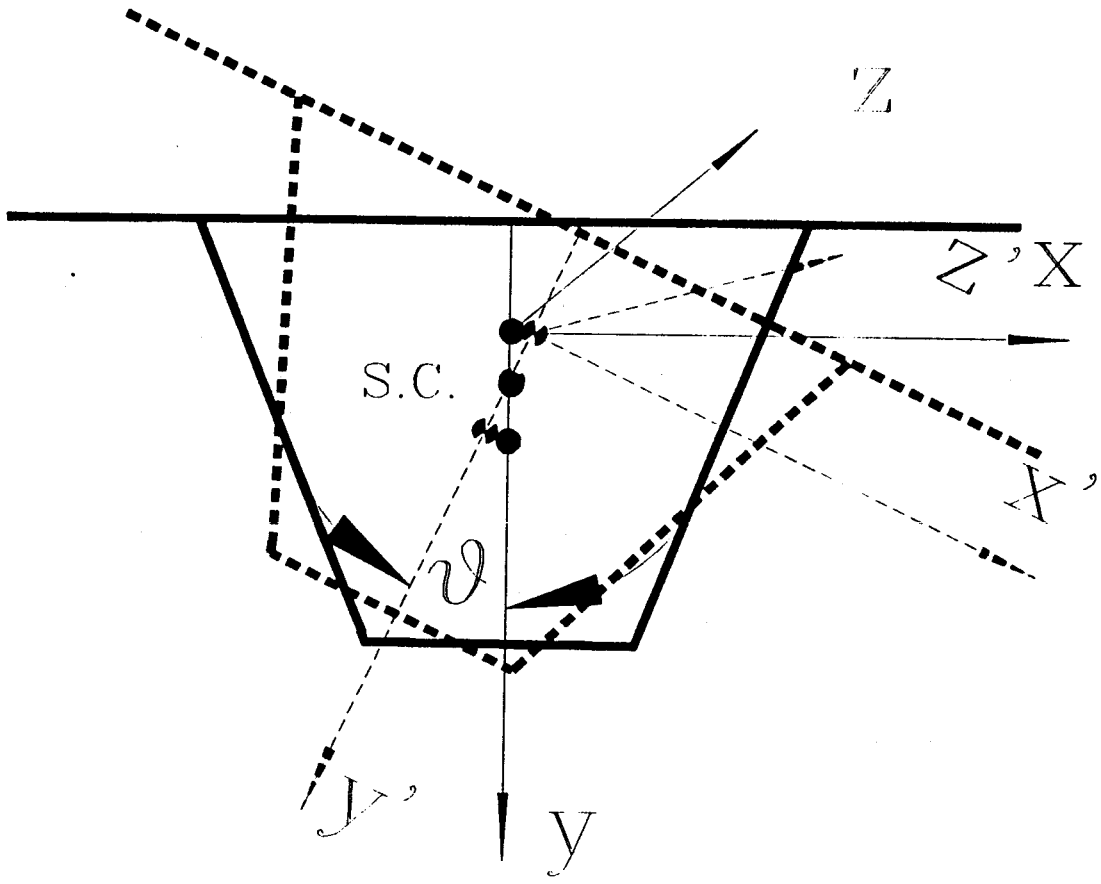

Fig. 2-4. Torsional Displacement of Box Girder

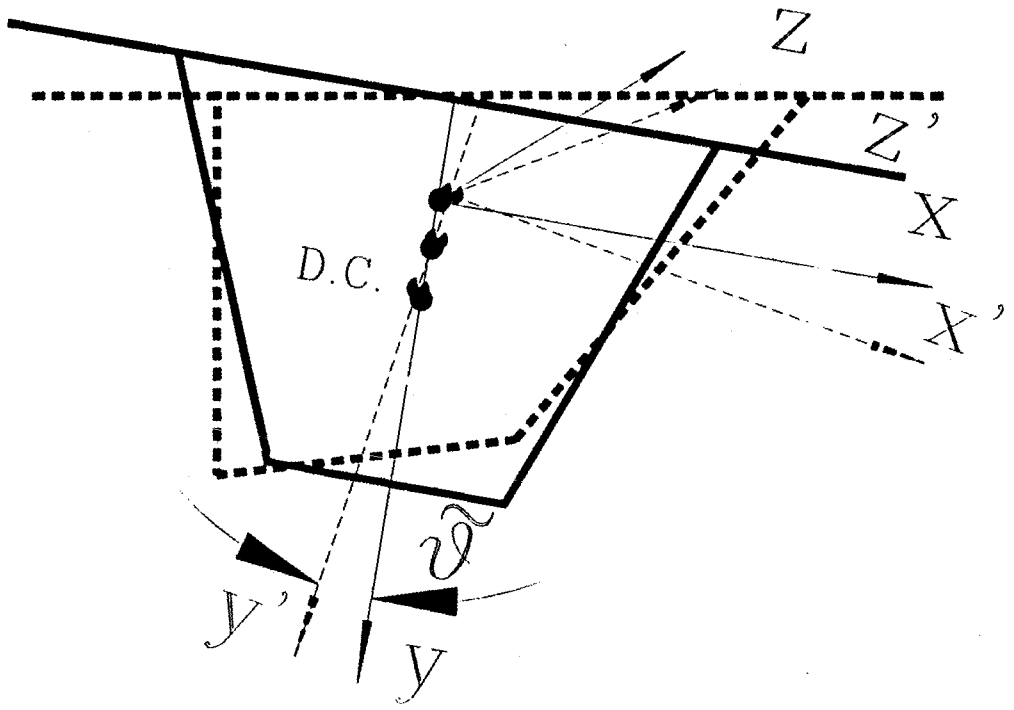

Fig. 2-5. Distortional Displacement of Box Girder

$$'\gamma_N = (1+v)\theta \qquad 2\text{-}2$$

where the factor v is used in order to ensure the continuity of distortion warping and can be determined by

$$v = \frac{\rho_1 d_1 + \rho_3 d_3}{\rho_2 d_2 + \rho_4 d_4} \qquad 2\text{-}3$$

where p; is the perpendicular from distortional center (D.C.) to the side i whose length is d; (see Fig. 2-6). For a rectangular box v = 1.

2.3 Finite Element Method of Thin-Walled Box Girders for Dynamic Analysis

In order to determine the response of the box girder bridges with variable height of cross sections, deformable cross sections over supports and intermediate diaphragms, the finite element method of thin-walled beam will be used in the dynamic analysis. The box girder bridge is divided into finite thin-walled beam elements (see Figs. 2-7 and 2-8). The element axis is defined as the locus of the centroid. To better ;satisfy the accuracy of normal stress concerned, we take the nodal displacement parameter vector of an element as

$$\{\delta\}^e = \begin{Bmatrix} \delta_i \\ \delta_j \end{Bmatrix} \qquad 2\text{-}4$$

in which {S;} = [u u v v θ θ θ θ θ θ]

{S;} = [u u v v θ θ θ θ θ θ]

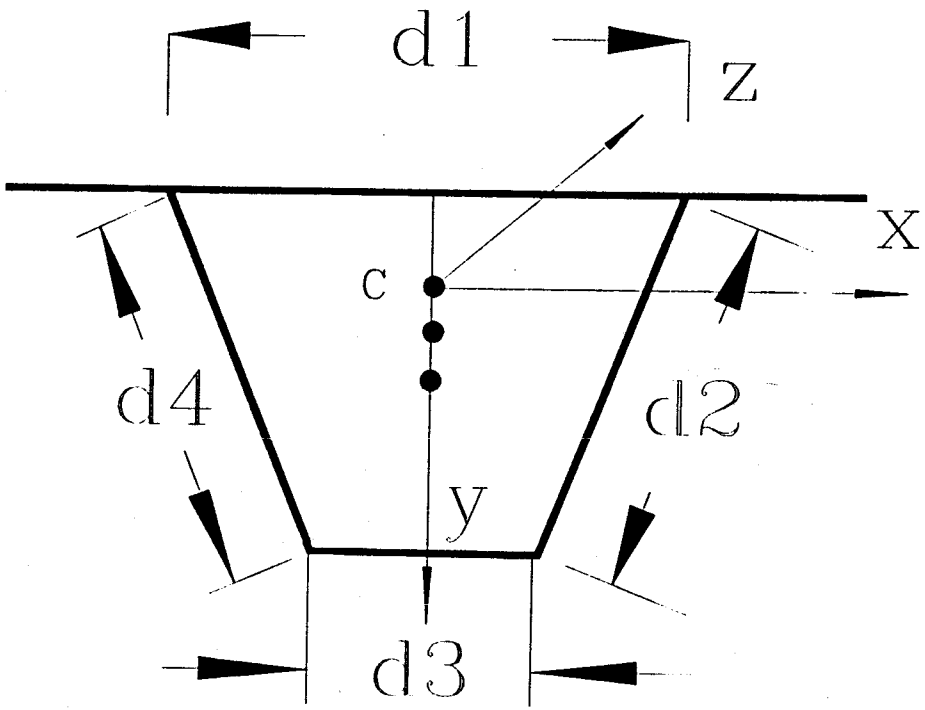

Fig. 2-6. Notation of the Sides of Box Girder

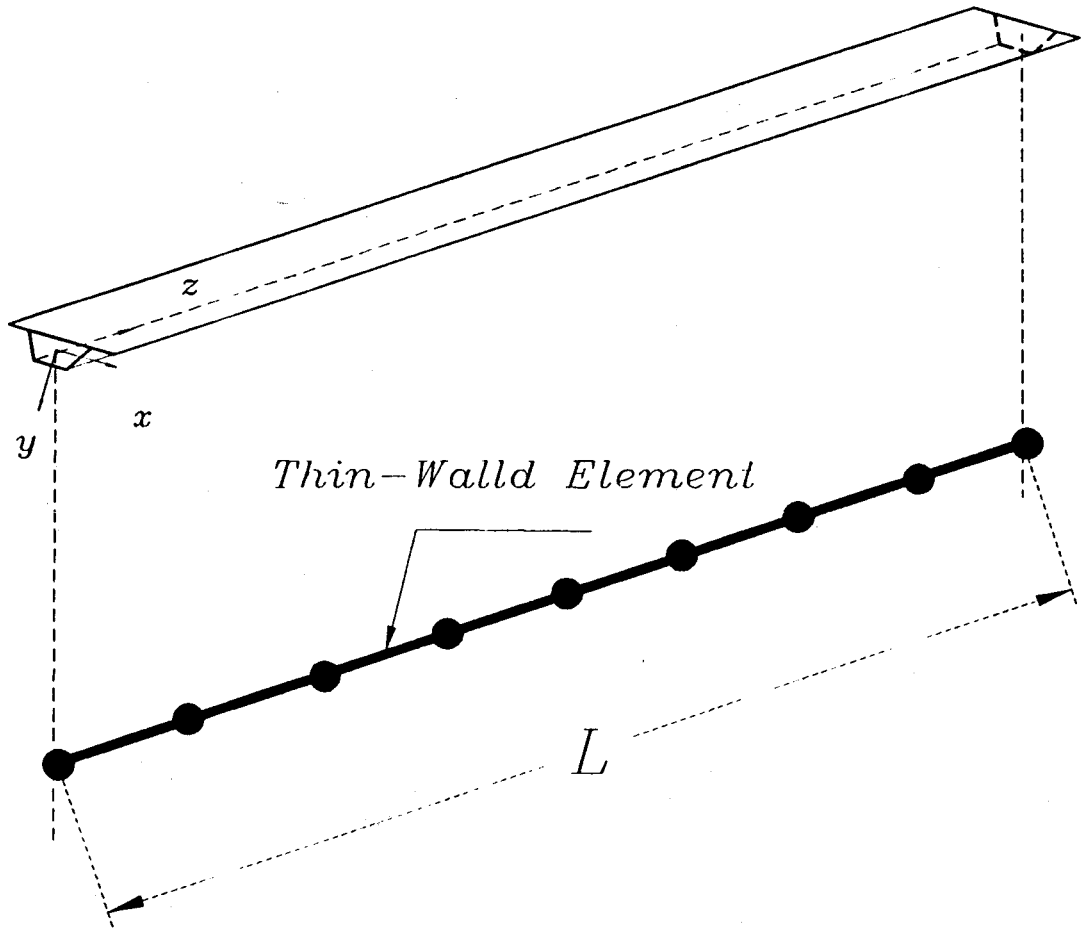

Fig. 2-7. Model of Box Girder Bridge

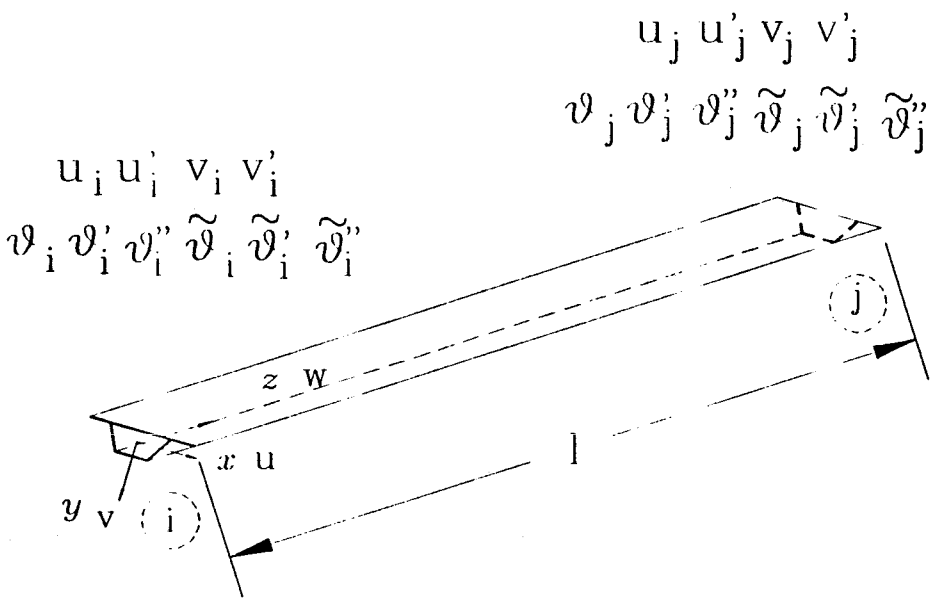

Fig. 2-8. Thin-Walled Beam Element

' and " represents the first and second derivatives with respect to longitudinal displacement z. A third order polynomial is assumed for the displacement functions of u and v; and a fifth order polynomial is assumed for θ and δ

Based on the geometric relations between strains and displacements as well as the relations between stresses and strains [35, 59], then applying the principle of virtual displacement, the stiffness matrix of the thin-walled element can be obtained as follows

$$[k]^e = \begin{bmatrix} [k_{u11}] & 0 & 0 & [k_{u12}] & 0 & 0 \\ & [k_{v11}] & 0 & 0 & [k_{v12}] & 0 \\ & & [k_{\theta 11}] & 0 & 0 & [k_{\theta 12}] \\ & & & [k_{u22}] & 0 & 0 \\ & Sym. & & & [k_{v22}] & 0 \\ & & & & & [k_{\theta 22}] \end{bmatrix} \qquad 2\text{-}5$$

where $[k_{u11}]$, $[k_{u12}]$, $[k_{u22}]$, $[k_{v11}]$, $[k_{v12}]$, $[k_{v22}]$ are 2 X 2 order matrices which can be obtained from the stiffness matrix of general beam element [59]; and

$$[k_{\theta 11}] = E \begin{bmatrix} J_{11}[A_1] & J_{12}[A_1] \\ Sym. & J_{22}[A_1] \end{bmatrix} + G \begin{bmatrix} J_T[B_1] & 0 \\ Sym. & 0 \end{bmatrix} + \begin{bmatrix} 0 & 0 \\ Sym. & A_R[C_1] \end{bmatrix} \qquad 2\text{-}6$$

$$[k_{\theta 12}] = E\begin{bmatrix} J_{11}[A_2] & J_{12}[A_2] \\ Sym. & J_{22}[A_2] \end{bmatrix} + G\begin{bmatrix} J_T[B_2] & 0 \\ 0 & 0 \end{bmatrix} + \begin{bmatrix} 0 & 0 \\ 0 & A_R[C_2] \end{bmatrix} \qquad 2\text{-}7$$

$$[k_{\theta 22}] = E\begin{bmatrix} J_{11}[A_3] & J_{12}[A_3] \\ Sym. & J_{22}[A_3] \end{bmatrix} + G\begin{bmatrix} J_T[B_3] & 0 \\ 0 & 0 \end{bmatrix} + \begin{bmatrix} 0 & 0 \\ 0 & A_R[C_3] \end{bmatrix} \qquad 2\text{-}8$$

$$[A_1] = \frac{1}{7l^3}\begin{bmatrix} 120 & 60l & 3l^2 \\ & \frac{192}{5}l^2 & \frac{11}{5}l^3 \\ & Sym. & \frac{3}{5}l^4 \end{bmatrix} \qquad 2\text{-}9$$

$$[A_2] = \frac{1}{7l^3}\begin{bmatrix} -120 & 60l & -3l^2 \\ & \frac{108}{5}l^2 & -\frac{4}{5}l^3 \\ & Sym. & \frac{1}{10}l^4 \end{bmatrix} \qquad 2\text{-}10$$

$$[A_3] = \frac{1}{7l^3}\begin{bmatrix} 120 & -60l & 3l^2 \\ & \frac{192}{5}l^2 & -\frac{11}{5}l^3 \\ & Sym. & \frac{3}{5}l^4 \end{bmatrix} \qquad 2\text{-}11$$

$$[B_1] = \frac{1}{7l}\begin{bmatrix} 10 & \frac{3}{2}l & \frac{1}{12}l^2 \\ & \frac{8}{5}l^2 & \frac{7}{10}l^3 \\ & Sym. & \frac{1}{90}l^4 \end{bmatrix} \qquad 2\text{-}12$$

$$[B_2] = \frac{1}{7l}\begin{bmatrix} -10 & \frac{3}{2}l & -\frac{1}{12}l^2 \\ & -\frac{1}{10}l^2 & \frac{1}{30}l^3 \\ & Sym. & \frac{1}{180}l^4 \end{bmatrix} \qquad 2\text{-}13$$

$$[B_3] = \frac{1}{7l}\begin{bmatrix} 10 & -\frac{3}{2}l & \frac{1}{12}l^2 \\ & \frac{8}{5}l^2 & -\frac{1}{60}l^3 \\ & Sym. & \frac{1}{90}l^4 \end{bmatrix} \qquad 2\text{-}14$$

$$[C_1] = \frac{l}{14}\begin{bmatrix} \frac{181}{33} & \frac{311}{330}l & \frac{281}{3960}l^2 \\ & \frac{104}{495}l^2 & \frac{23}{1320}l^3 \\ & Sym. & \frac{1}{660}l^4 \end{bmatrix} \qquad 2\text{-}15$$

$$[C_2] = \frac{l}{14}\begin{bmatrix} \frac{50}{33} & -\frac{151}{330}l & \frac{181}{3960}l^2 \\ & -\frac{133}{990}l^2 & \frac{13}{990}l^3 \\ & Sym. & \frac{1}{792}l^4 \end{bmatrix} \qquad 2\text{-}16$$

$$[C_3] = \frac{l}{14}\begin{bmatrix} \frac{181}{33} & -\frac{311}{330}l & \frac{281}{3960}l^2 \\ & \frac{104}{495}l^2 & -\frac{23}{1320}l^3 \\ & Sym. & \frac{1}{660}l^4 \end{bmatrix} \qquad 2\text{-}17$$

where E is modulus of elasticity;

G is shear modulus;

$J_{11} = \int_F \omega\omega dF$, warping torsional constant;

$J_{22} = \int_F \bar{\omega}\bar{\omega}\, dF$, distortional constant;

$J_{12} = \int_F \omega\bar{\omega}\, dF$, torsional and distortional cross constant;

F = area of cross section;

ω = the unit torsional warping function; and

ϖ = the unit distortional warping function;

J_T = pure torsional constant;

$A_R = (1+\nu)K$; and

K = the stiffness of the box section against the distortion.

Element consistent-mass matrix can be derived as follows:

$$[m]^e = \begin{bmatrix} [m_{u11}] & 0 & [m_{\theta 12}] & [m_{u12}] & 0 & [m_{\theta 13}] \\ & [m_{v11}] & 0 & 0 & [m_{v12}] & 0 \\ & & [m_{\theta 11}] & [m_{\theta 13}]^T & 0 & [m_{\theta 14}] \\ & Sym. & & [m_{u22}] & 0 & [m_{\theta 23}] \\ & & & & [m_{v22}] & 0 \\ & & & & & [m_{\theta 22}] \end{bmatrix} \qquad 2\text{-}18$$

where $[m_{u11}]$, $[m_{v11}]$, $[m_{u12}]$, $[m_{v12}]$, $[m_{u22}]$, and $[m_{v22}]$ are 2x2 matrices and can be obtained easily from conventional beam element consistent-mass matrix [59]; and

$$[m_{\theta 11}] = \begin{bmatrix} M_A[C_1] & 0 \\ 0 & M_A[C_1] \end{bmatrix} \qquad 2\text{-}19$$

$$[M_{\theta 12}] = \begin{bmatrix} \alpha_1[C_4] & \alpha_2[C_4] \end{bmatrix} \qquad 2\text{-}20$$

$$[M_{\theta 13}]=\begin{bmatrix}\alpha_1[C_5] & \alpha_2[C_5]\end{bmatrix} \qquad 2\text{-}21$$

$$[M_{\theta 14}]=\begin{bmatrix}\alpha_3[C_2] & \alpha_4[C_2] \\ Sym. & \alpha_5[C_2]\end{bmatrix} \qquad 2\text{-}22$$

$$[M_{\theta 22}]=\begin{bmatrix}\alpha_3[C_3] & \alpha_4[C_3] \\ Sym. & \alpha_5[C_3]\end{bmatrix} \qquad 2\text{-}23$$

$$[M_{\theta 23}]=\begin{bmatrix}\alpha_1[C_6] & \alpha_2[C_6]\end{bmatrix} \qquad 2\text{-}24$$

$$[C_4]=\frac{l}{21}\begin{bmatrix}-8 & \frac{11}{8}l & -\frac{5}{48}l^2 \\ -\frac{9}{8}l & -\frac{1}{8}l^2 & -\frac{1}{48}l^3\end{bmatrix} \qquad 2\text{-}25$$

$$[C_5]=\frac{l}{42}\begin{bmatrix}-5 & \frac{29}{20}l & -\frac{17}{120}l^2 \\ \frac{5}{4}l & \frac{7}{20}l^2 & \frac{1}{30}l^3\end{bmatrix} \qquad 2\text{-}26$$

$$[C_6]=\frac{l}{21}\begin{bmatrix} -8 & \frac{11}{8}l & -\frac{5}{48}l^2 \\ \frac{9}{8}l & -\frac{1}{4}l^2 & \frac{1}{48}l^3 \end{bmatrix} \qquad 2\text{-}27$$

where $\alpha_1 = -S_x + y_s M_A$,

$\alpha_2 = -S_x + y_D M_A$,

$\alpha_3 = J_{mx} + J_{my} - 2y_s S_x + y_s^2 M_A$,

$\alpha_4 = J_{mx} - J_{my} - (y_s + y_D)S_x - y_s y_D M_A$,

$\alpha_5 = J_{mx} + J_{my} - 2y_D S_x + y_D^2 M_A$,

M_A is mass per unit along z-axis,

y_s and y_D are the distances measured from centroid to shear center and distortion center, respectively;

S_x is the static moment of mass of whole section about y-axis; and

J_{mx} and J_{my} are the mass inertia moments about x-axis and y-axis, respectively.

The equations of motion of the bridge are

$$[M_B]\{\ddot{\delta}\} + [D_B]\{\dot{\delta}\} + [K_B]\{\delta\} = \{F_{BT}\} \qquad 2\text{-}28$$

in which $[M_B]$ = global mass matrix,

$[K_B]$ = global stiffness matrix,

$[D_B]$ = global damping matrix,

$\{\delta\}$, $\{\dot{\delta}\}$, $\{\ddot{\delta}\}$ = global nodal displacement, velocity, and acceleration vectors, and

$\{F_{BT}\}$ = global nodal loading vector, due to the interaction between the bridge and vehicle.

The boundary conditions of thin-walled box girder are somewhat different from those of conventional beam. At a simple support with diaphragm of infinite rigidity in-plane while zero out-plane, the boundary conditions are

$u=0,$

$v=0,$

$\theta=0,$

$\bar{\theta}=0,$

$\theta^{*}=0,$ and

$\bar{\theta}^{*}=0.$

If the diaphragm over the support can be deformable in-plane, the boundary conditions can be formulated as

$u=(y_s + y_D)\theta,$

$v=0,$

$\theta=\bar{\theta},$

$\theta^{*}=0,$

$\bar{\theta}^{*}=0.$

2.4. Interaction Equations

The interaction force of the ith tire between the bridge and vehicle is given as:

$$F^i_{BT} = K_{tyi}U_{tyi} + D_{tyi}\dot{U}_{tyi} \qquad 2\text{-}29$$

in which K_{tyi} = the stiffness of the ith tire, D_{tyi} = the damping coefficient of the ith tire, U_{tyi} = the relative displacement between the ith tire and bridge = y_{ai} - ($-u_{sri}$) - w_{bi}, y_{ai} = the vertical displacement of the ith tire, u_{sri} = the road surface roughness under the ith tire (positive upwards), and w_{bi} = the bridge vertical displacement under the ith tire (positive downwards), and a dot superscript denotes differential with respect to time. The w_{bi} can be evaluated by the nodal displacements of $\{\delta\}^e$ of the element and expressed as follows:

$$w_{bi} = v(z) + x\theta(z) - x\tilde{\theta}(z) \qquad 2\text{-}30$$

where

$$\begin{Bmatrix} v \\ \theta \\ \tilde{\theta} \end{Bmatrix} = \begin{bmatrix} 0 & 0 & N_1 & N_2 & 0 & 0 & 0 & 0 & 0 & 0 & 0 & 0 & N_3 & N_4 & 0 & 0 & 0 & 0 & 0 & 0 \\ 0 & 0 & 0 & 0 & N_5 & N_6 & N_7 & 0 & 0 & 0 & 0 & 0 & 0 & 0 & N_8 & N_9 & N_{10} & 0 & 0 & 0 \\ 0 & 0 & 0 & 0 & 0 & 0 & 0 & N_5 & N_6 & N_7 & 0 & 0 & 0 & 0 & 0 & 0 & 0 & N_8 & N_9 & N_{10} \end{bmatrix}$$

$$*\{\delta\}^e \qquad 2\text{-}31$$

$N_1 = 1 - 3z_1^2 + 2z_1^3$

$N_2 = (z_1 - 2z_1^2 + z_1^3)l$

$N_3 = (3z_1^2 - 2z_1^3)$

$N_4 = (- z_1^2 + z_1^3)l$

$N_5 = 1 - 10z_1^3 + 15z_1^4 - 6z_1^5$

$N_6 = (z_1 - 6z_1^3 + 8z_1^4 - z_1^5)l$

$N_7 = 1/2\ (z_1^2 - 3z_1^3 + 3z_1^4 - z_1^5\ )l^2$

$N_8 = 10z_1^3 - 15z_1^4 + 6z_1^5$

$N_9 = (-4z_1^3 + 7z_1^4 - 3z_1^5)l$

$N_{10} = 1/2(z_1^3 - 2z_1^4 + z_1^5)l^2$

$z_1 = z/l.$

2.5. Validation

In order to validate the whole dynamic model of box girder bridges, extensive model testing was conducted. Herein, only two box girder bridges investigated by Li [35] and Jones [26] as well as Jones and Chu [27] are presented.

Numerical Example 1 [35]:

Dimension of a cross-section of a simply supported steel box girder are illustrated in Fig. 2-9,

$l = 24.0$ m, span length;

$E = 2.06 \times 10^5$ MPa, modulus of elasticity; and

$G = 7.848 \times 10^4$ MPa, modulus of shearing.

The box girder is divided into 20 equal elements. Two loading cases are considered: (1) uniform torque $m_z = 1$ kN-m/m; (2) uniform distortional torque $\tilde{m}_z = 1$ kN-m/m. The computed angle of torsion, θ, St. Venant's torsion, T_c, Wagner's torsional moment/warping torsion, T_ω, and bi-moment B_ω, for loading case 1 of both analytic method [38] and the presented finite element method, are shown in Figs 2-10 to 2-12. The angles of distortion $\tilde{\theta}$ and distortional bi-moment $B_{\tilde{\omega}}$ are shown in Figs. 2-13 and 2-14. Those figures demonstrated that the computed results well agree with the results from Li [35]. It can be concluded from the

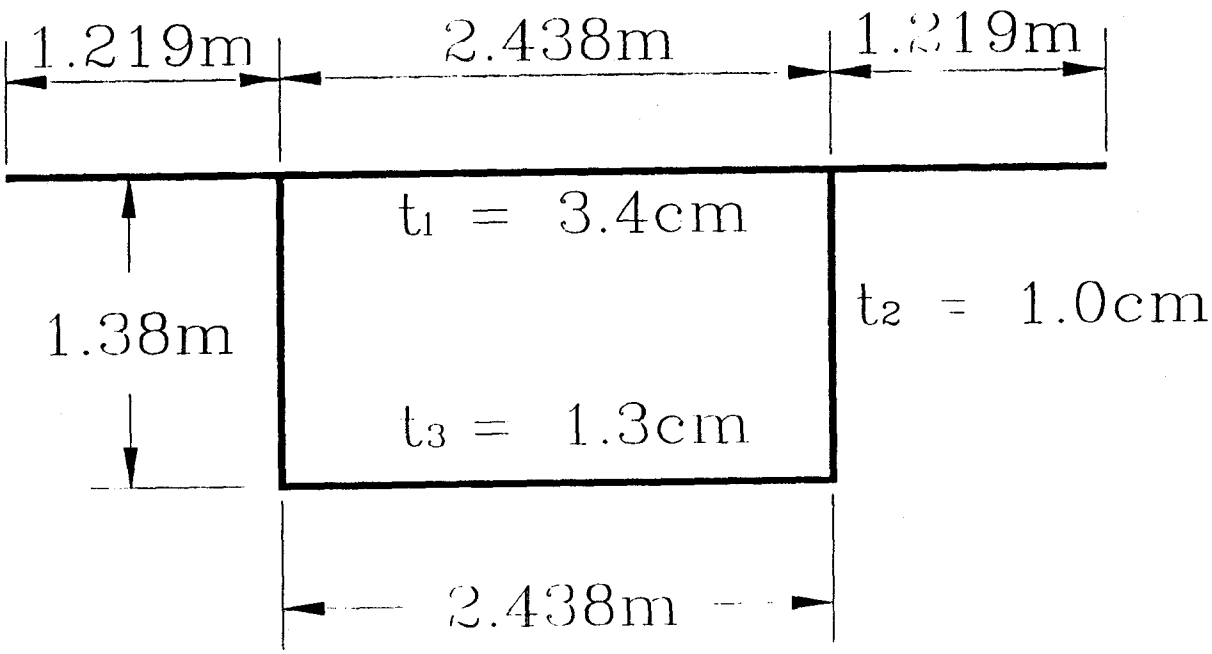

Fig. 2-9. Cross-Section of the Bridge for Example 1

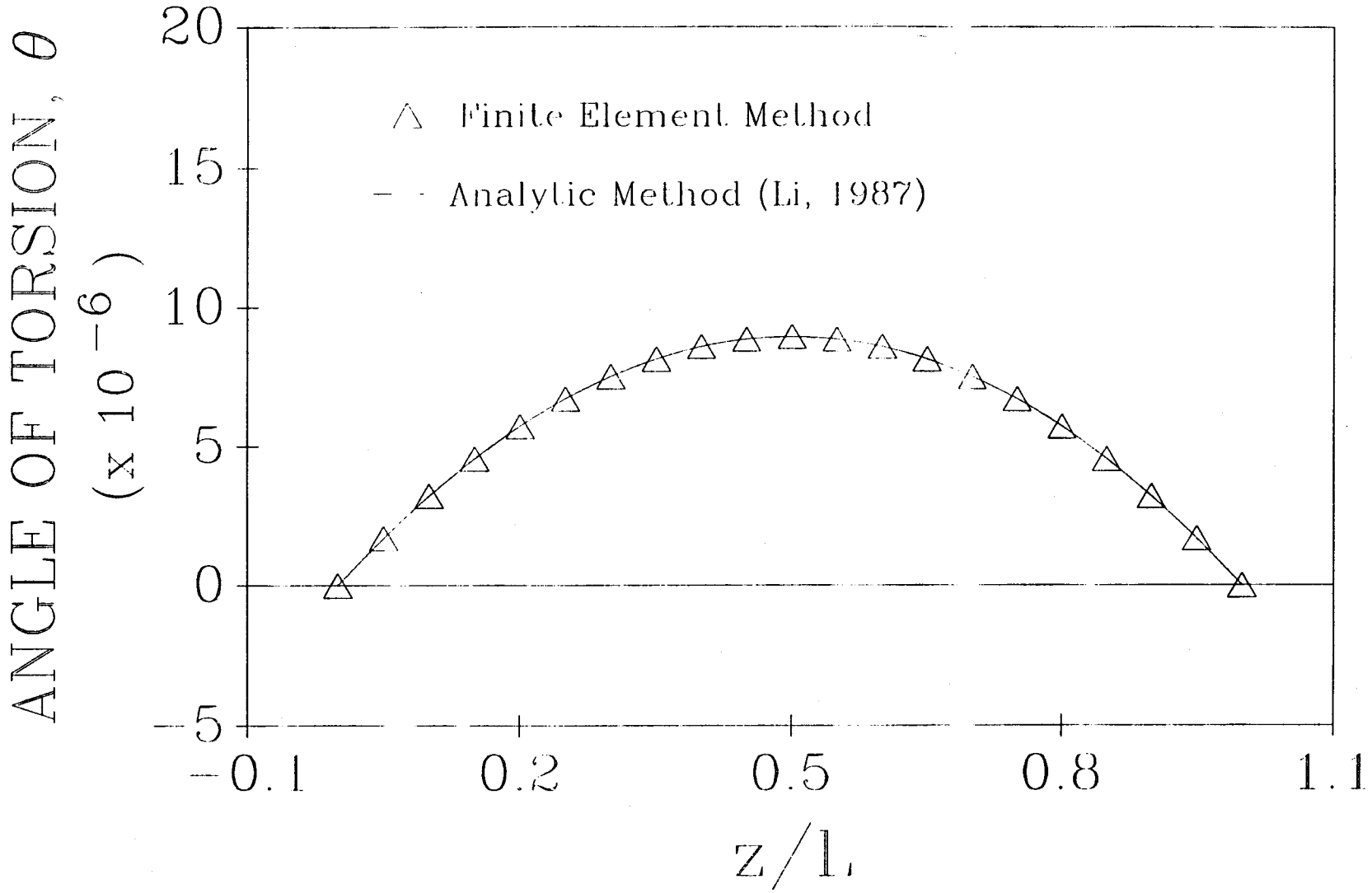

Fig. 2-10. Angle of Torsion as a Function of z/L

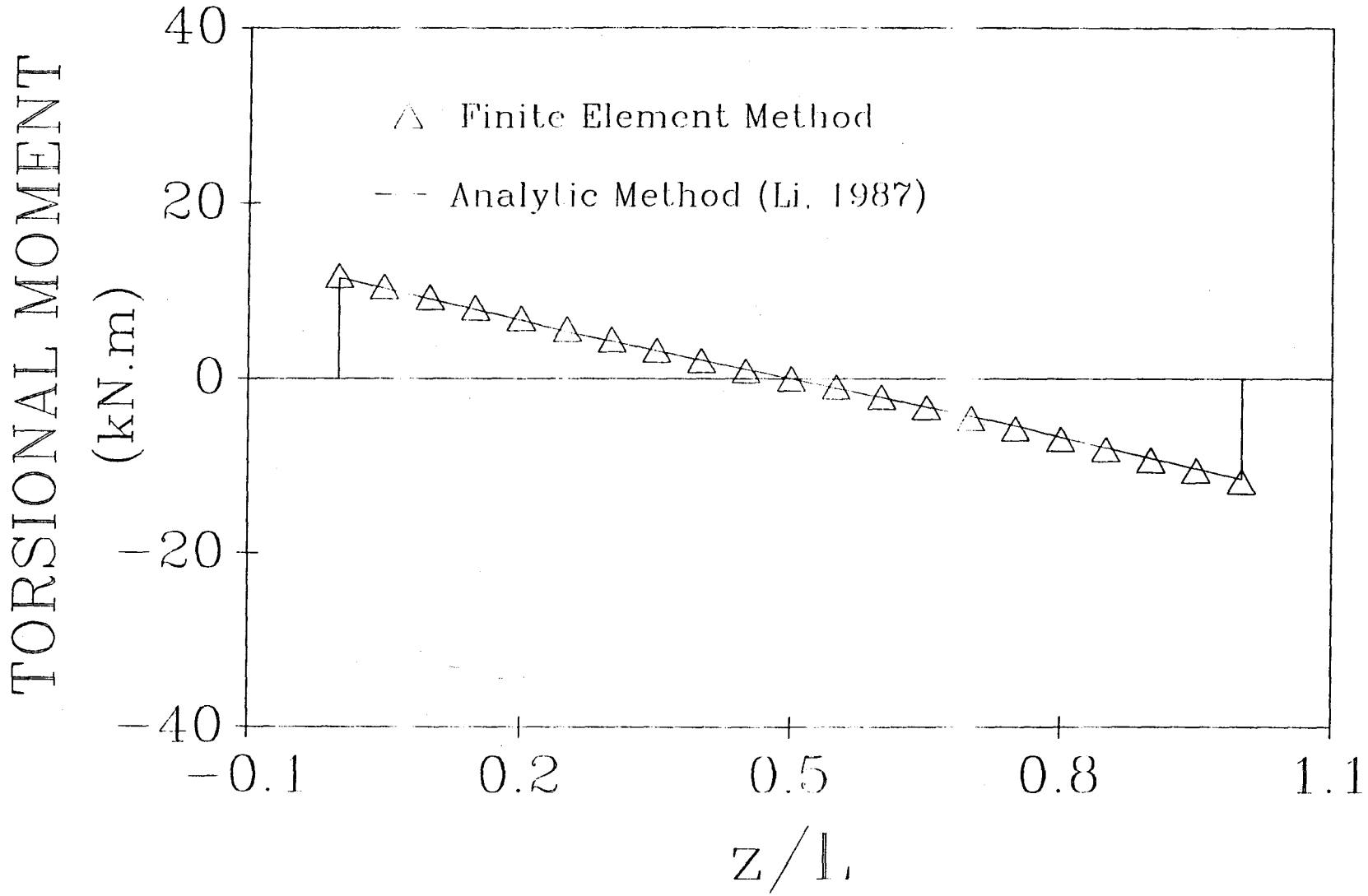

Fig. 2-11. Torque as a Function of z/L

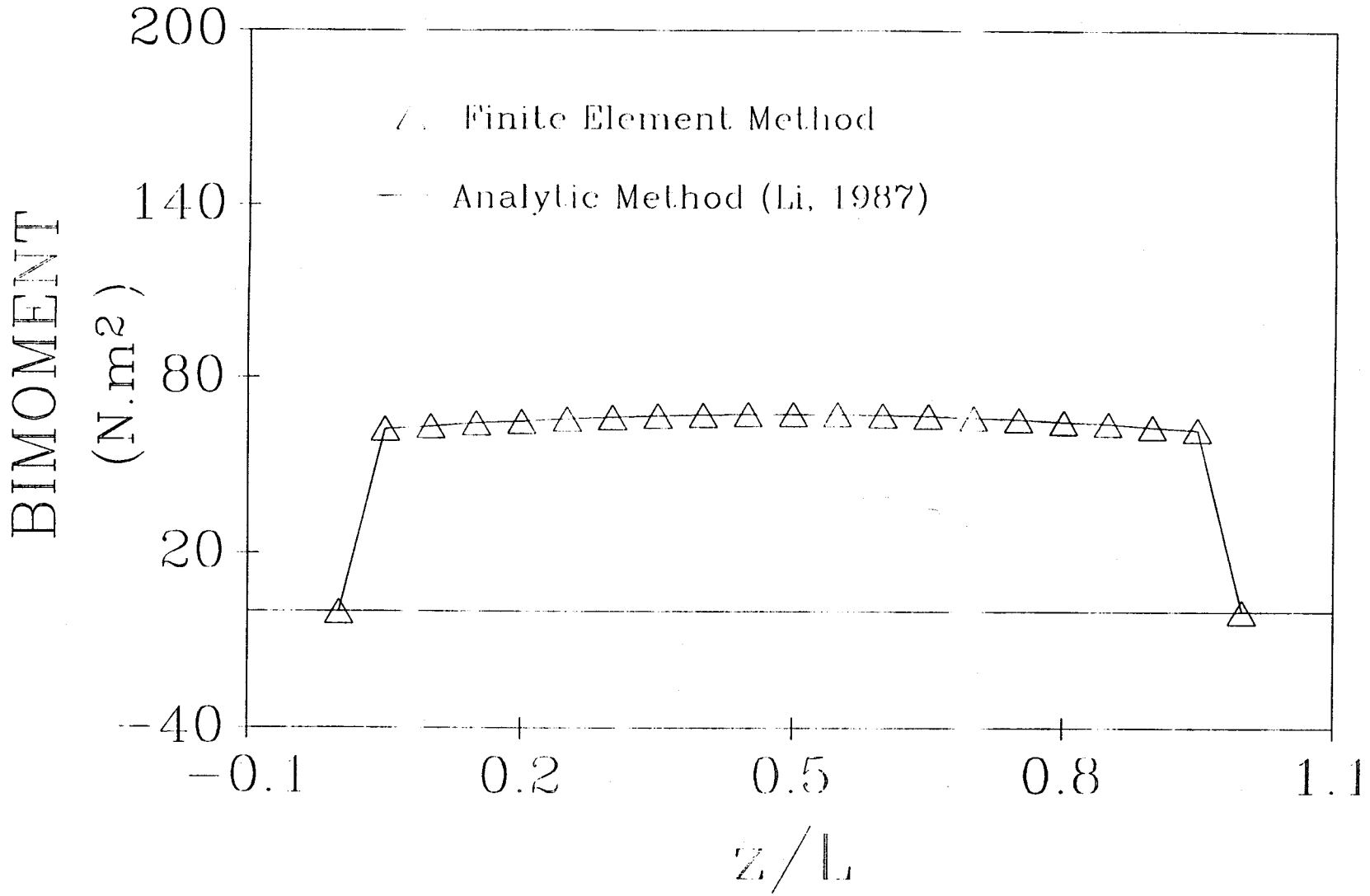

Fig. 2-12. Bi-moment as a Function of z/L

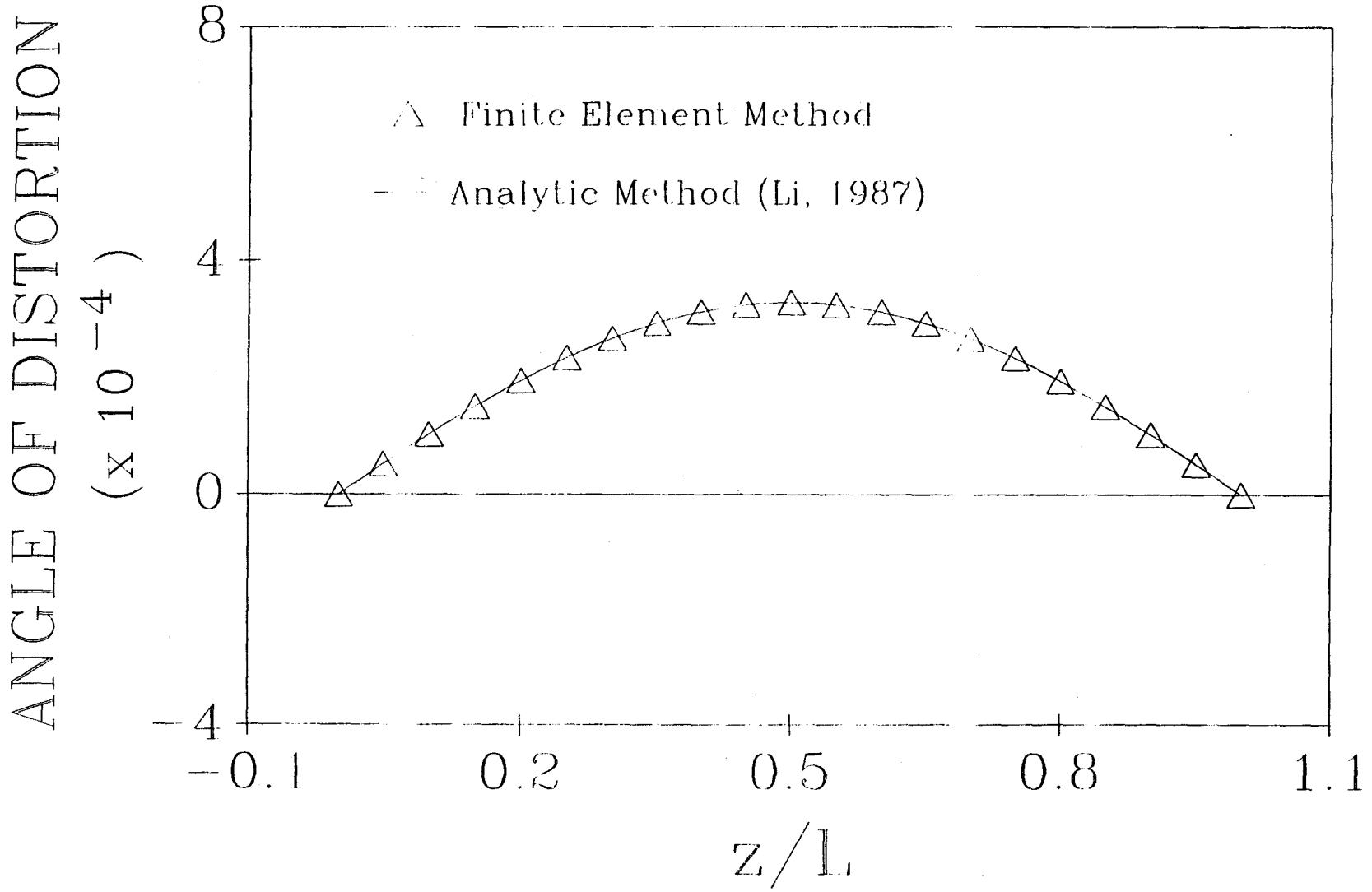

Fig. 2-13. Distortional angle as a Function of z/L

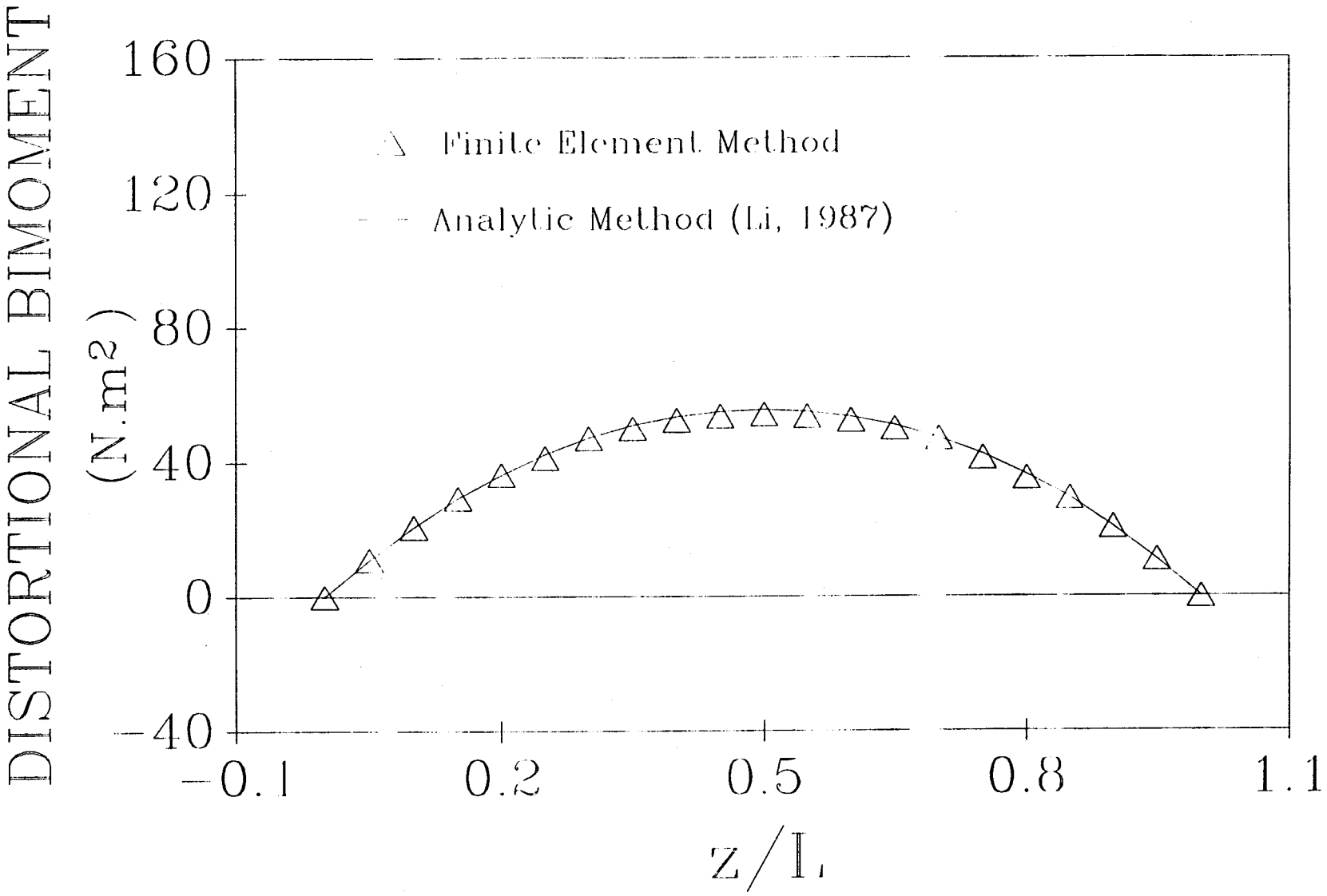

Fig. 2-14. Distortional Bi-moment as a Function of z\L

numerical example that both the finite element formulae and the computer program are reliable for static analysis of box girders.

Numerical Example 2 [26, 27];

Fig. 2-15 shows the cross section of the box girder bridge used in Jones [26], which is simply supported with 30.48 m span. The bridge has end rigid diaphragms but no intermediate ones. The mass density is taken as 2570 kg/m^3; the modulus of elasticity as 2.069 x 10' MPa, and Poisson's Ratio as 0.2. The live load of truck is simplified as consisting of four identical wheel loads (see Fig. 2-16). Each wheel load is taken as 71.168 kN represented by spring supported mass with the force in the spring distributed over a rectangular area of 60.96 cm transverse by 20.32 cm longitudinal (see Fig. 2-17). The spring constant is taken as 7.588 kN/cm. Internal damping of the truck as well as bridge damping are neglected. The two axles (four spring born loads) keep 4.267 m apart with exterior wheel touching the inside of the right curb (see Fig. 2-18). The vehicle speed is taken as 109.41 km/hr (68 mph). The springs are considered as staring at zero vertical displacement and zero velocity when the load entering the bridge. The road surface is assumed to be smooth.

The dynamic responses of 8 points at mid-span for vertical deflection and longitudinal stress are shown in Table 2-1. The numbering of the points are shown in Fig. 2-17. From Table 2-1, we can observe that the results calculated by the presented procedure agree very well with those evaluated by folded plate method [26], just slightly larger by less than 1.5% for almost all dynamic responses.

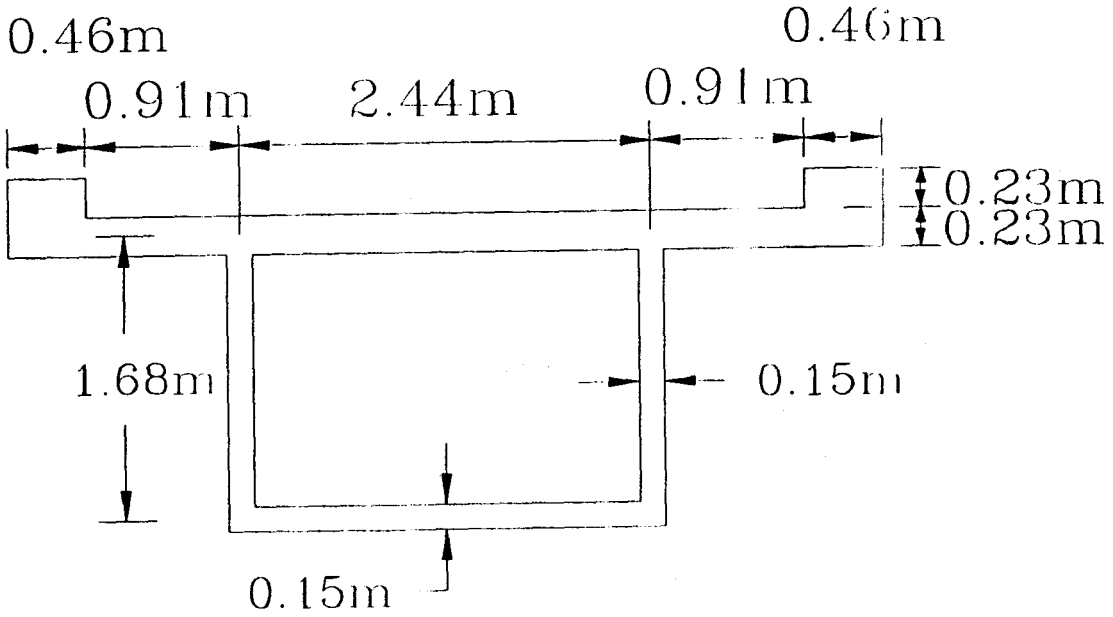

Fig. 2-15. Cross-Section of the Bridge for Example 2

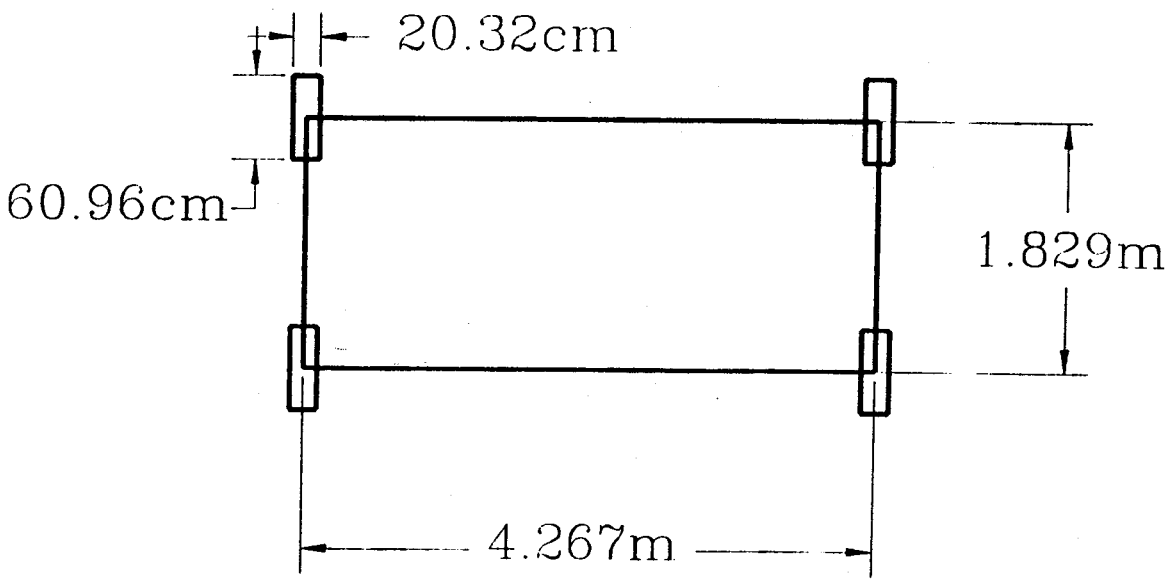

Fig. 2-16. Plane of The Simplified Live Loading Model

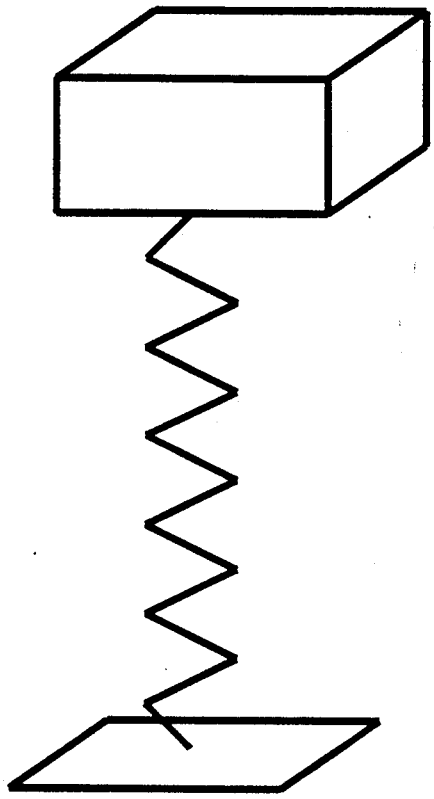

Fig. 2-17. Simplified Wheel Load

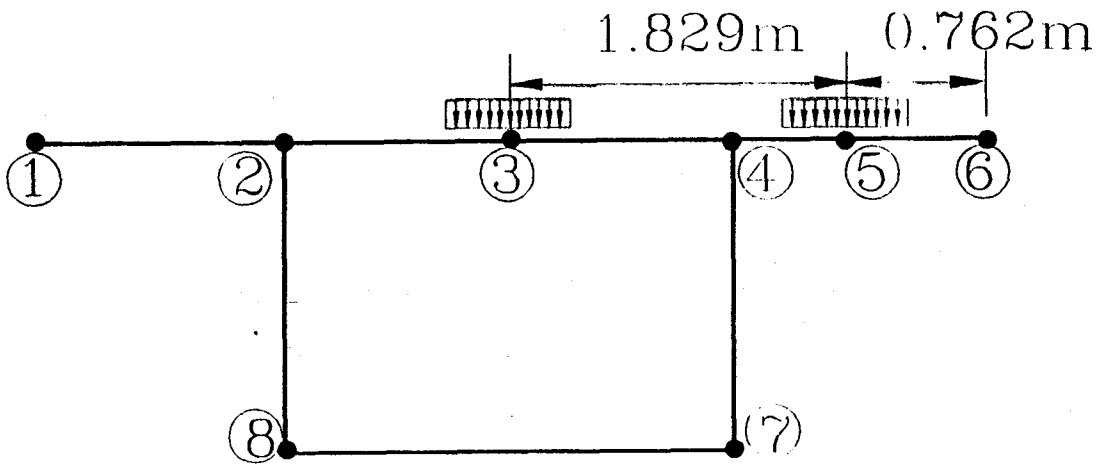

Fig. 2-18. Numbering of Stress Points

Table 2-1. Comparison of Dynamic Responses

Method	Type of Response	Points							
		1	2	3	4	5	6	7	8
Folded Plate	Deflec.(cm)	0.6248	0.6552	0.6829	0.7100	0.7319	0.7344	0.7122	0.6559
	Normal Stress (MN/m^2)	-0.9111	-0.9162	-0.9493	-1.0078	-1.0016	-0.9939	2.5261	2.1544
Thin-walled Beam	Deflec.(cm)	0.6285	0.6602	0.6883	0.7165	0.7376	0.7482	0.7165	0.6602
	Normal Stress (MN/m^2)	-0.9236	-0.9251	-0.9595	-1.0172	-1.0094	-1.0065	2.5545	2.1724

CHAPTER III

VIBRATION OF SIIVIPLY SUPPORTED BOX GIRDER BRIDGES

3.1 General

As described in Chapter 2, the former investigators used simple planar model of vehicle and simple road profile simulation. This may not reflect the real behavior of practical box girder bridges. The fundamental purpose of this chapter is to analyze the bridge impact characteristics to be considered in the practical design and further impact studies of box girder bridges, with space truck models.

3.2. Vehicle Model

Figs. 3-1 and 3-2 illustrate the side and front views of a nonlinear vehicle model developed according to HS20-44 trucks which is a major design vehicle in AASHTO specifications [49]. Five rigid masses represent the tractor, semi-trailer, steer wheel/axle set, tractor wheel/axle set, and trailer wheel/axle set, respectively. In the model, the tractor, semi-trailer were each assigned three degrees of freedom (DOF'S), corresponding to the vertical displacement (y), rotation about the transverse axis (pitch or B), and rotation about the longitudinal axis (roll or 0). Each wheel/axle set is provided with two DOF's in the vertical and roll directions. The total degrees of freedom are twelve. The tractor and semi-trailer were interconnected at the pivot point (so-called fifth wheel point, see Fig.3-1).

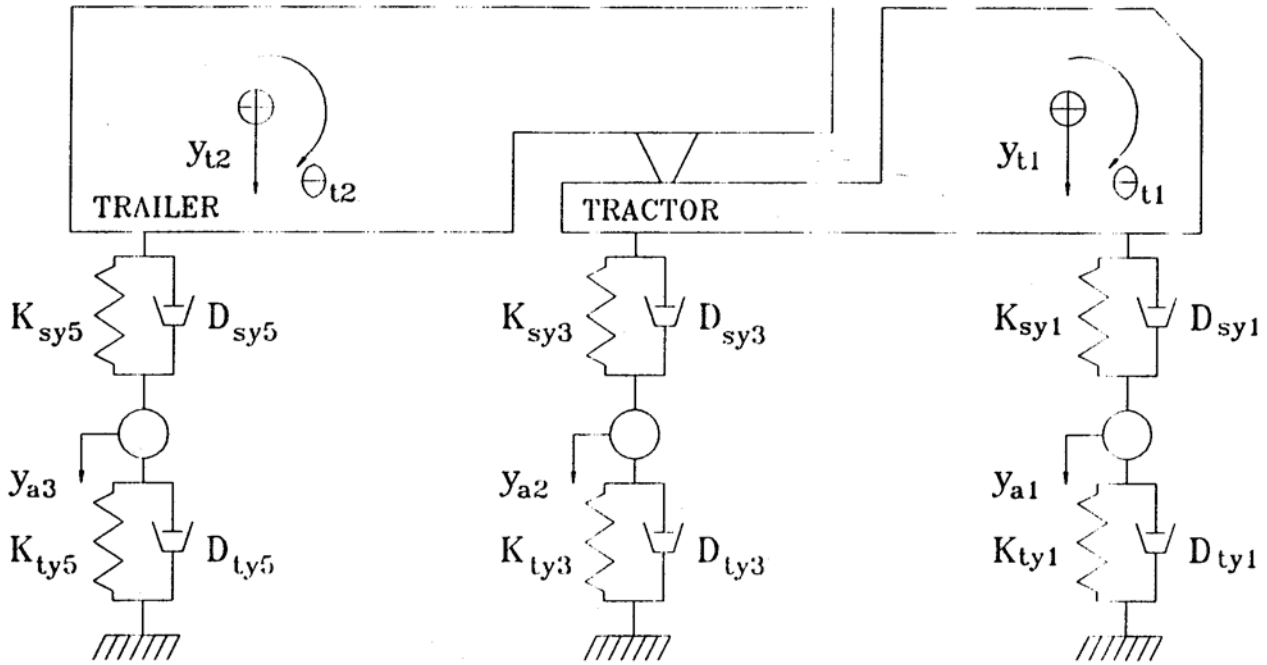

Fig. 3-1. Front View of HS20-44 Vehicle Model

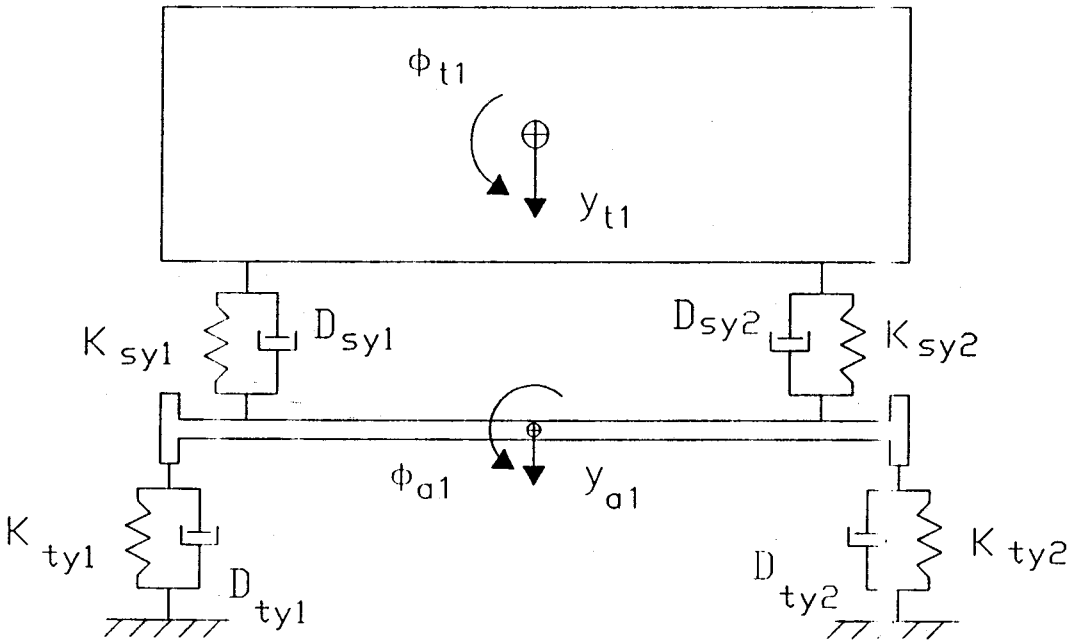

Fig. 3-2. Side View of HS20-44 Vehicle Model

Suspension force consists of the linear elastic spring force and the constant interleaf friction force [22]. The tire springs and all dampers are assumed to be linear. The equations of motion of the system were derived by using Lagrange's formulation. Details of derivation and data are presented in Reference [53, 54].

3.3. Model of Road Surface Roughness

The Power Spectral Density (PSD) functions for highway surface roughness have been developed by Dodds and Robson [7] and modified by Wang and Huang [53, 58]. They are shown as:

$$s(\phi) = A_r \left(\frac{\phi}{\phi} \right)^{-2} \qquad 3\text{-}1$$

where: S(¢) = PSD (m^2/cycle/m)

ϕ = wave number (cycle/m)

A_r = roughness coefficient (m^s/cycle)

ϕ_o = discontinuity frequency = 1/(27r) (cycle/in)

The detail of the procedure for the road surface roughness generation has been discussed by Wang and Huang [53]. In this study, the values of 5x 10^{-6}, 20x 10^{-6}, 80x 10^{-6}, and 256x $10^{'6}$ m^3/cycle were used according to International Organization for Standardization (ISO) specifications [7] as the roughness coefficient A, for the classes of very good, good, average, and poor roads, respectively. The sample length was taken as 256 rn (839.9 ft) and 2048 (2")

data points were generated for this distance. The average vertical highway surface profiles from ten simulations are shown in Figs. 3-3 to 3-10 for very good, good, average, and poor roads, respectively.

3.4. Dynamic Analytical Procedure

The fourth-order Runge-Kutta Integration scheme [19, 53, 54] was used to solve the equations of motion of the vehicle. The equations of bridge were determined by Newmark method [2]. The main procedure for dynamic analysis of the bridges is demonstrated in Fig. 3-11.

3.5. Description of Analytic Bridge

In order to obtain more general dynamic characteristics of box girder bridges, a prestressed concrete box girder bridge presented in Ishac and Smith [25] is chosen in this study and shown' in Fig. 3-12. The box girder bridge has a span length of 45.72 m (150 ft.) and roadway width of 9.144 m (30 ft). The bridge is simply supported and has diaphragms at both ends with distortional rigidity of 4.763 kN-m x 10'. The density of the box girder is 2570 kg/m^3. The effect of parapets is neglected in the analysis.

3.6. Characteristics of Free Vibration

The first six frequencies for four different cases of the analytic bridge are listed in Table

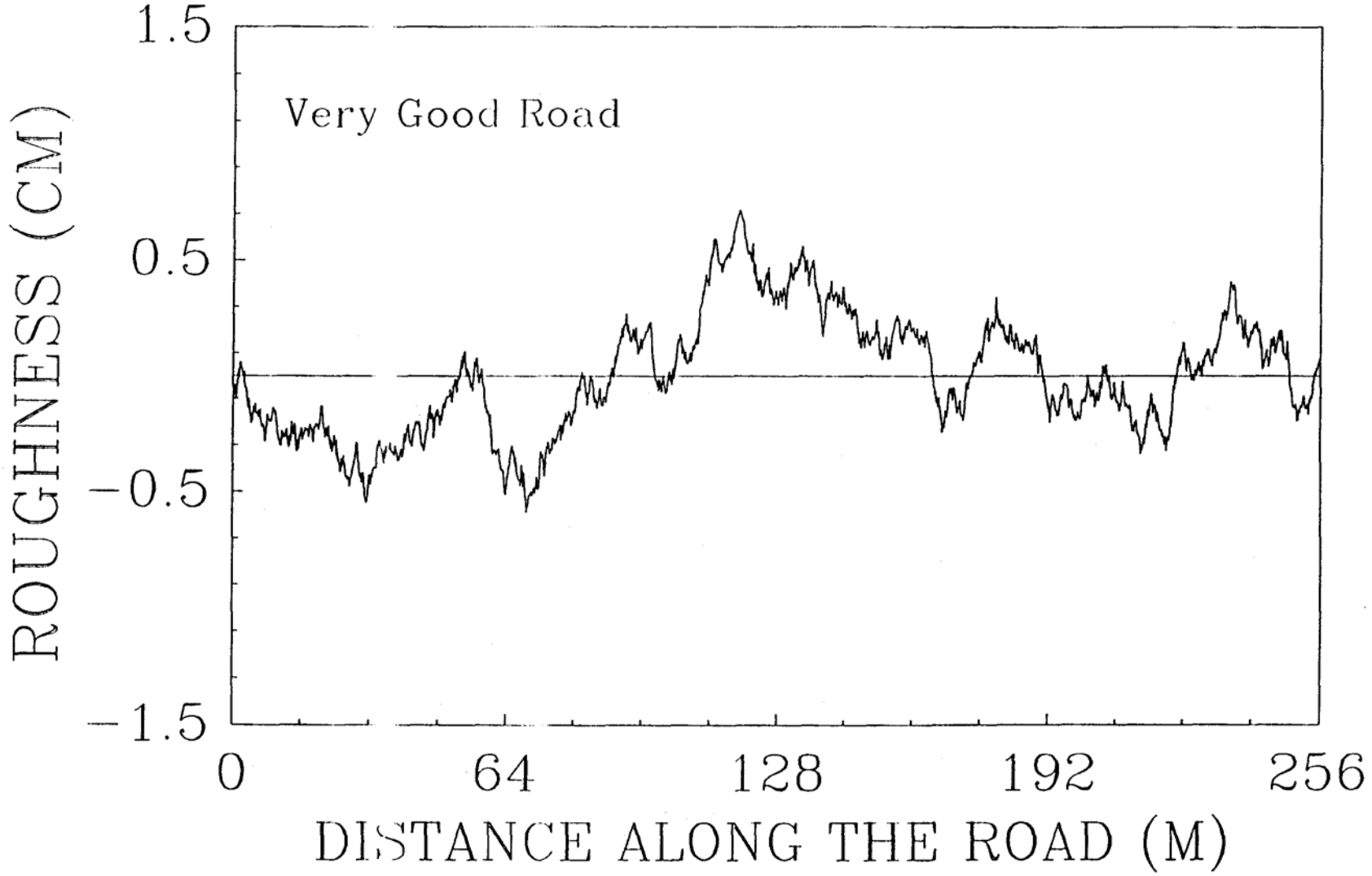

Fig. 3-3. Right Line of Vertical Highway Surface Profile in a Very Good Road

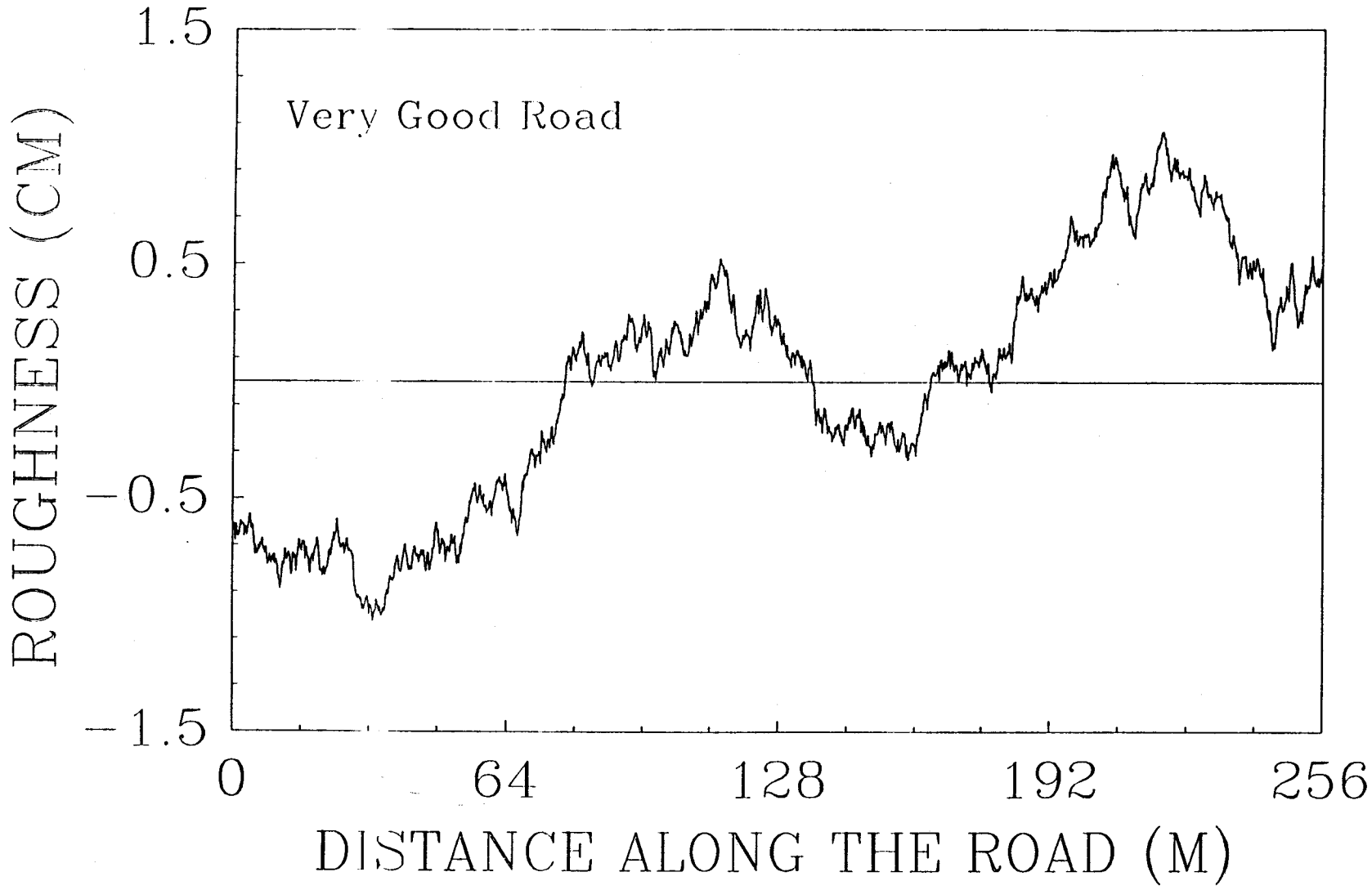

Fig. 3-4. Left Line of Vertical Highway Surface Profile in a Very Good Road

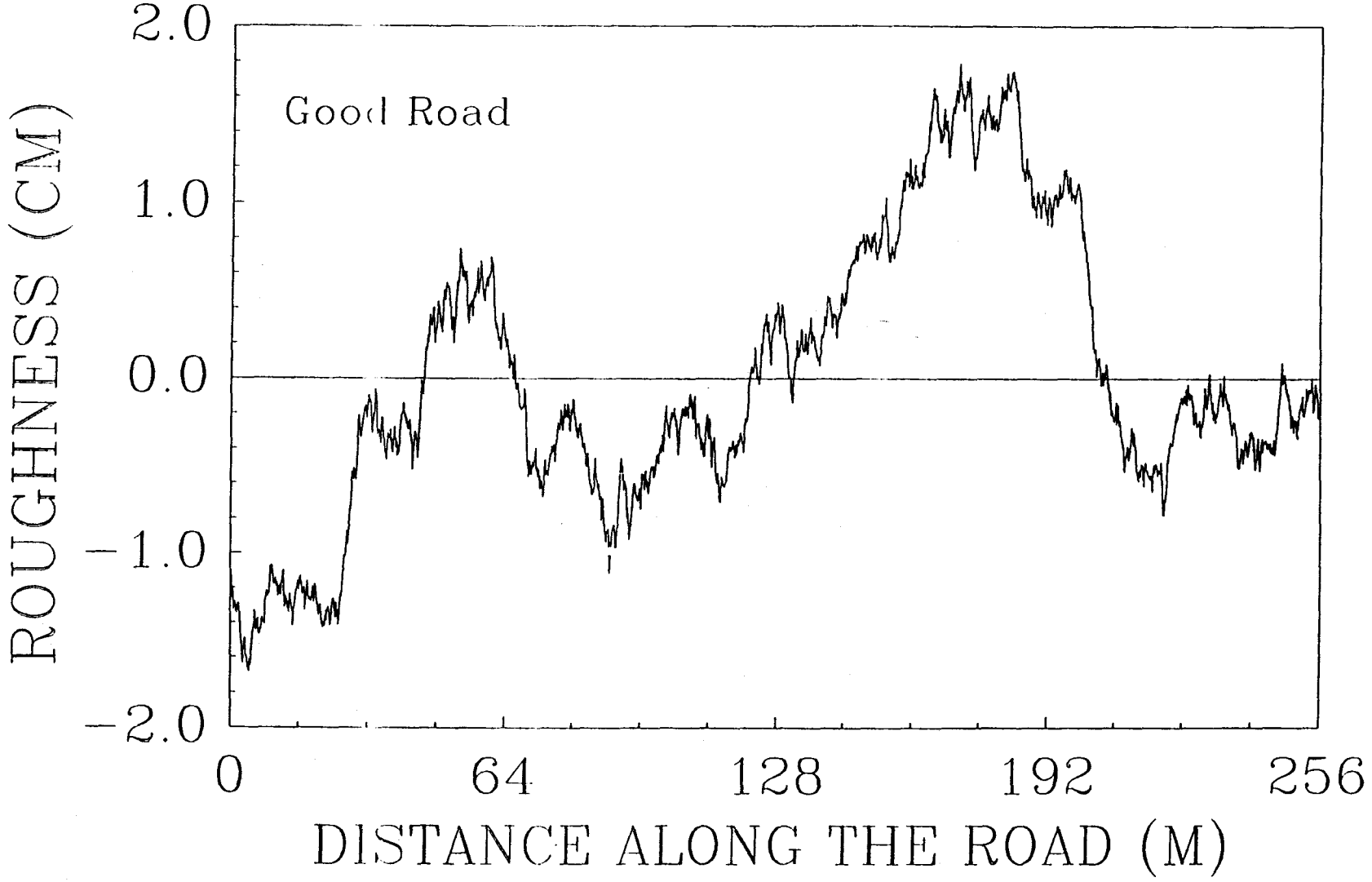

Fig. 3-5. Right Line of Vertical Highway Surface Profile in a Good Road

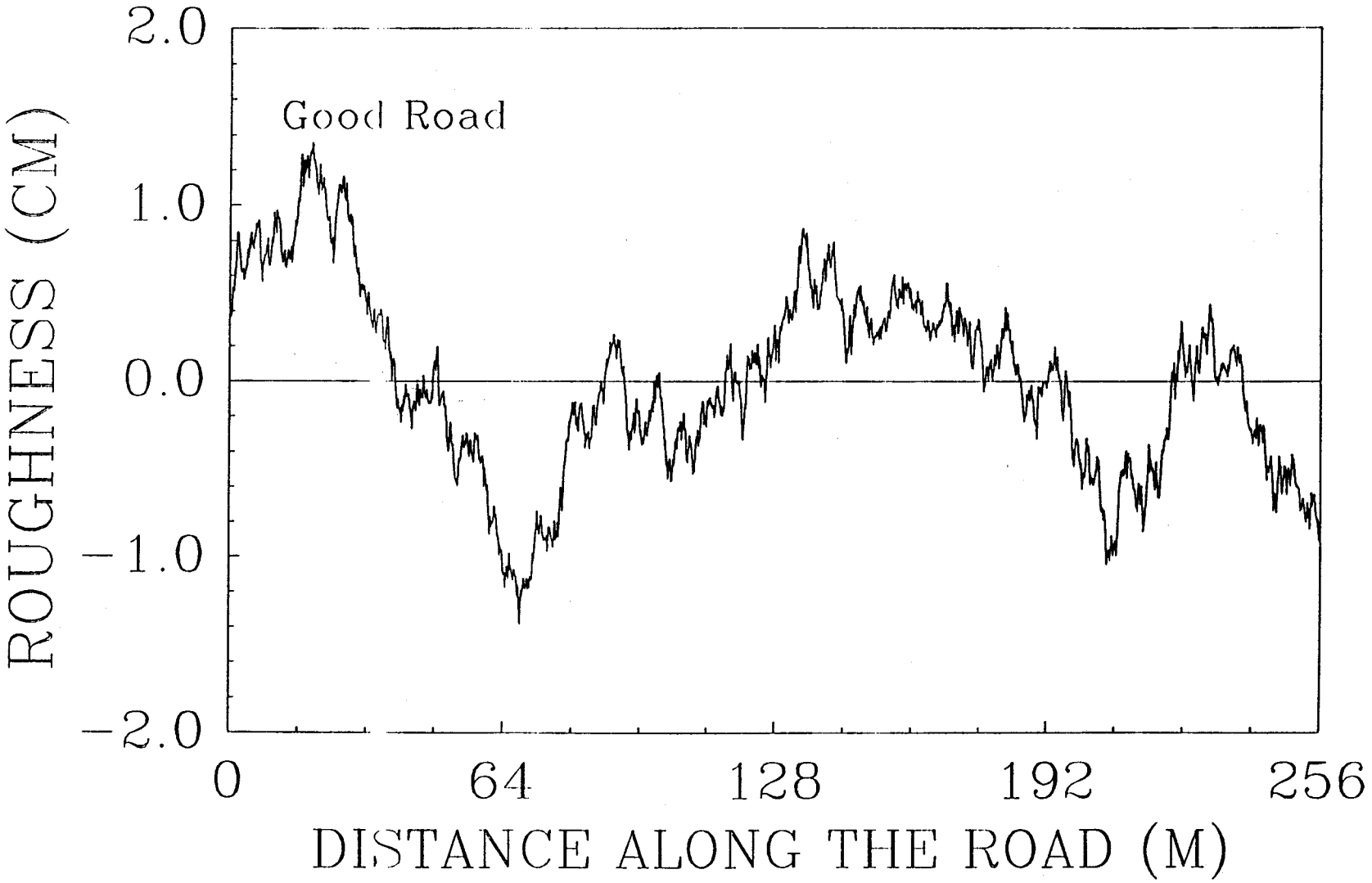

Fig. 3-6. Left Line of Vertical Highway Surface Profile in a Good Road

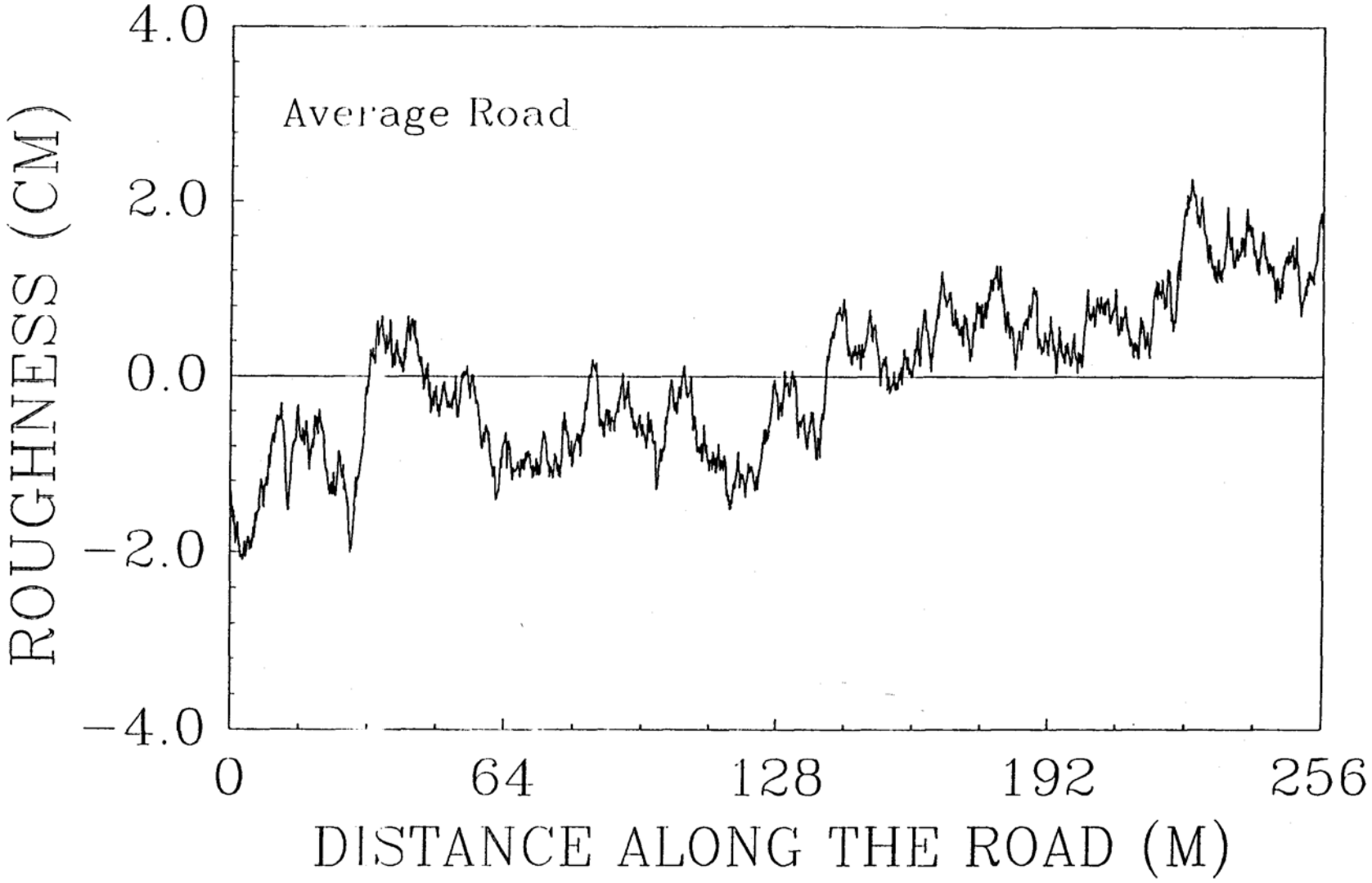

Fig. 3-7. Right Line of Vertical Highway Surface Profile in an Average Road

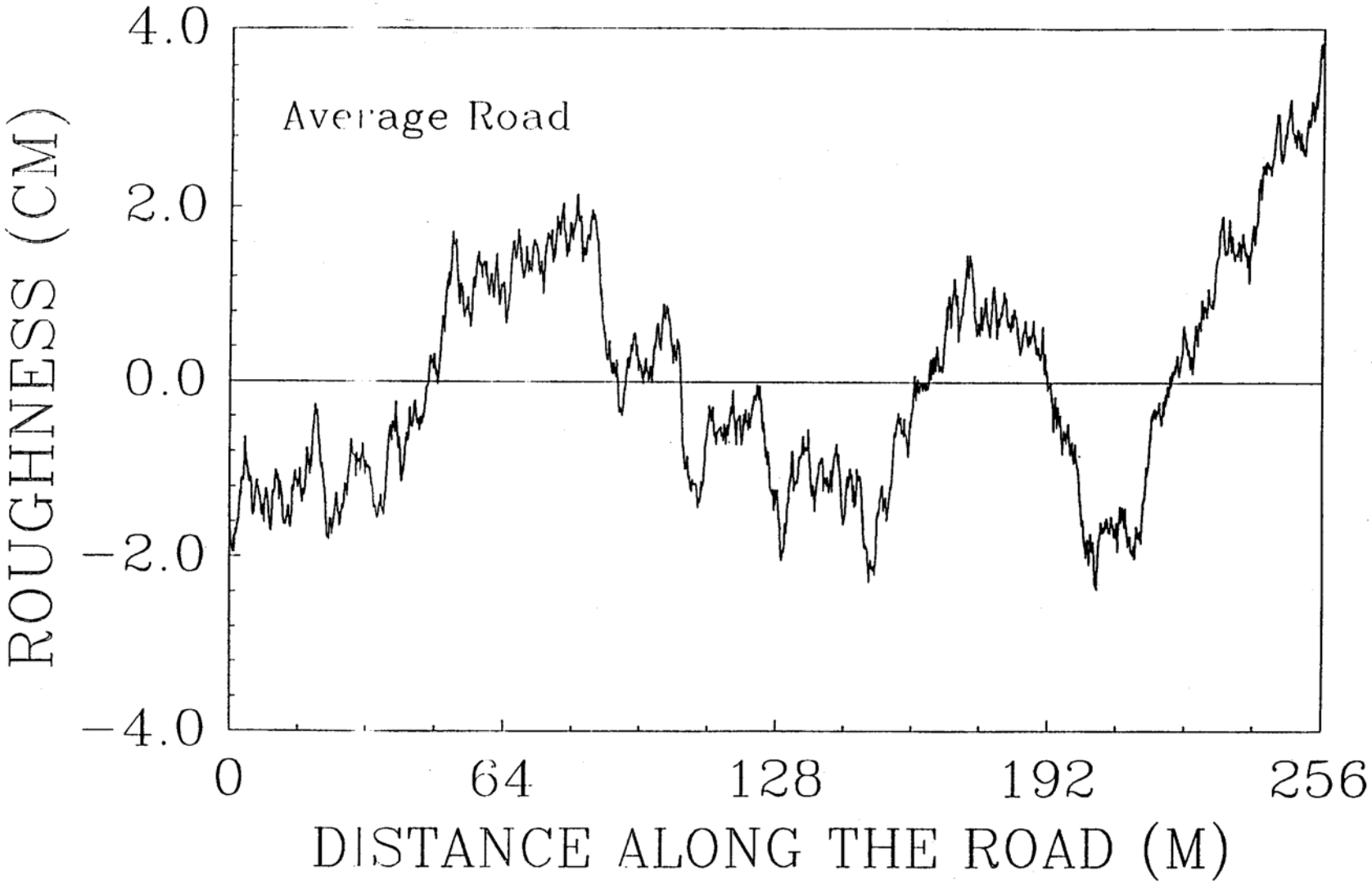

Fig. 3-8. Left Line of Vertical Highway Surface Profile in an Average Road

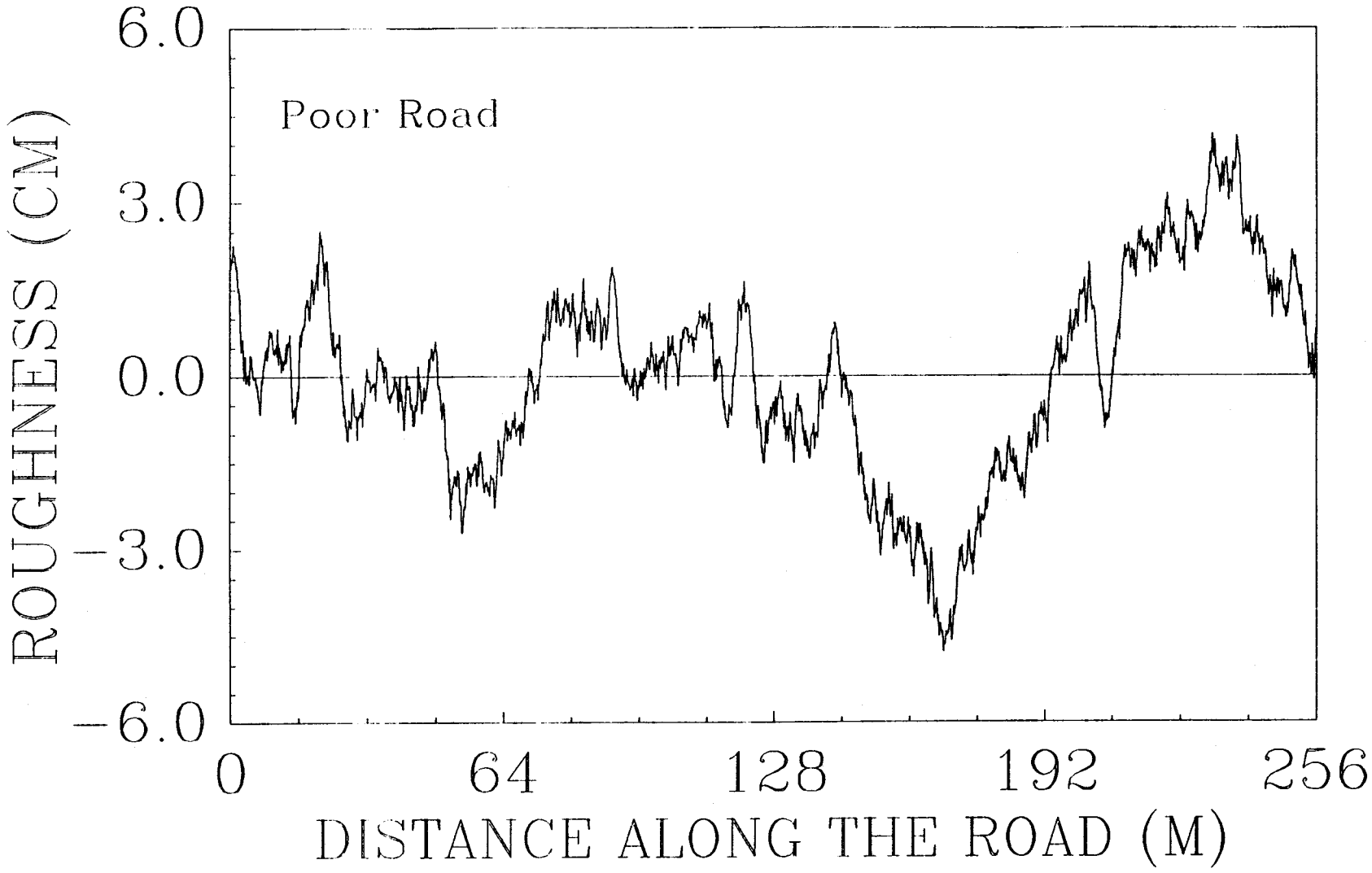

Fig. 3-9. Right Line of Vertical Highway Surface Profile in a Poor Road

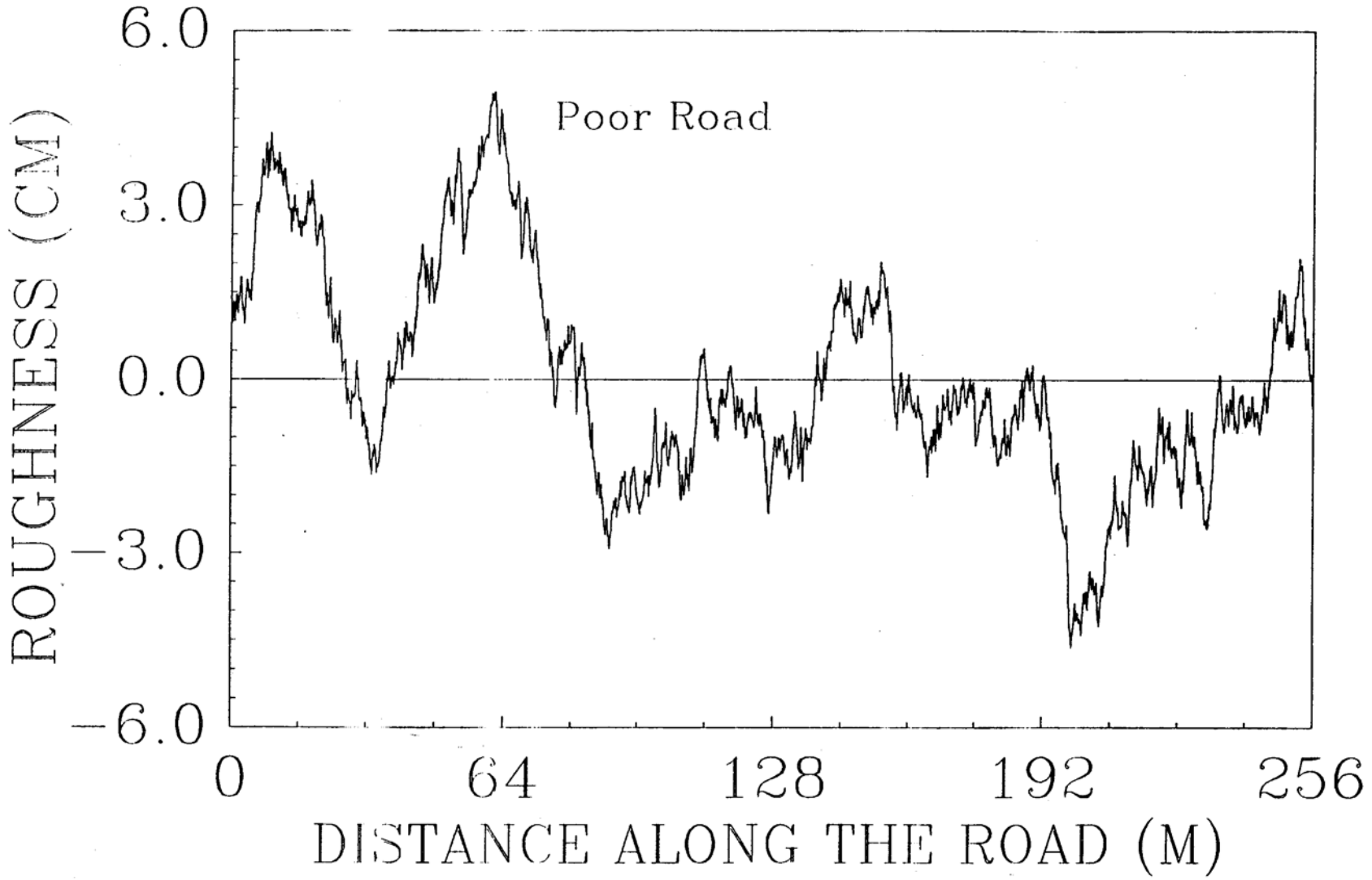

Fig. 3-10. Left Line of Vertical Highway Surface Profile in a Poor Road

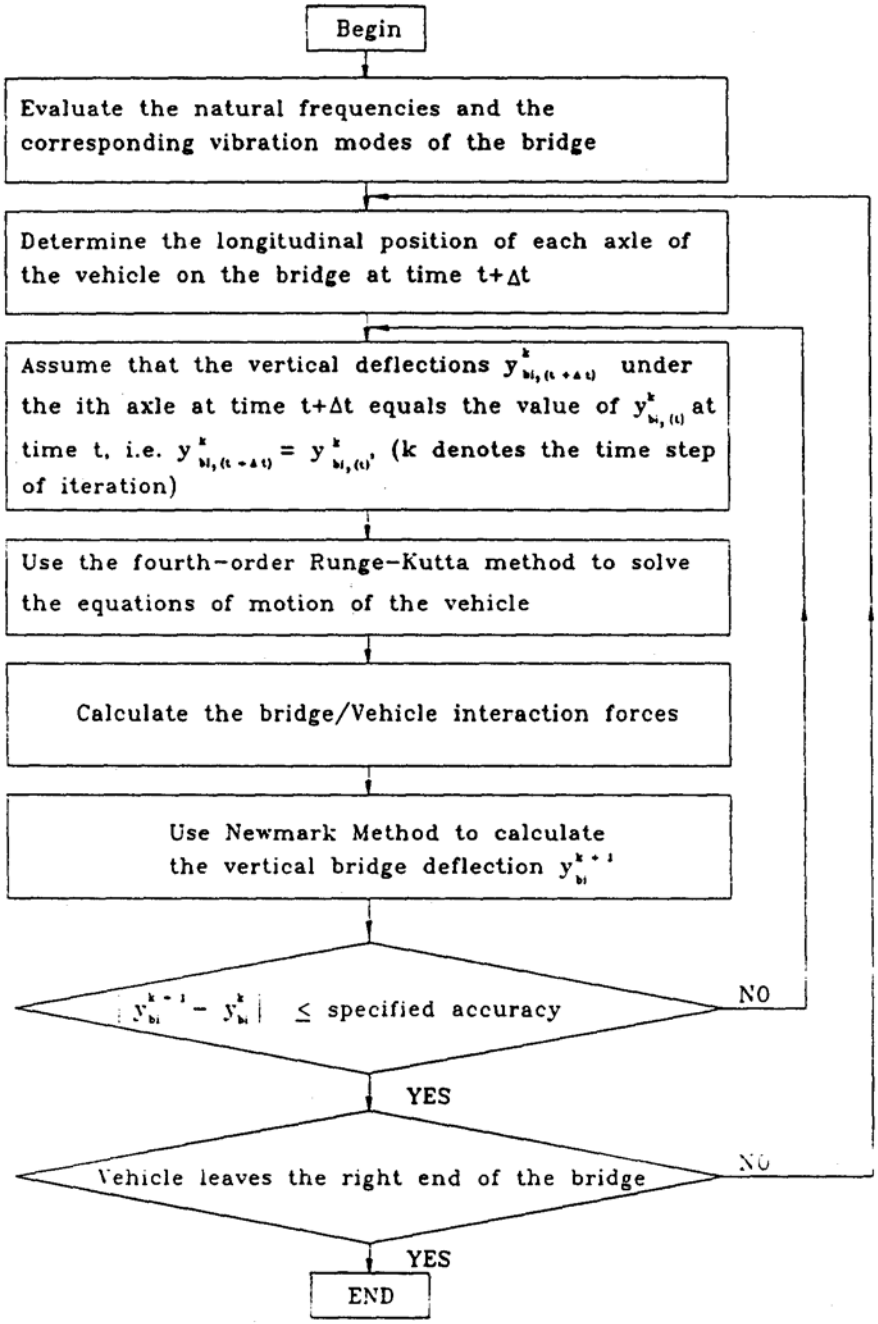

Fig. 3-11. Overall Computational Scheme

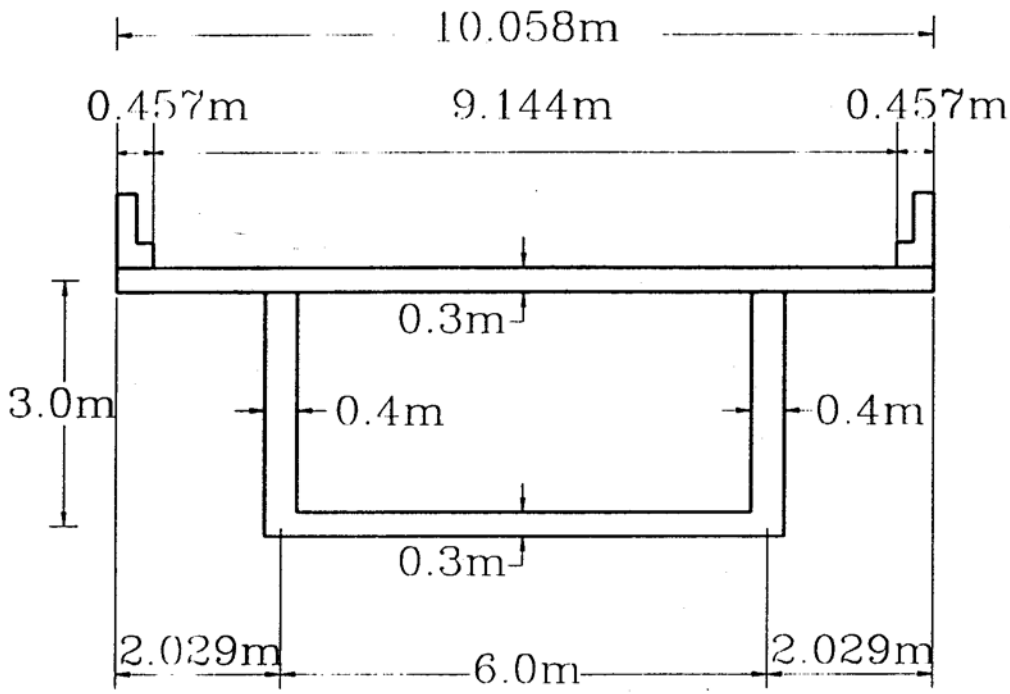

Fig. 3-12. Cross-Section of Analytical Simply Supported Bridge

3-1. In case I, the bridge is assumed to have two rigid diaphragms at both end supports. Case II is the original design with two deformable end diaphragms. In Case III, the bridge is assumed to be added a mid-span diaphragm with the same rigidity as the end diaphragms. No diaphragm is considered in Case IV. From Table 3-1, it can be seen that frequencies have little difference among Cases I, II, and III. However, the frequencies of lateral bending and torsion decrease greatly if the bridge has no end diaphragm. Figs. 3-13 to 3-42 shows the first fifteen vibration modes of the bridges for Cases I and IV respectively. An examination of these figures shows that lateral vibration (u) and torsional ones (8,6) are always coupled together and that the lowest frequency is the vertical bending vibration mode. Figs. 3-29 to 3-42 indicates 'that end diap

3.7. Forced Vibration Analysis

It is assumed that the bridge has damping characteristics that can be modeled as viscous. The damping matrix is assumed to be proportional to mass and stiffness and be made up of combinations of these [5]. One percent of damping is supposed for the first and second modes according to Ruhl [45] and Wang et al [57].The solutions of Eq.2-28 are obtained by the Newmark method. By trial, it is found that the time step of 0.0005 sec. can give very good accuracy for all kinds of dynamic responses. In order to get the initial displacements and velocities of vehicle DOF's when the vehicles entered the bridge, the vehicles were started the motion at a distance of 42.67 m (140 ft), i.e. five-car length) away from the left end of the bridge and continued moving until the entire vehicle cleared the right end of the bridge.All trucks have the same left and right road surface roughnesses. The same class of road surface

Table 3-1. Frequencies of

Case	No. of frequency					
	1	2	3	4	5	6
1	3.220	6.644	12.962	14.961	19.975	20.960
2	3.220	6.442	12.962	16.688	19.610	23.992
3	3.220	6.436	12.962	14.458	19.080	19.610
4	3.220	3.528	9.788	12.126	12.962	16.247

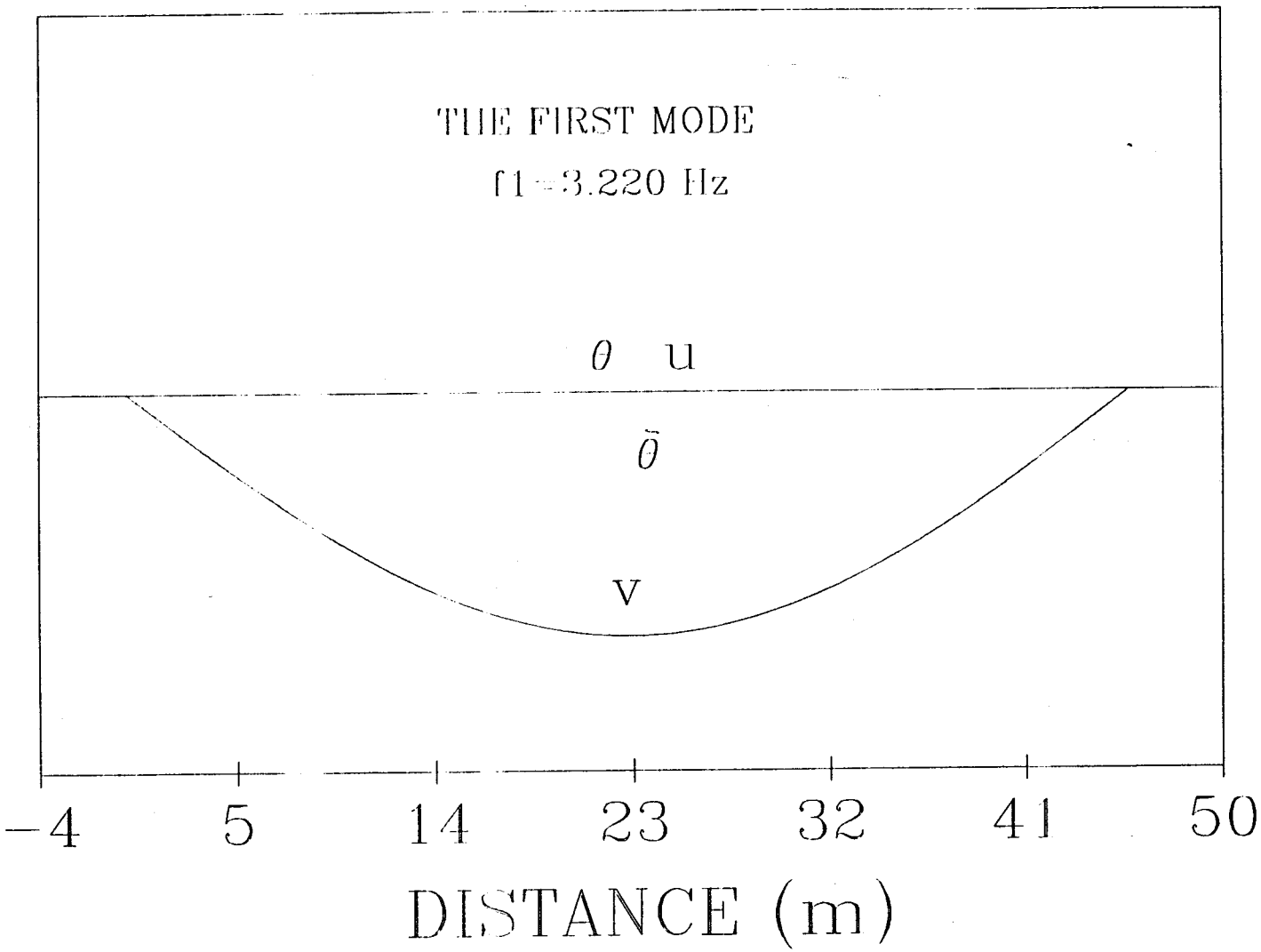

Fig. 3-13. The First Vibration Mode of Simply Supported Bridge

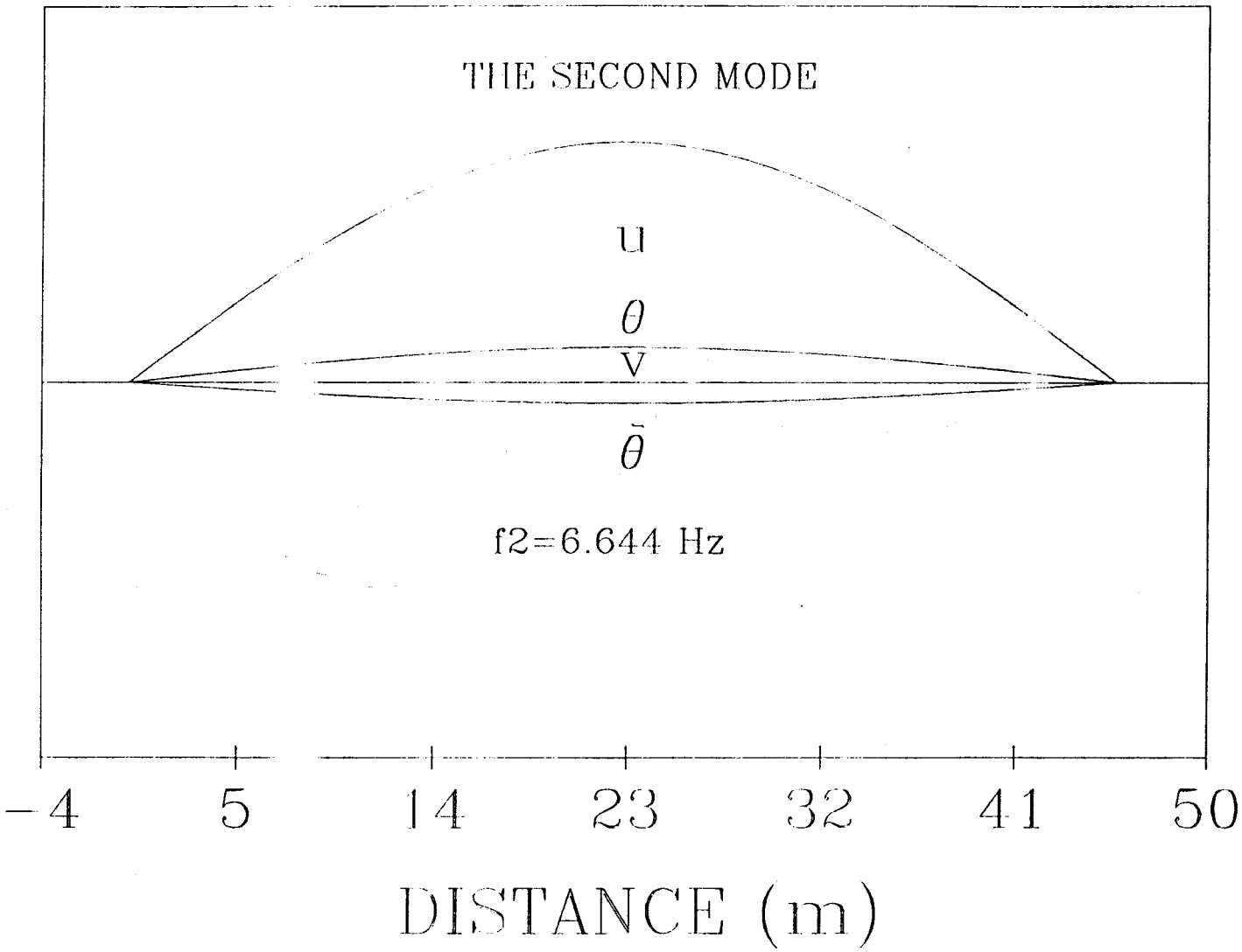

Fig. 3-14. The Second Vibration Mode of Simply Supported Bridge

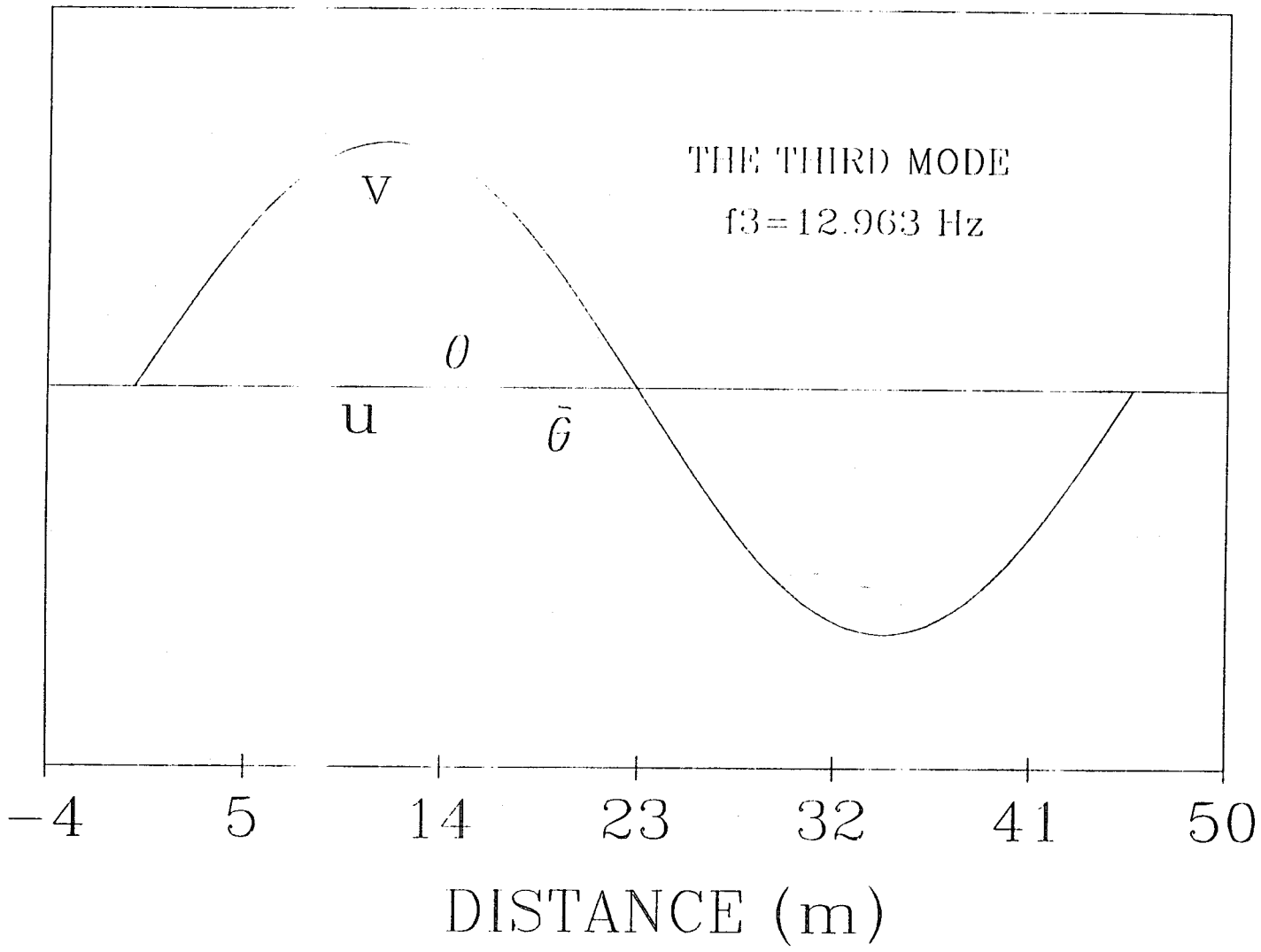

Fig. 3-15. The Third Vibration Mode of Simply Supported Bridge

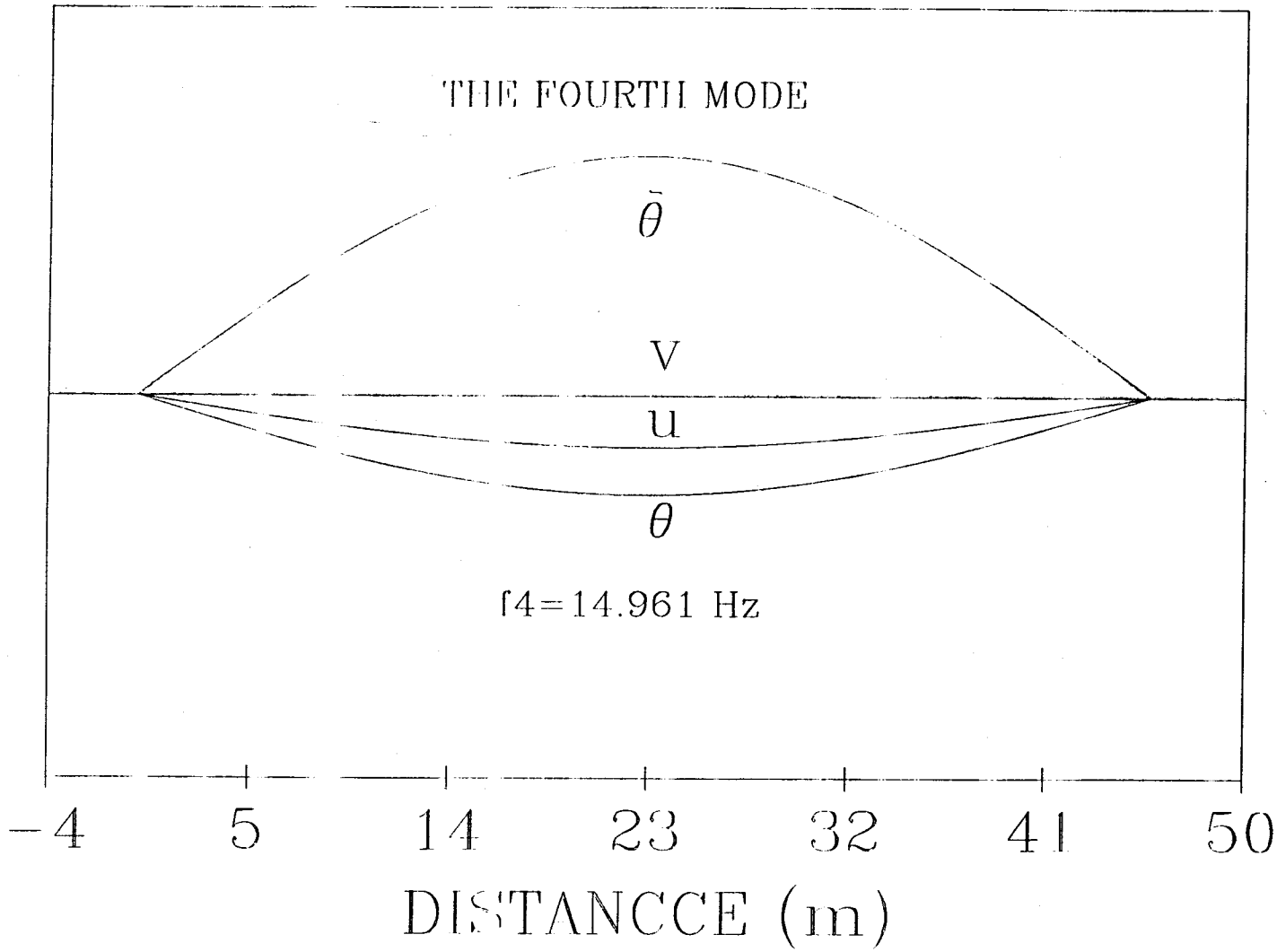

Fig. 3-16. The Fourth Vibration Mode of Simply Supported Bridge

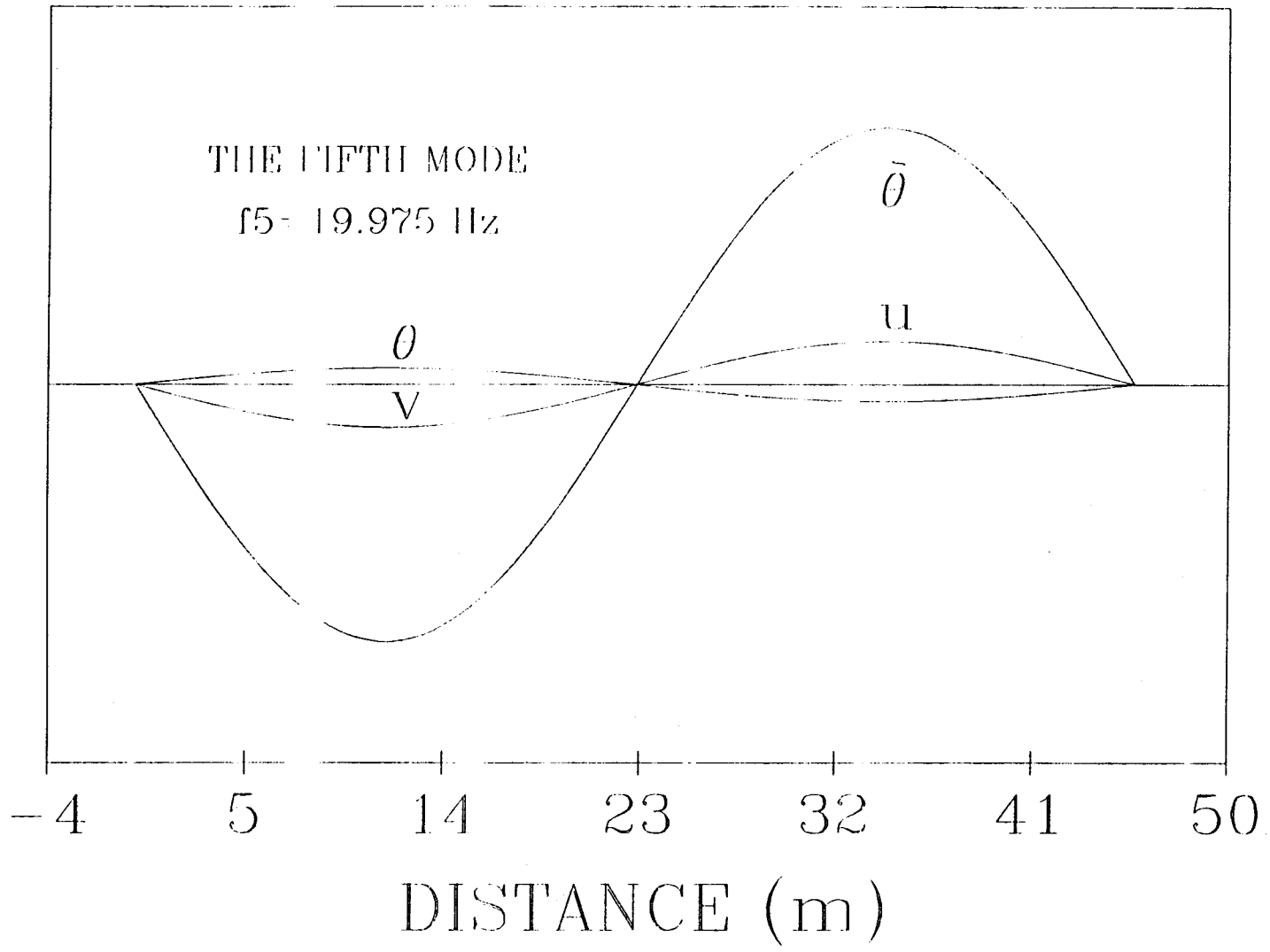

Fig. 3-17. The Fifth Vibration Mode of Simply Supported Bridge

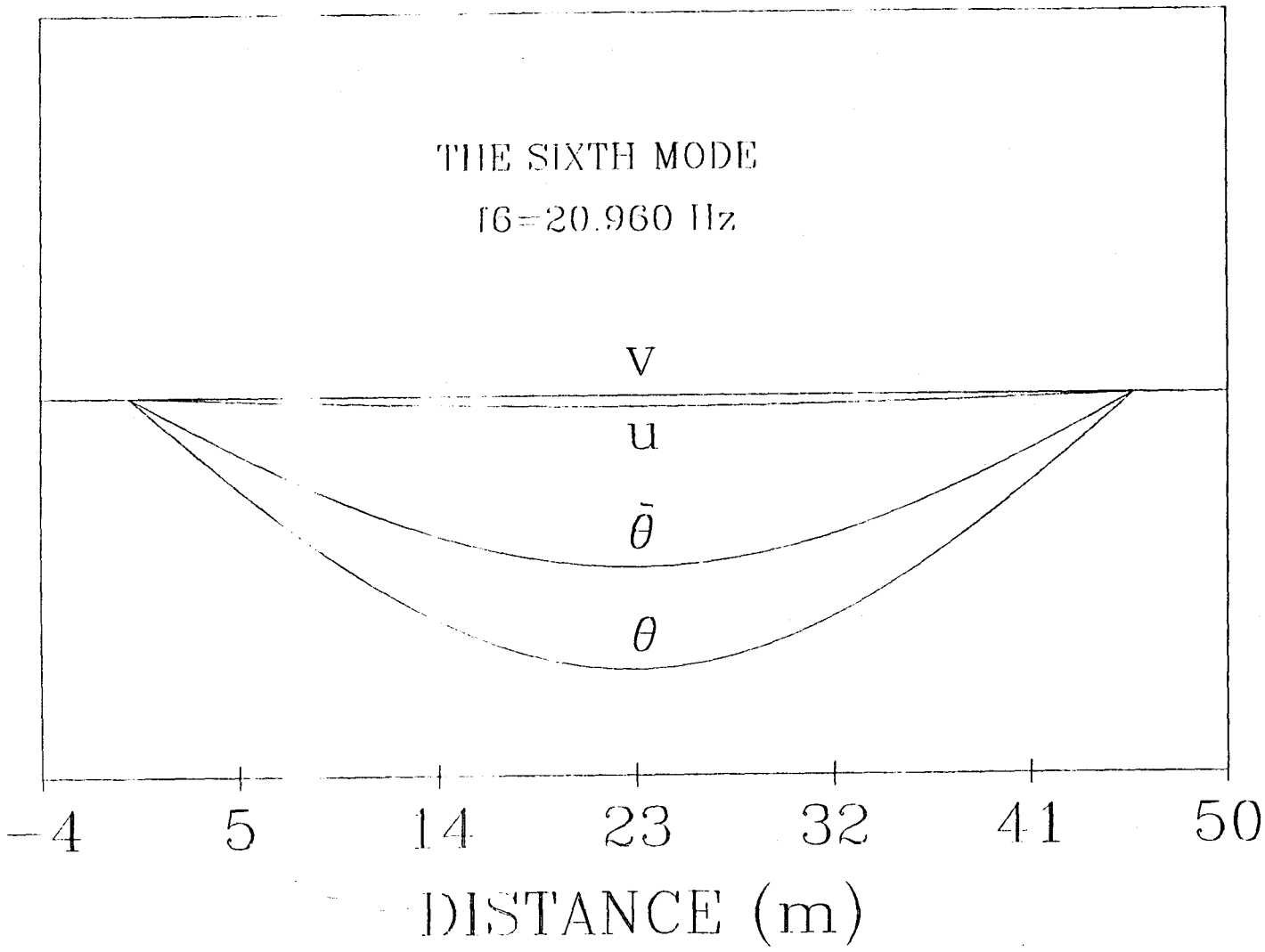

Fig. 3-18. The Sixth Vibration Mode of Simply Supported Bridge

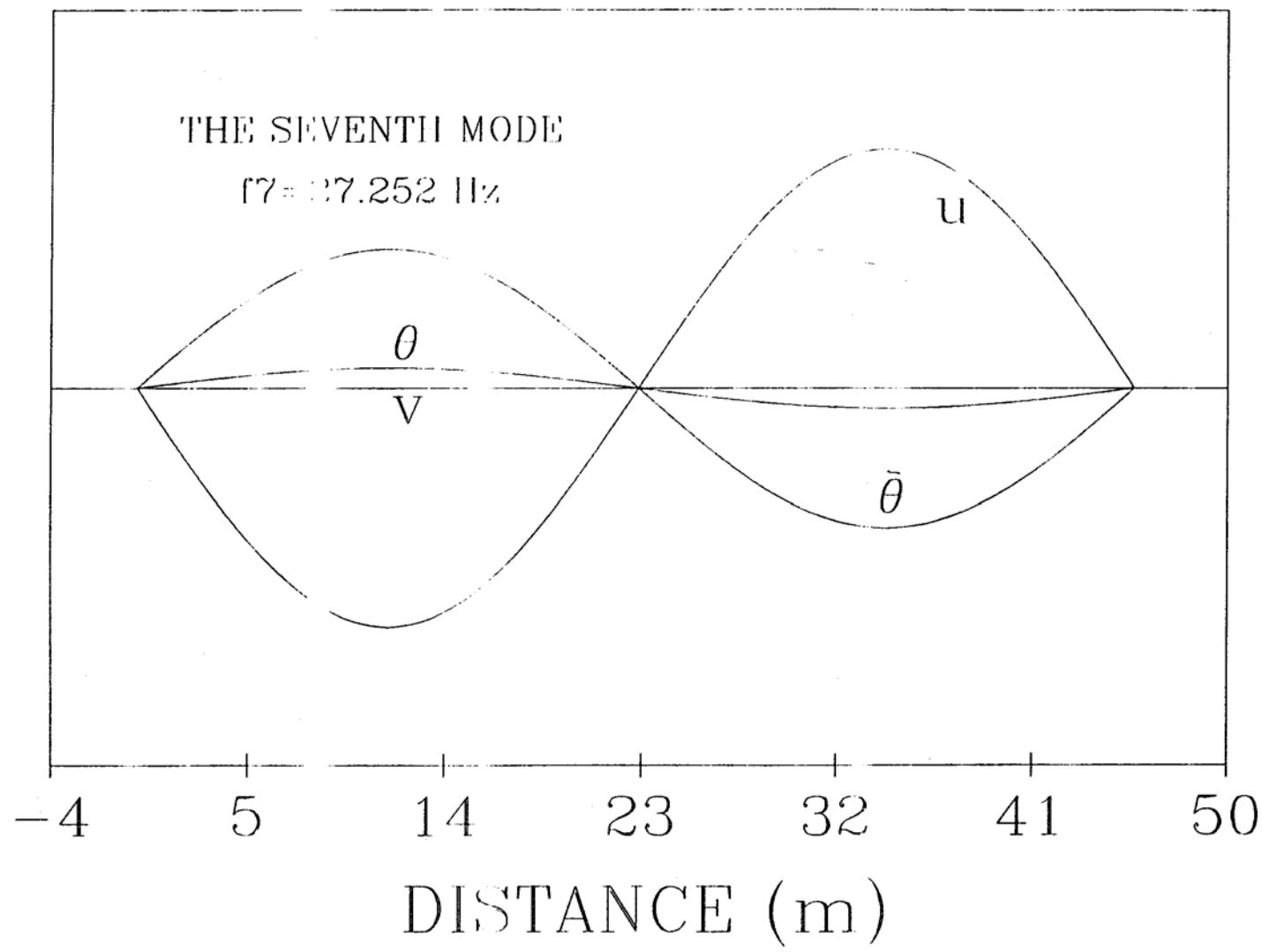

Fig. 3-19. The Seventh Vibration Mode of Simply Supported Bridge

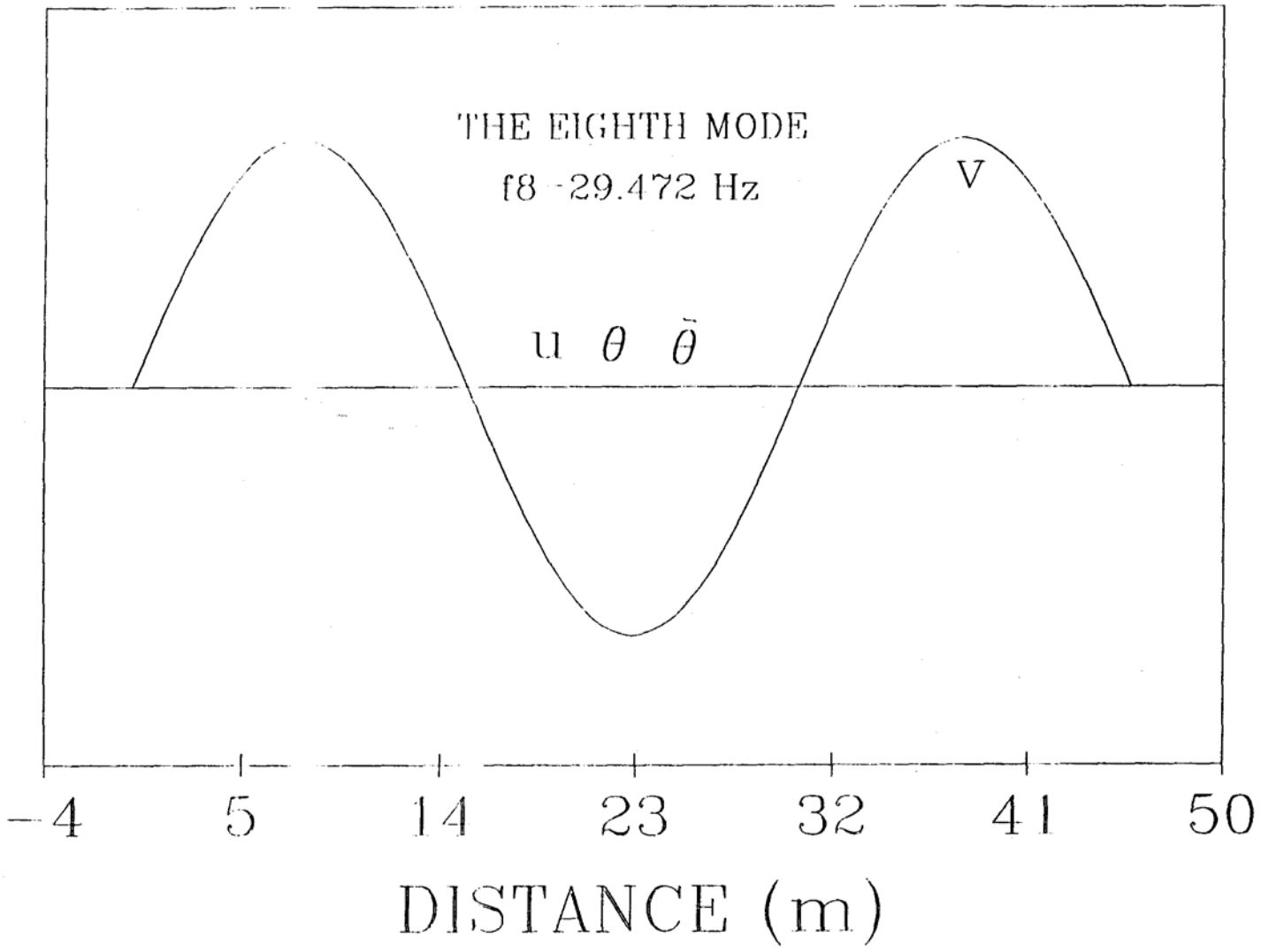

Fig. 3-20. The Eighth Vibration Mode of Simply Supported Bridge

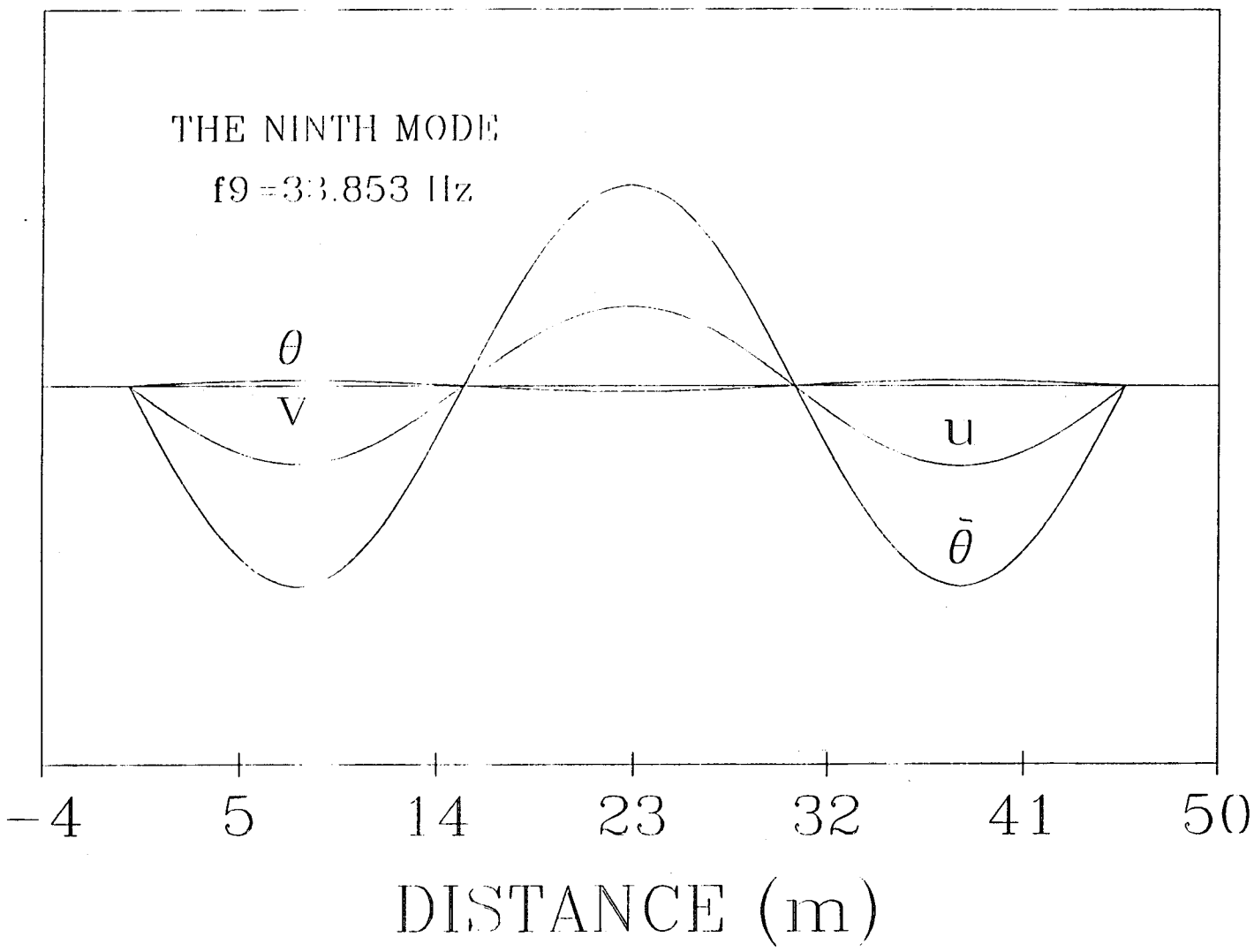

Fig. 3-21. The Ninth Vibration Mode of Simply Supported Bridge

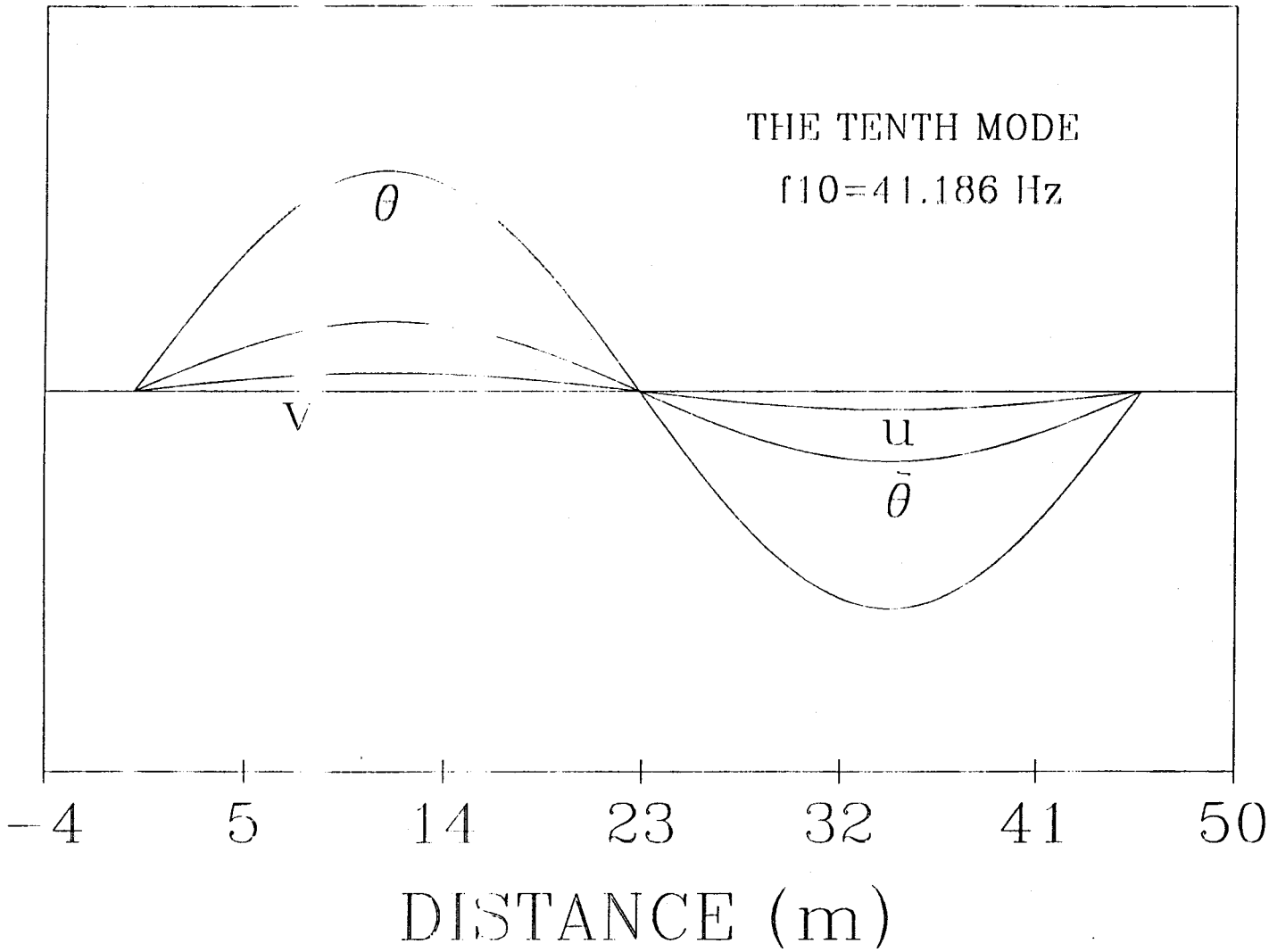
THE TENTH MODE
f10=41.186 Hz
θ
V
u
θ̃
−4
5
14
23
32
41
50
DISTANCE (m)

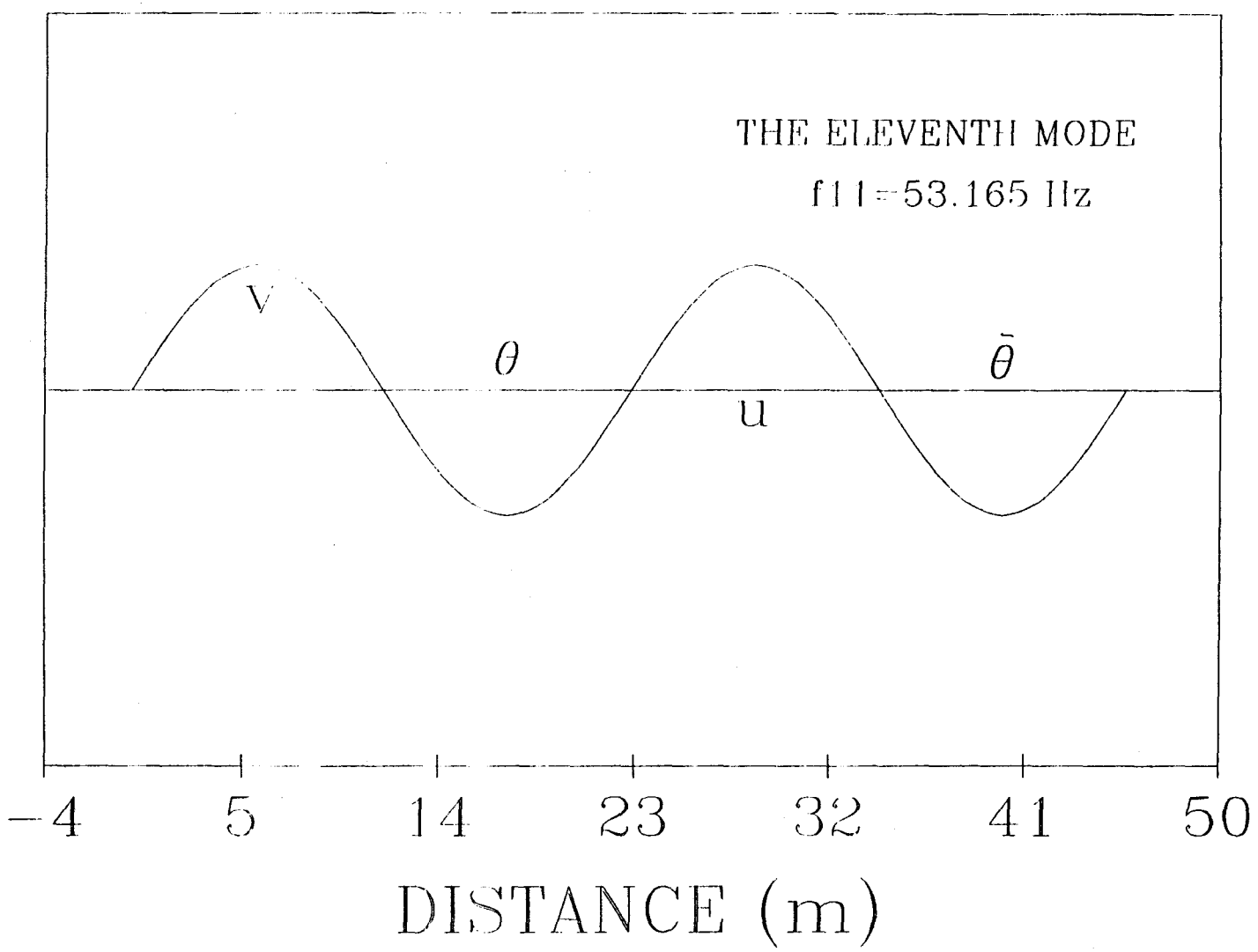

Fig. 3-23. The Eleventh Vibration Mode of Simply Supported Bridge

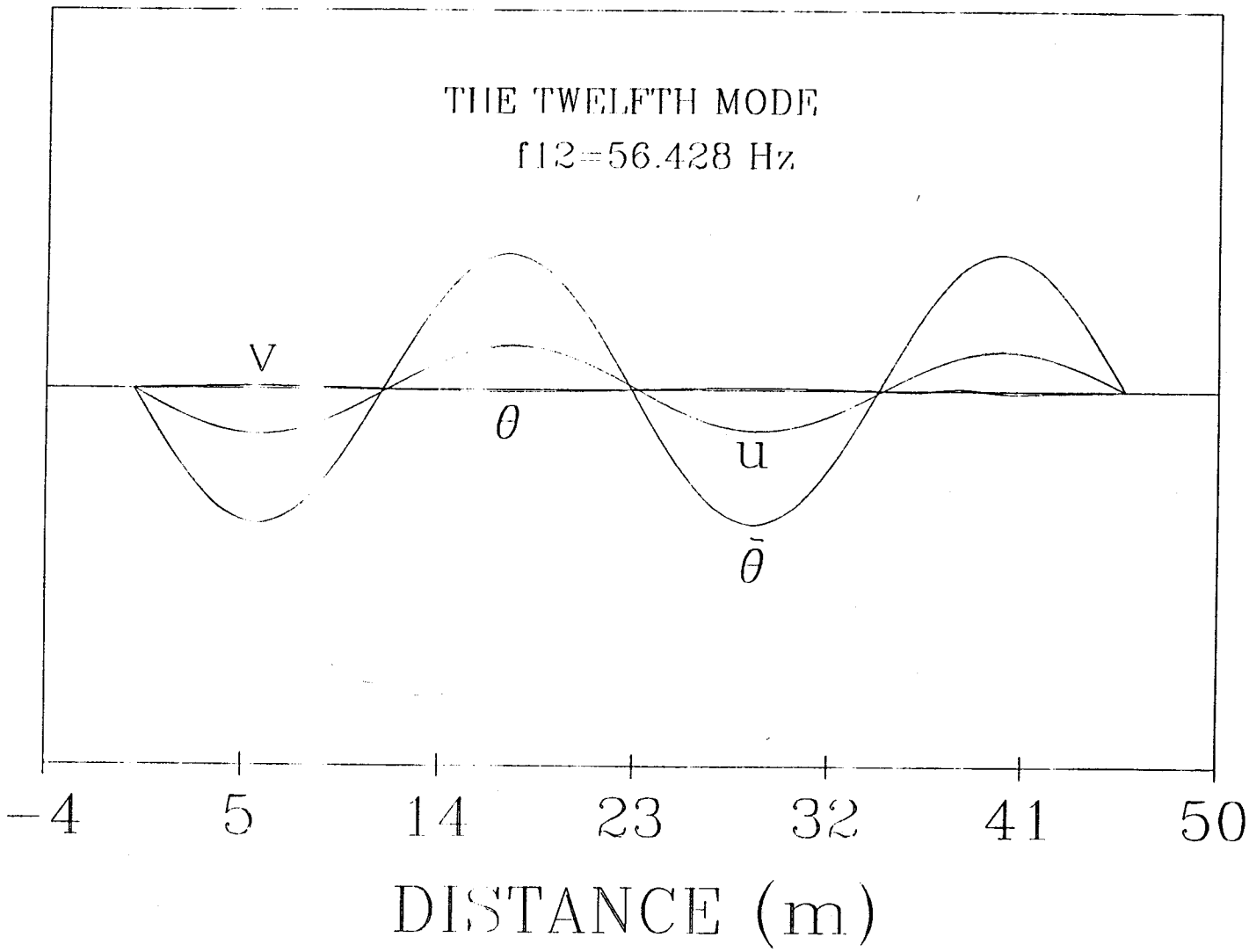

Fig. 3-24. The Twelfth Vibration Mode of Simply Supported Bridge

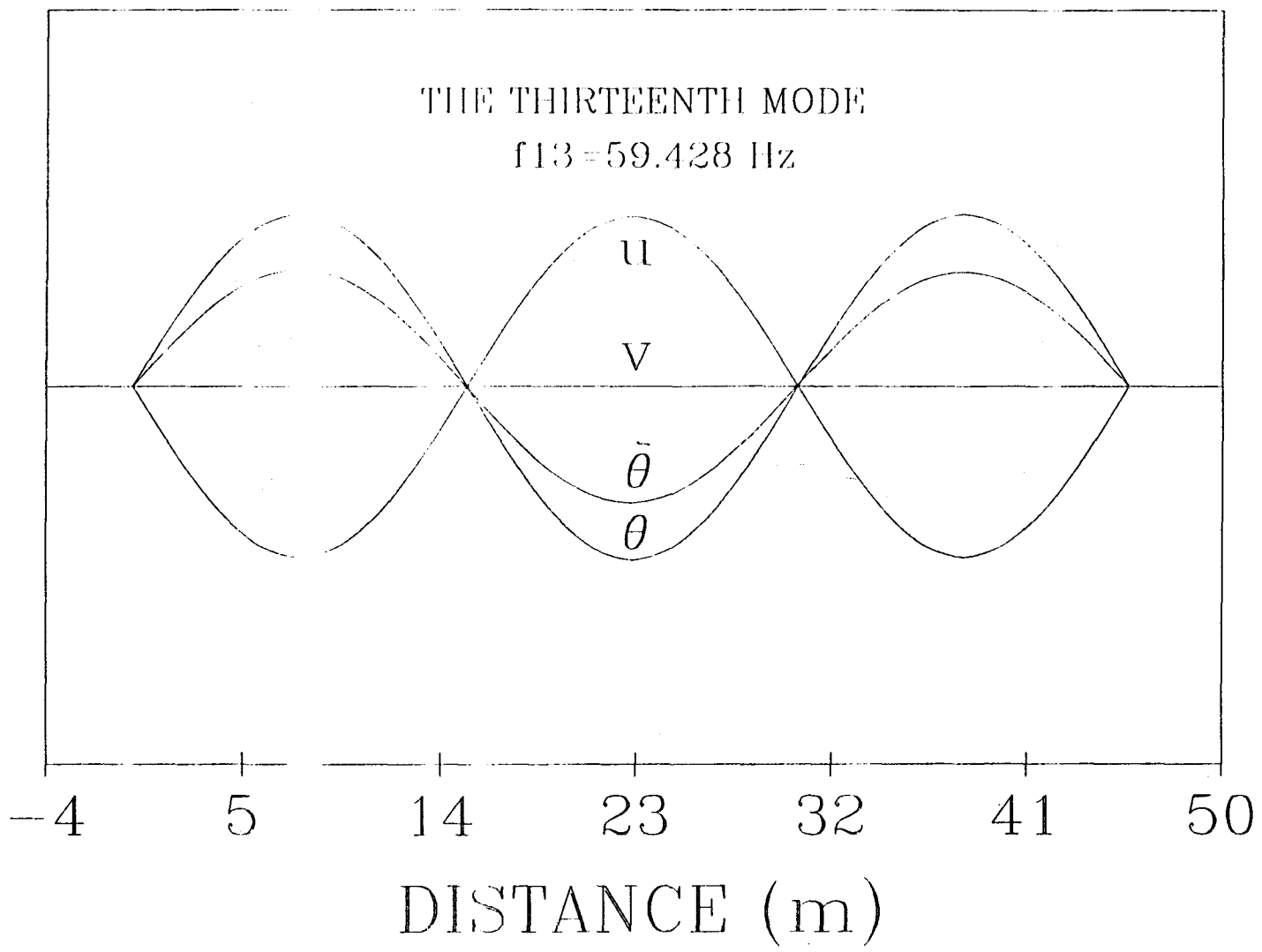

Fig. 3-25. The Thirteenth Vibration Mode of Simply Supported Bridge

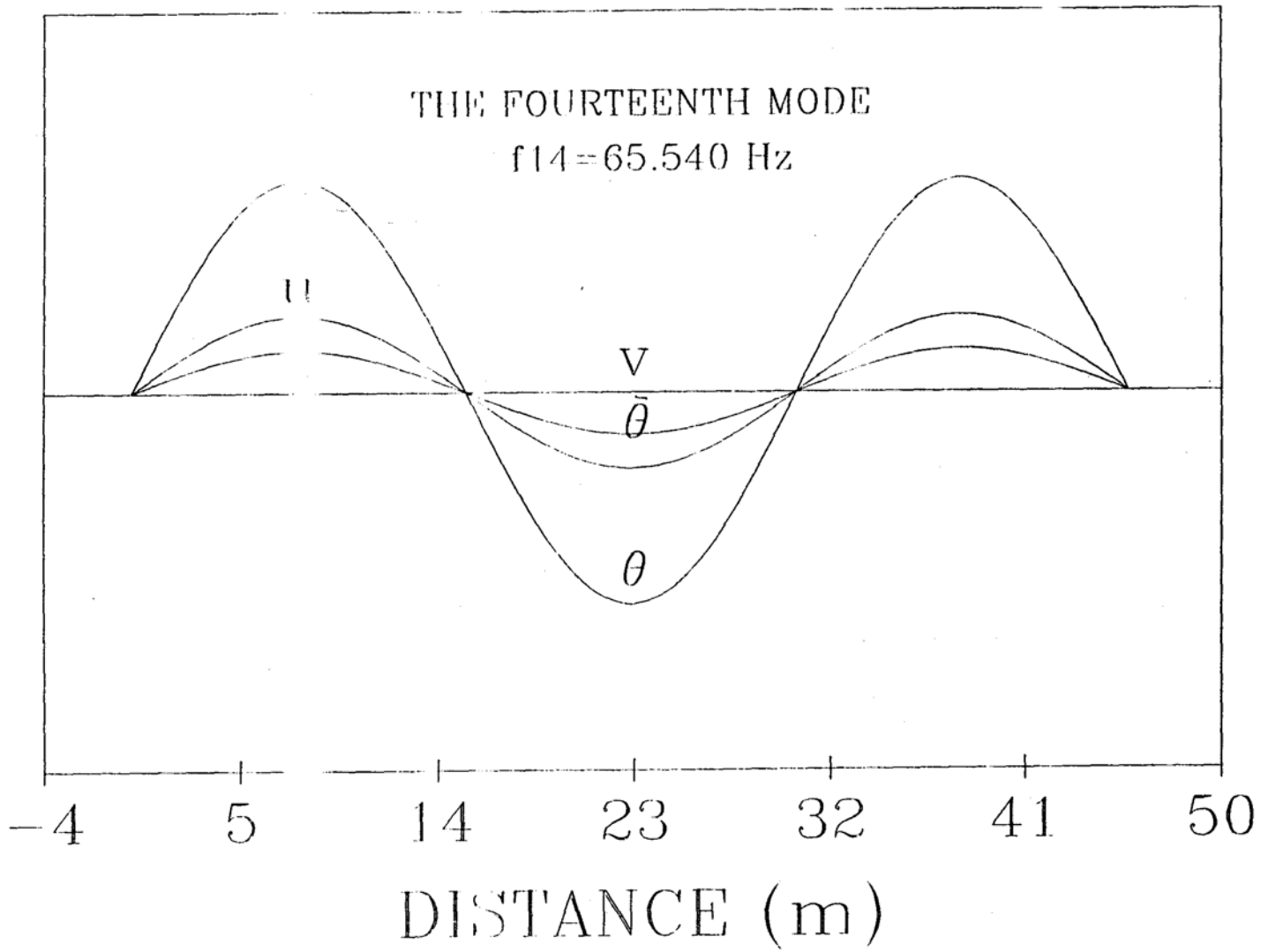

Fig. 3-26. The Fourteenth Vibration Mode of Simply Supported Bridge

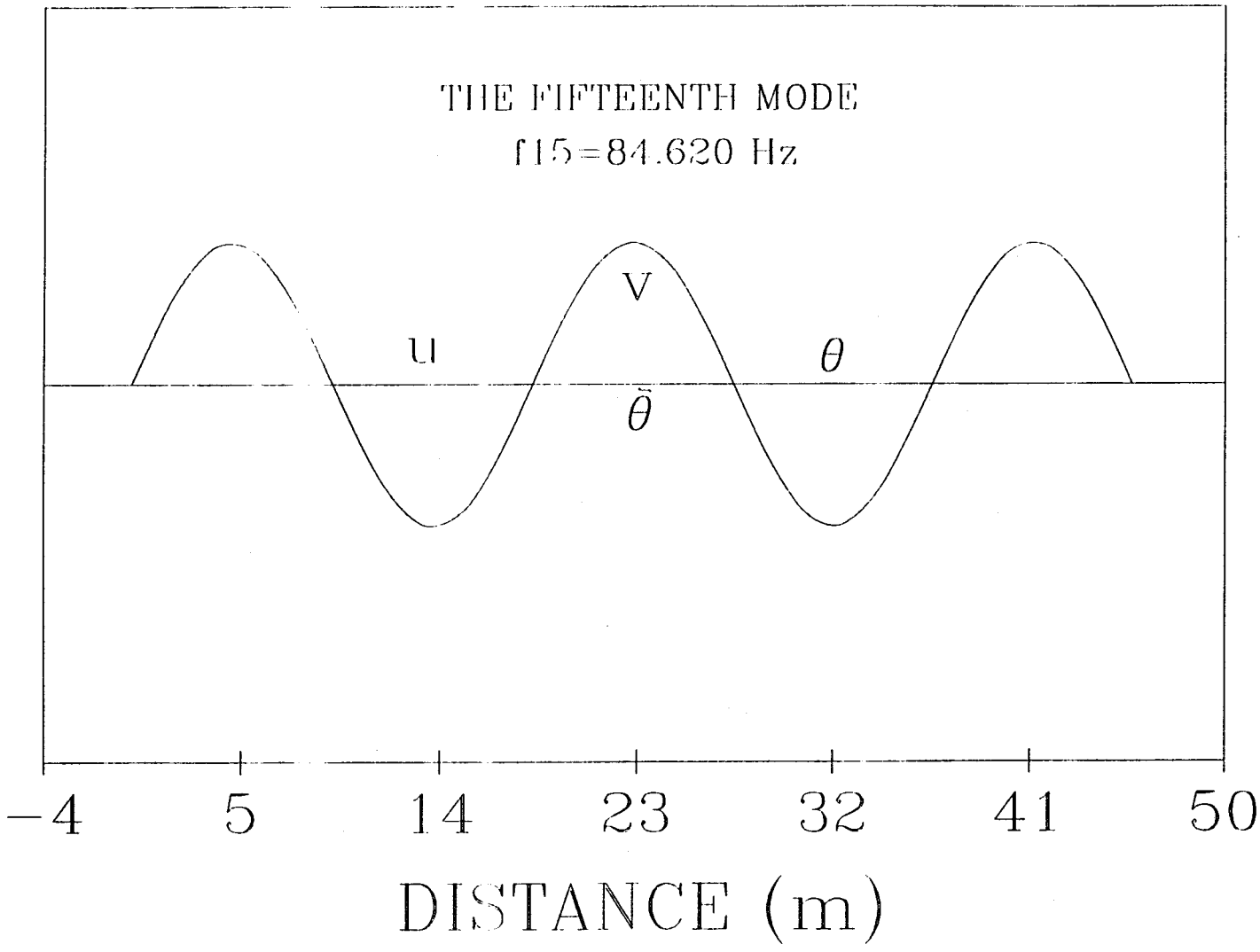

Fig. 3-27. The Fifteenth Vibration Mode of Simply Supported Bridge

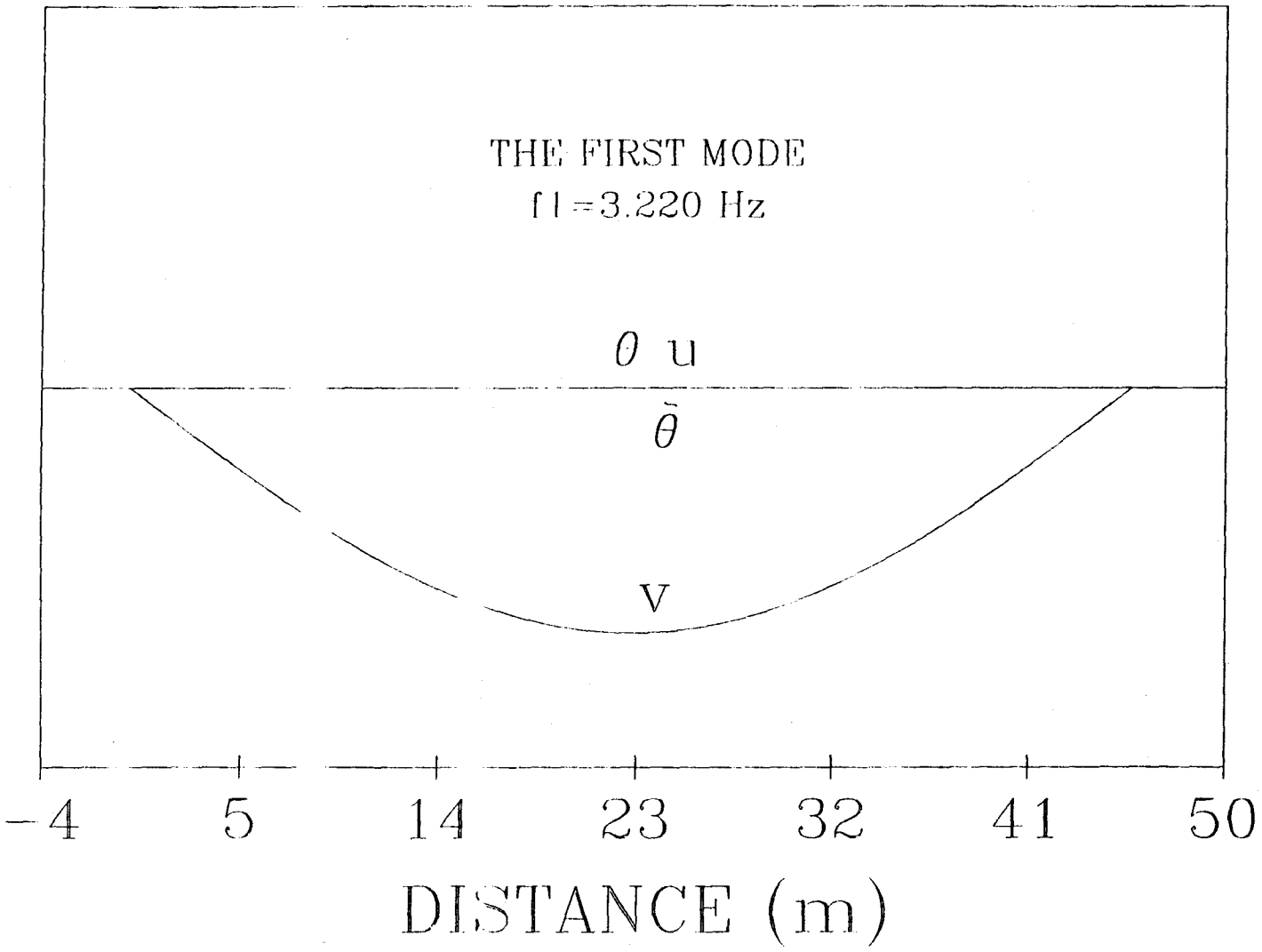

Fig. 3-28. The First Vibration Mode of Simply Supported Bridge without Diaphragm

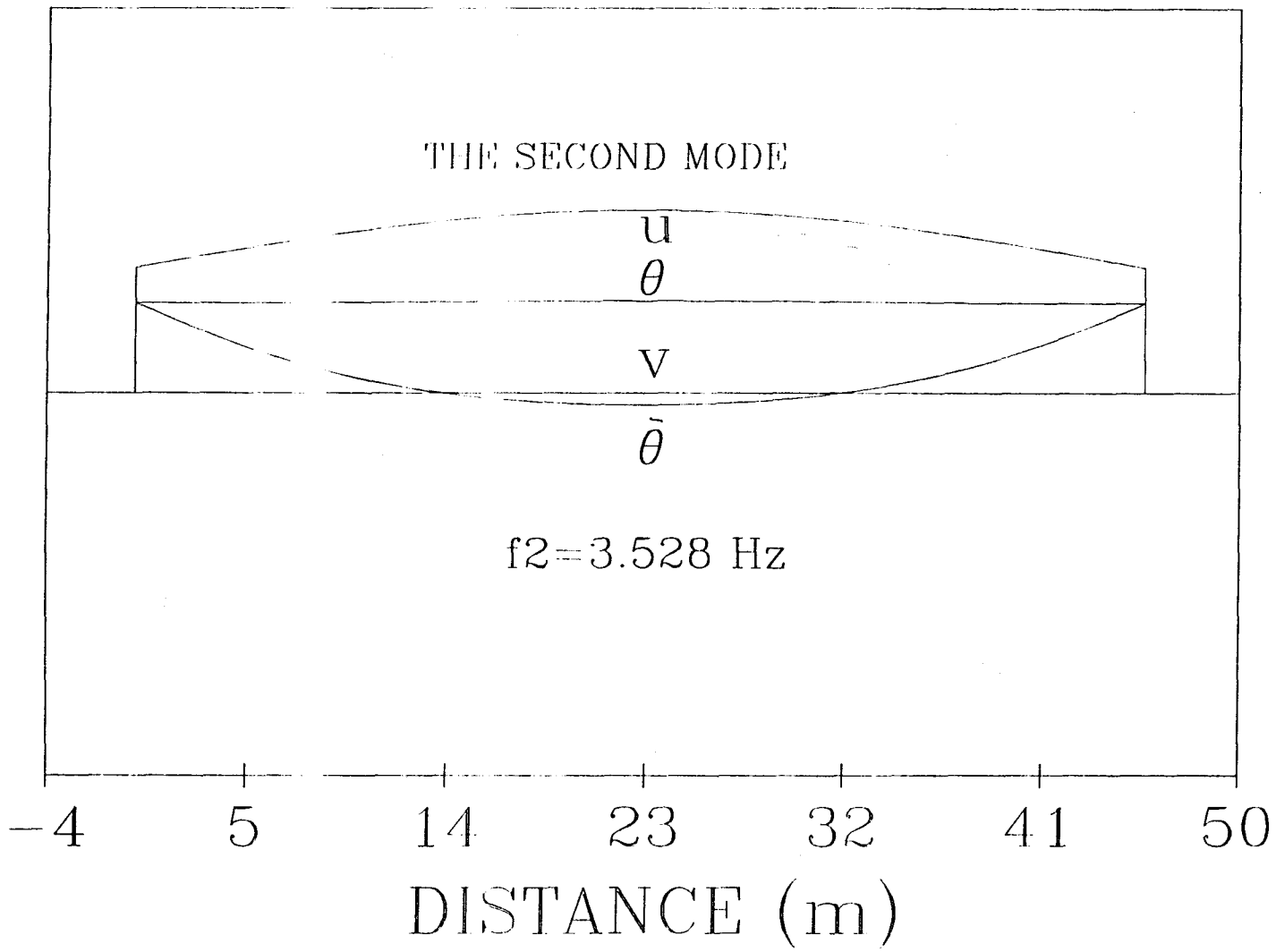

Fig. 3-29. The Second Vibration Mode of Simply Supported Bridge without Diaphragm

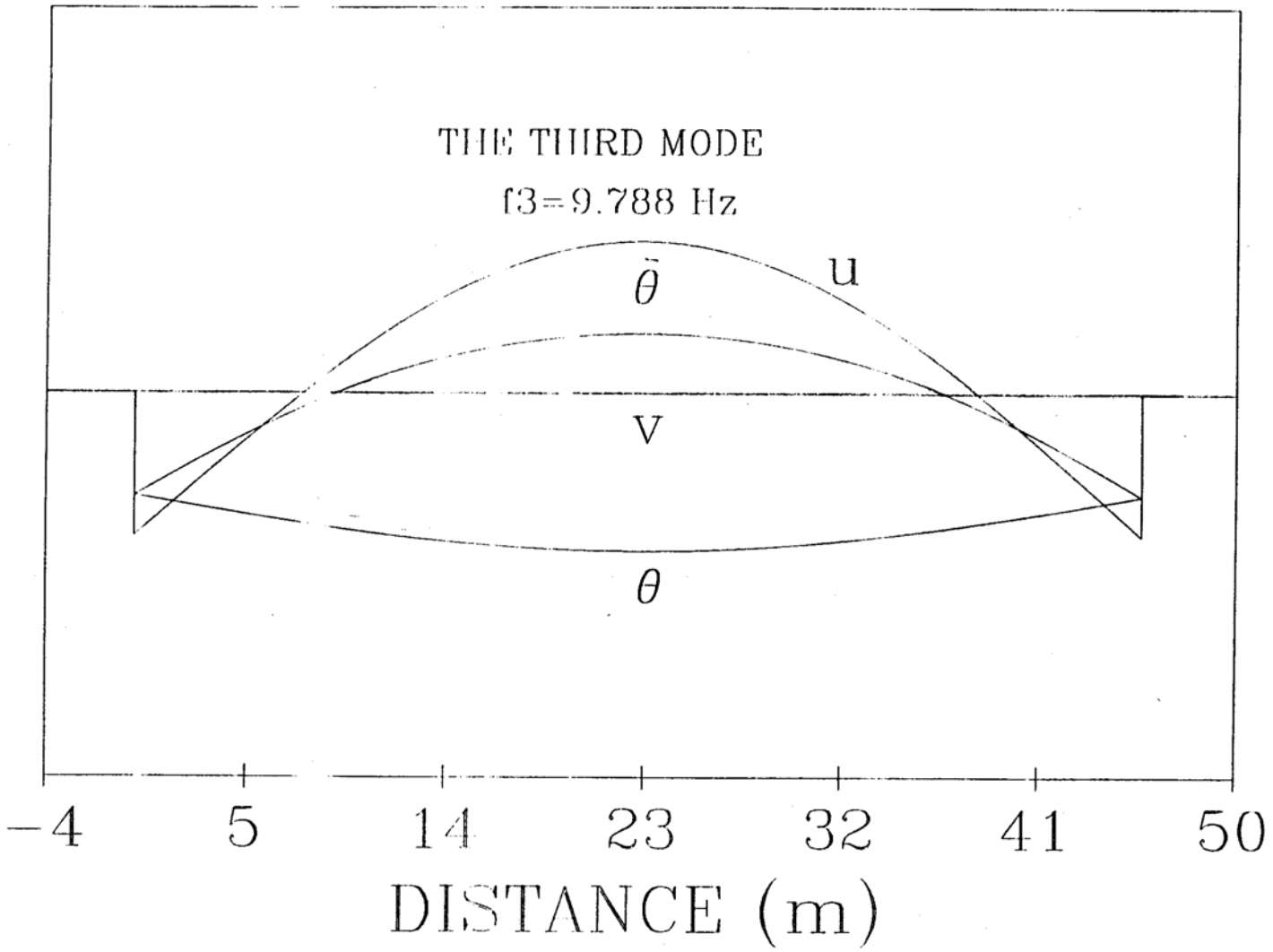

Fig. 3-30. The Third Vibration Mode of Simply Supported Bridge without Diaphragm

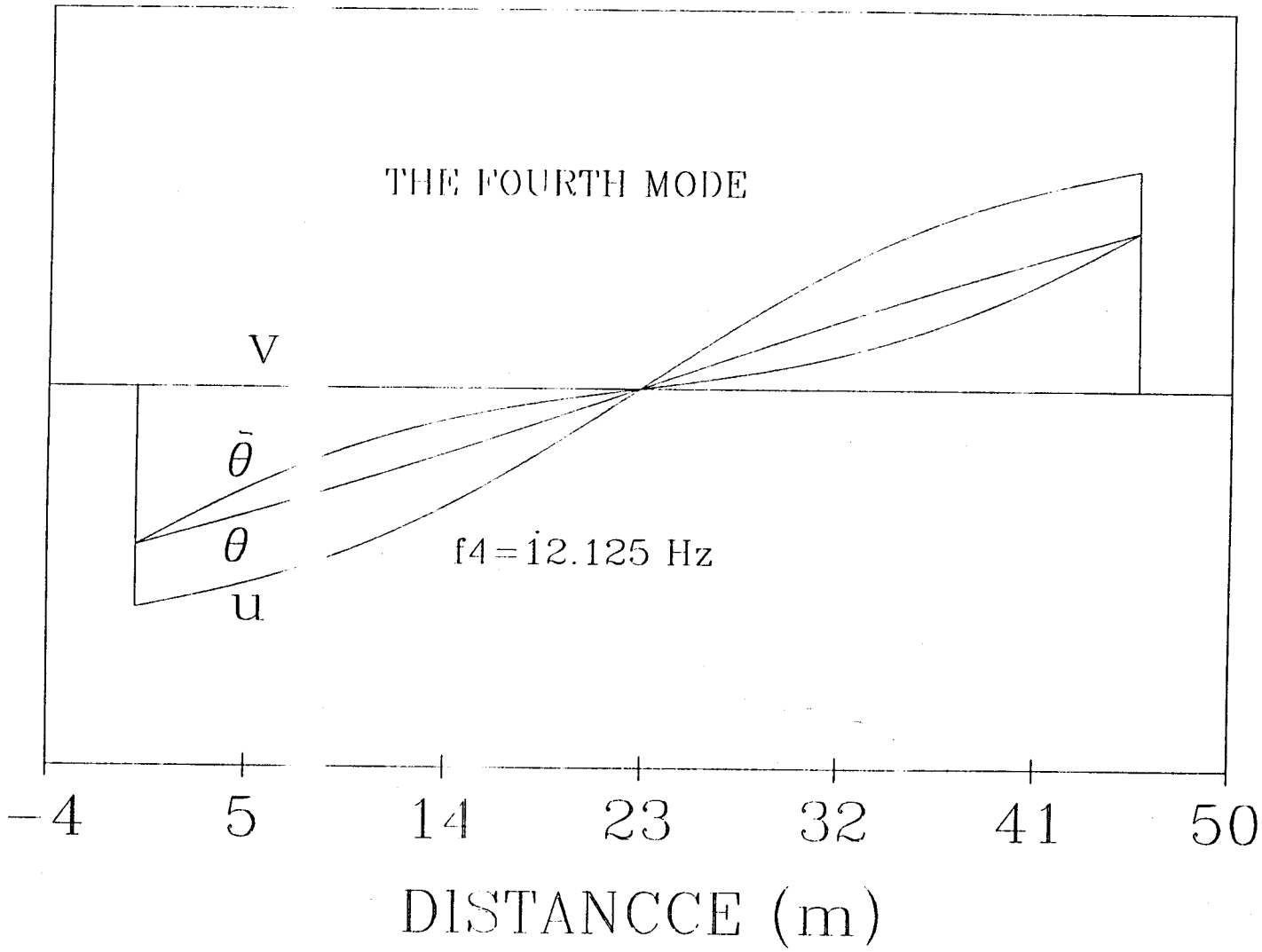

Fig. 3-31. The Fourth Vibration Mode of Simply Supported Bridge without Diaphragm

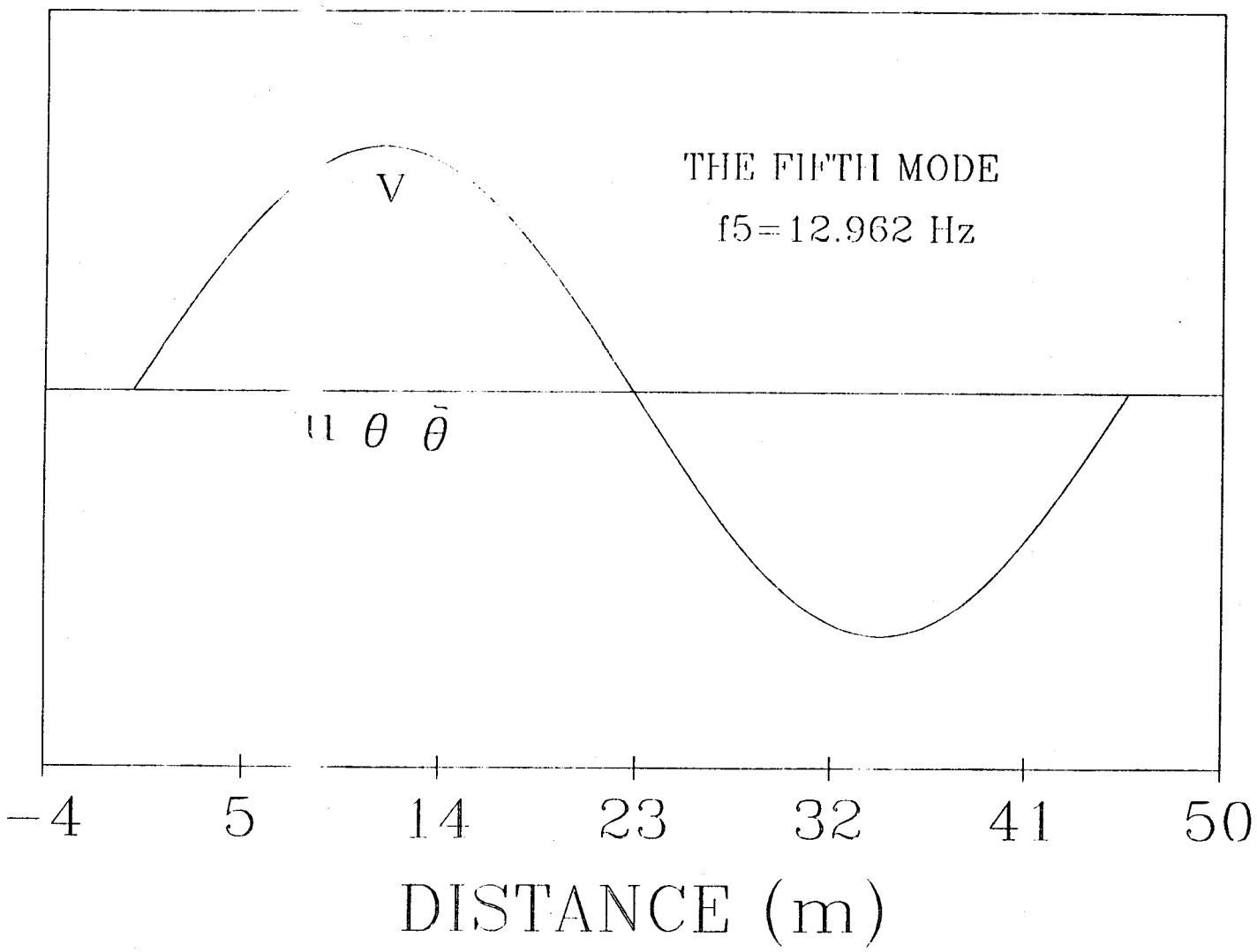

Fig. 3-32. The Fifth Vibration Mode of Simply Supported Bridge without Diaphragm

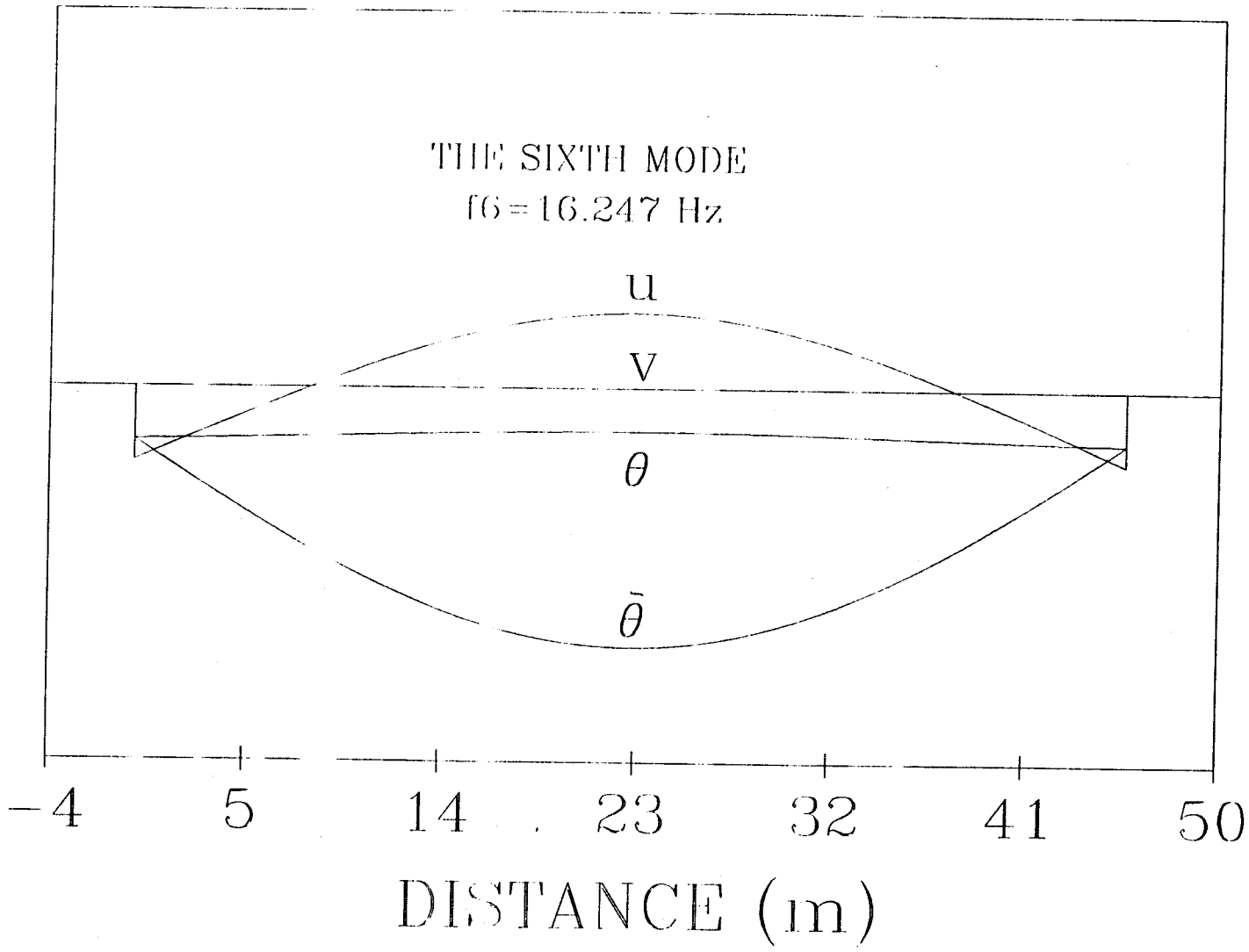

Fig. 3-33. The Sixth Vibration Mode of Simply Supported Bridge without Diaphragm

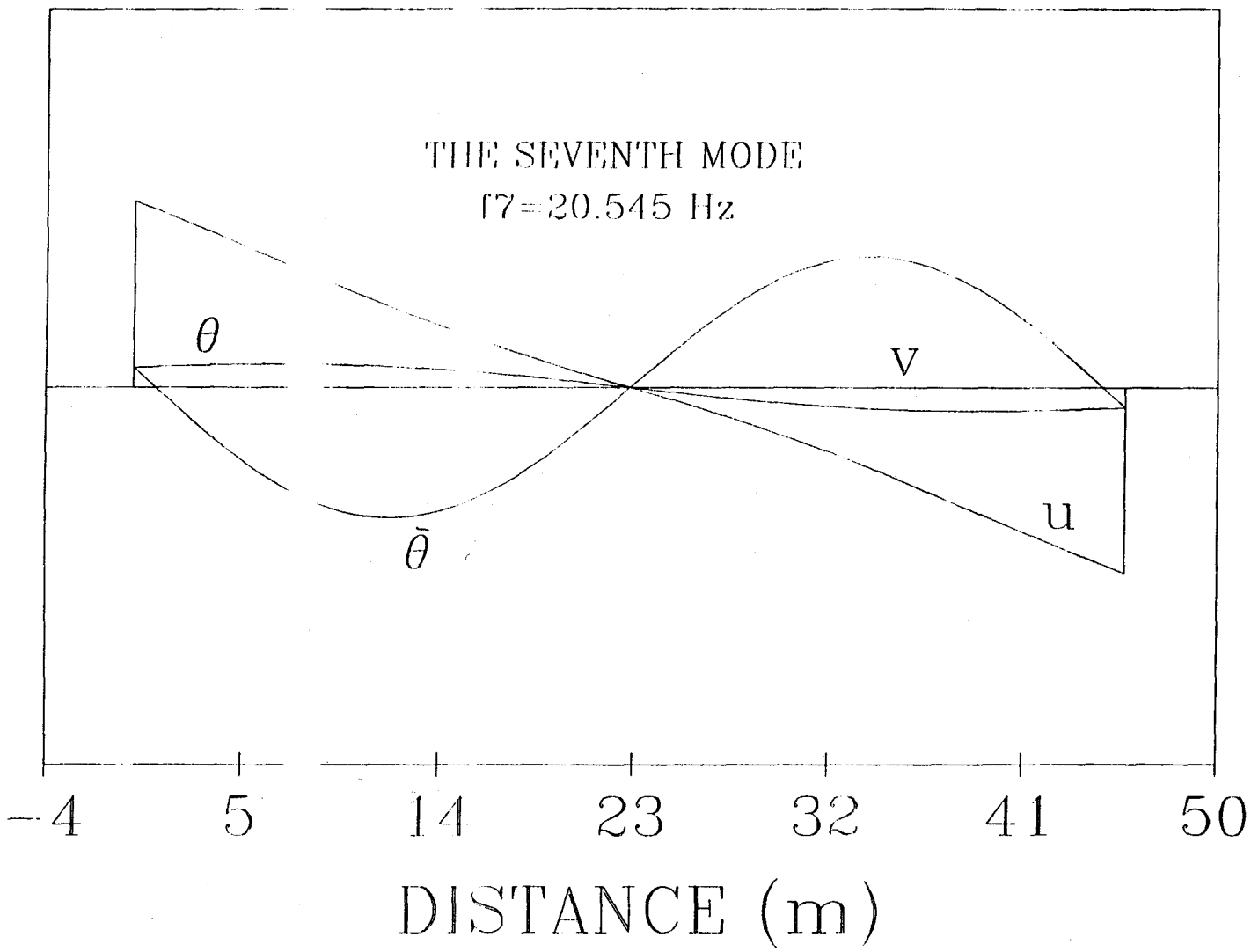

Fig. 3-34. The Seventh Vibration Mode of Simply Supported Bridge without Diaphragm

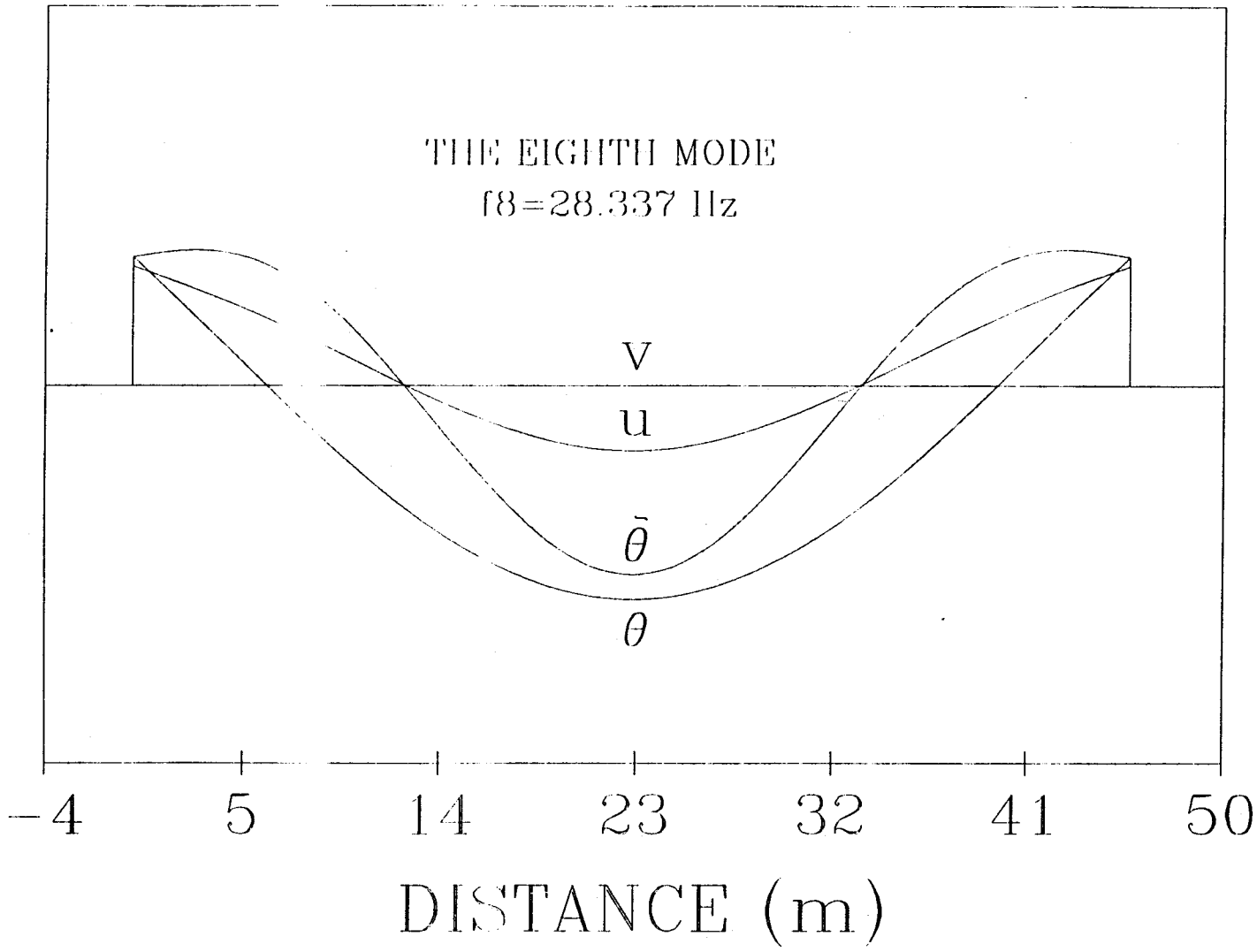

Fig. 3-35. The Eighth Vibration Mode of Simply Supported Bridge without Diaphragm

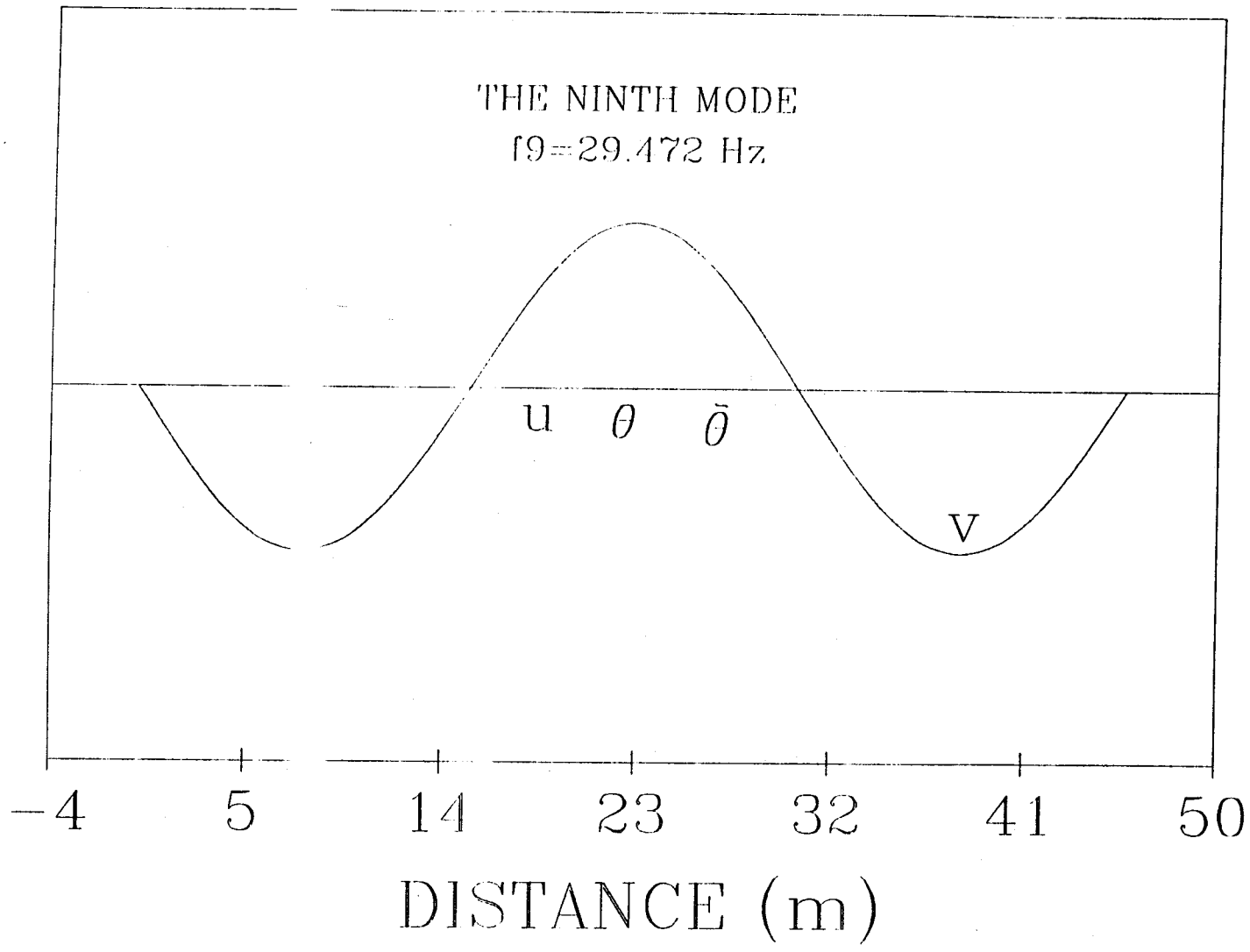

Fig. 3-36. The Ninth Vibration Mode of Simply Supported Bridge without Diaphragm

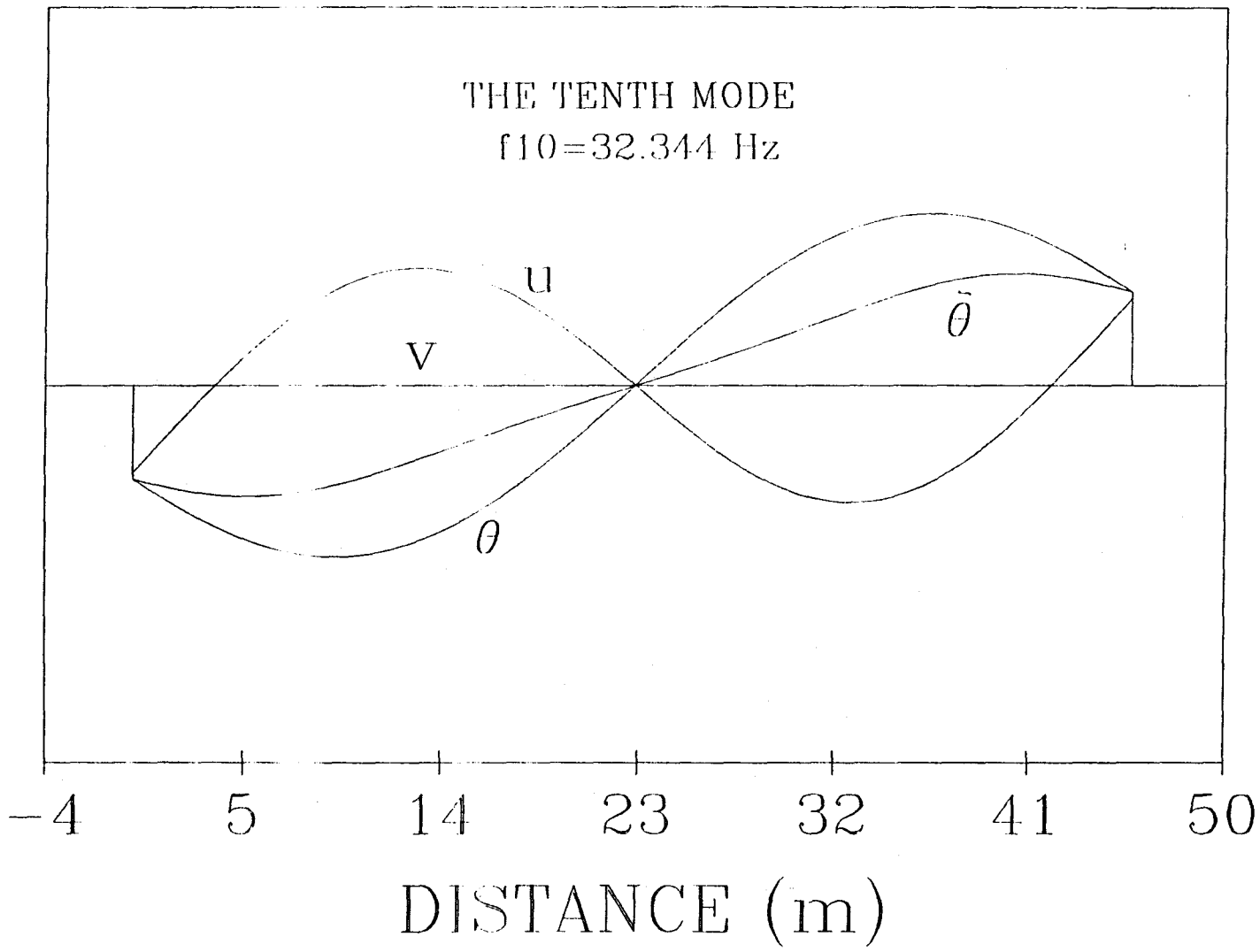

Fig. 3-37. The Tenth Vibration Mode of Simply Supported Bridge without Diaphragm

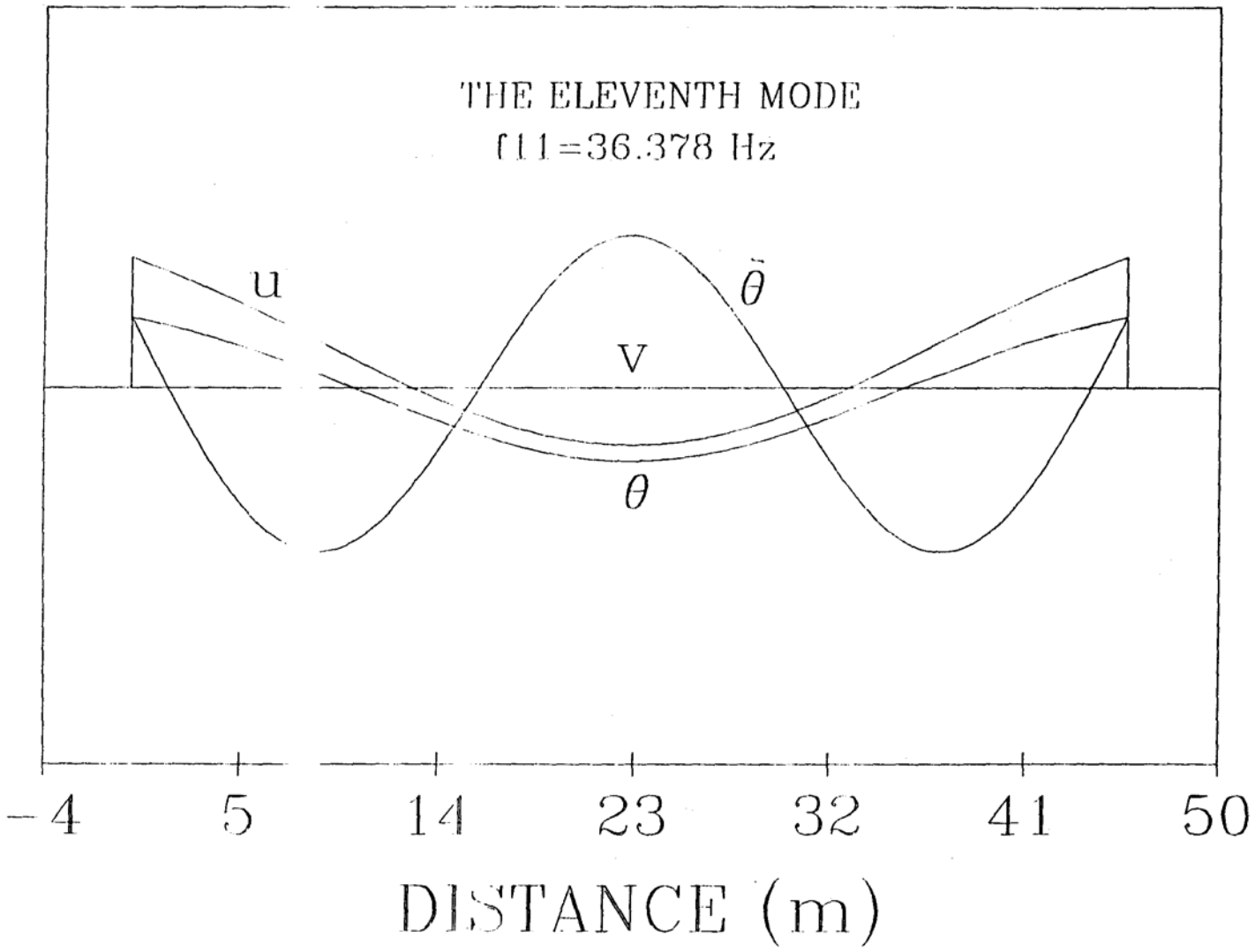

Fig. 3-38. The Eleventh Vibration Mode of Simply Supported Bridge without Diaphragm

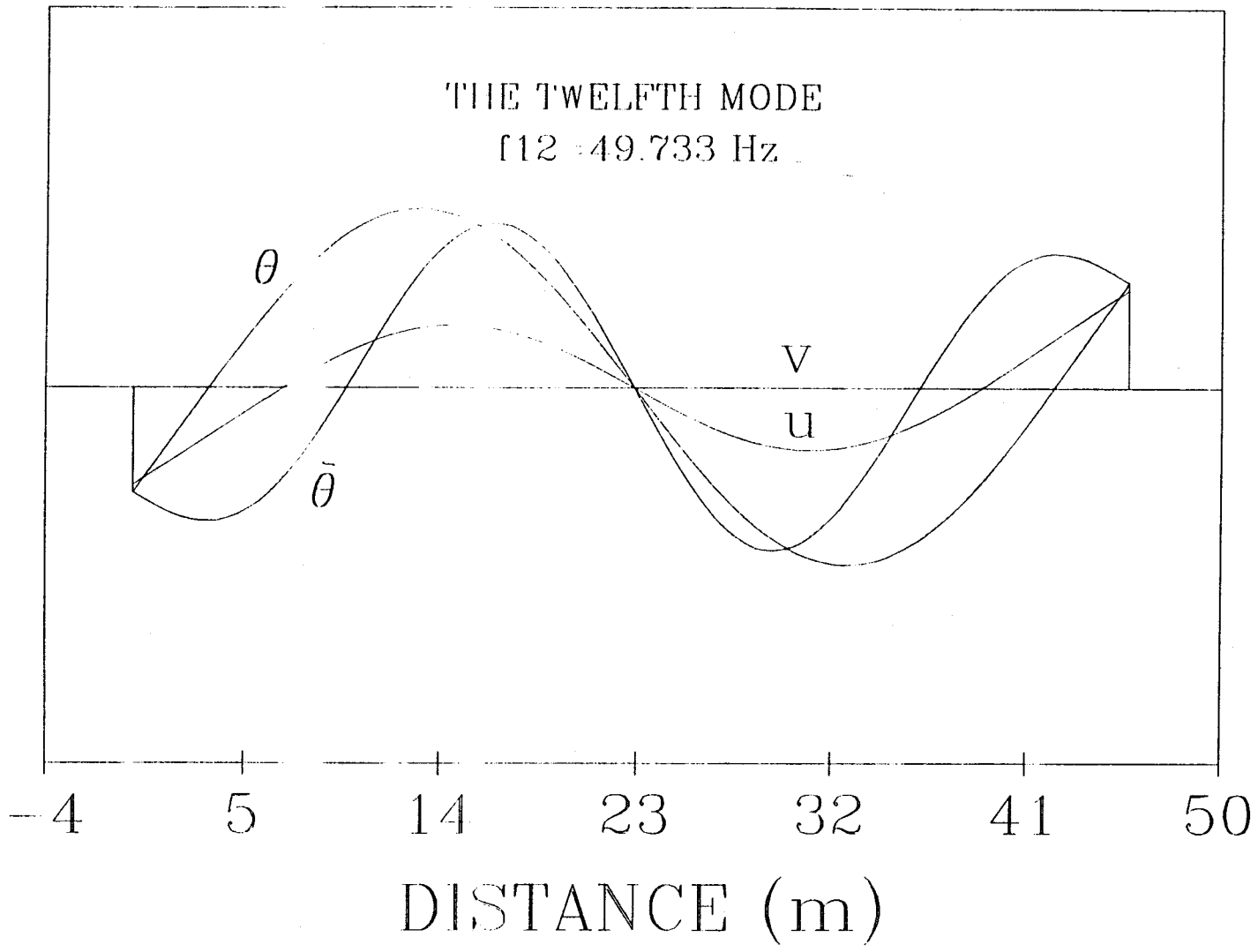

Fig. 3-39. The Twelfth Vibration Mode of Simply Supported Bridge without Diaphragm

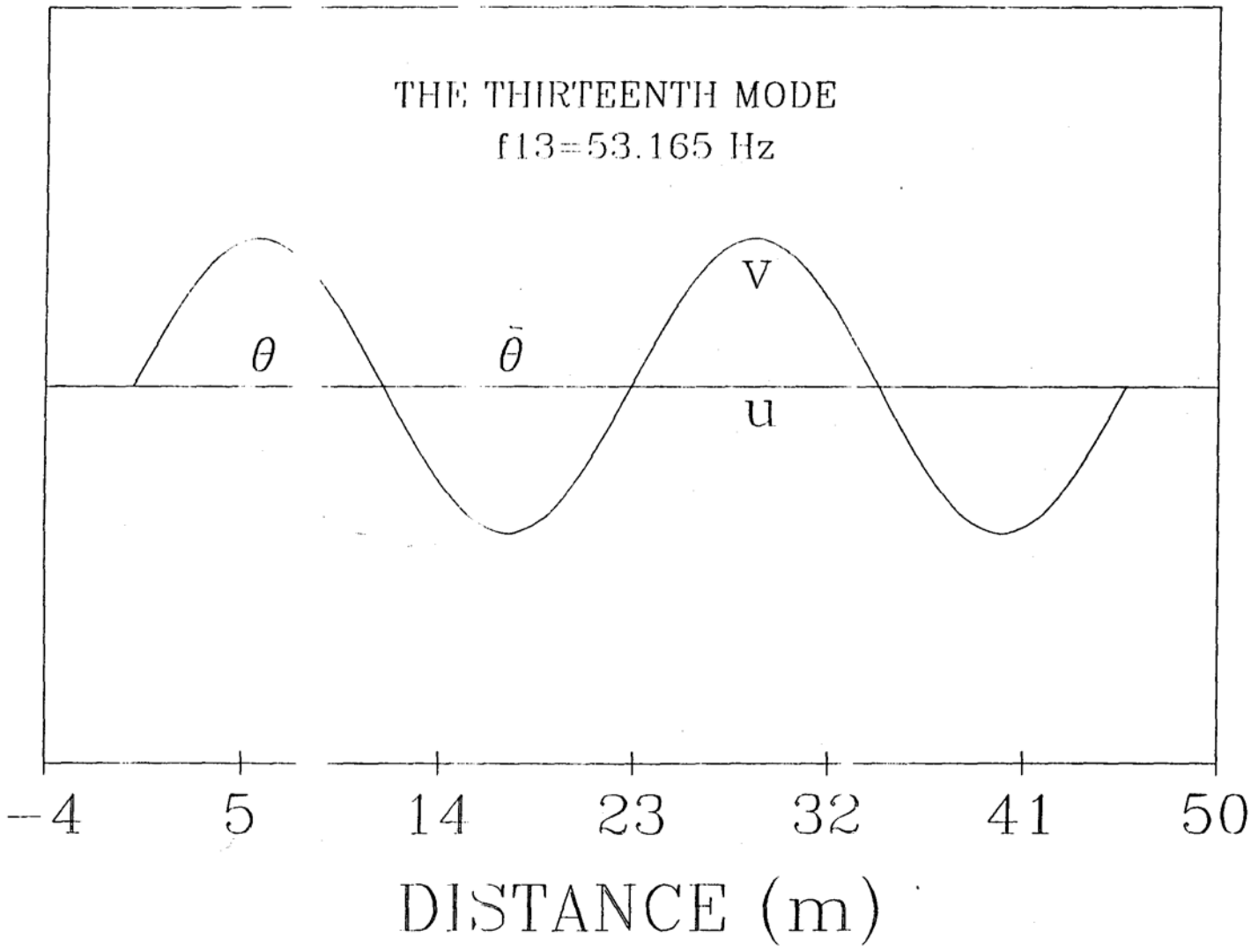

Fig. 3-40. The Thirteenth Vibration Mode of Simply Supported Bridge without Diaphragm

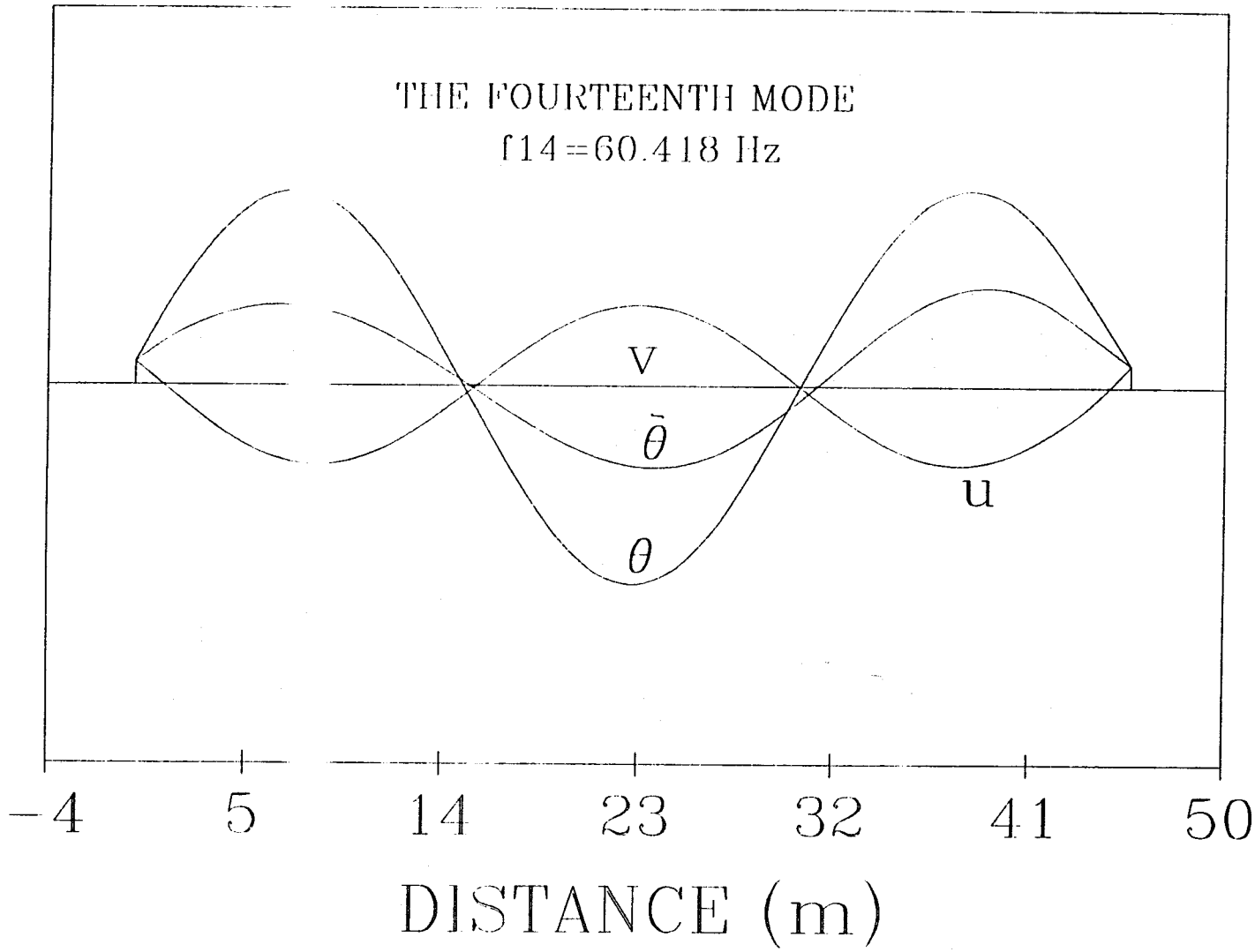

Fig. 3-41. The Fourteenth Vibration Mode of Simply Supported Bridge without Diaphragm

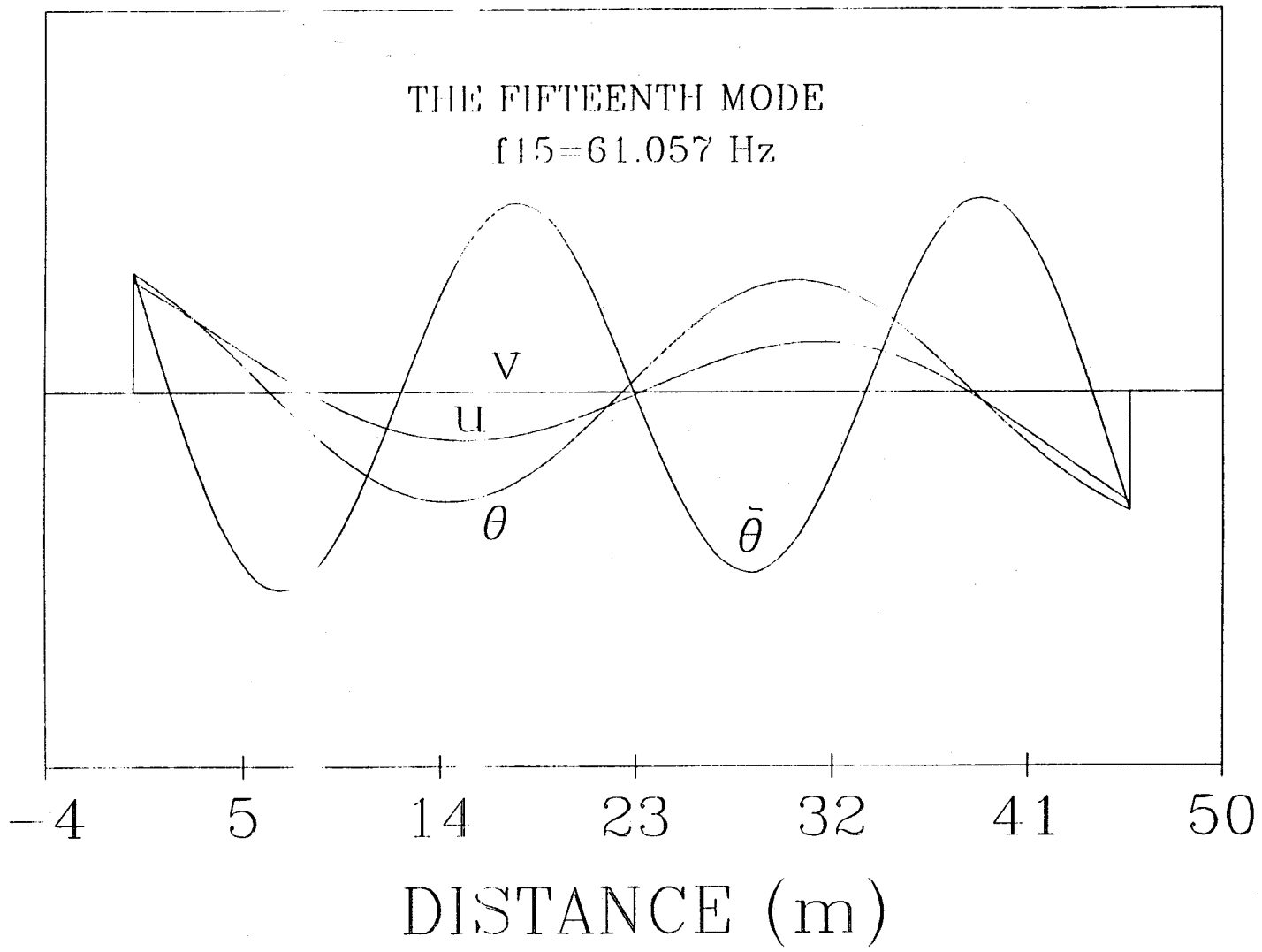

Fig. 3-42. The Fifteenth Vibration Mode of Simply Supported Bridge without Diaphragm

is assumed for both the approach roadways and bridge decks.

Figs.3-43 to 3-59 show seventeen time-history curves of the bridge under conditions of average road surface roughness and vehicle speed of 72.405 km/hr. (45 mph). Figs.3-43 to 3-45 are the time histories of vertical shear Q_y, bi-moment $B_{,,,,}$ and distortional bi-moment B_j, at left end support of the bridge, respectively. The histories of lateral bending moment M_y, vertical shear Q_y, vertical bending moment M_x, torque $T_{G,,,}$ $B_{,,,}$ distortional torque $T_{z;,,}$ and B, at span fourth point are shown in Figs.3-46 to 3-52 individually. The histories of $M_{,,,}$ Q_Y, MX, $T_{cc,,}$ $B_{u,,}$ $T_{j,,}$ and B~ at mid-span are indicated in Figs. 3-53 to 3-59, separately. All of those histories are obtained based on Loading 4 of two-truck (see Fig.3-60). It can be observed from those time histories that first several lower vibration modes dominate the response of vertical bending moment at mid-span, while higher modes greatly affect the other responses of torque, bimoment, and lateral bending moment.

In order to know the effect of lateral loading position on the dynamic response of the box girder bridge, the static response and impact factors at mid-span for symmetric and asymmetric one-truck loading cases (see Fig.3-61, Loadings 1 to 3) are evaluated and given in Tables 3-2 and 3-3, in which MX, T.., $B_{.,,}$ T_z, $B_{z,,}$ D_y, B, & express vertical bending moment, torque, bi-moment, torque due to distortion, distortional bi-moment, vertical displacement, twist angle, and distortional angle, respectively. The impact factor is defined as

$$I_{.P}(\%) = [R_{dm}/R_{sm} - 1\ ]x\ 100\% \qquad 3\text{-}2$$

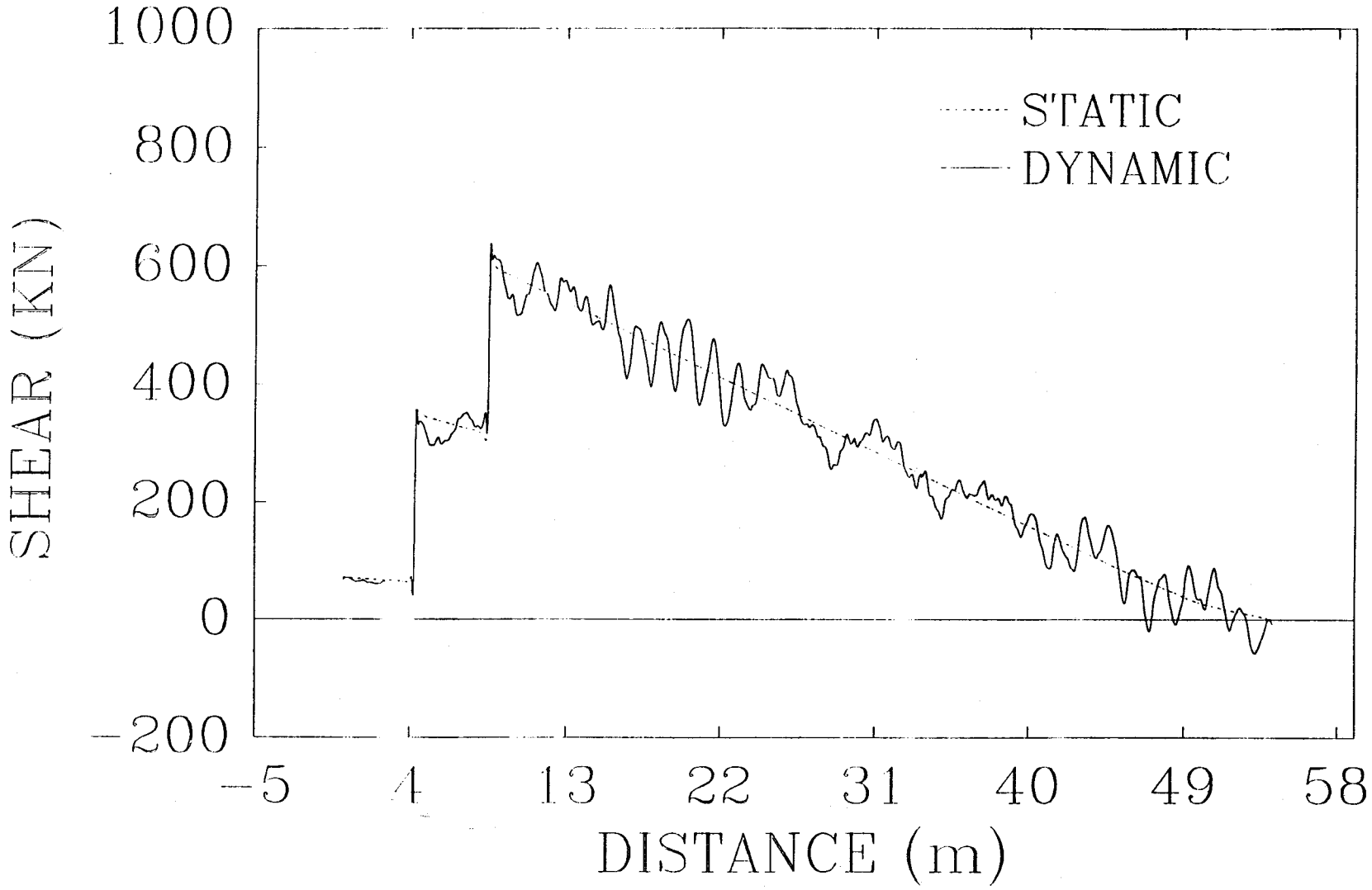

Fig. 3-43. Histories of Shear at Left End Support

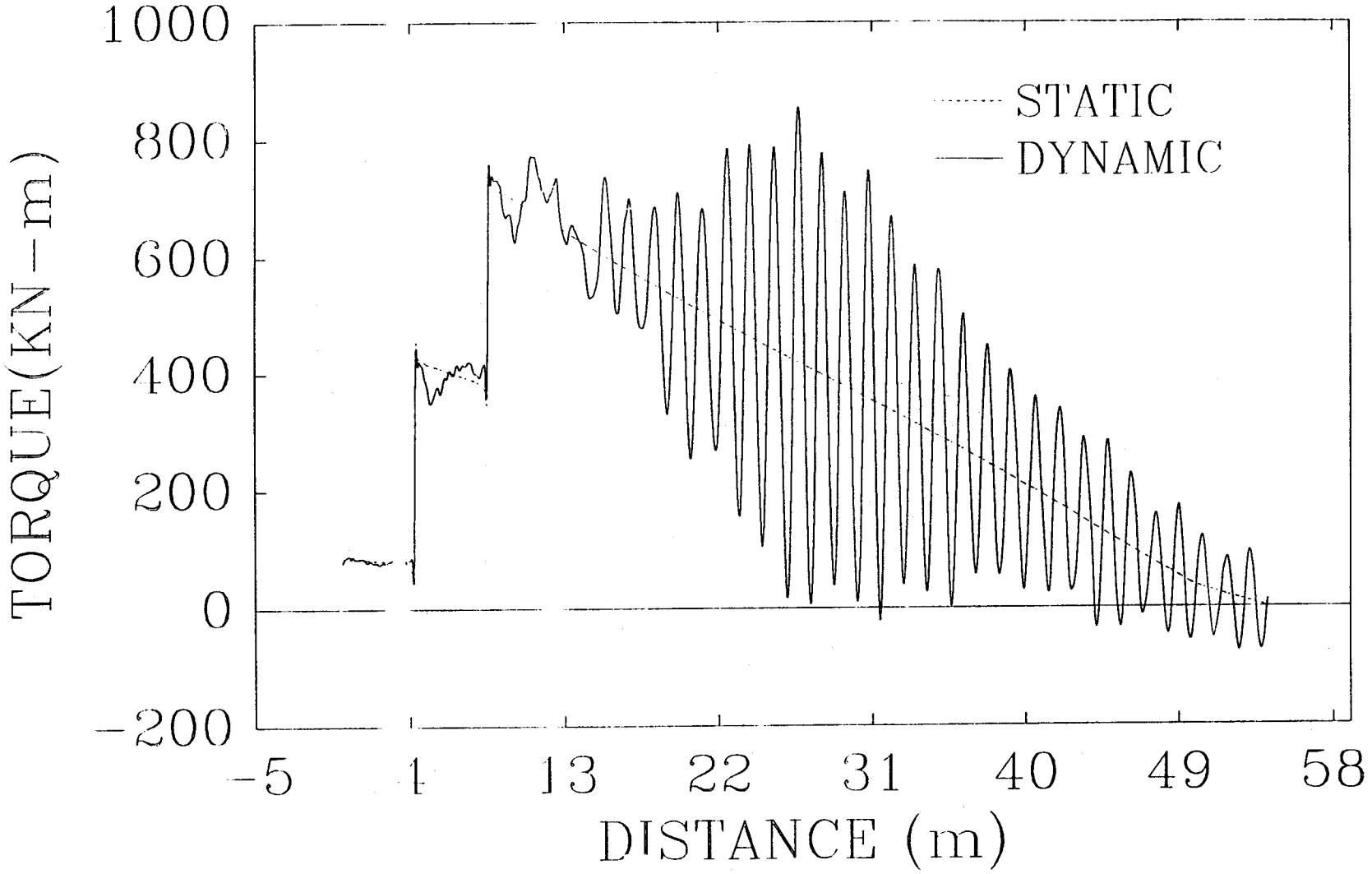

Fig. 3-44. Histories of Torque at Left End Support

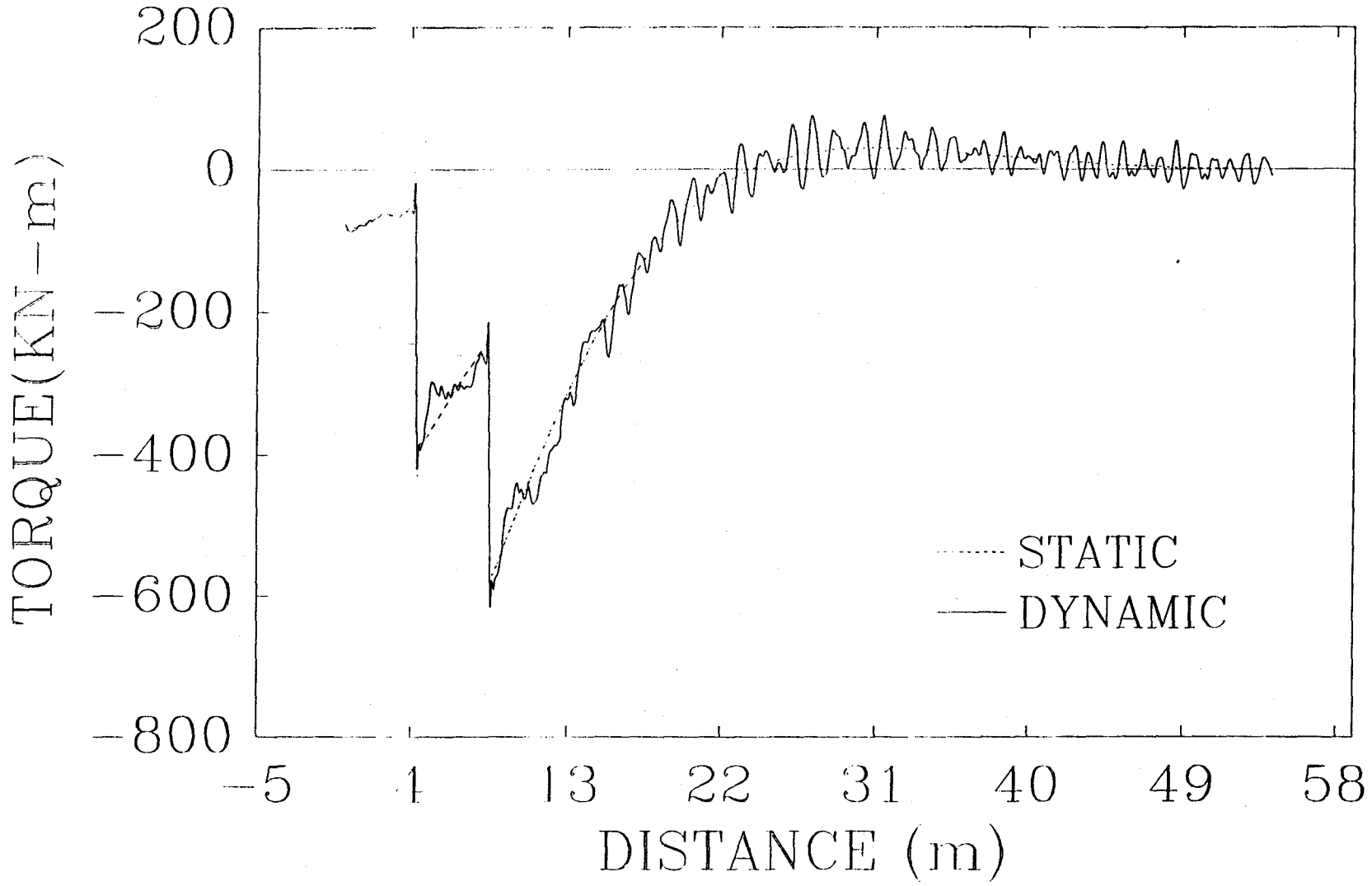

Fig. 3-45. Histories of Torque due to Distortion at Left End Support

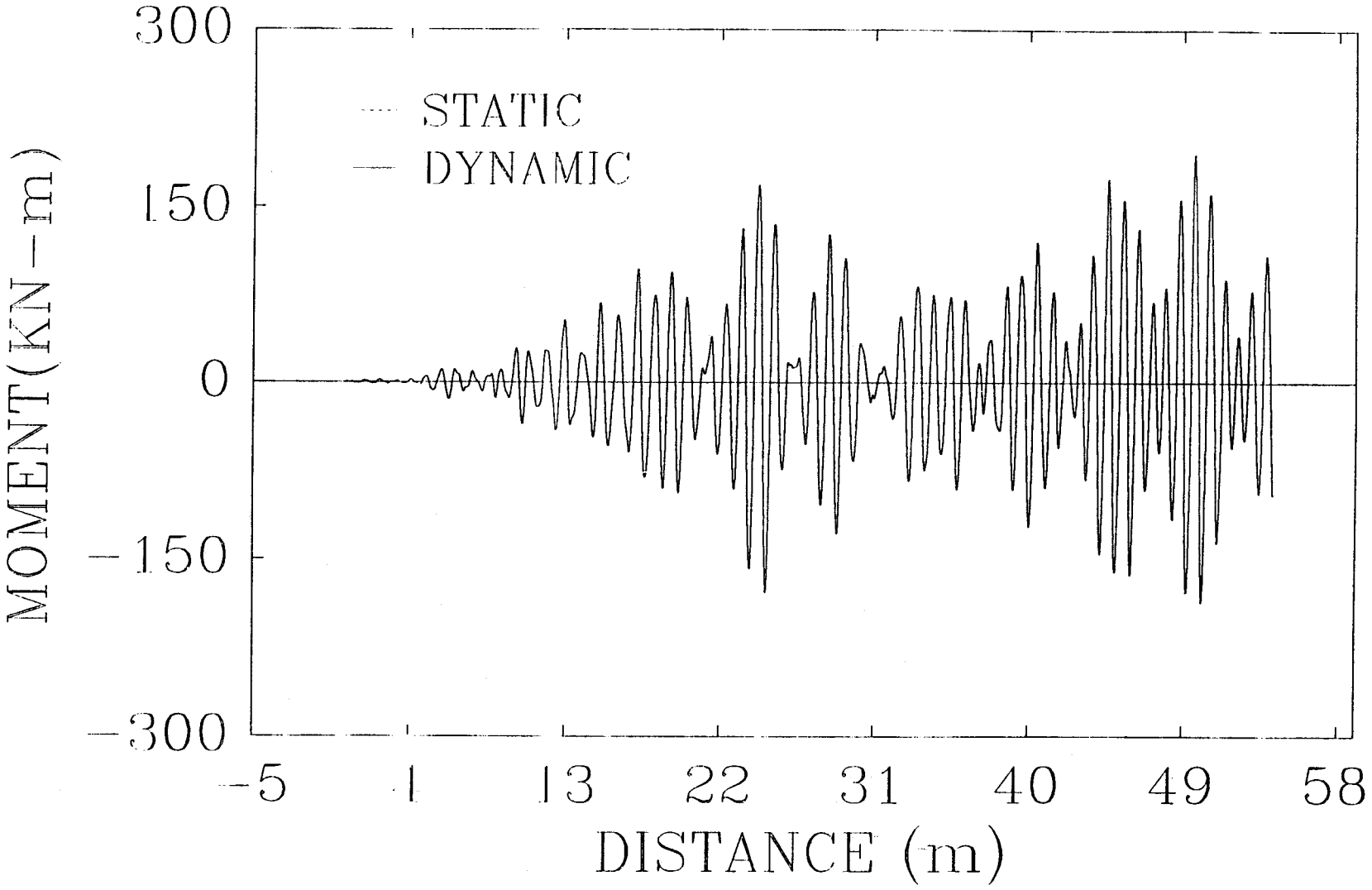

Fig. 3-46. Histories of Lateral Bending Moment at Span Fourth Point

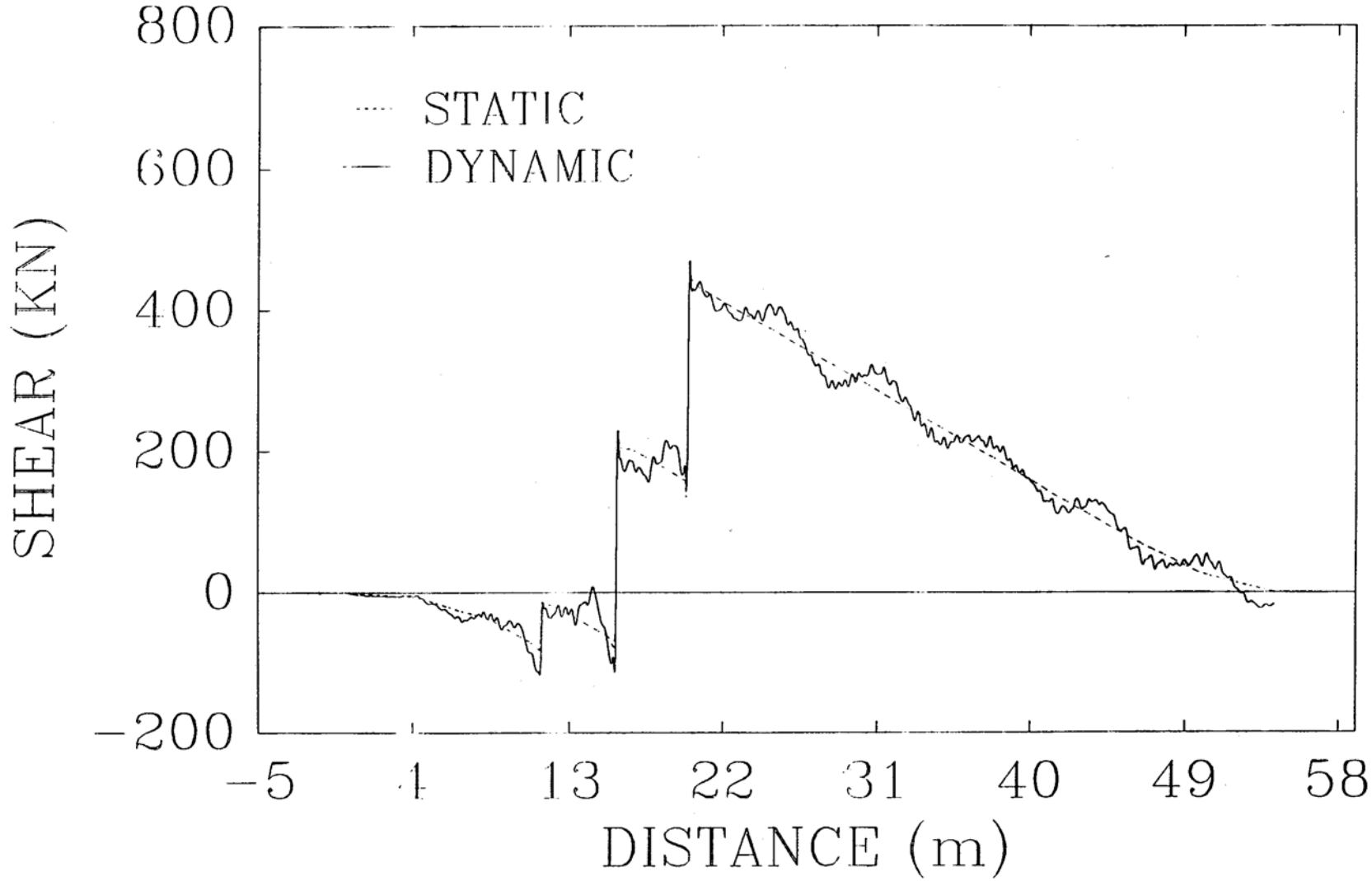

Fig. 3-47. Histories of Shear at Span Fourth Point

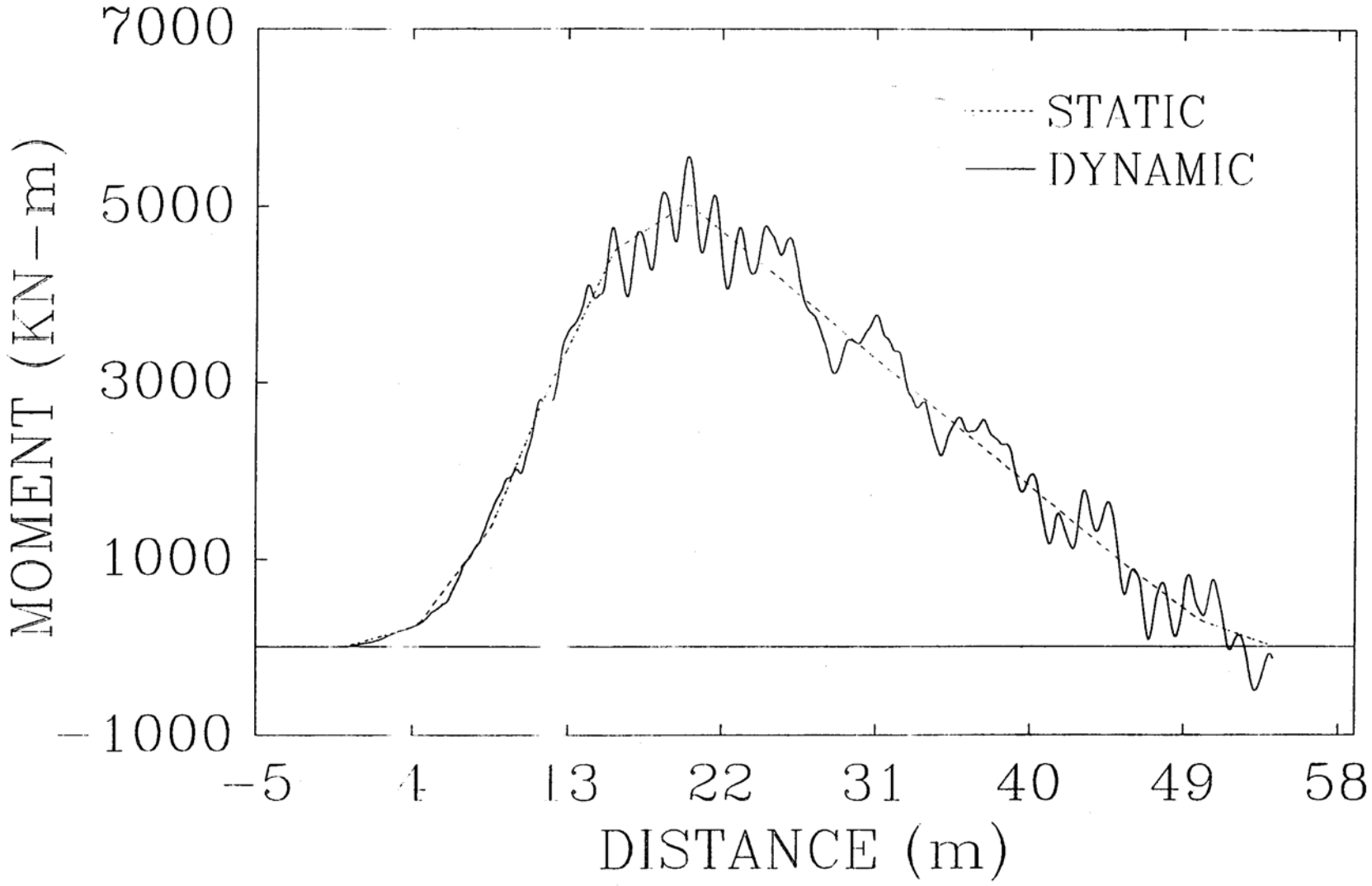

Fig. 3-48. Histories of Vertical Bending Moment at Span Fourth Point

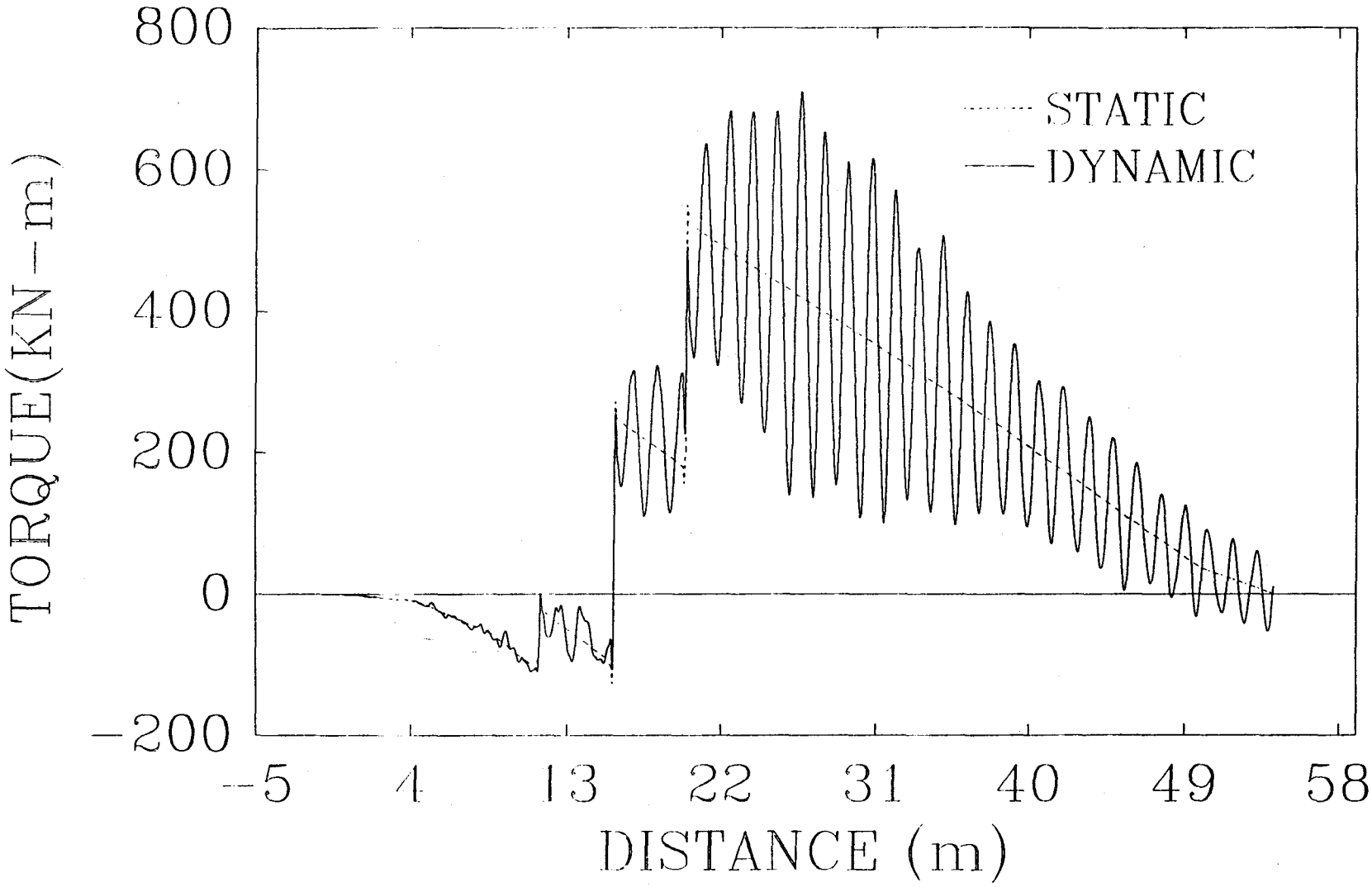

Fig. 3-49. Histories of Torque at Span Fourth Point

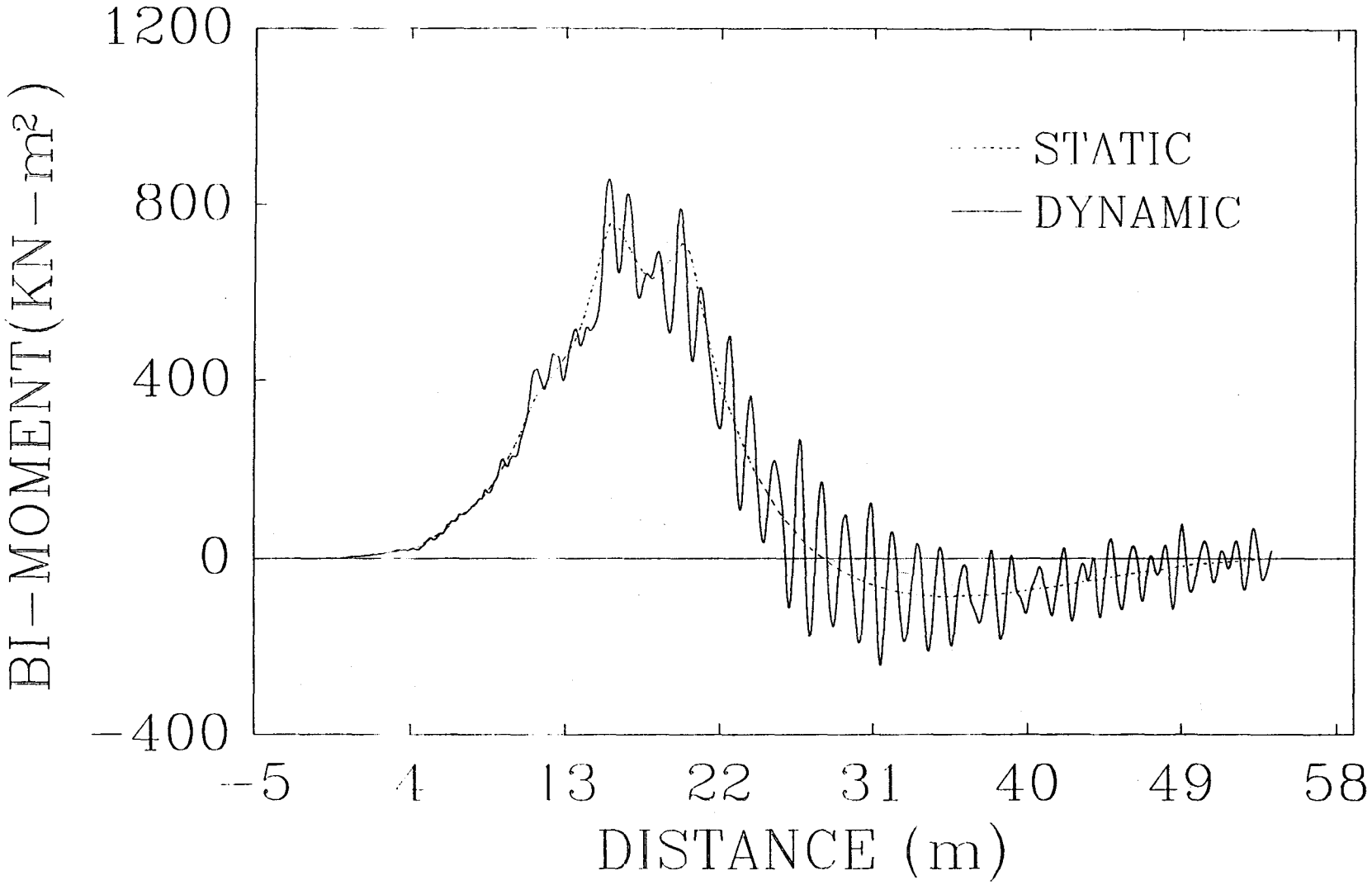

Fig. 3-50. Histories of Bi-Moment at Span Fourth Point

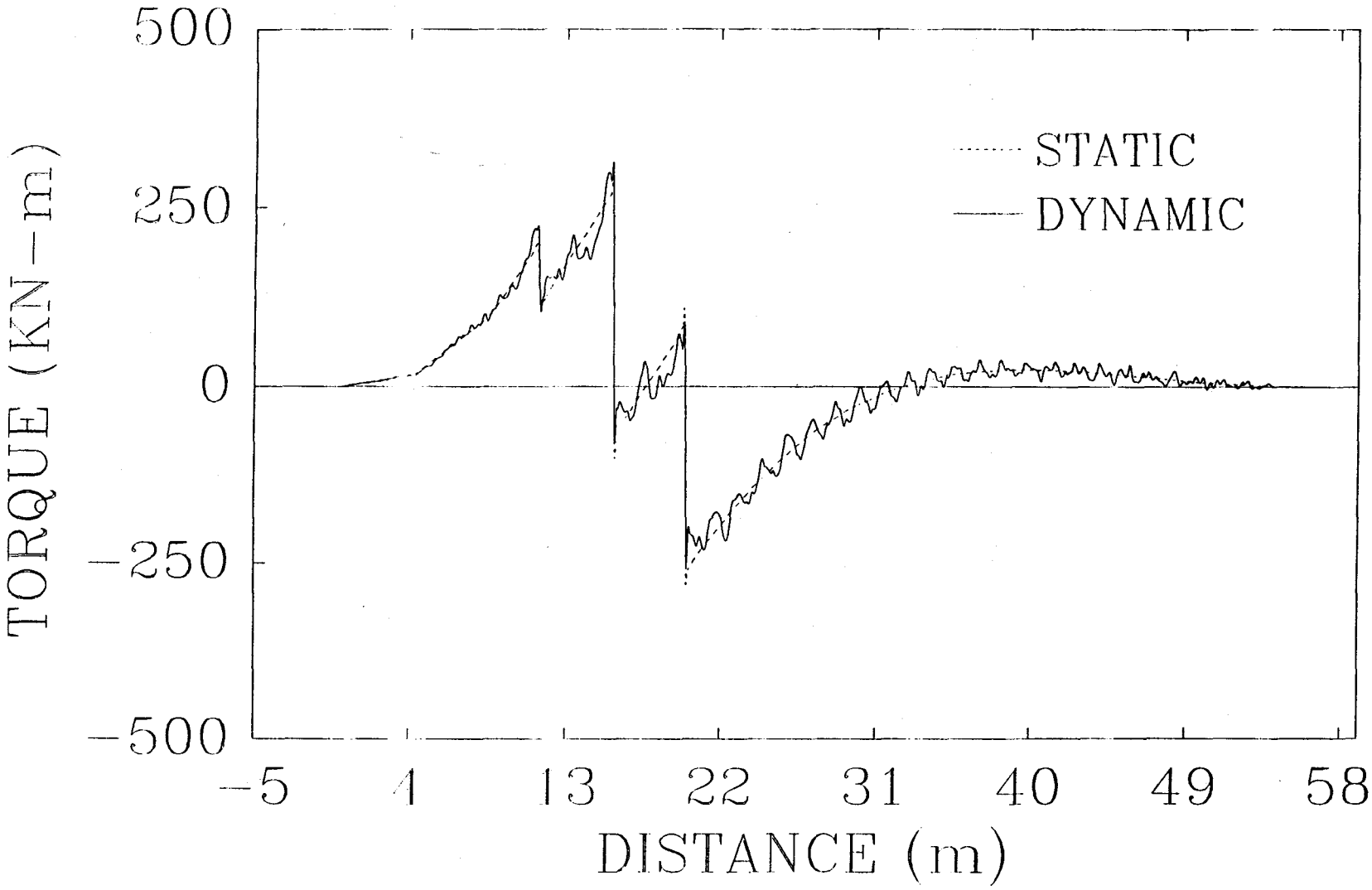

Fig. 3-51. Histories of Torque due to Distortion at Span Fourth Point

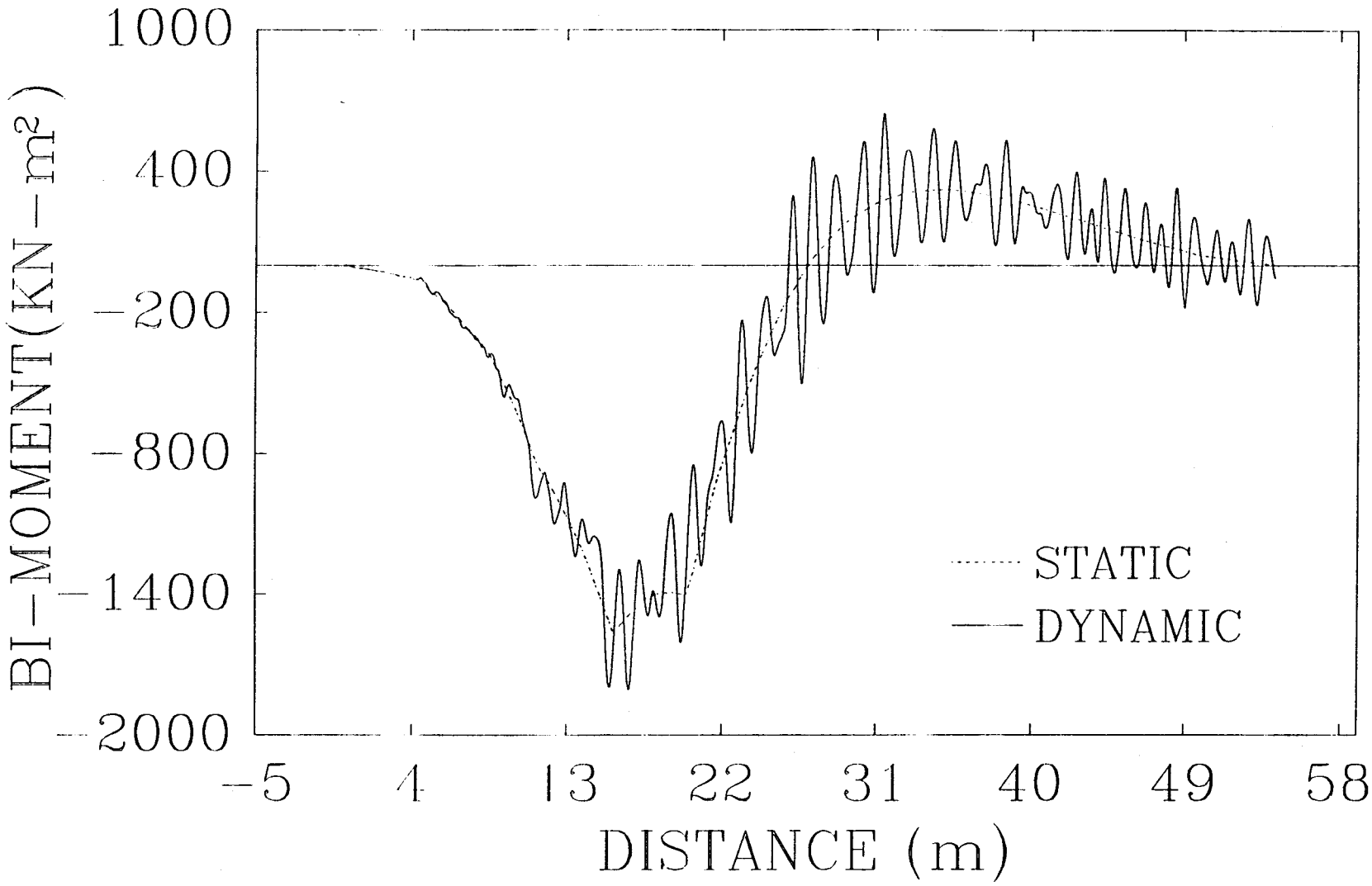

Fig. 3-52. Histories of Bi-moment due to Distortion at Span Fourth Point

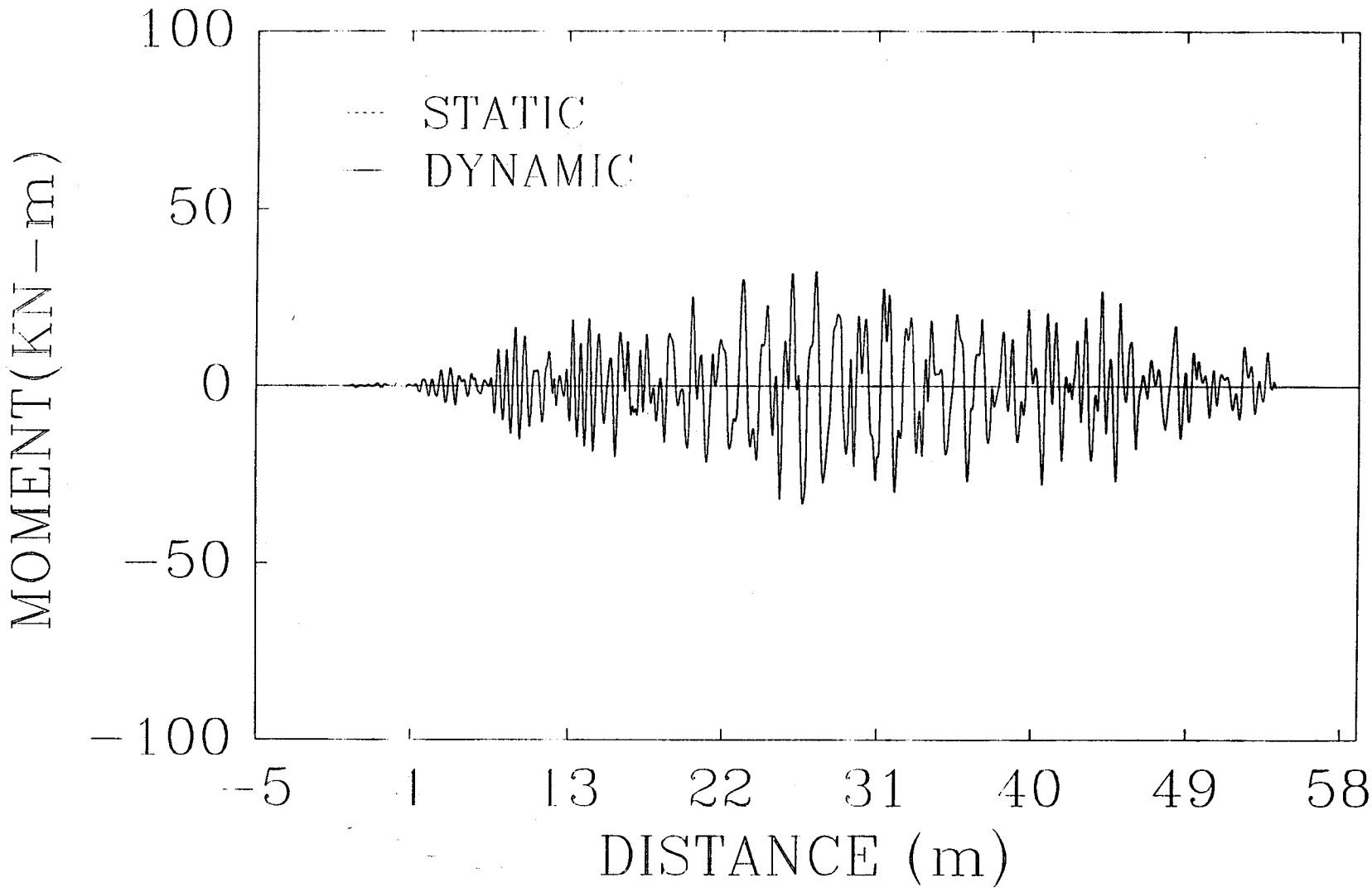

Fig. 3-53. Histories of Lateral Bending Moment at Mid-span

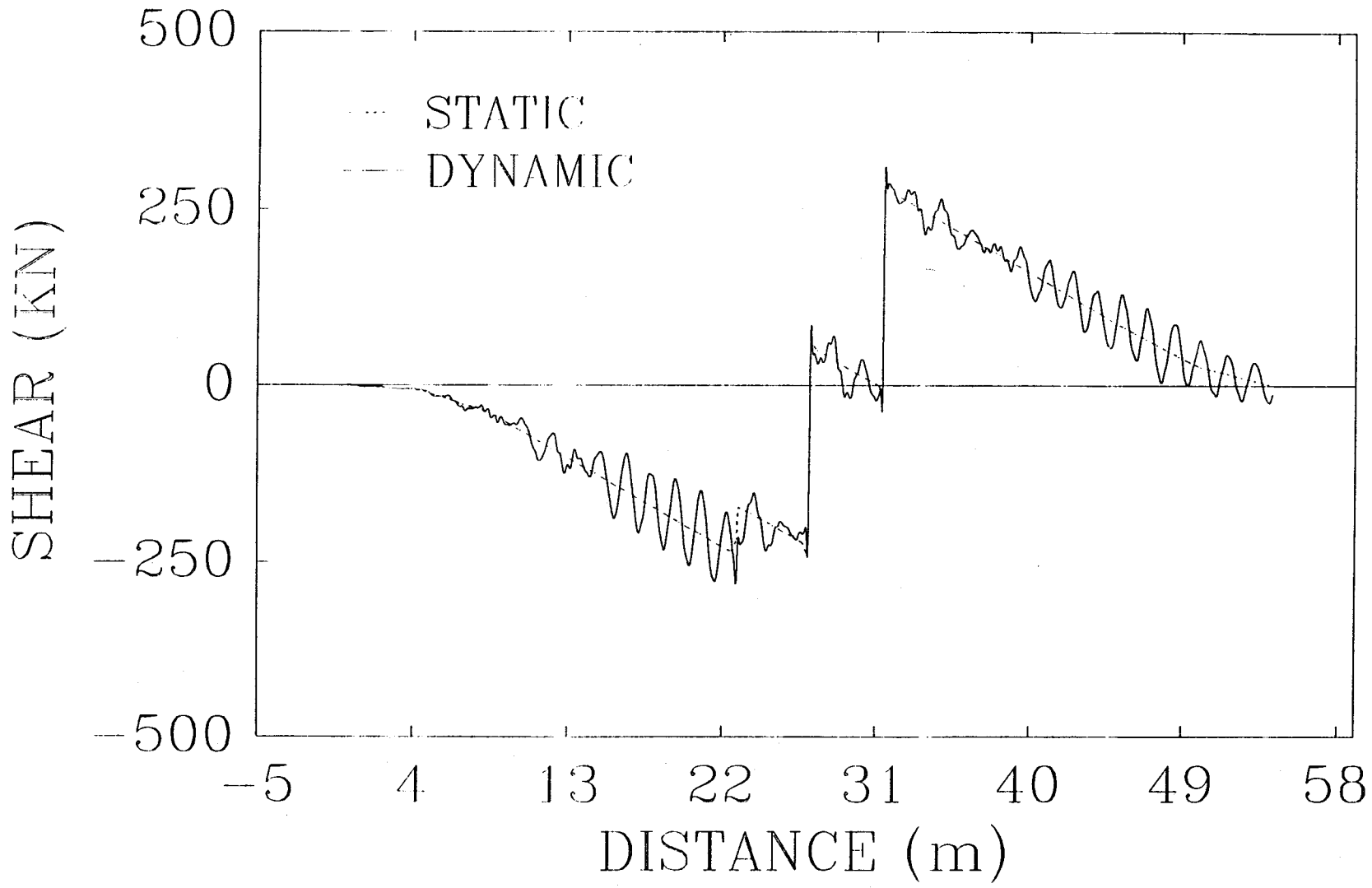

Fig. 3-54. Histories of Shear at Mid-span

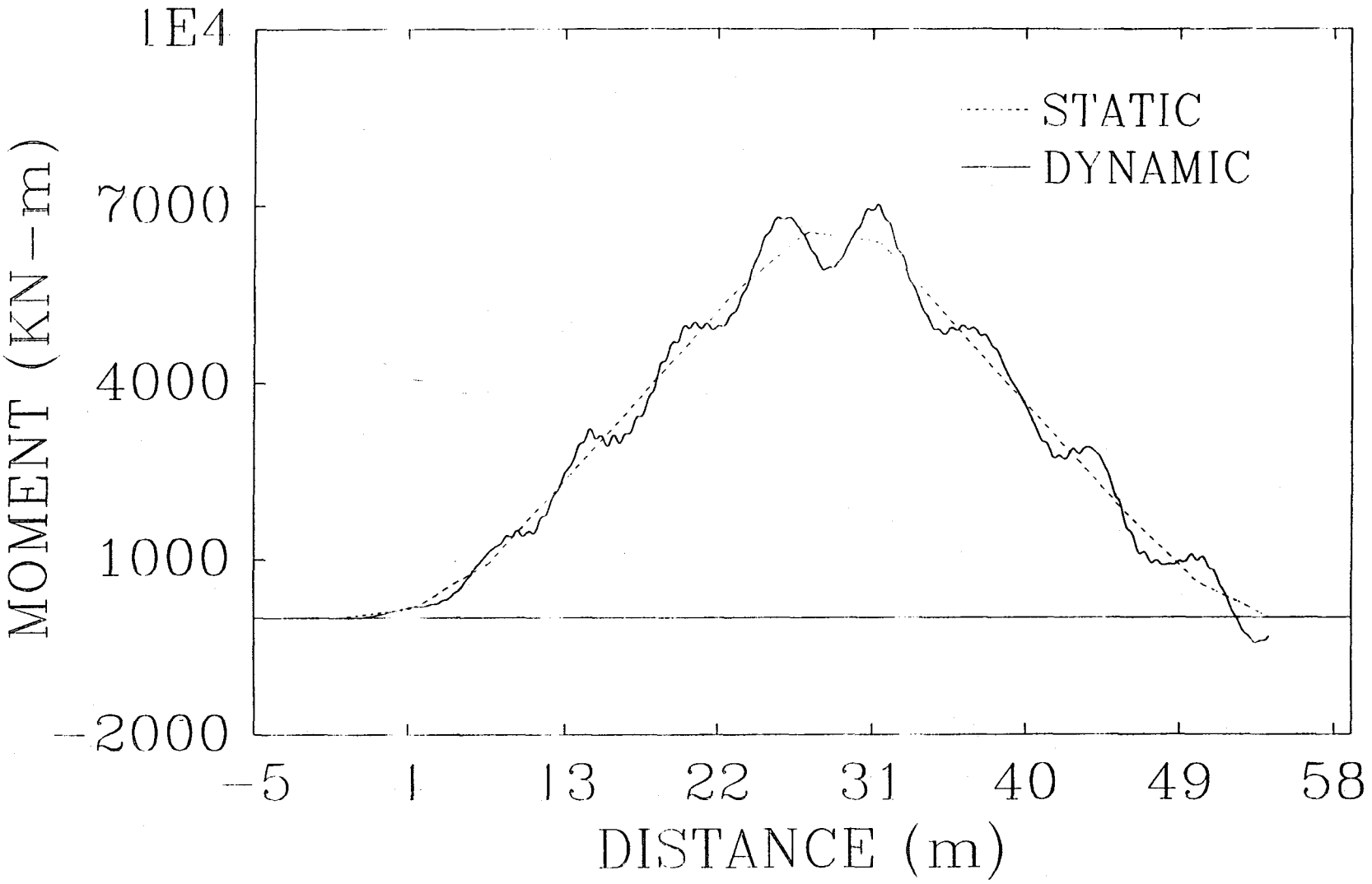

Fig. 3-55. Histories of Vertical Bending Moment at Mid-span

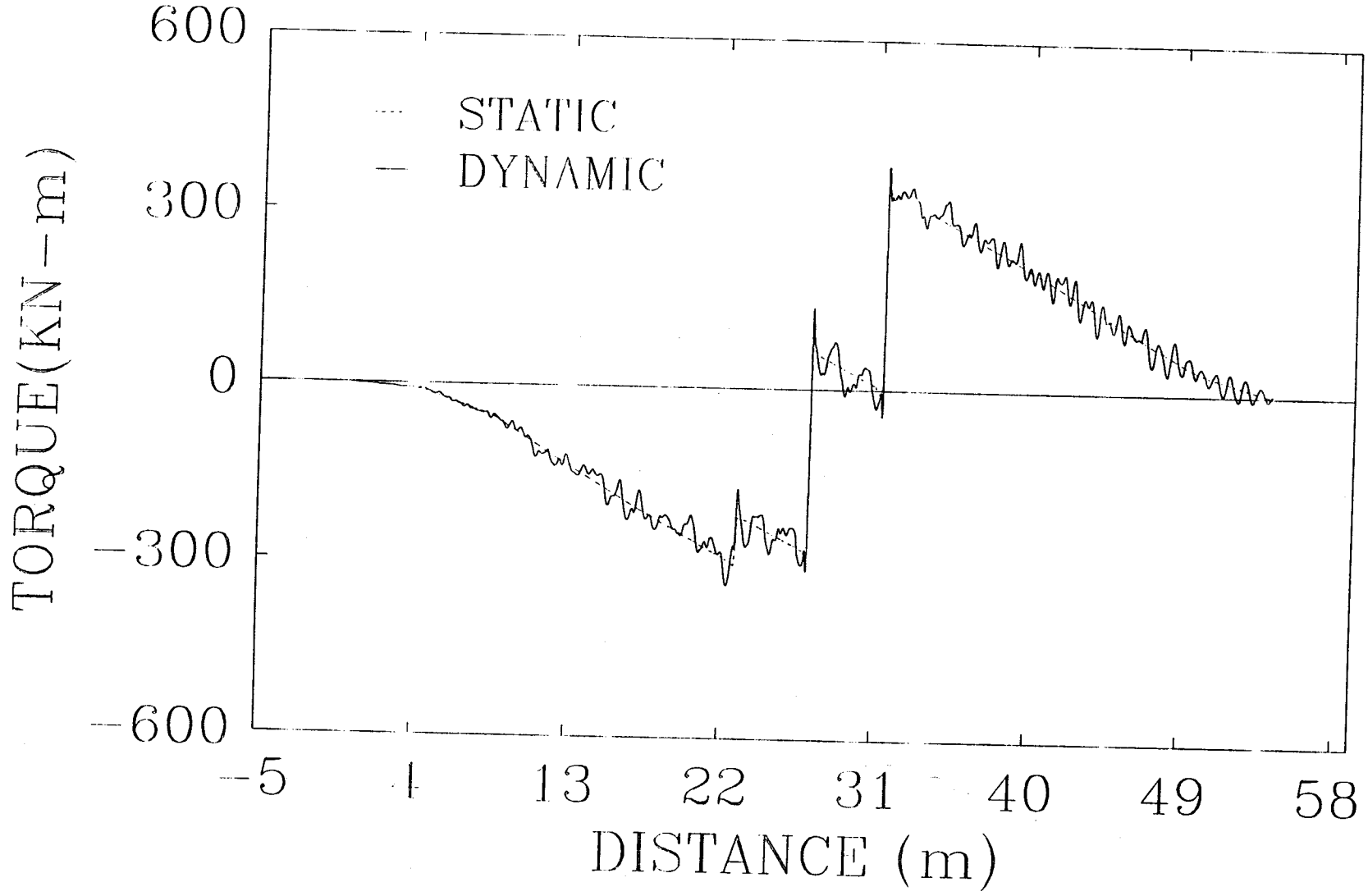

Fig. 3-56. Histories of Torque at Mid-span

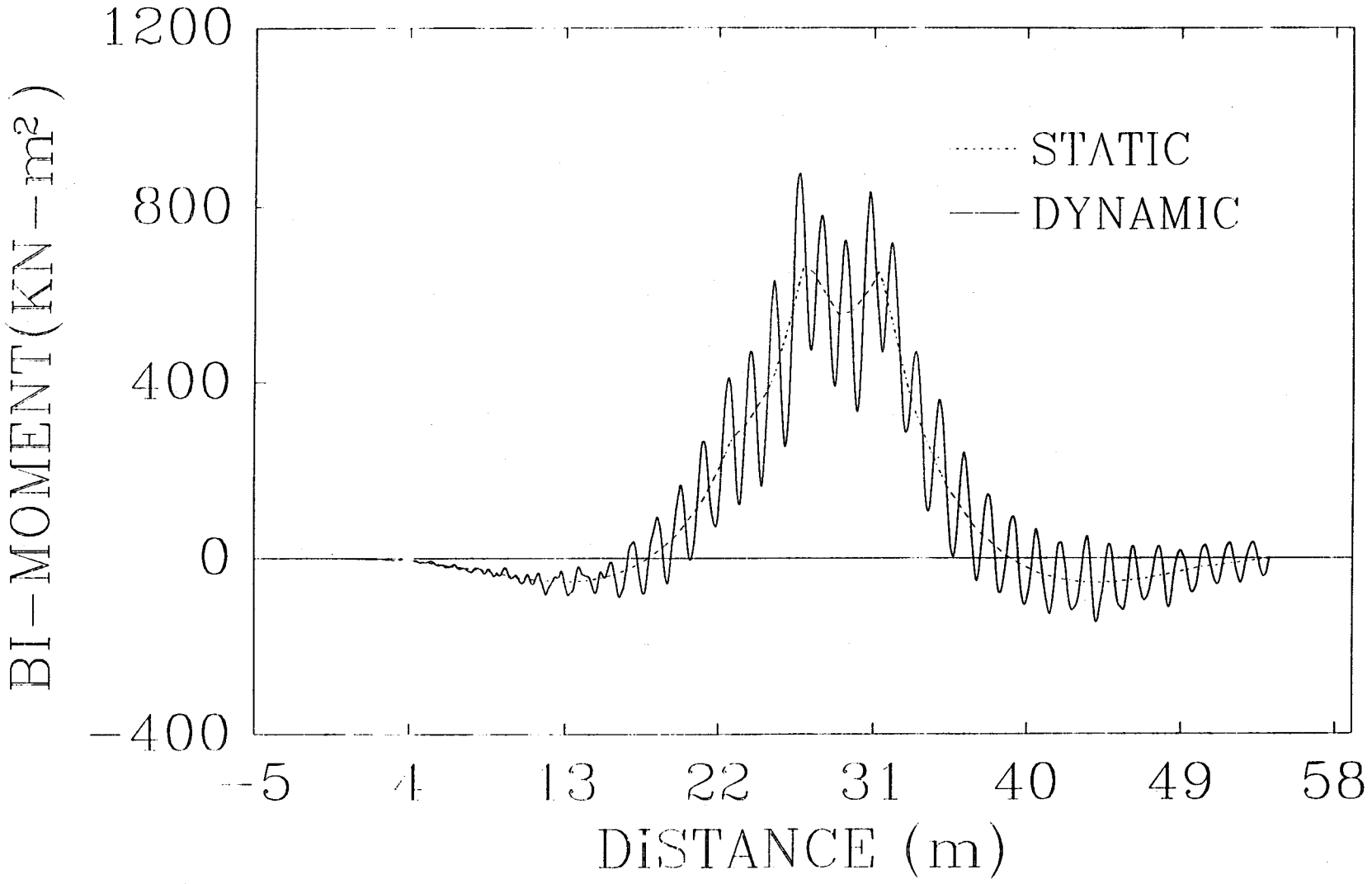

Fig. 3-57. Histories of Bi-Moment at Mid-span

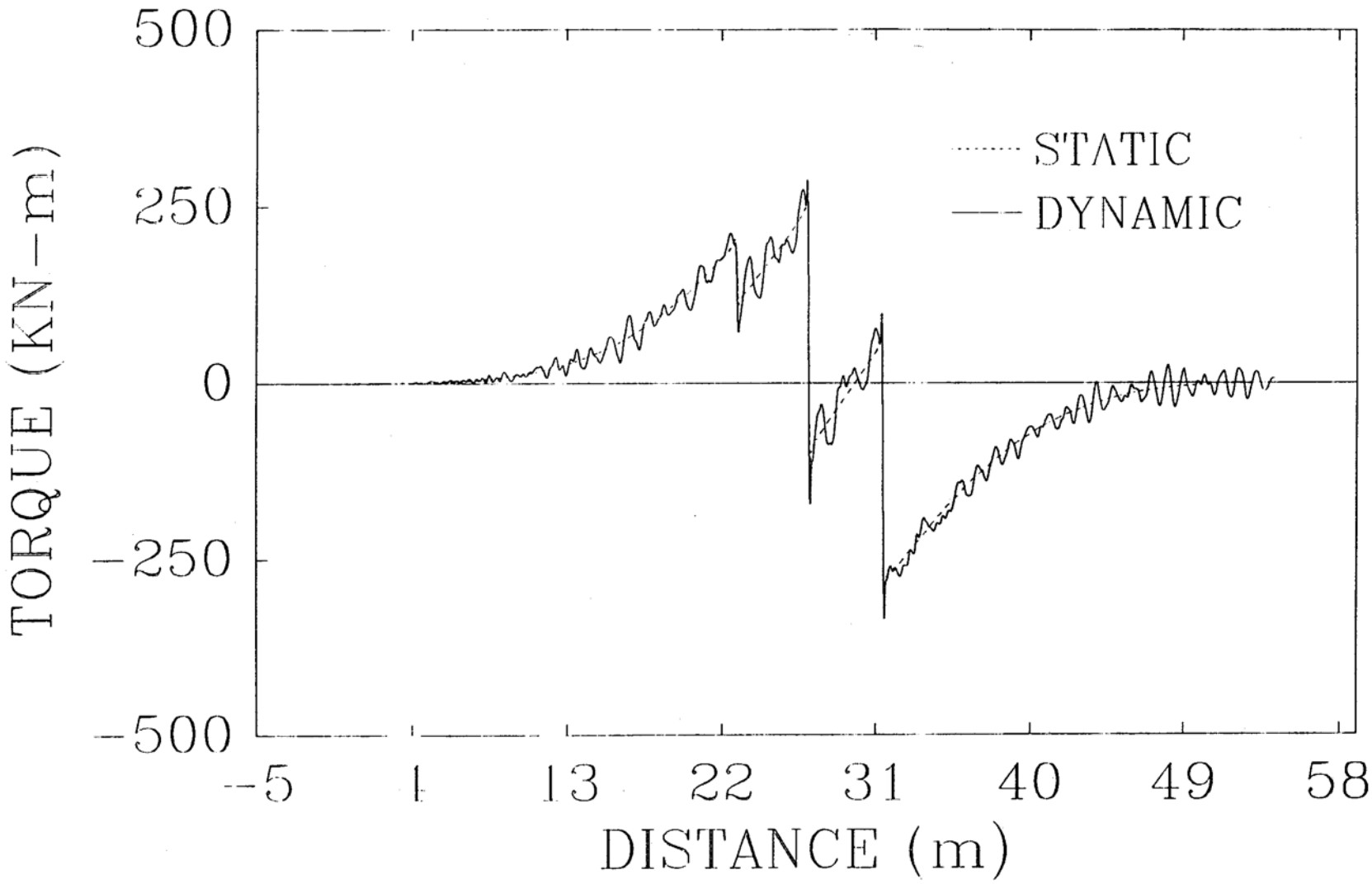

Fig. 3-58. Histories of Torque due to Distortion at Mid-span

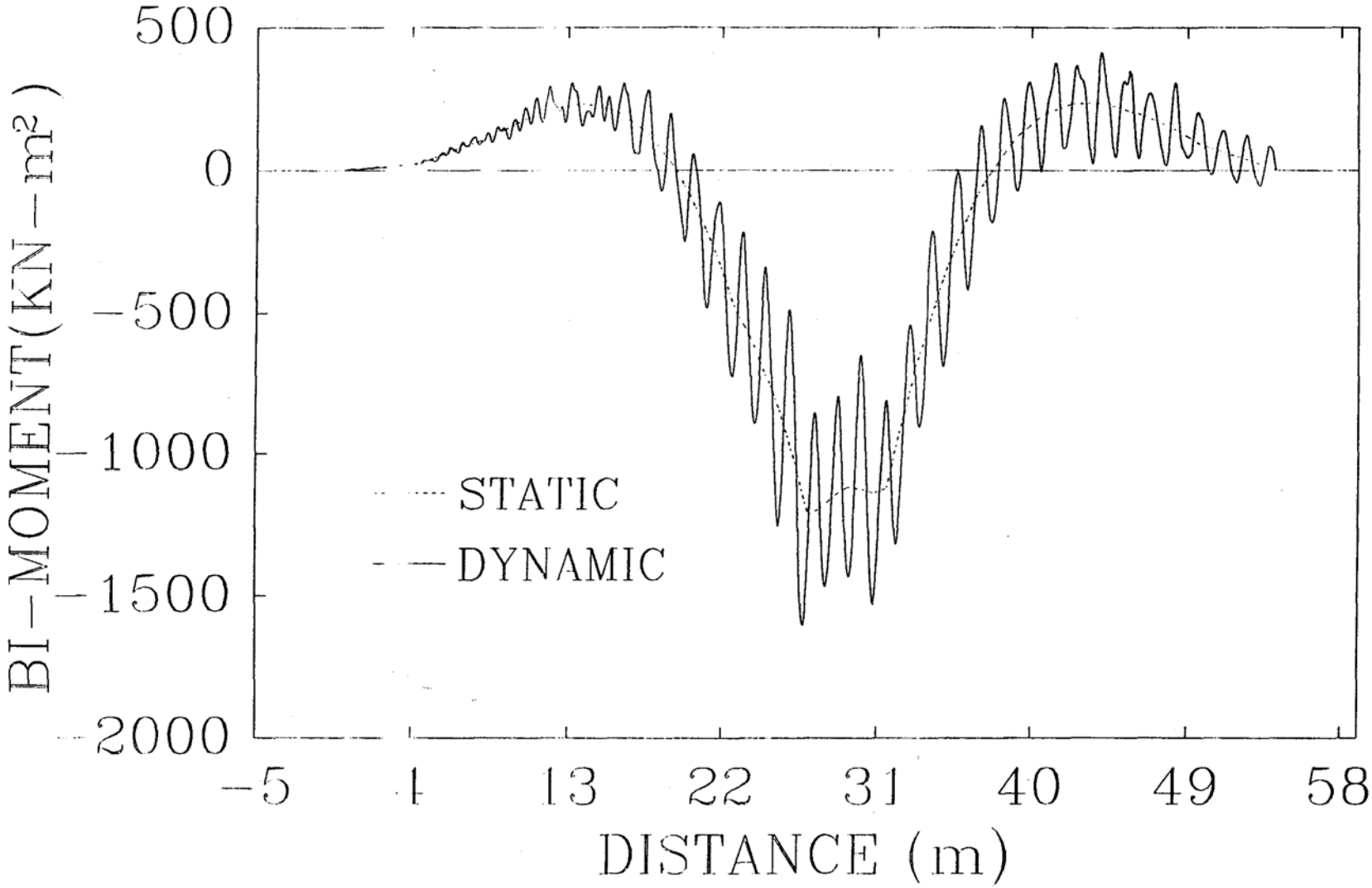

Fig. 3-59. Histories of Bi-moment due to Distortion at Mid-span

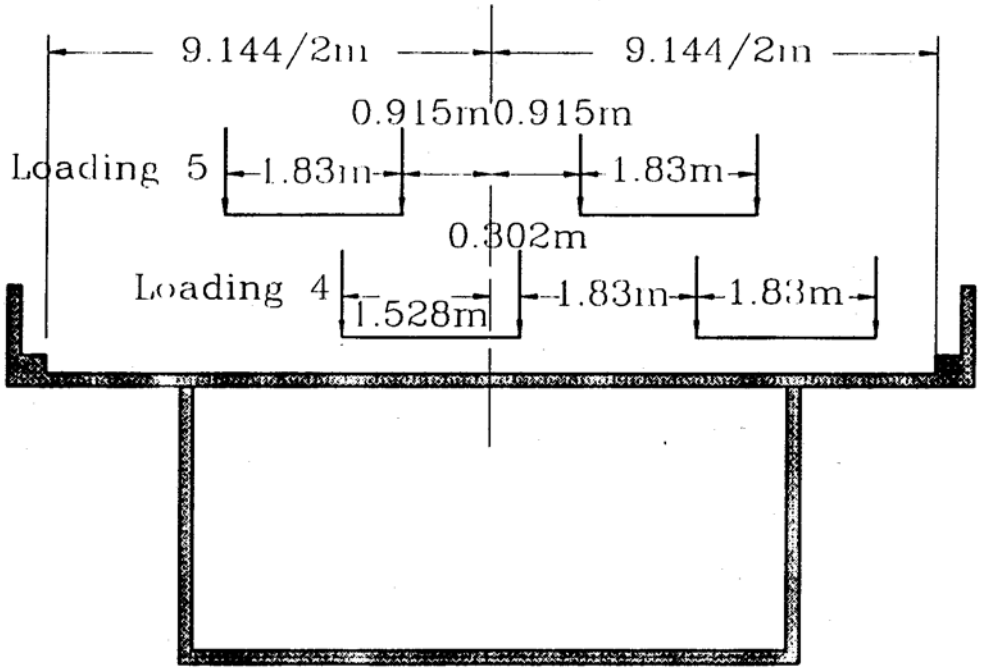

Fig. 3-60. Two-truck Loading Model

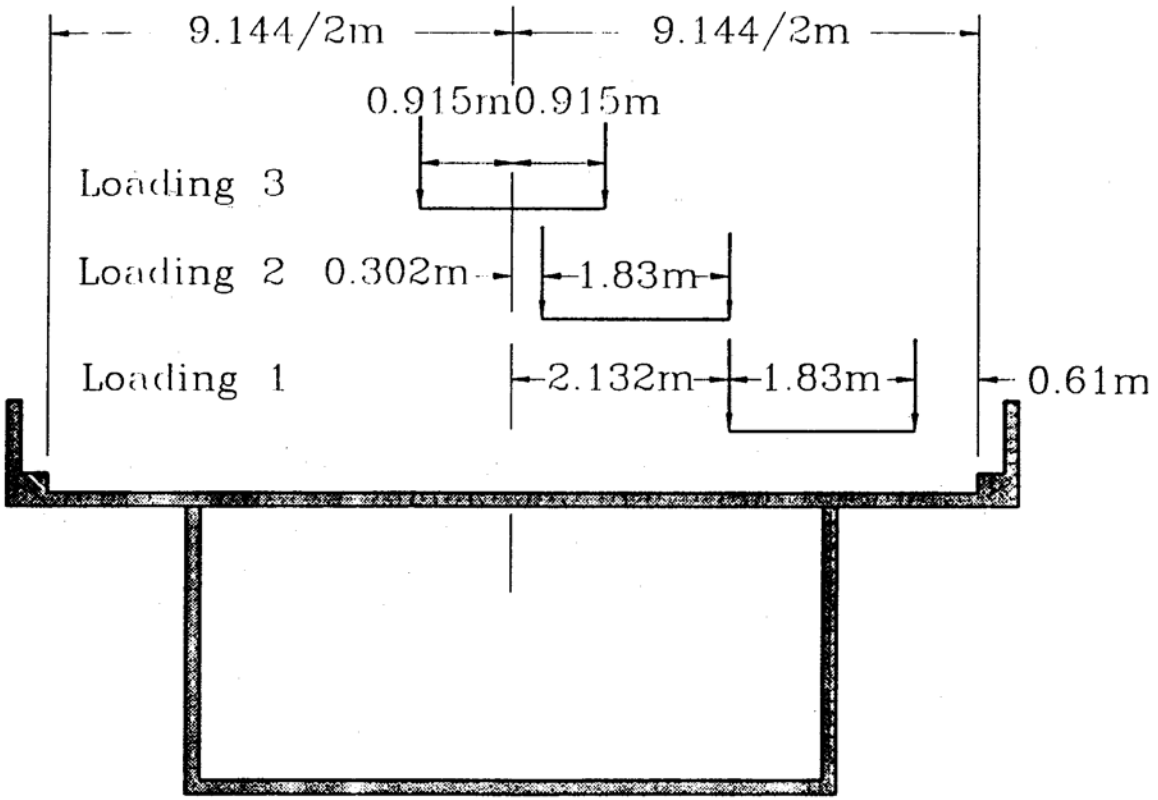

Fig. 3-61. One-truck Loading Model

in which R_d. and R,. = the absolute maximum dynamic and static responses, respectively. The results listed in Tables 3-2 and 3-3 are determined according to average road surface and 72.405 km/hr. (45 mph).

From Tables 3-2 and 3-3, it can be inferred that: (1) The change of transverse loading position has little effect on the impact of vertical bending moment; (2) The impact of torque and bi-moment will be significantly affected by transverse loading positions, especially for bi-moment; that is the smaller the static response, the larger the impact will be. Table 3-2 also gives the response of two-truck loadings (see Fig.3-60, Loadings 4 and 5). It can be seen from this table that the number of loading vehicle has significant influence on the impact. Generally, the impact of vertical bending moment will decrease with increasing the number of loading vehicles. For the presented bridge, it is reasonable to choose Loading 1 and Loading 4 to calculate the impact factors of torque and bending moment/bi-moment, respectively, because these two Loadings control the design for shear and normal stress.

Table 3-4 demonstrates the effect of damping ratio. The results shown in Table 3-4 are determined based on average road surface roughness, vehicle speed of 72.405 km/hr(45 mph). and Loading 4 (see Fig.6-60). Table 3-4 expresses that damping greatly decreases the dynamic response of torsion and distortion by damping out the effect of high vibration modes.

The effect of diaphragms can be seen from Tables 3-5 and 3-6 which shows the impact factors at mid-span evaluated according to average road surface roughness, vehicle speed of 72.405 km/hr (45 mph), and Loading 4, for three cases. Case I is the original design of the

Table 3-2. Influence of Loading Cases - Static Response

Loading Cases	M_x x 10^3 kN-m	$T_{c\omega}$ x 10^2 kN-m	B_ω x 10^2 kN-m^2	$T_{\tilde{\omega}}$ x10^2 kN-m	$B_{\tilde{\omega}}$ x 10^3 kN-m^2	D_y cm	θ x10^{-5} rad.	$\tilde{\theta}$ x10^{-5} rad.
1	3.276	4.327	8.638	-3.638	-1.550	0.184	3.92	-5.58
2	3.276	1.740	3.444	-1.457	0.620	0.184	1.57	-2.23
3	3.276	N/A	N/A	N/A	N/A	0.184	N/A	N/A
4	6.564	3.468	6.915	-2.869	-1.240	0.368	3.13	-4.46
5	6.564	N/A	N/A	N/A	N/A	0.368	N/A	N/A

Table 3-3. Influence of Loading Cases - Dynamic Response

Loading Cases	Impact Factors (%)							
	M_x	$T_{c\omega}$	B_ω	$T_{\tilde{\omega}}$	$B_{\tilde{\omega}}$	D_y	θ	$\tilde{\theta}$
1	8.77	6.06	17.9	7.37	21.0	10.2	64.9	66.7
2	8.33	8.52	33.2	10.8	35.9	9.64	93.6	96.2
3	9.19	N/A	N/A	N/A	N/A	10.9	N/A	N/A
4	7.13	5.55	27.1	7.30	29.7	8.53	80.2	82.5
5	6.99	N/A	N/A	N/A	N/A	8.48	N/A	N/A

Table 3-4. Influence of Damping Ratio

Damping Ratio	Impact Factors (%)							
	M_x	$T_{c\omega}$	B_ω	$T_{\tilde{\omega}}$	$B_{\tilde{\omega}}$	D_y	θ	$\tilde{\theta}$
0	9.25	20.90	43.5	32.80	49.0	9.09	123.0	129.0
1	7.13	5.55	27.1	7.30	29.7	8.53	80.2	82.5
2	6.33	2.76	18.9	3.32	20.9	8.04	58.8	59.8
4	4.93	1.57	10.5	1.78	12.0	7.02	36.6	36.7

Table 3-5. Influence of Distortional Rigidity of Diaphragms - Static Response

Diaphr. Cases	M_x x 10^3 kN-m	$T_{c\omega}$ x 10^1 kN-m	B_ω x 10^2 kN-m^2	$T_{\bar{\omega}}$ x10^2 kN-m	$B_{\bar{\omega}}$ x 10^3 kN-m^2	D_y cm	θ x 10^{-5} rad.	θ x 10^{-5} rad.
1	6.564	3.468	6.915	-2.869	-1.240	0.368	3.13	-4.46
2	6.564	3.615	7.375	-2.926	-1.389	0.368	5.93	-4.84
3	6.564	3.740	8.666	-2.937	-1.791	0.368	13.4	-5.84

Table 3-6. Influence of Distortional Rigidity of Diaphragms - Dynamic Response

Diaphr. Cases	Impact Factors (%)							
	M_x	$T_{c\omega}$	B_ω	$T_{\tilde{\omega}}$	$B_{\tilde{\omega}}$	D_y	θ	$\tilde{\theta}$
1	7.13	5.55	27.1	7.30	29.7	8.53	80.2	82.5
2	6.94	7.63	12.2	0.31	11.4	8.54	28.4	22.4
3	6.47	6.29	6.21	-0.40	4.5	8.22	21.3	15.7

bridge with two end diaphragms. In Case II, the distortional rigidity of the two end diaphragms of the bridge is reduced by 0.1 times. No diaphragm is considered in Case III. From Tables 3-5 and 3-6, we can observe that with decreasing distortional rigidity of diaphragms, the static responses of torsion and distortion increase, while the impact factors decrease.

Figs. 3-62 to 3-67 demonstrates the variation of impact factor at mid-span with vehicle speeds. The curves of impact factor as a function of vehicle speed for moment and twist angle are shown in Figs. 3-62 to 3-67, respectively. Figs. 3-63 and 3-64 present the variation of impact factors with vehicle speeds for torsional moment and distortional moment, separately. The variation of impact factors of bi-moment due to torsion and distortion is illustrated in Fig. 3-65 and 3-66, individually. It can be seen, from those figures, that: (1) Under the conditions of good or very good surface roughness, the variation of impact factor with vehicle speed is slight, and generally the maximum impact factors for inner forces are less than 10%; (2) With increasing road surface roughness, the impact factors increase rapidly, and high impact factors may be reached, especially for bi-moments whose dynamic responses are greatly influenced by high frequencies; (3) The impact factors of displacements are generally larger than those of inner forces, especially for angular displacements. Therefore, taking the impact factors of angular displacements as those of inner forces is not suitable in design practice.

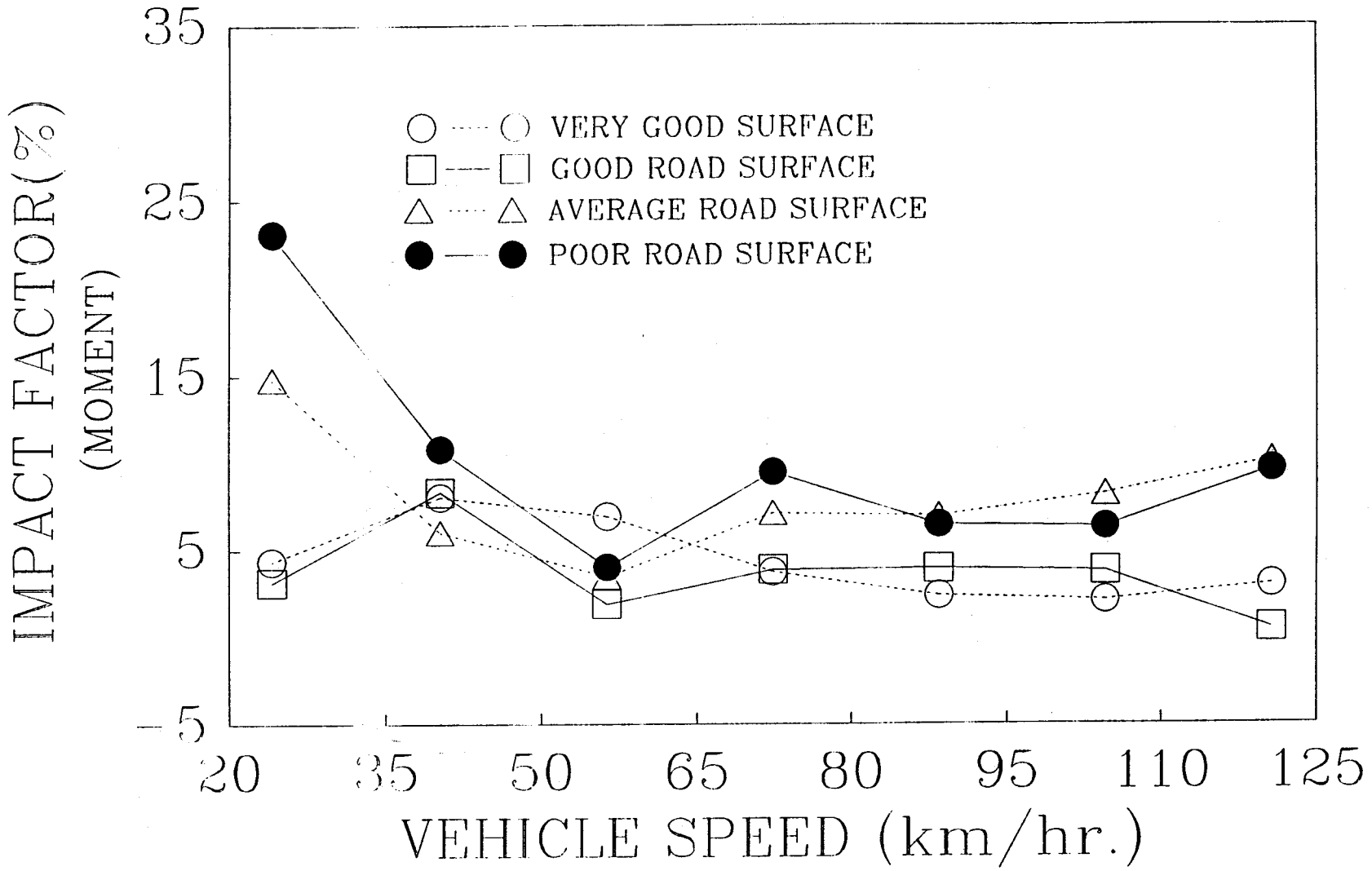

Fig. 3-62. Variation of Impact Factors of Vertical Moment at Mid-span with Vehicle Speeds

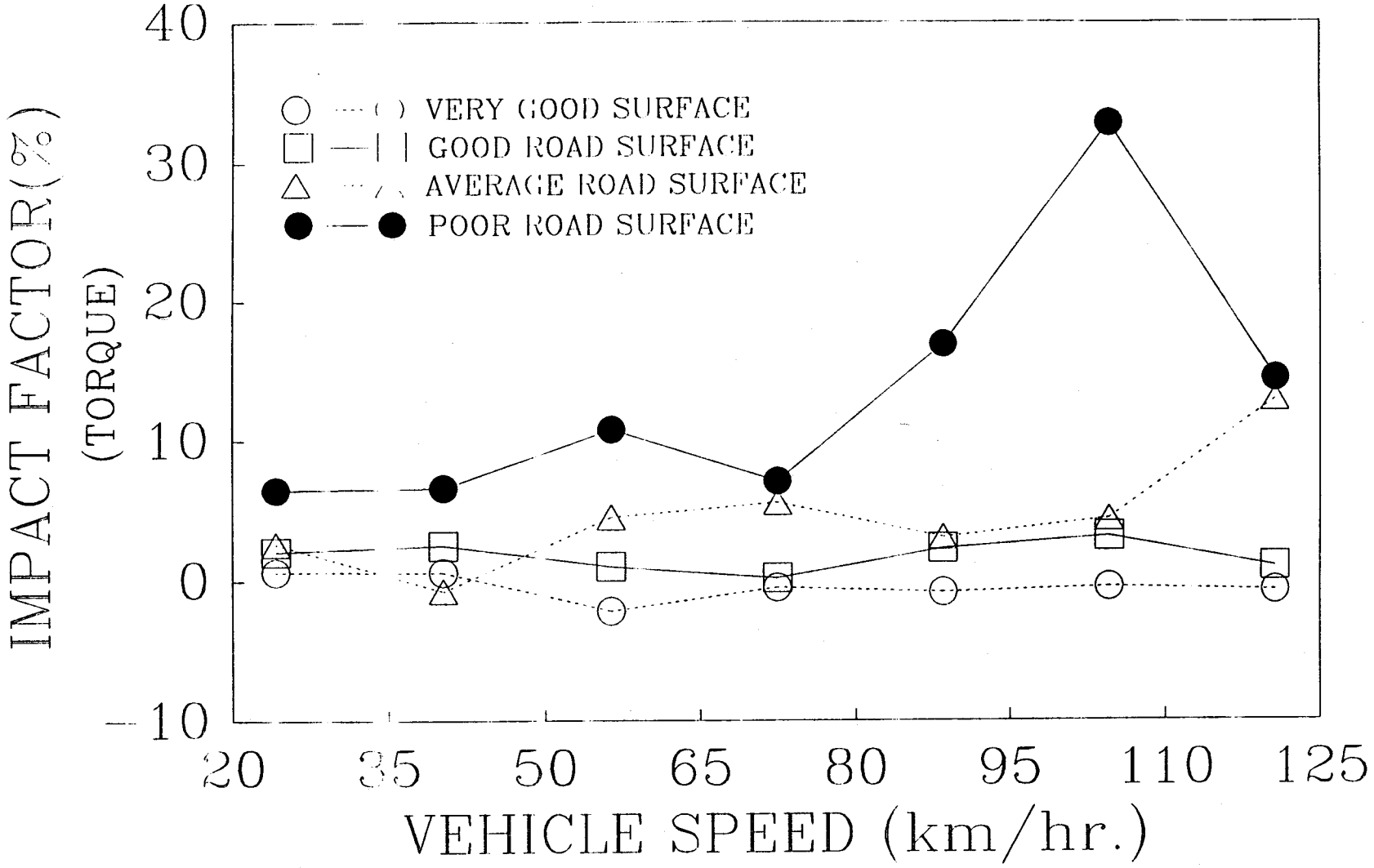

Fig. 3-63. Variation of Impact Factors of Torque at Mid-span with Vehicle Speeds

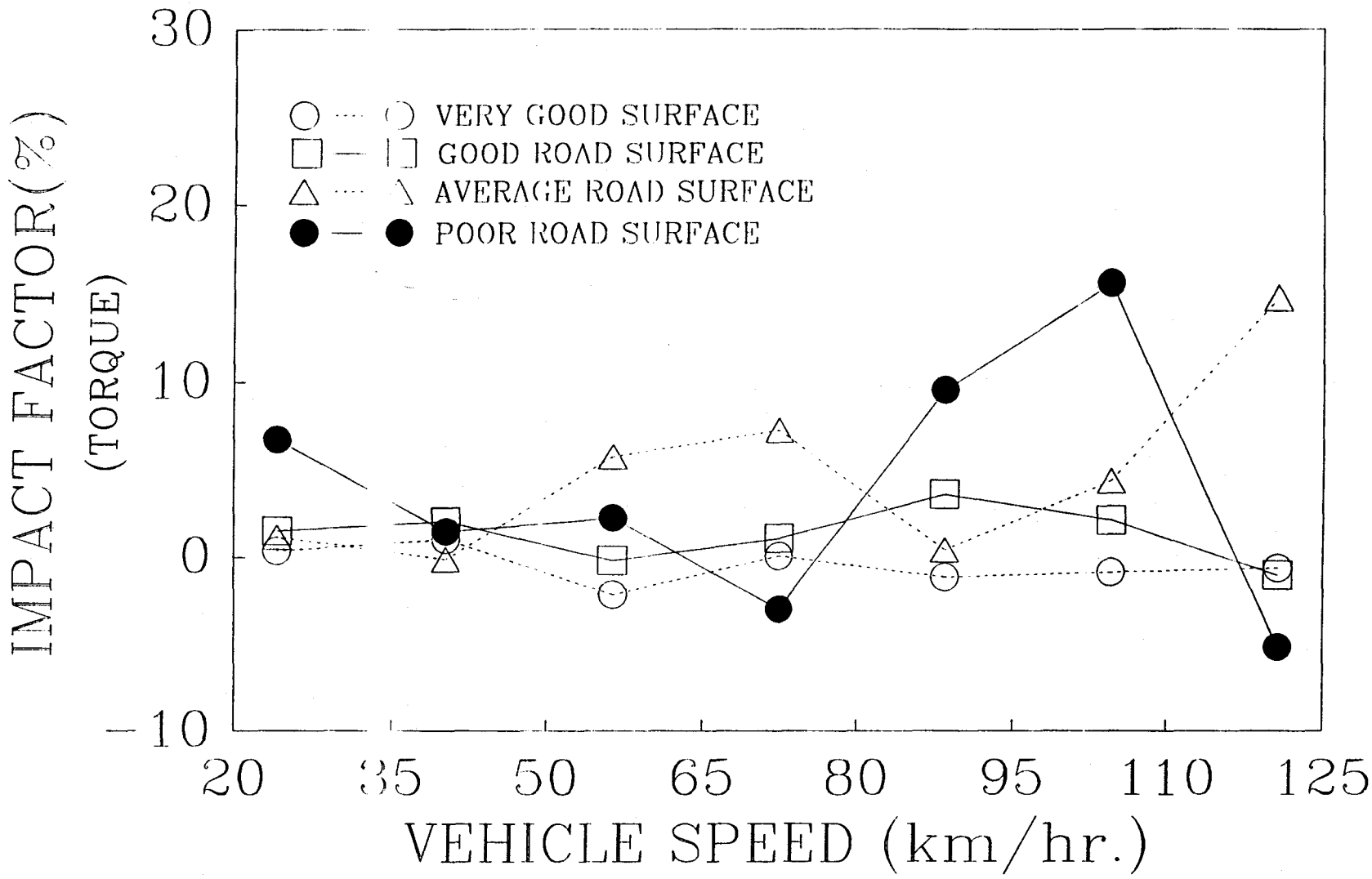

Fig. 3-64. Variation of Impact Factors of Torque due to Distortion at Mid-span with Vehicle Speeds

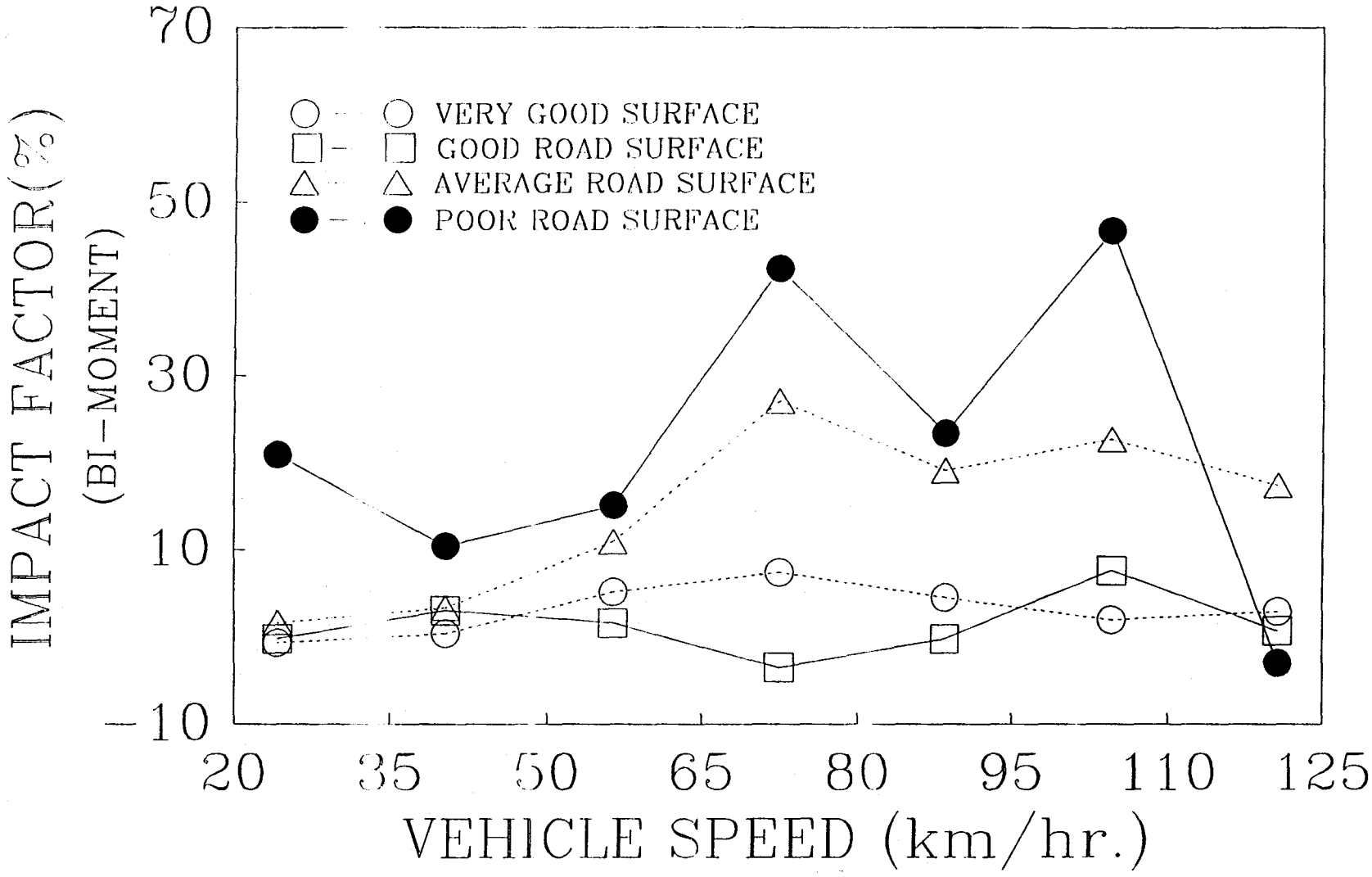

Fig. 3-65. Variation of Impact Factors of Bi-moment at Mid-span with Vehicle Speeds

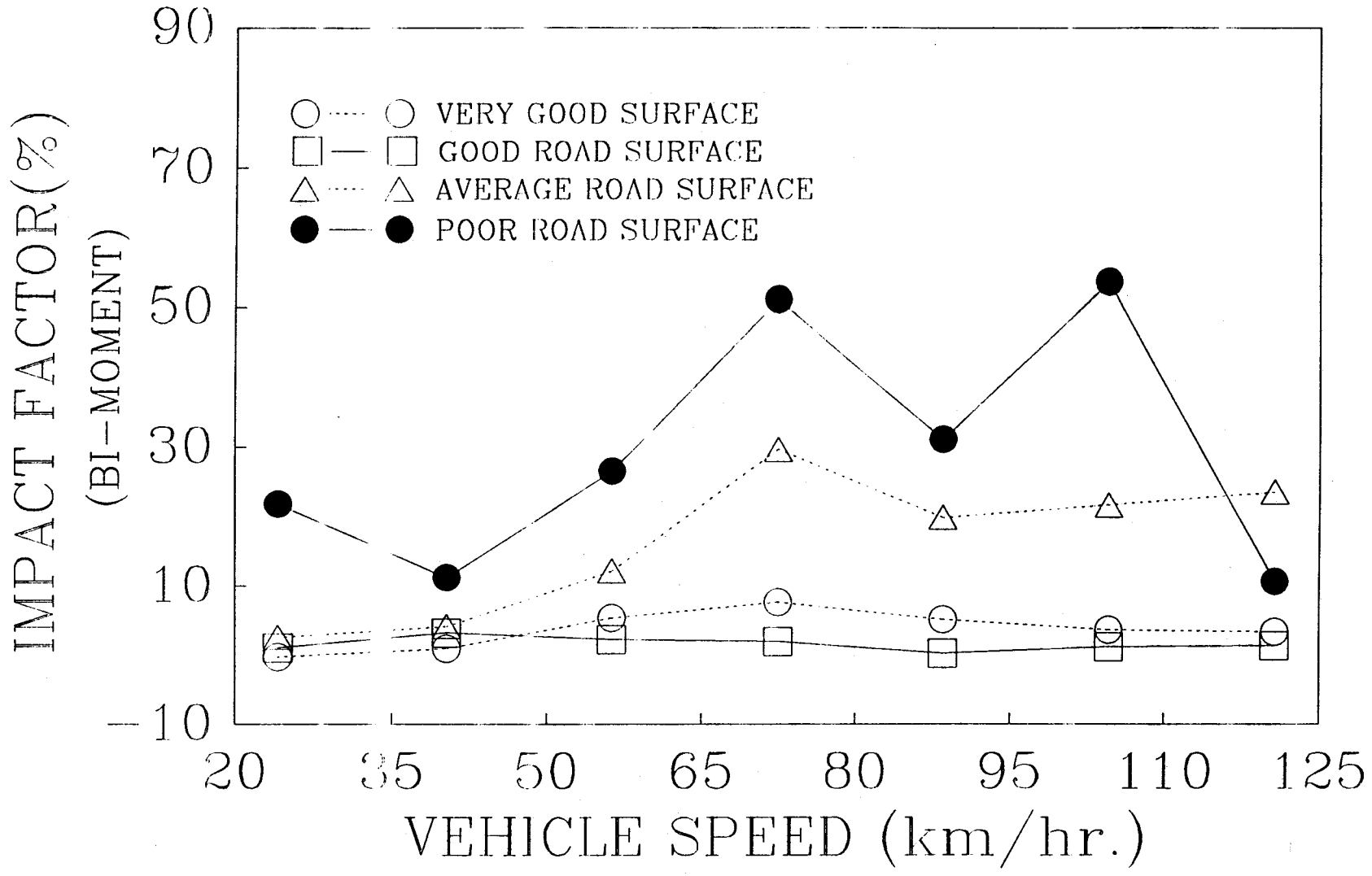

Fig. 3-66. Variation of Impact Factors of Bi-moment due to Distortion at Mid-span with Vehicle Speeds

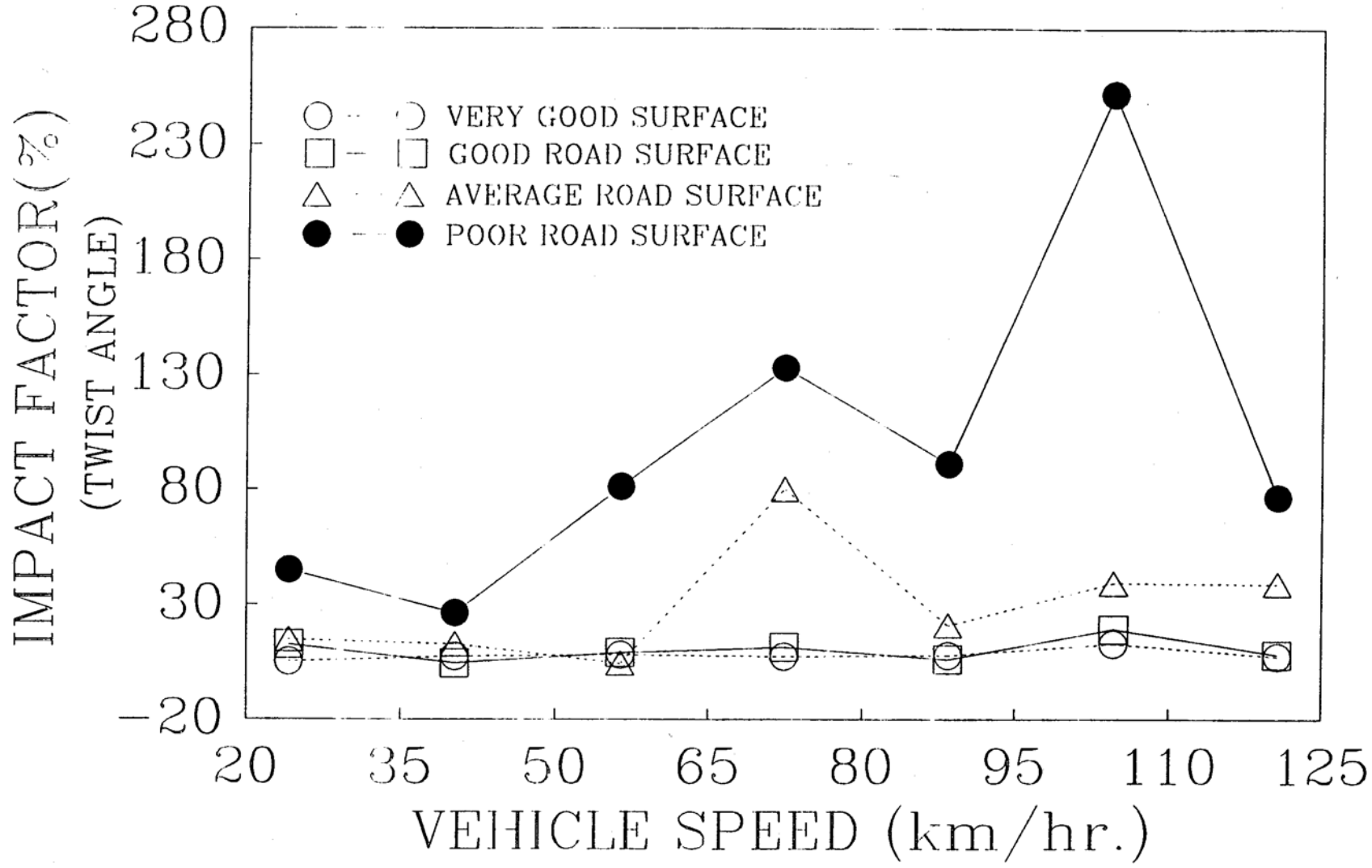

Fig. 3-67. Variation of Impact Factors of Torsional Angle at Mid-span with Vehicle Speeds

CHAPTER IV

DYNAMIC BEHAVIOR OF CONTINUOUS AND CANTILEVER BOX GIRDER BRIDGES

4.1. Introduction

The design and construction of continuous and cantilever thin-walled box girders in the recent decades have increased dramatically. Former investigations on this type of bridge emphasized the static behavior [15, 41]. However, little was known on the characteristics of bending and torsional vibration of the bridges, especially those caused by moving vehicles. Some valuable research work has been conducted on the subject of dynamic response of continuous and cantilever beam bridges. Fleming and Romnaidi [11] studied the dynamic response of the three-span continuous beams by modeling the vehicle as a single sprung mass and bridge as a system of concentrated masses. Veletsos and Huang [53] presented a successful numerical approach for evaluating the response of continuous.and cantilever beam bridges. In that study, the bridge was idealized as a single beam, the distributed mass as a number of masses, and vehicle as a planar model. Wen and Toridis [60] treated the vehicle as a moving force of constant magnitude and performed numerous investigations on three-span cantilever bridges. Wu and Dai [62] used a transfer matrix method to predicate the free and forced vibration behaviors of multi-span nonuniform beam due to moving loads. Recently, a comprehensive study on multigirder continuous bridges was reported by Huang, et al [19]. In that study, the emphasis was on the impact of I-beam bridges. In all previous studies, no consideration of bending and torsional vibration of box girder bridges was given. Also, authors

used one vehicle loading in longitudinal direction, which may not reflect the real practice of continuous and cantilever bridges. Moreover, there is little information available concerning the comparison of dynamic characteristics among continuous and different types of cantilever bridges, under the conditions of different road profiles, vehicle speeds, and others.

The objective of this chapter is to investigate the dynamic characteristics and impact of continuous and cantilever box girder bridges with different vehicle models, road surface roughnesses, as well as vehicle speeds. In this study, the bridge model, road surface roughness, and vehicle model are same as those described in Chapter III. Multi-truck loading is considered in both transverse and longitudinal directions of the bridge. The results obtained in this study are significant for both practical bridge design and further theoretical study of continuous and cantilever box girder bridges.

4.2. Description of analytical bridges

Three analytical box girder bridges, which are designed based on the study of Heins and Lawrie [15] and AASHTO specifications [49], are shown in Fig 4-1. Fig. 4-1 (a) is a single-cell box girder continuous three-span structure with a center span of 76.17 m (249.91 ft) and end spans of 37.63 m (123.45 ft). The variable-depth girder is 4.572 m (15 ft) at the inner supports and 2.438 in (8 ft) at the sections 10.262 m (33.669 ft) from the inner supports to midspan and end supports. The single-cell trapezoidal box is 7.518 m (24.667 ft) wide at the top with the top cantilevering on each side of 2.718 m (8.917 ft). The top flange or deck is of constant dimension both longitudinally and transversely. The bottom flange is of constant dimension

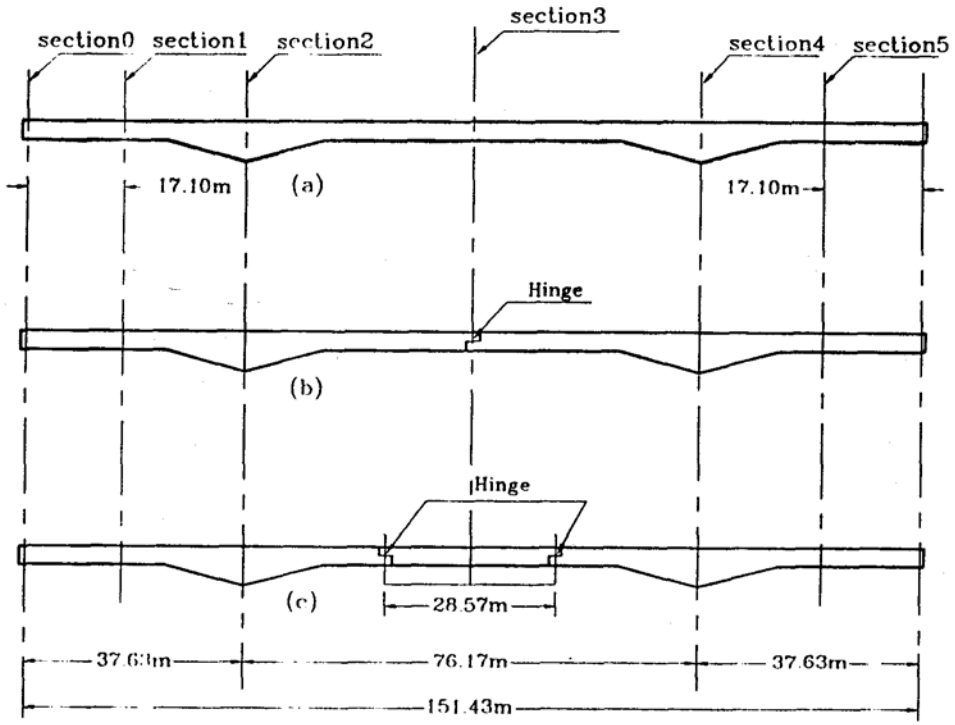

Fig. 4-1. Analytical Bridges: (a) Bridge Type I, (b) Bridge Type II, (c) Bridge Type III

transversely but varies in longitudinal direction from 0.457 m (1.5 ft) thick at inner supports to 0.229 m (0.75 ft) at the sections 10.262 m (33.669 ft) from the inner supports. The webs have a gradient of 1:4 and constant thickness of 0.406 m (1.333 ft). The typical sections are shown in Fig. 4-2. A diaphragm of 22.86 cm (9 in.) thick is added at the cross section over each support.

Fig. 4-1 (b) and (c) show two common types of cantilever box girder bridges with the dimension as that illustrated in Fig. 4-1 (a). The cantilever bridge shown in Fig. 4-1 (b) has one hinge at midspan. The one presented in Fig. 4-1 (c) has two hinges at center span. The suspended span length is 27.699 m (90.876 ft). It is assumed that the deflections, angles of torsion, and angles of distortion on both sides of each hinge are compatible. All the crosssections at hinges have diaphragms.

4.3. Characteristics of free vibration

The first eleven frequencies and their corresponding vibration mode shapes of the bridges shown in Fig. 4-1 are demonstrated in Figs. 4-3 to 4-46. Figs. 4-3 to 4-24 show the vibration modes of the continuous girder bridges with and without diaphragms at sections over supports. The vibration modes of cantilever box girder bridges with one and two hinges are illustrated in Figs. 4-25 to 4-46. It can be seen from Figs. 4-3 to 4-46 that: (1) The lowest first frequency among the three types of bridges occurs in Bridge Type II (see Fig. 4-1 (b)), while the lowest second frequency of those bridges is found in Bridge Type III, and (2) the torsional frequencies for the three different types of bridges have little difference because of the diaphragms added

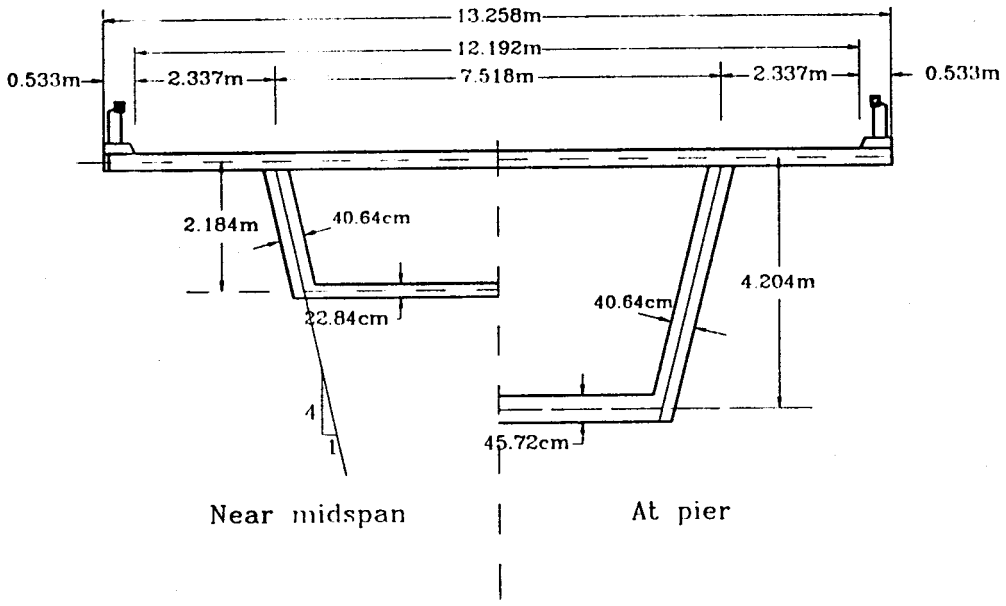
13.258m
12.192m
0.533m
2.337m
7.518m
2.337m
0.533m
2.184m
40.64cm
22.84cm
4
1
40.64cm
4.204m
45.72cm
Near midspan
At pier

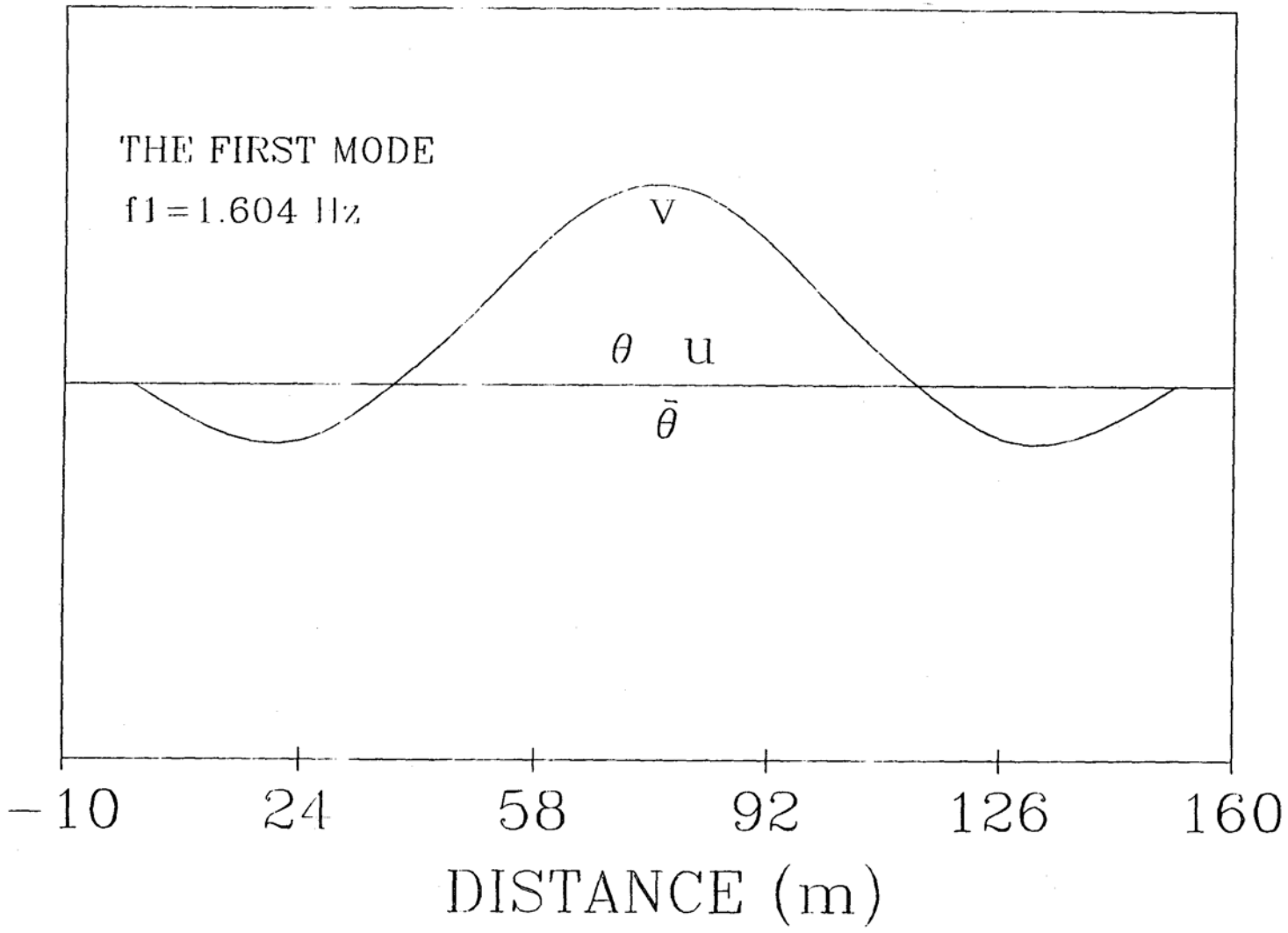

Fig. 4-3. The First Vibration Mode of the Continuous Bridge

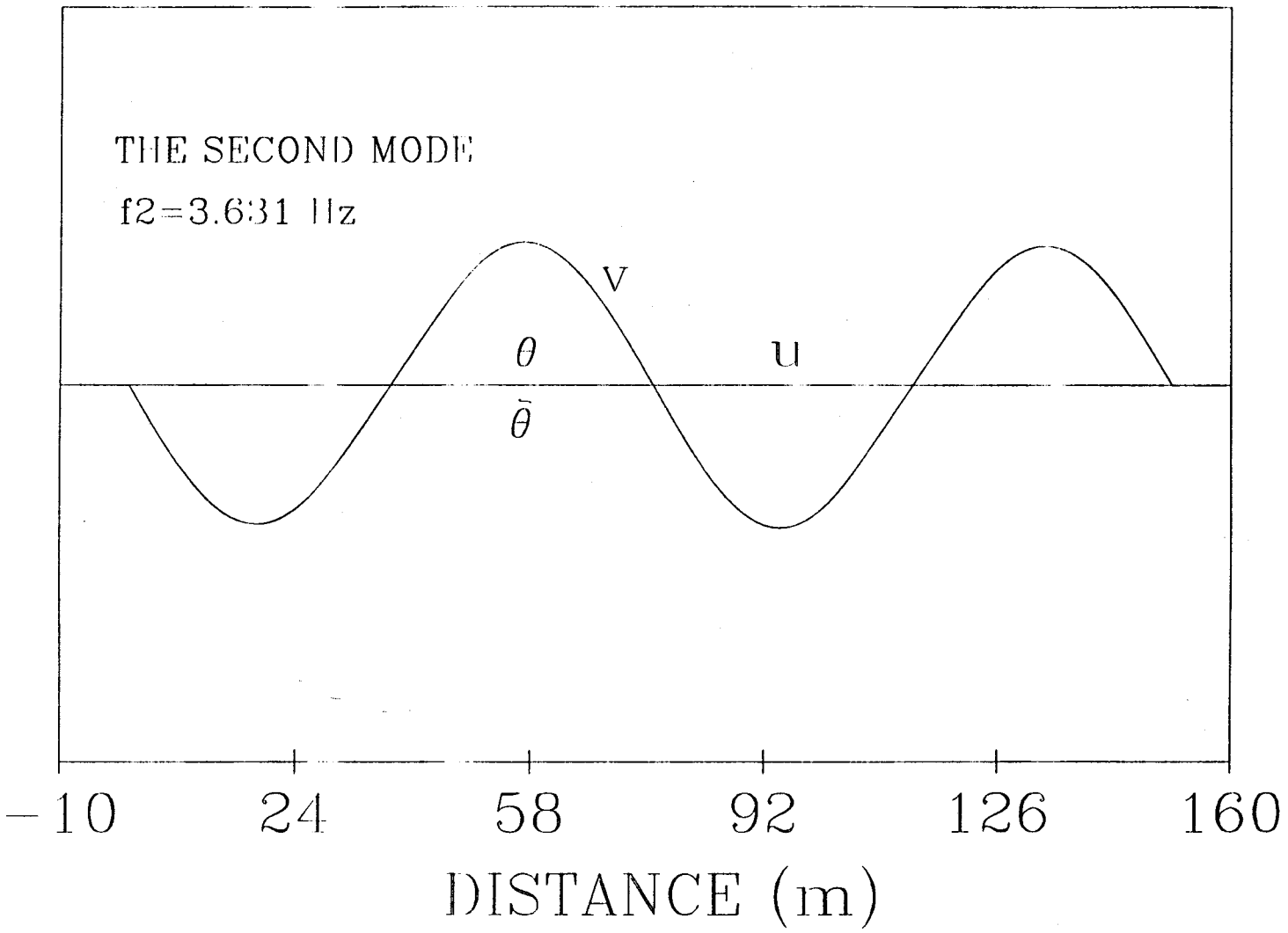

Fig. 4-4. The Second Vibration Mode of the Continuous Bridge

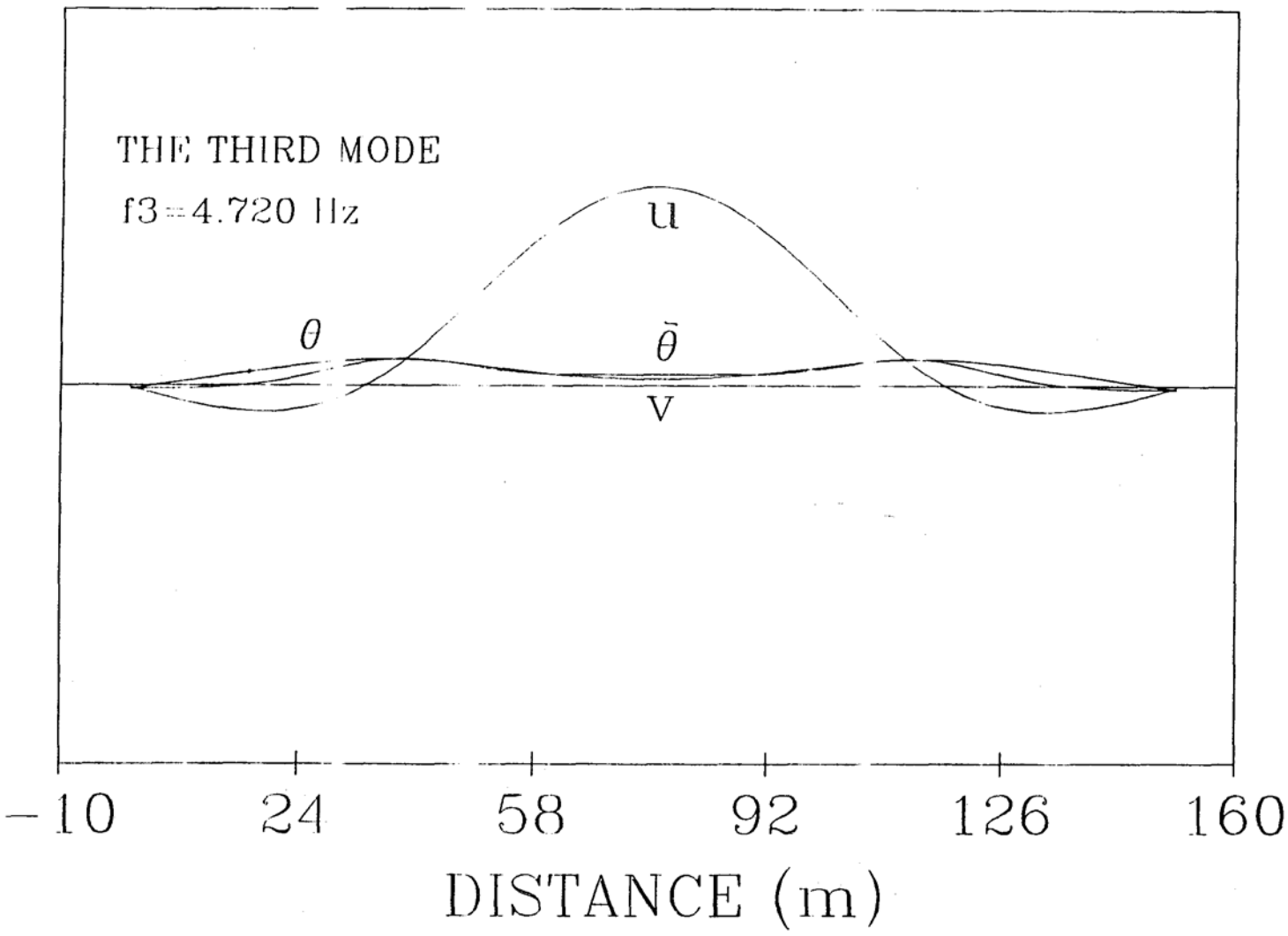

Fig. 4-5. The Third Vibration Mode of the Continuous Bridge

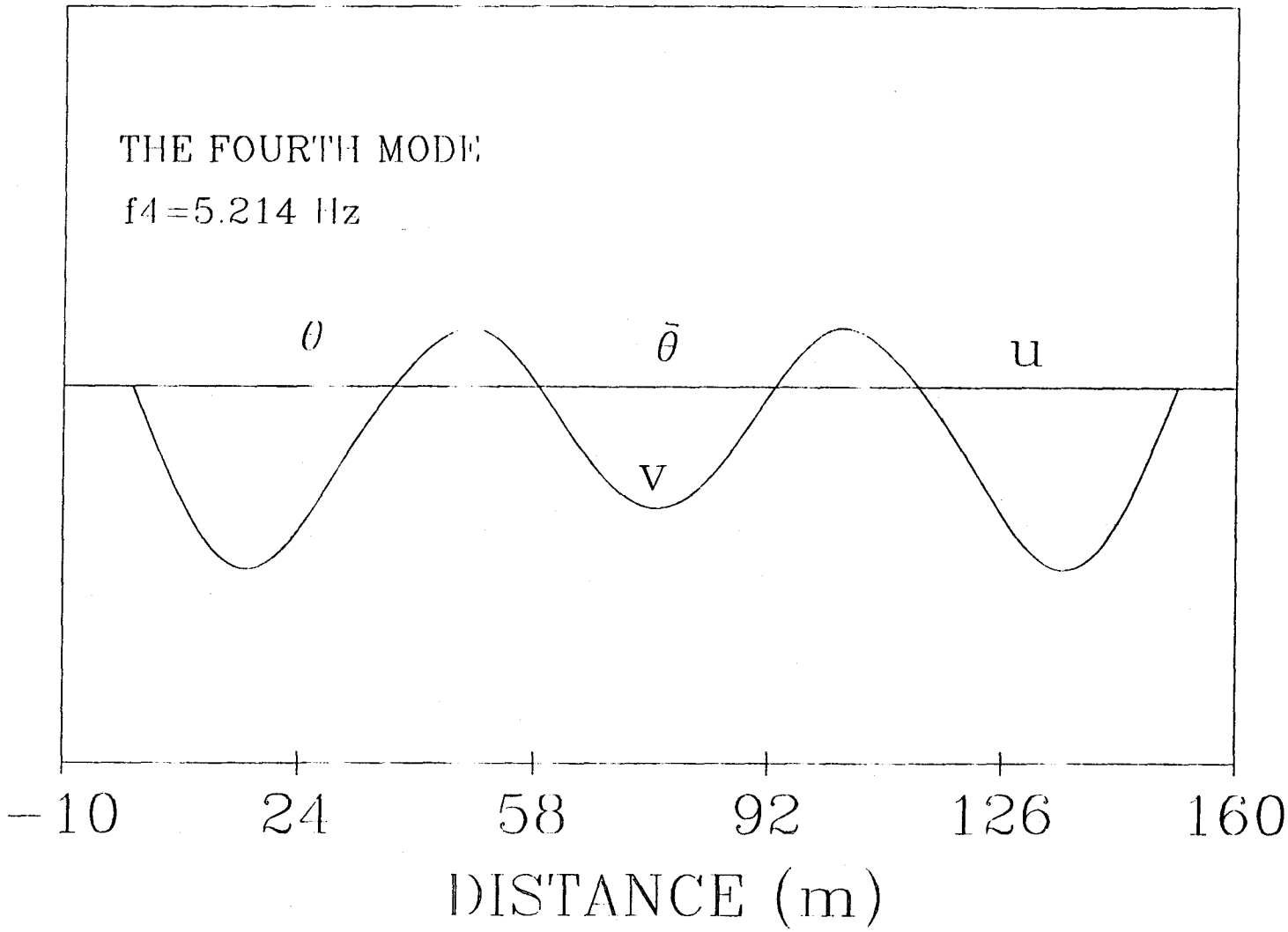

Fig. 4-6. The Fourth Vibration Mode of the Continuous Bridge

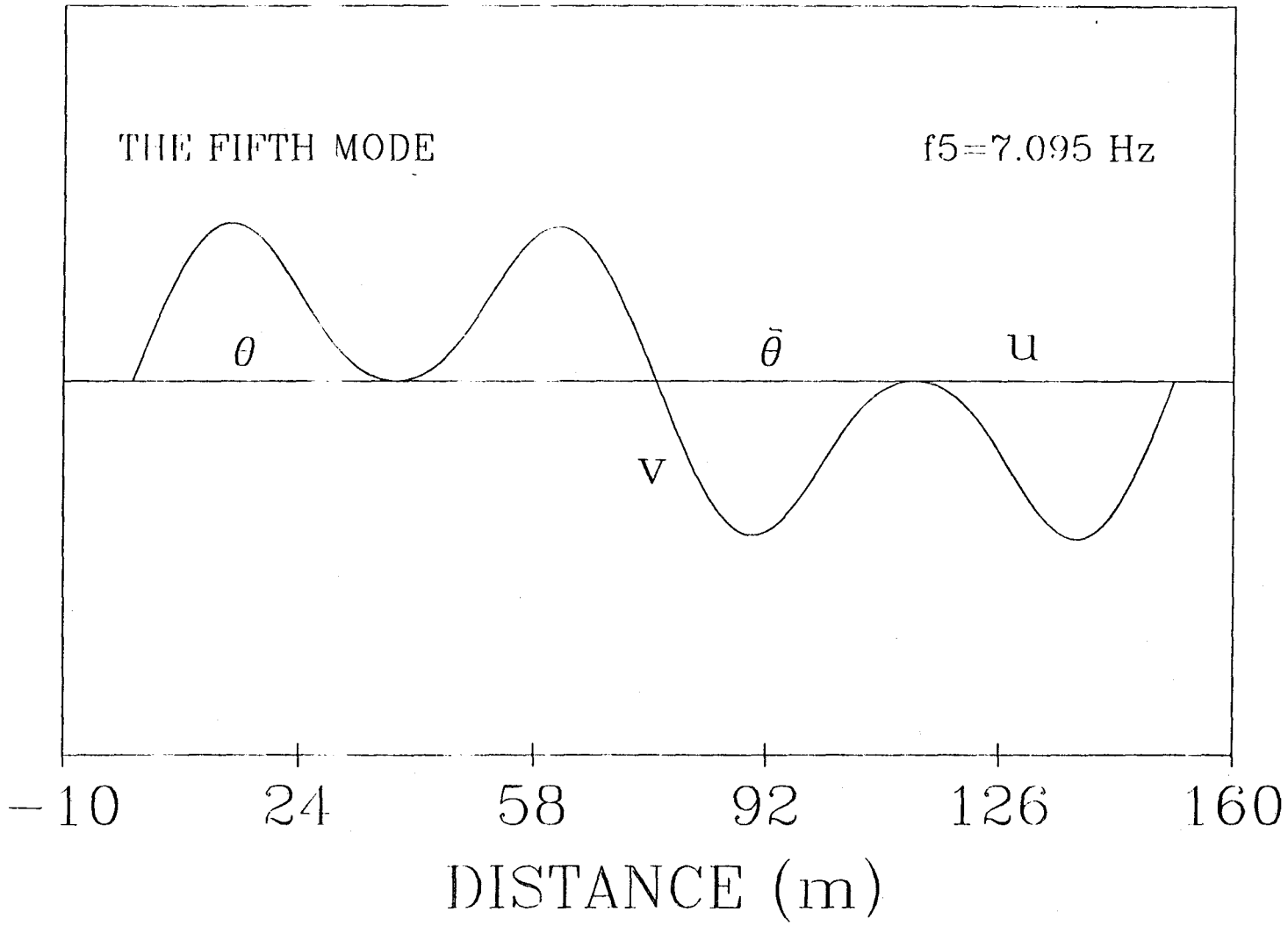

Fig. 4-7. The Fifth Vibration Mode of the Continuous Bridge

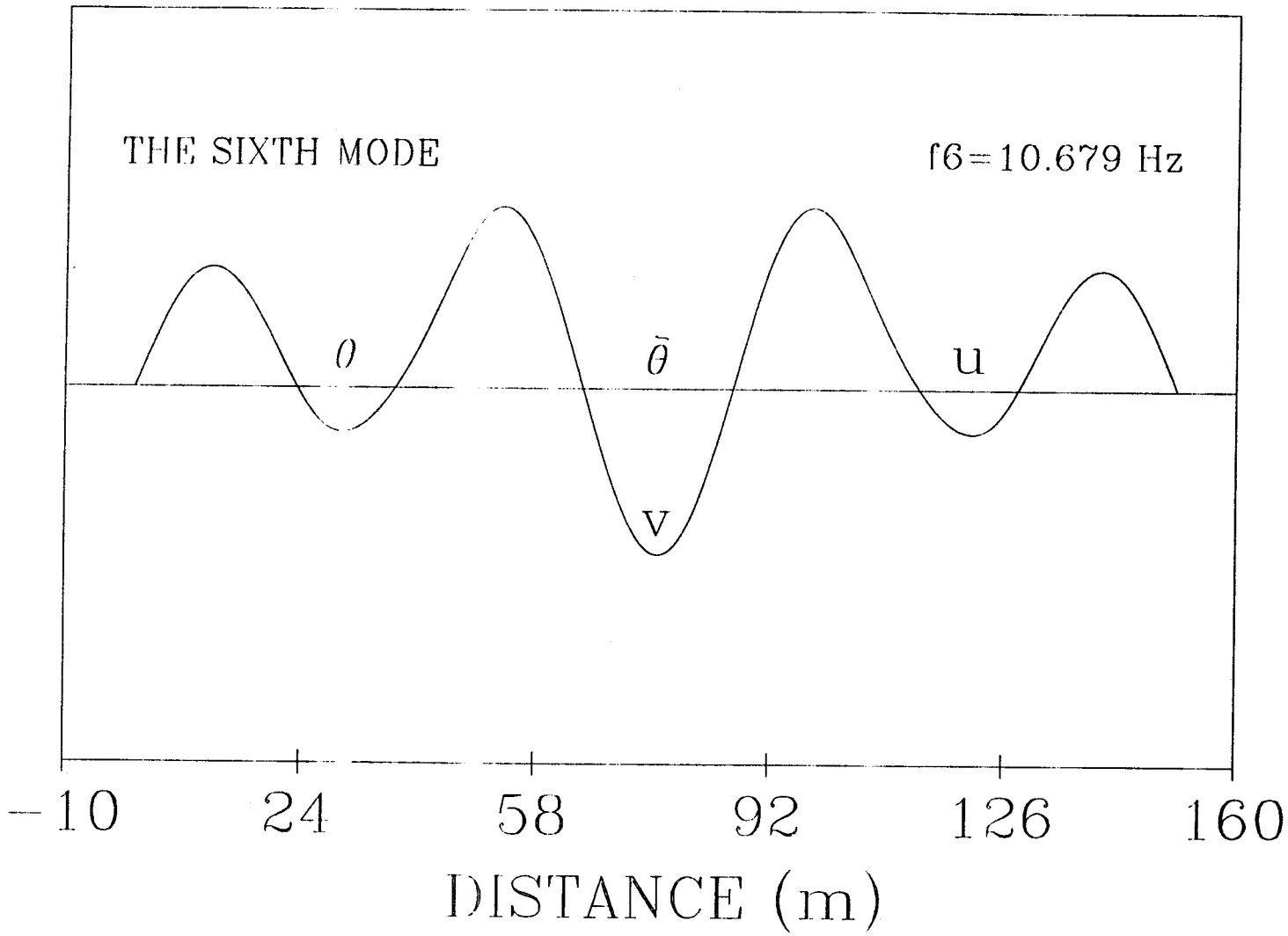

Fig. 4-8. The Sixth Vibration Mode of the Continuous Bridge

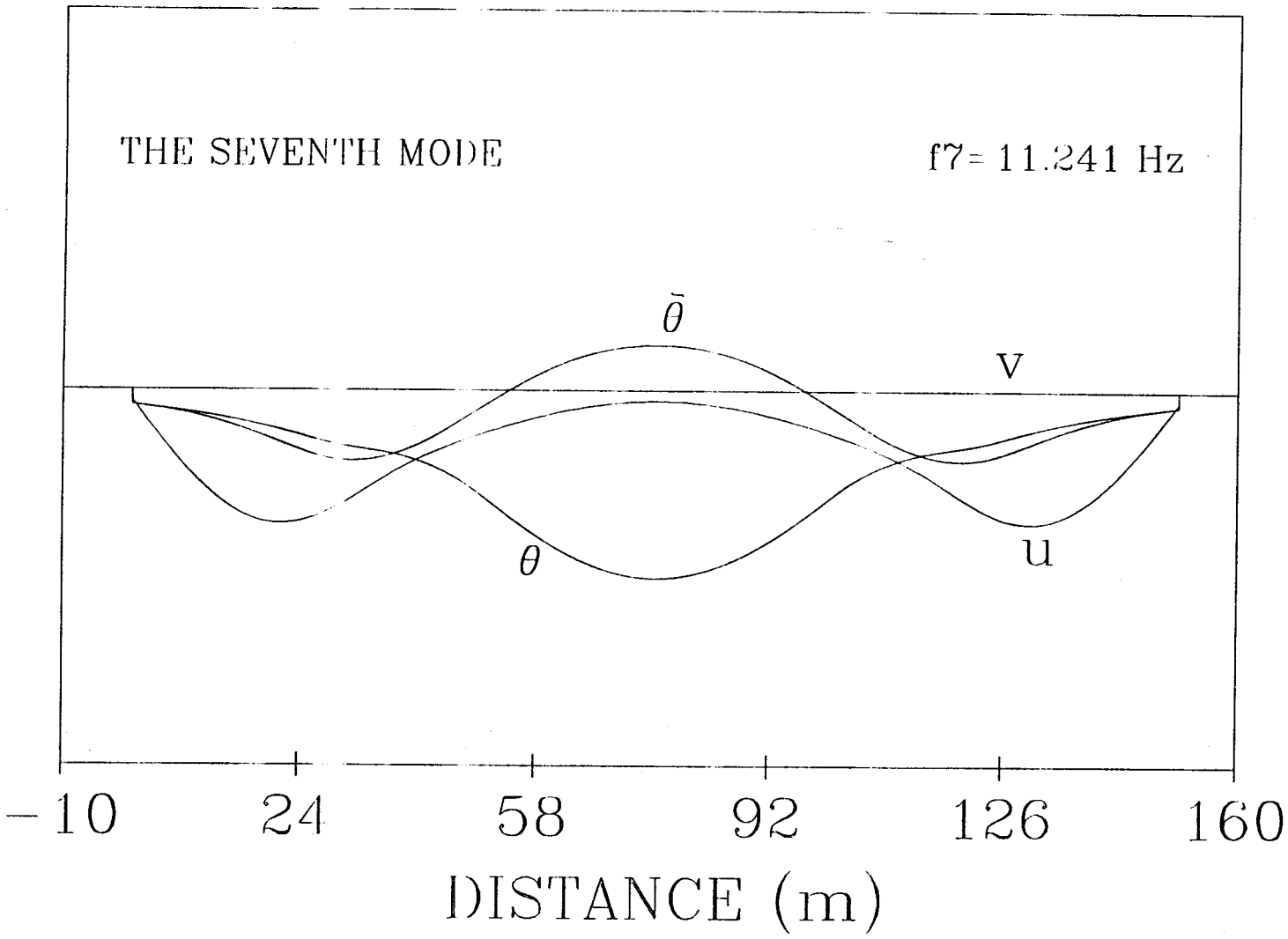

Fig. 4-9. The Seventh Vibration Mode of the Continuous Bridge

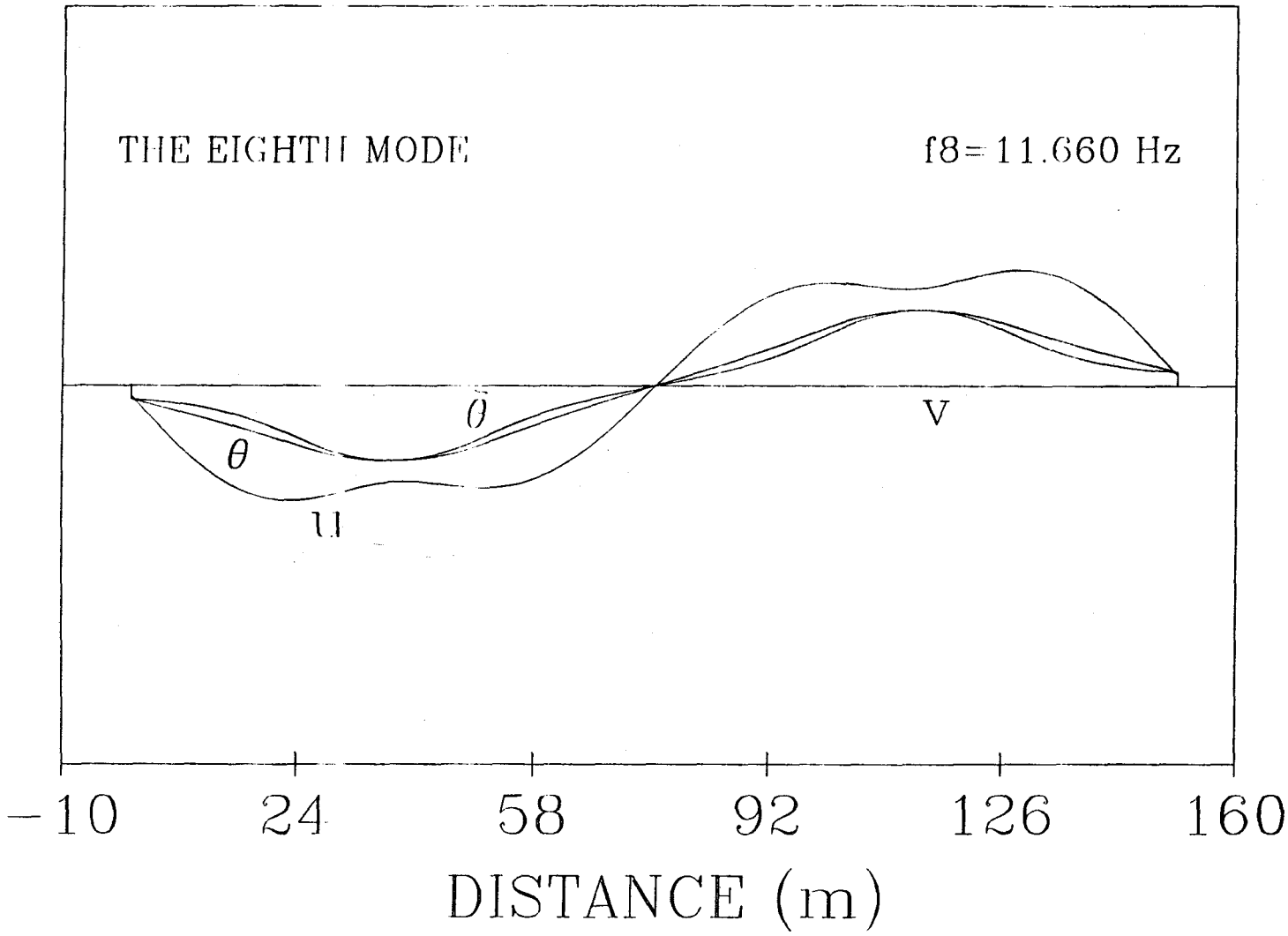

Fig. 4-10. The Eighth Vibration Mode of the Continuous Bridge

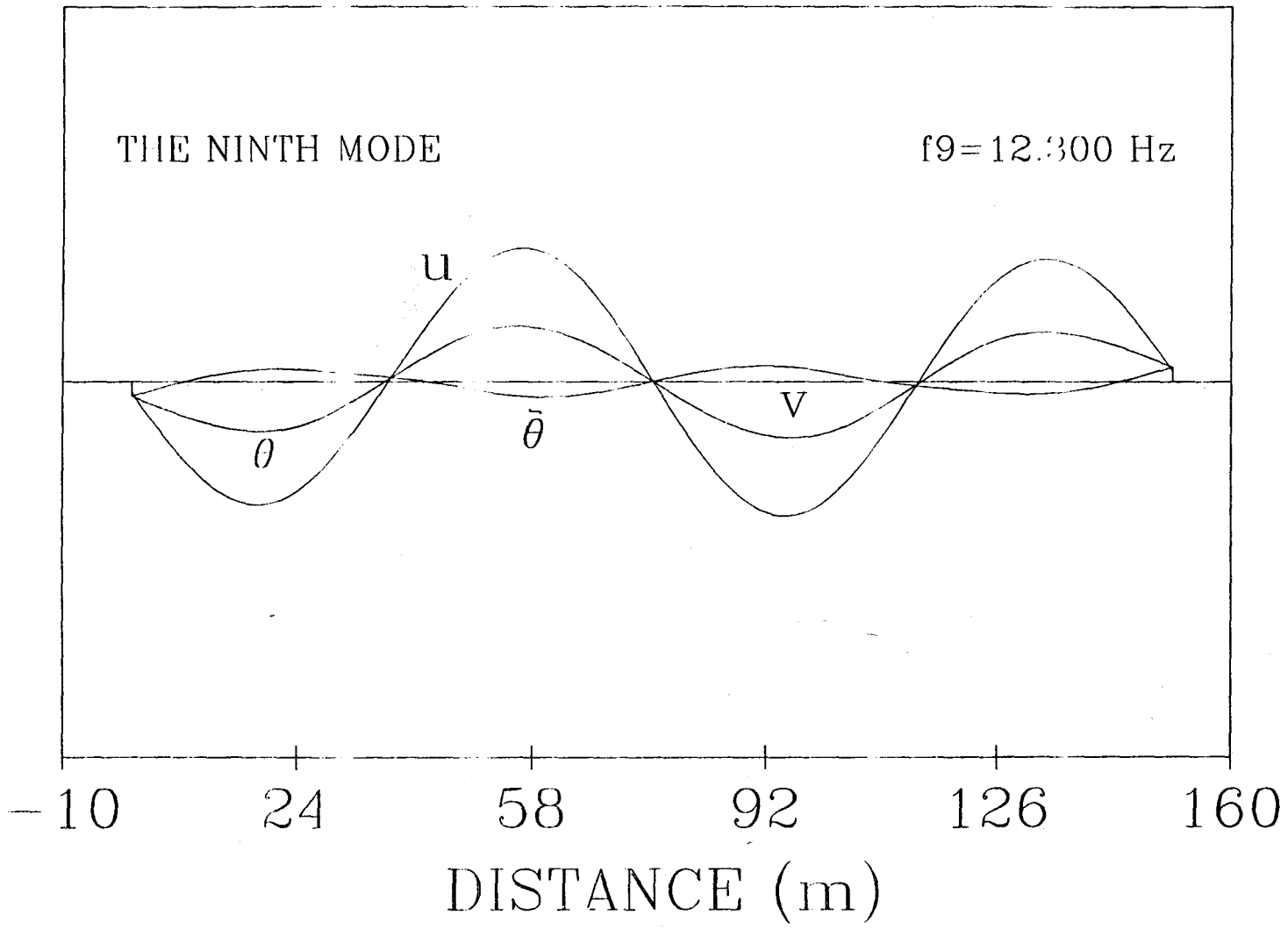

Fig. 4-11. The Ninth Vibration Mode of the Continuous Bridge

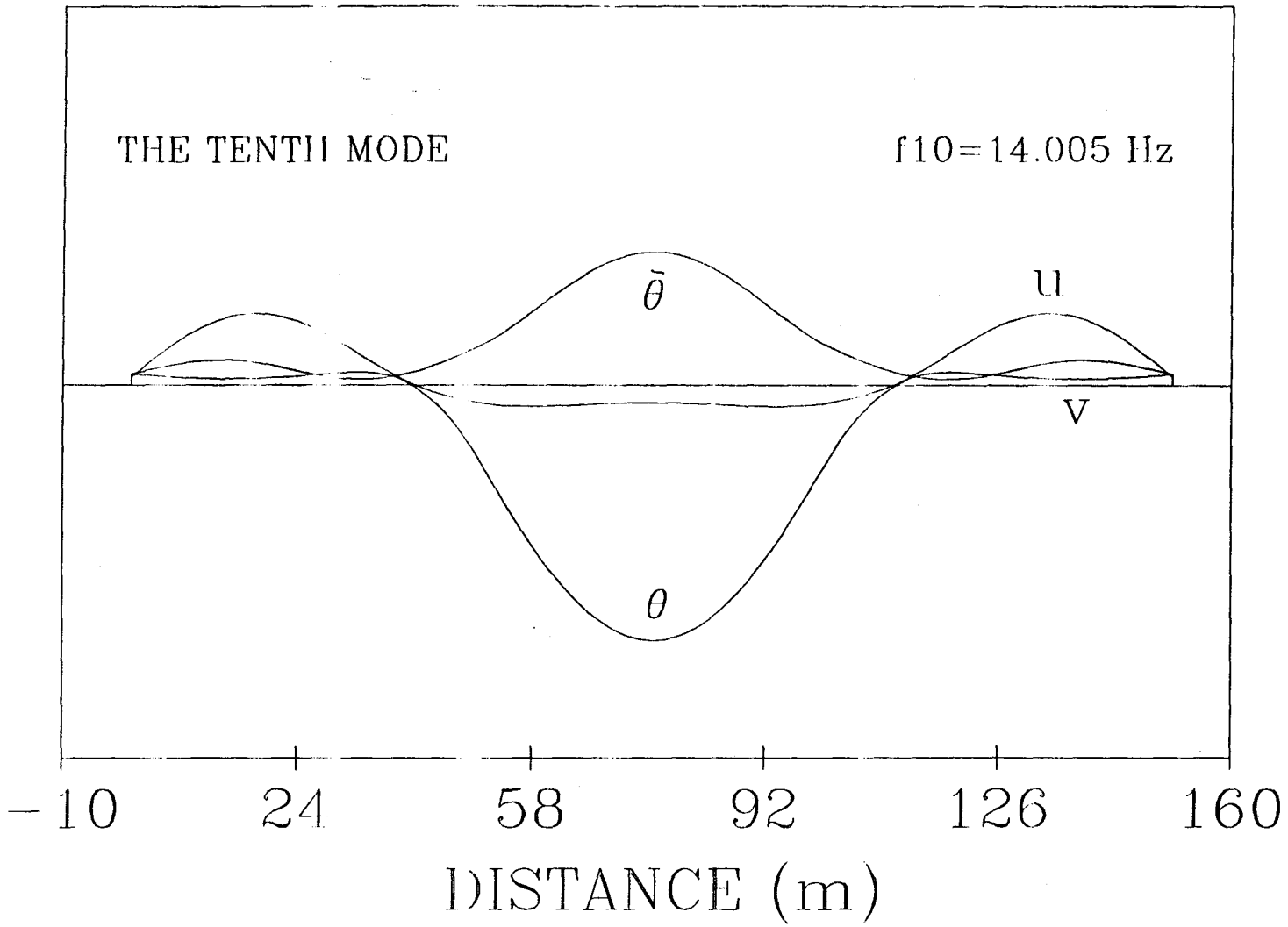

Fig. 4-12. The Tenth Vibration Mode of the Continuous Bridge

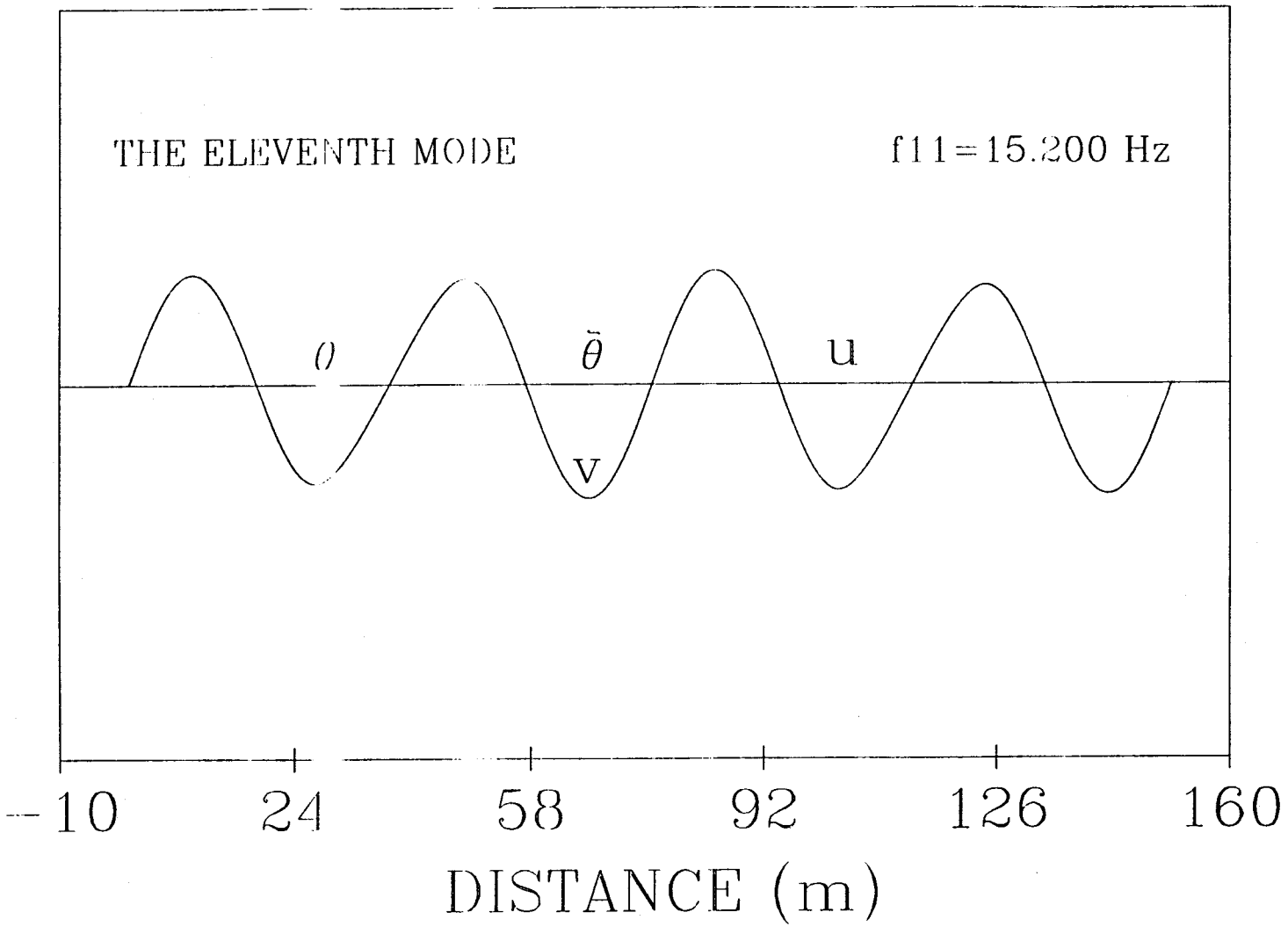

Fig. 4-13. The Eleventh Vibration Mode of the Continuous Bridge

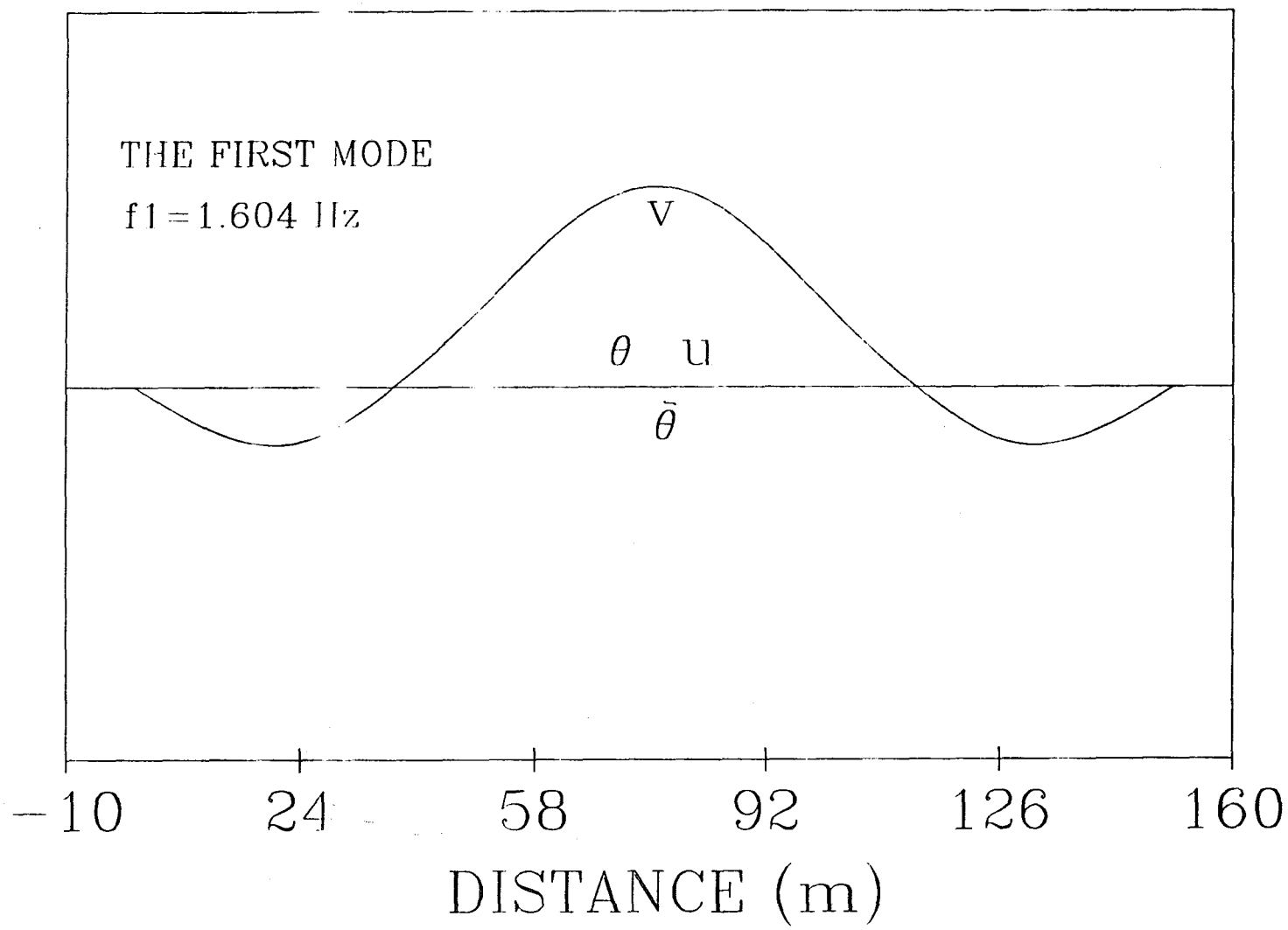

Fig. 4-14. The First Vibration Mode of the Continuous Bridge without Diaphragm

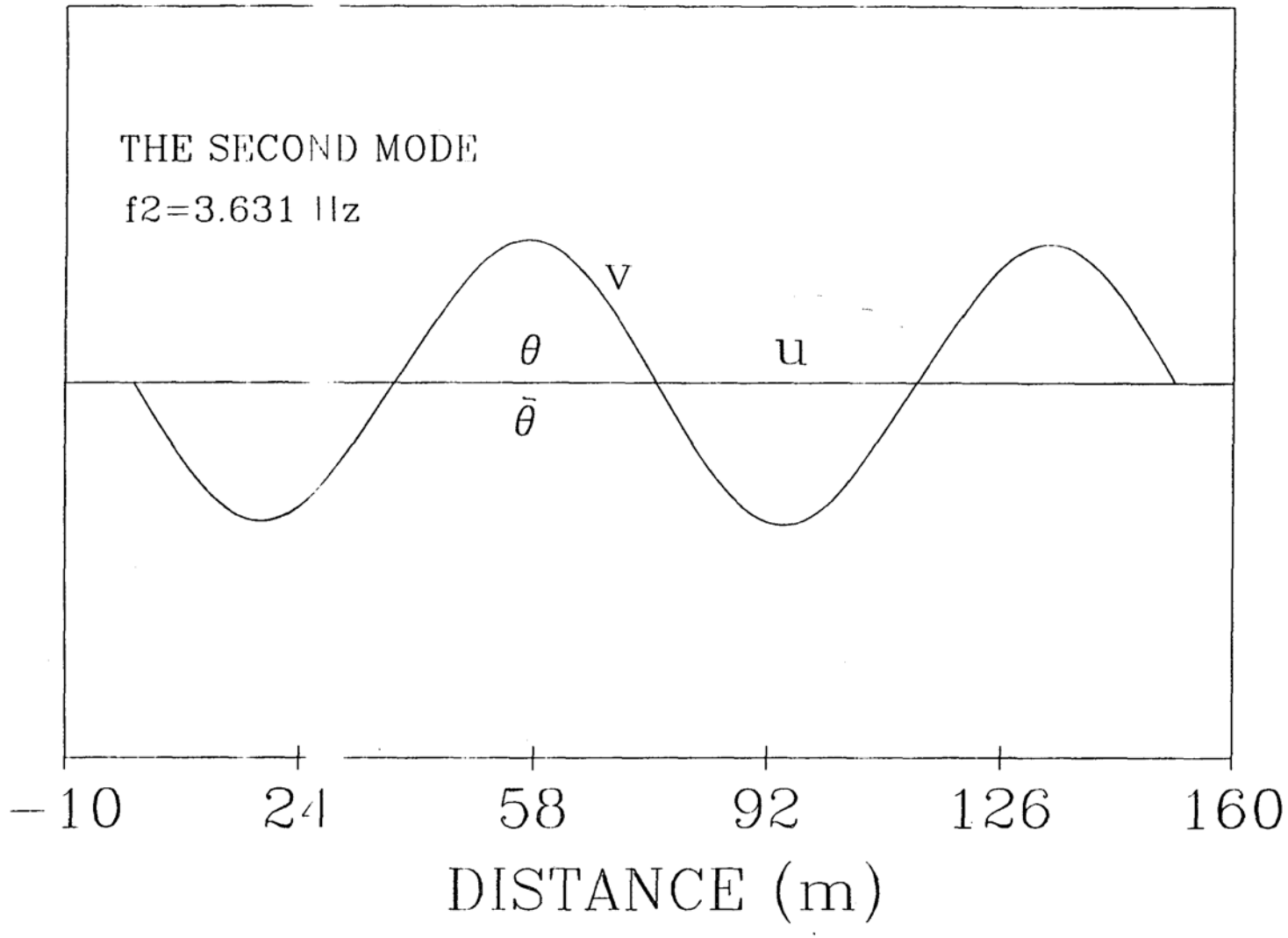

Fig. 4-15. The Second Vibration Mode of the Continuous Bridge without Diaphragm

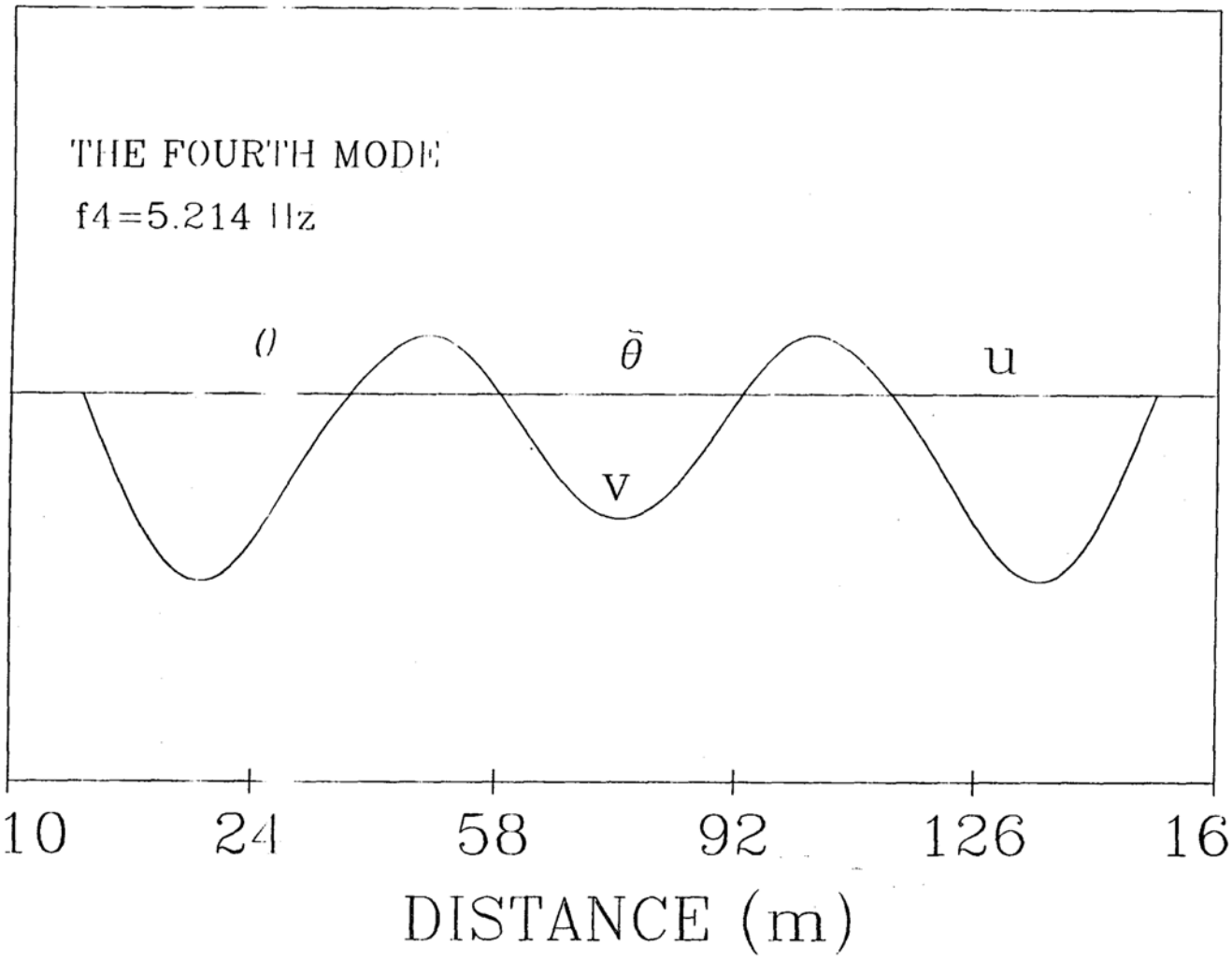

Fig. 4-17. The Fourth Vibration Mode of the Continuous Bridge without Diaphragm

Fig. 4-16. The Third Vibration Mode of the Continuous Bridge without Diaphragm

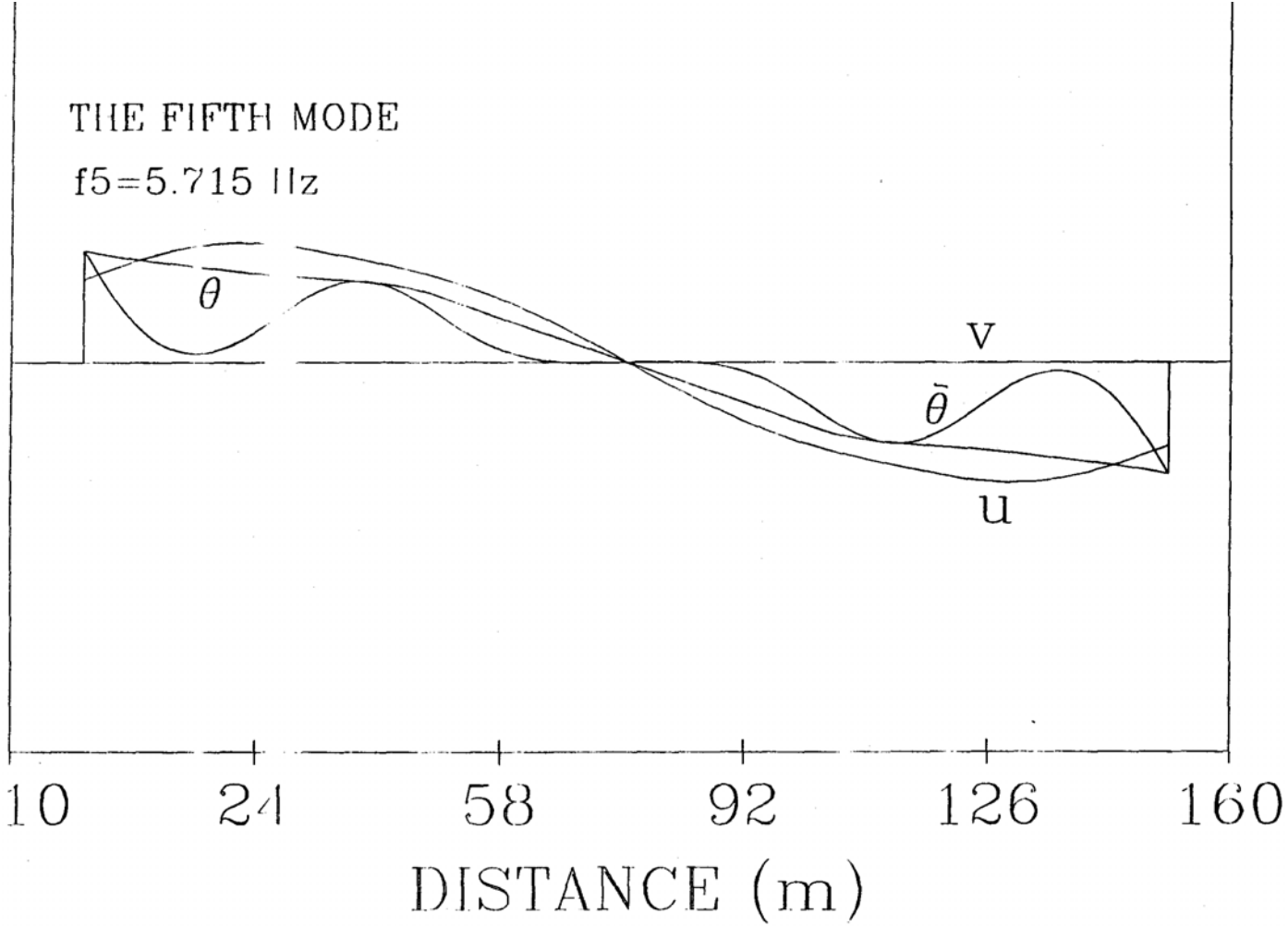

Fig. 4-18. The Fifth Vibration Mode of the Continuous Bridge without Diaphragm

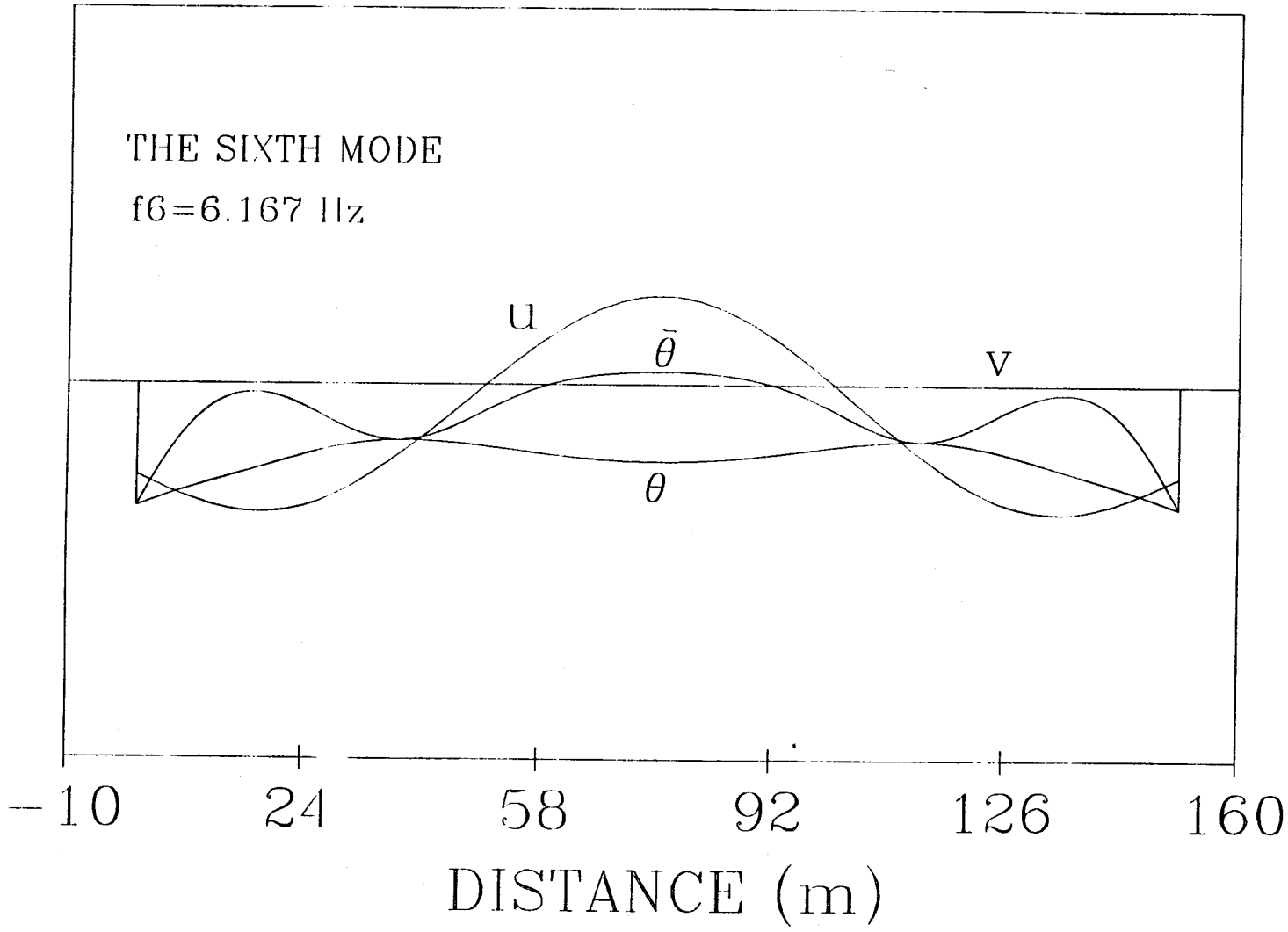

Fig. 4-19. The Sixth Vibration Mode of the Continuous Bridge without Diaphragm

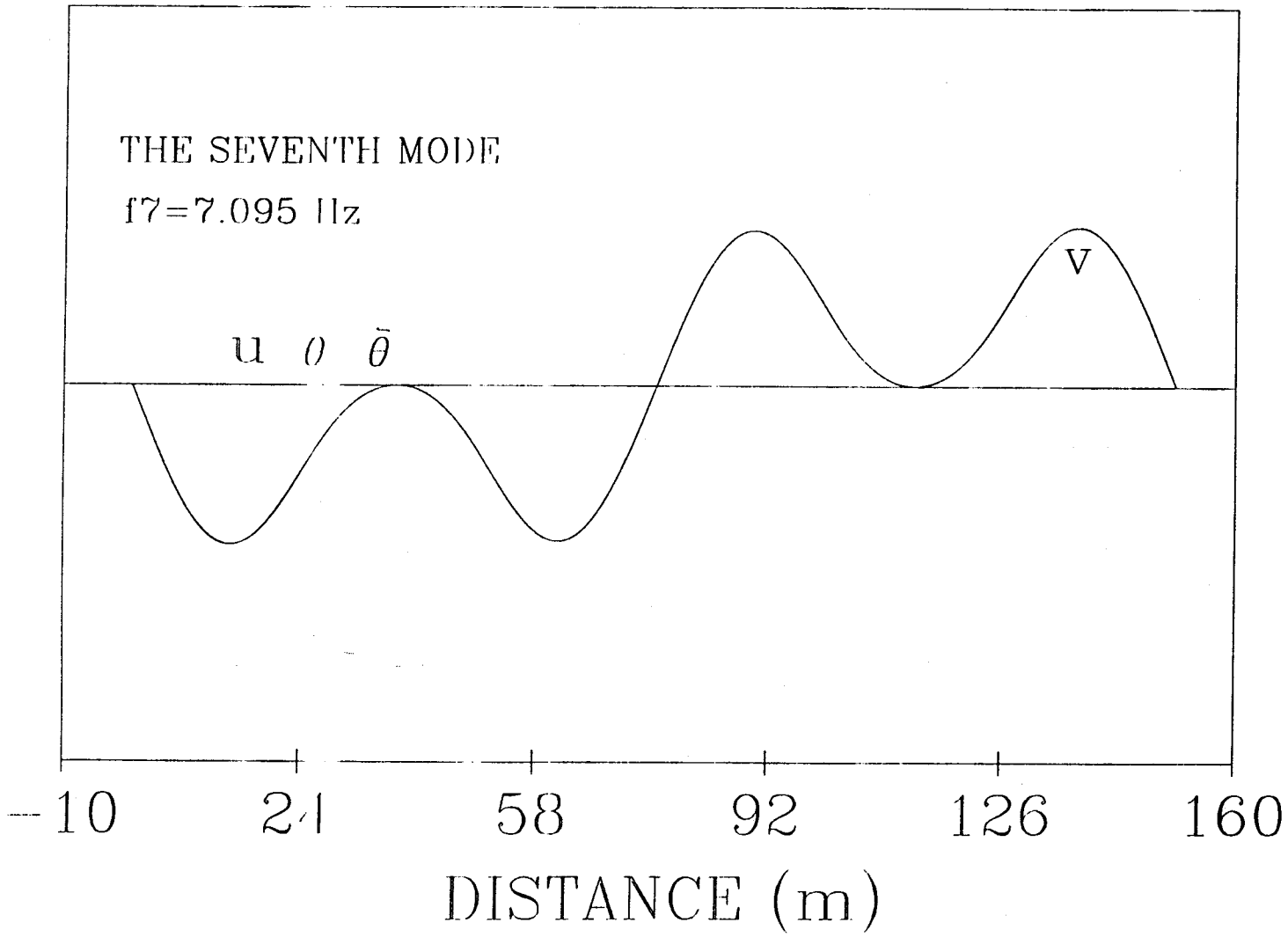

Fig. 4-20. The Seventh Vibration Mode of the Continuous Bridge without Diaphragm

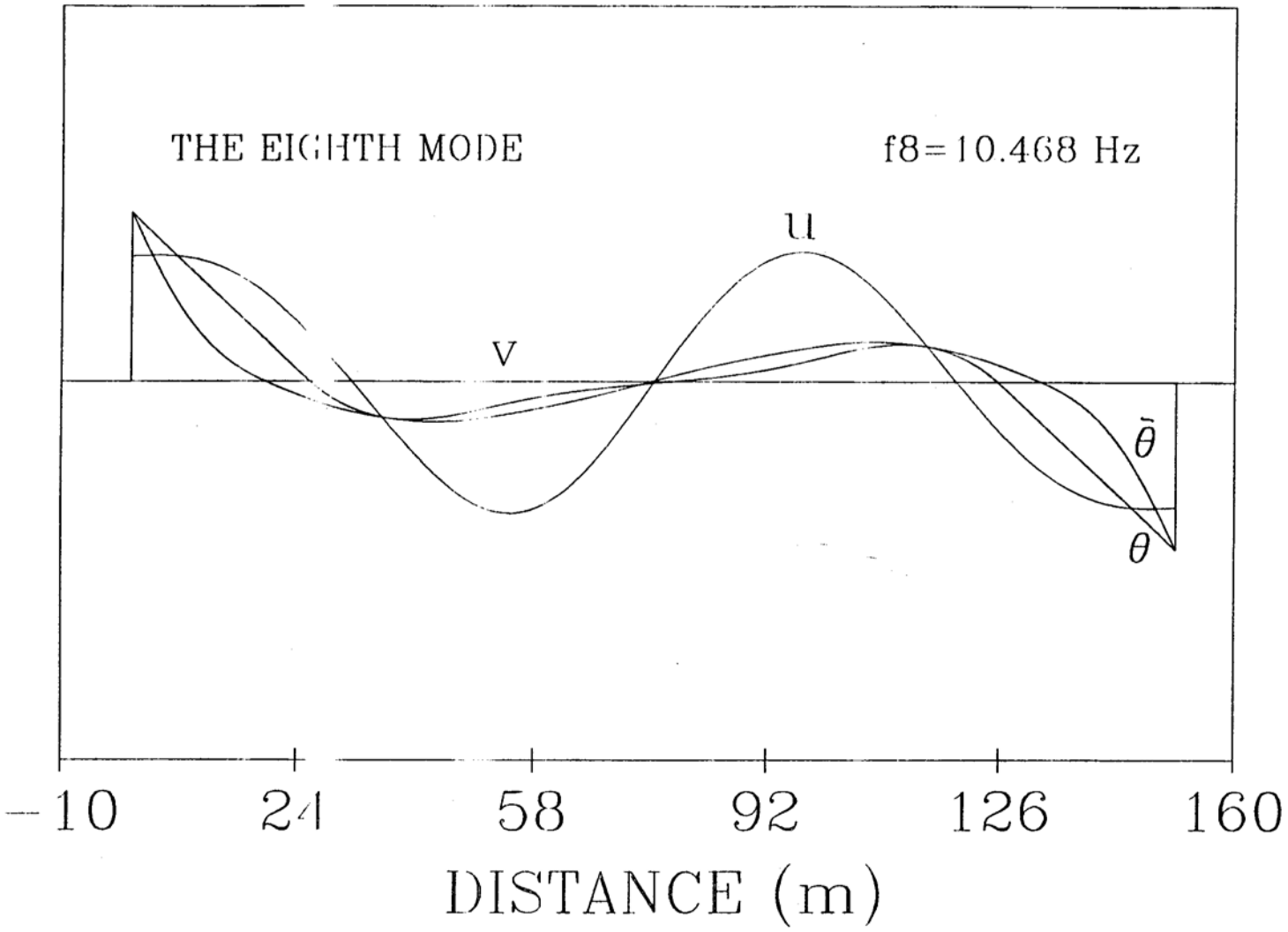

Fig. 4-21. The Eighth Vibration Mode of the Continuous Bridge without Diaphragm

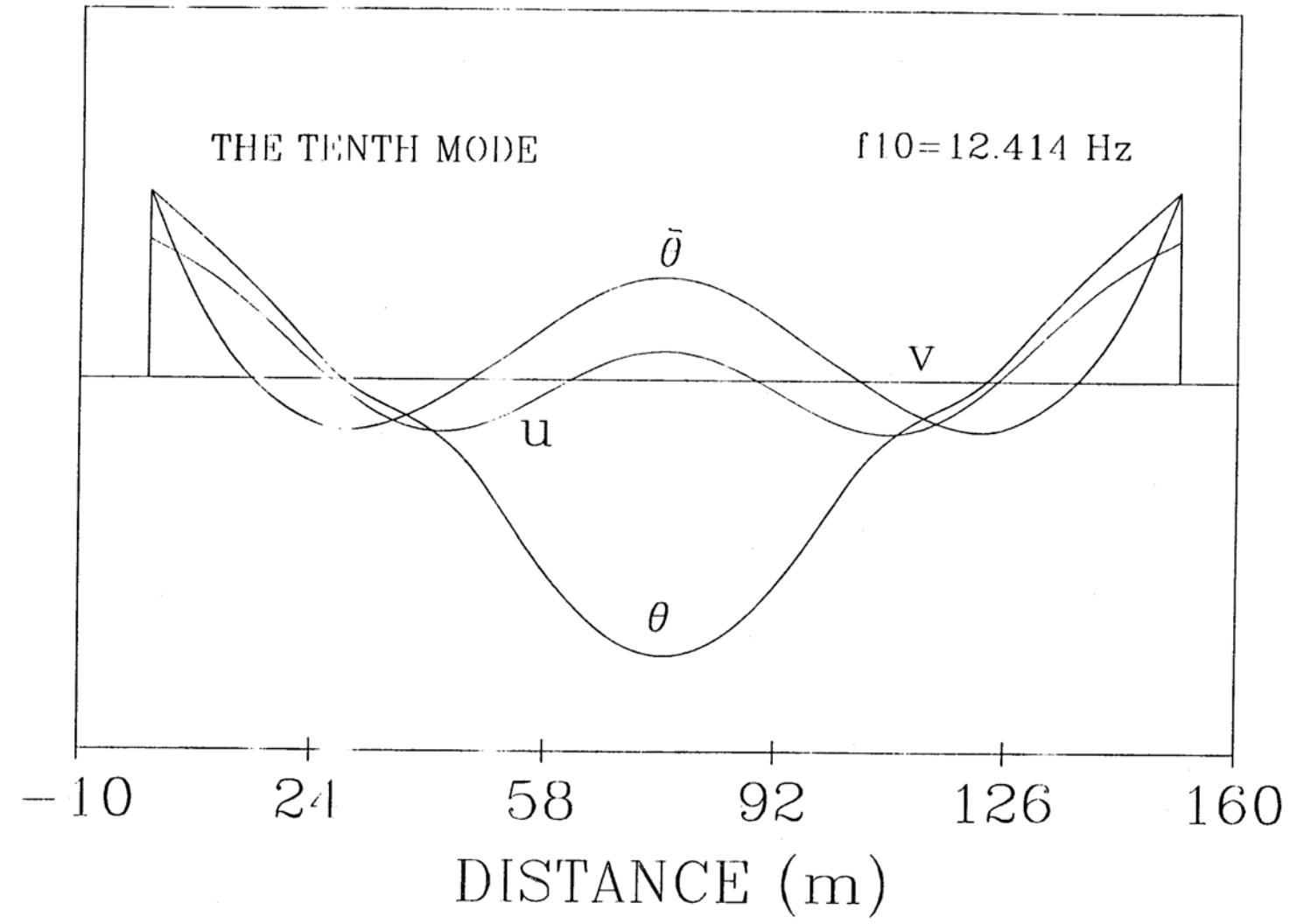

Fig. 4-23. The Tenth Vibration Mode of the Continuous Bridge without Diaphragm

Fig. 4-22. The Ninth Vibration Mode of the Continuous Bridge without Diaphragm

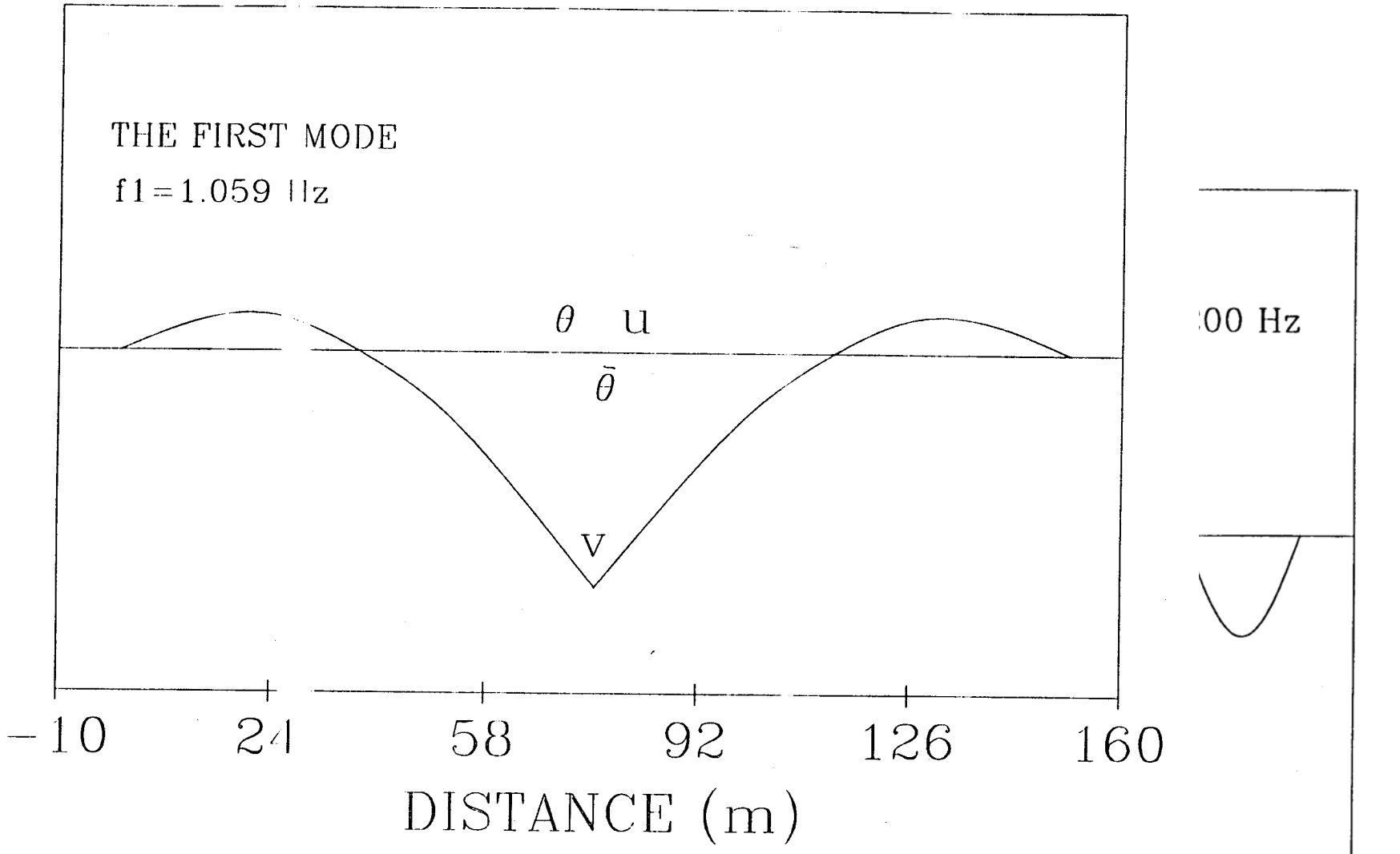

Fig. 4-25. The First Vibration Mode of the Cantilever Bridge with One Hinge

Fig. 4-24. The Eleventh Vibration Mode of the Continuous Bridge without Diaphragm

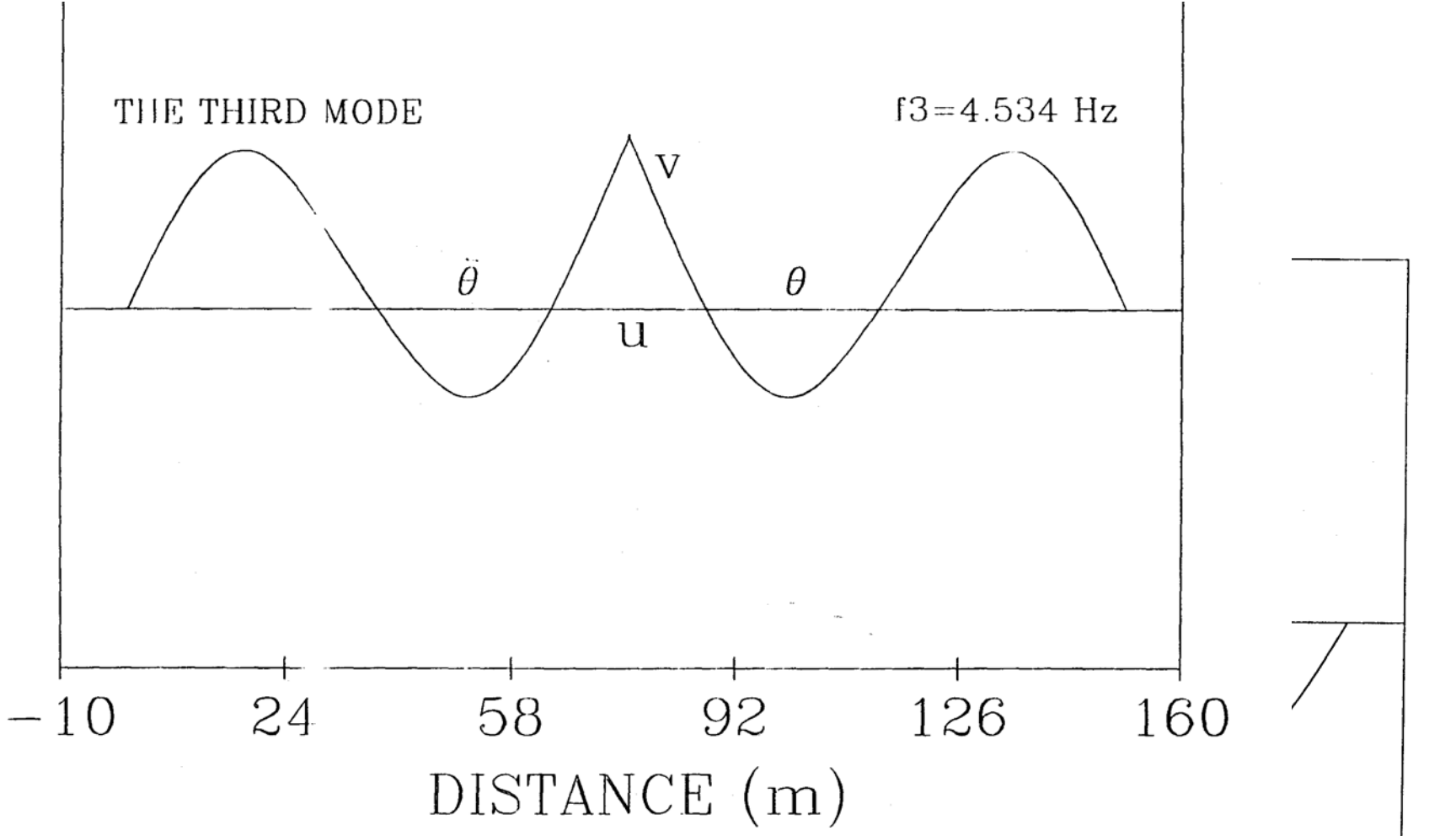

Fig. 4-27. The Third Vibration Mode of the Cantilever Bridge with One Hinge

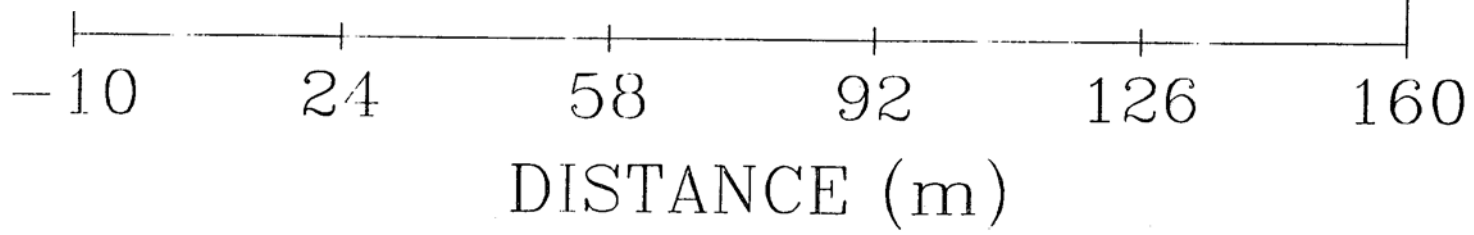

Fig. 4-26. The Second Vibration Mode of the Cantilever Bridge with One Hinge

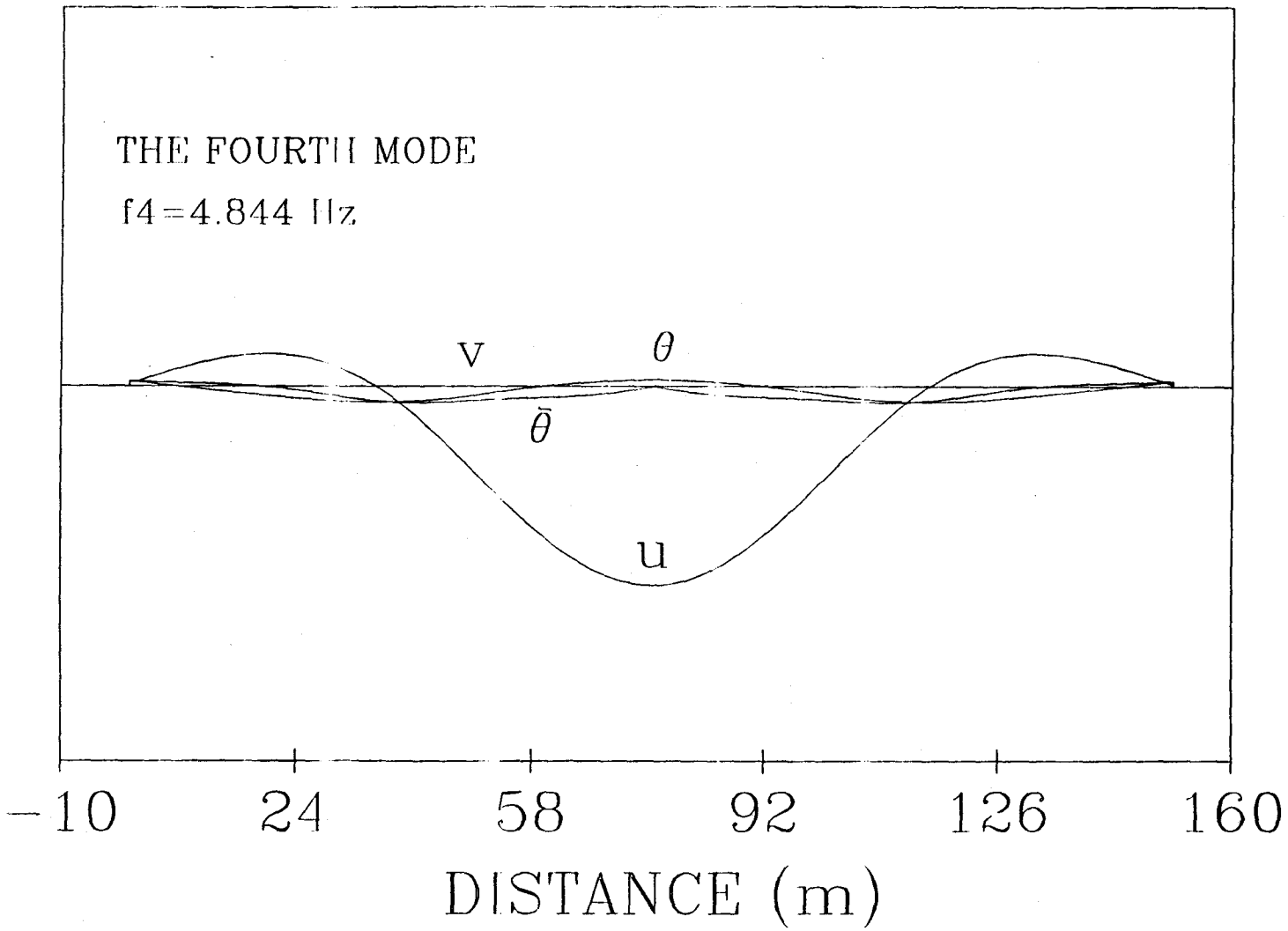

Fig. 4-28. The Fourth Vibration Mode of the Cantilever Bridge with One Hinge

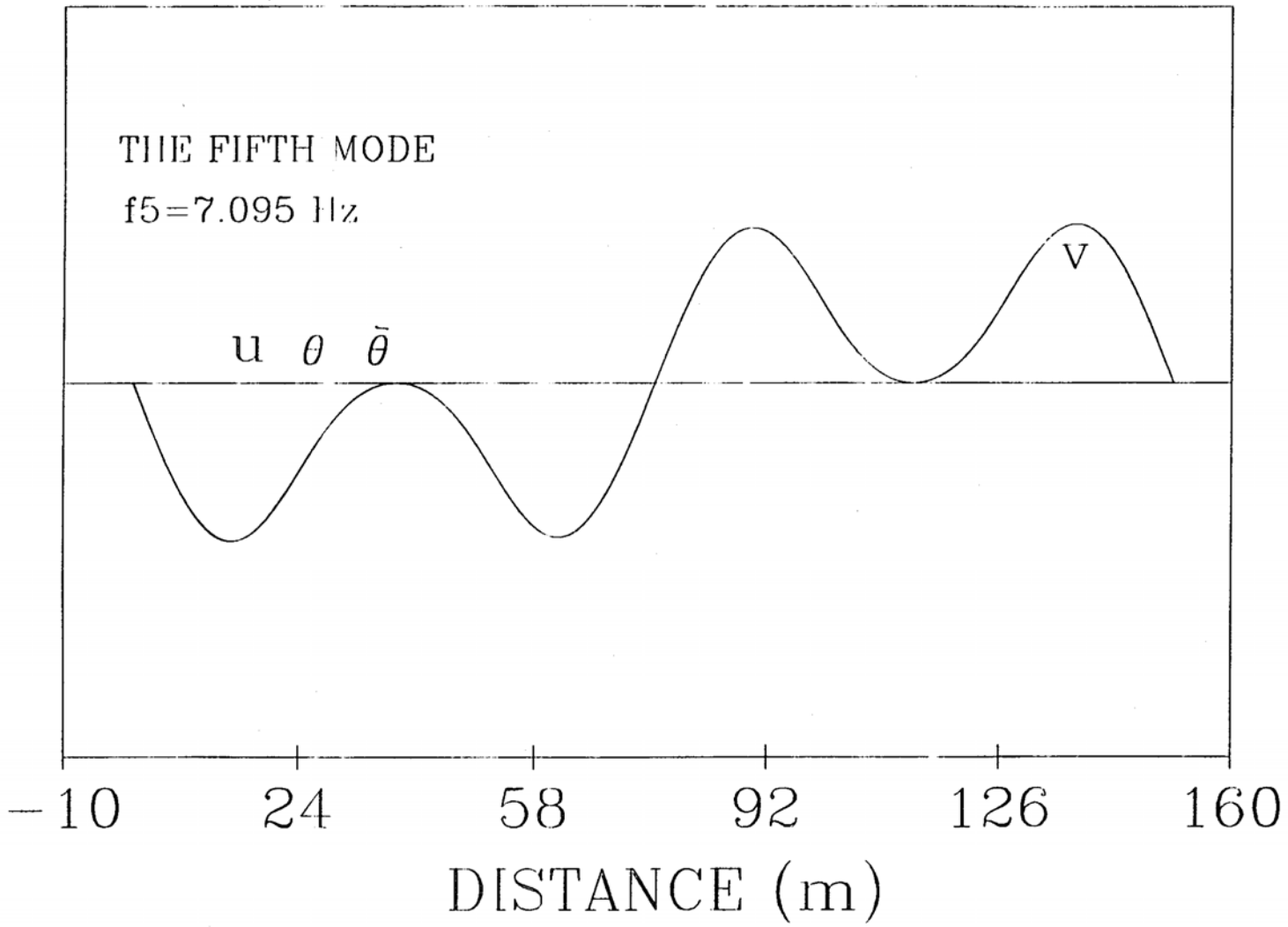

Fig. 4-29. The Fifth Vibration Mode of the Cantilever Bridge with One Hinge

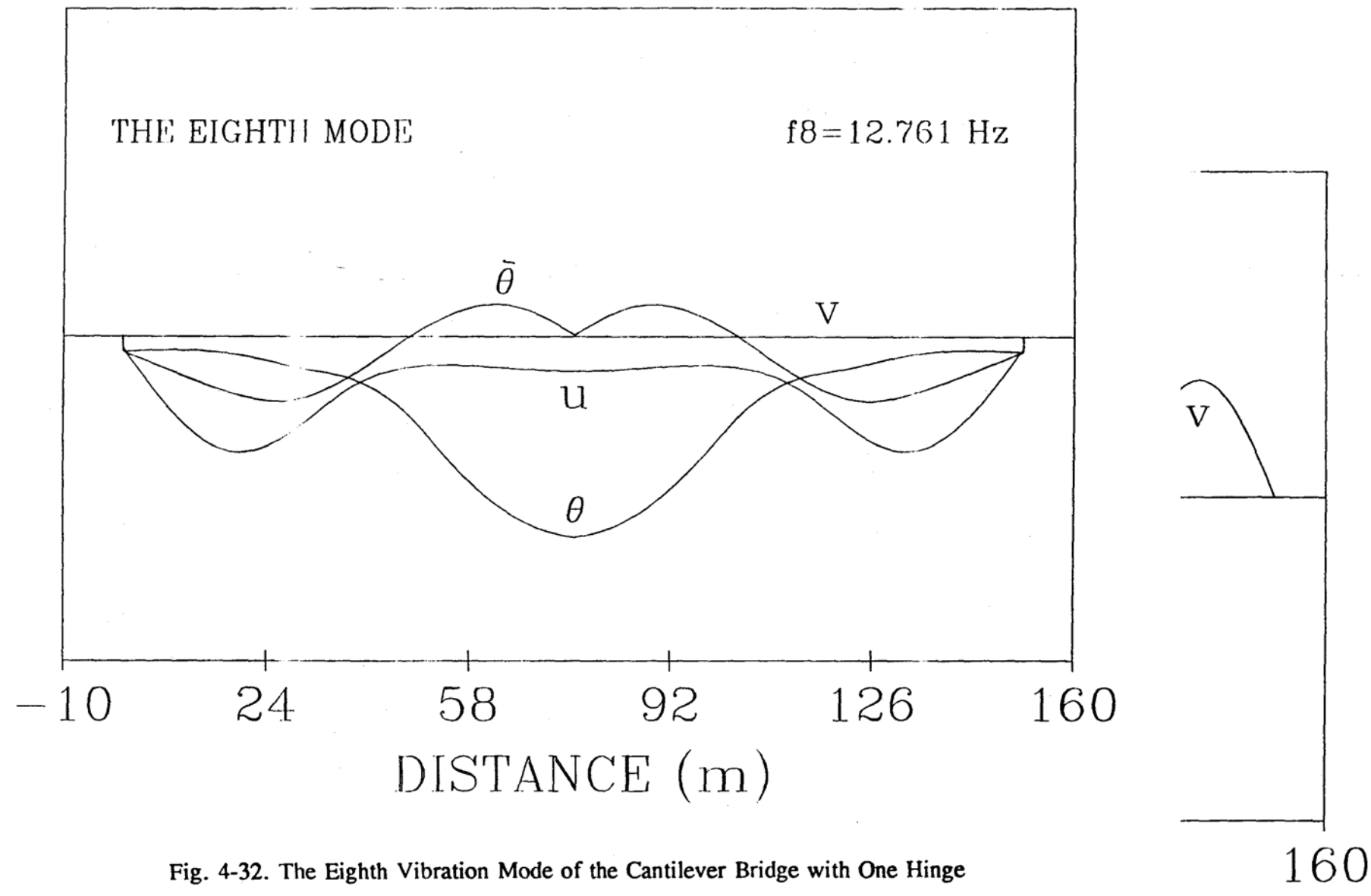

Fig. 4-32. The Eighth Vibration Mode of the Cantilever Bridge with One Hinge

Fig. 4-30. The Sixth Vibration Mode of the Cantilever Bridge with One Hinge

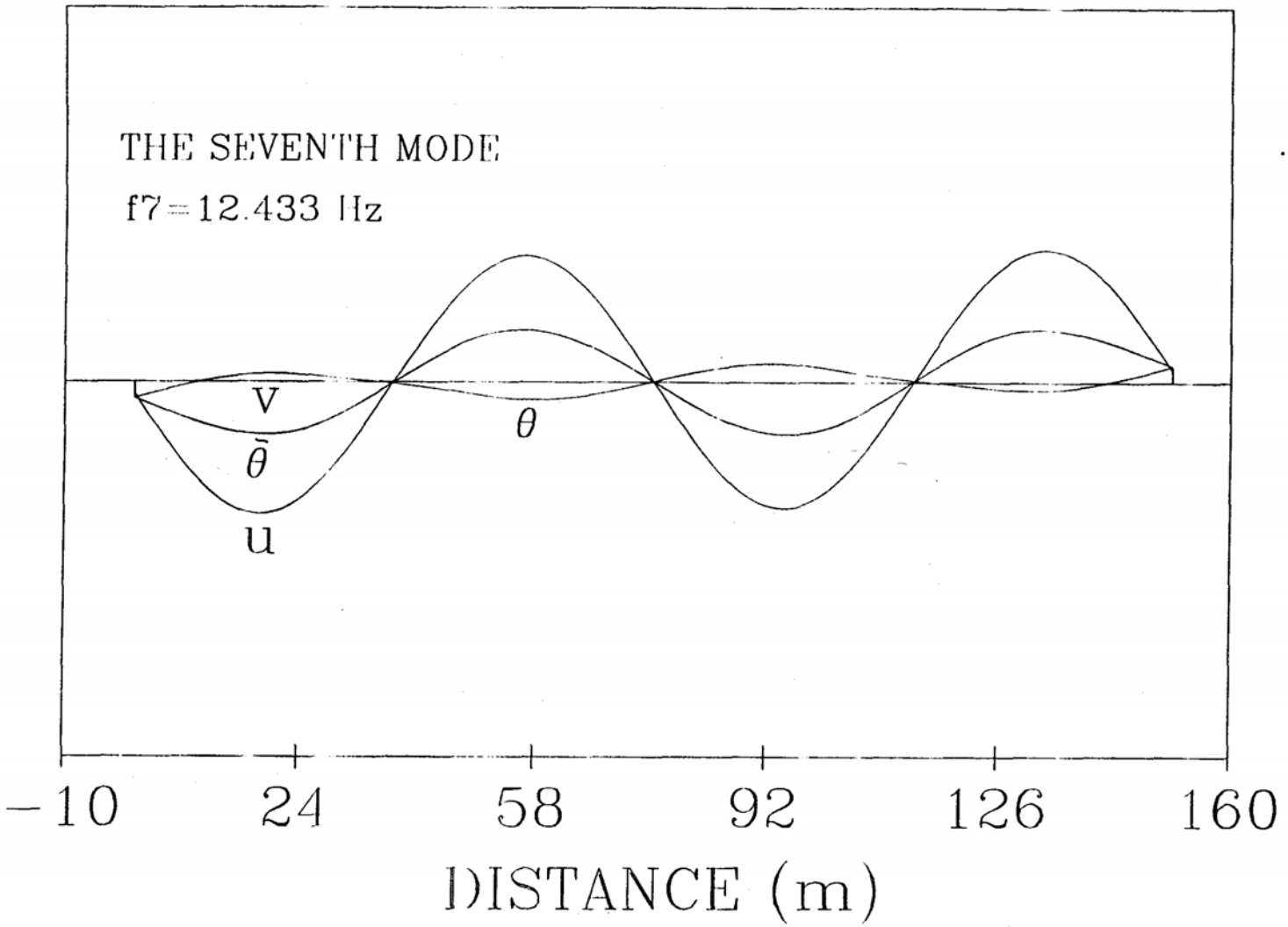

Fig. 4-31. The Seventh Vibration Mode of the Cantilever Bridge with One Hinge

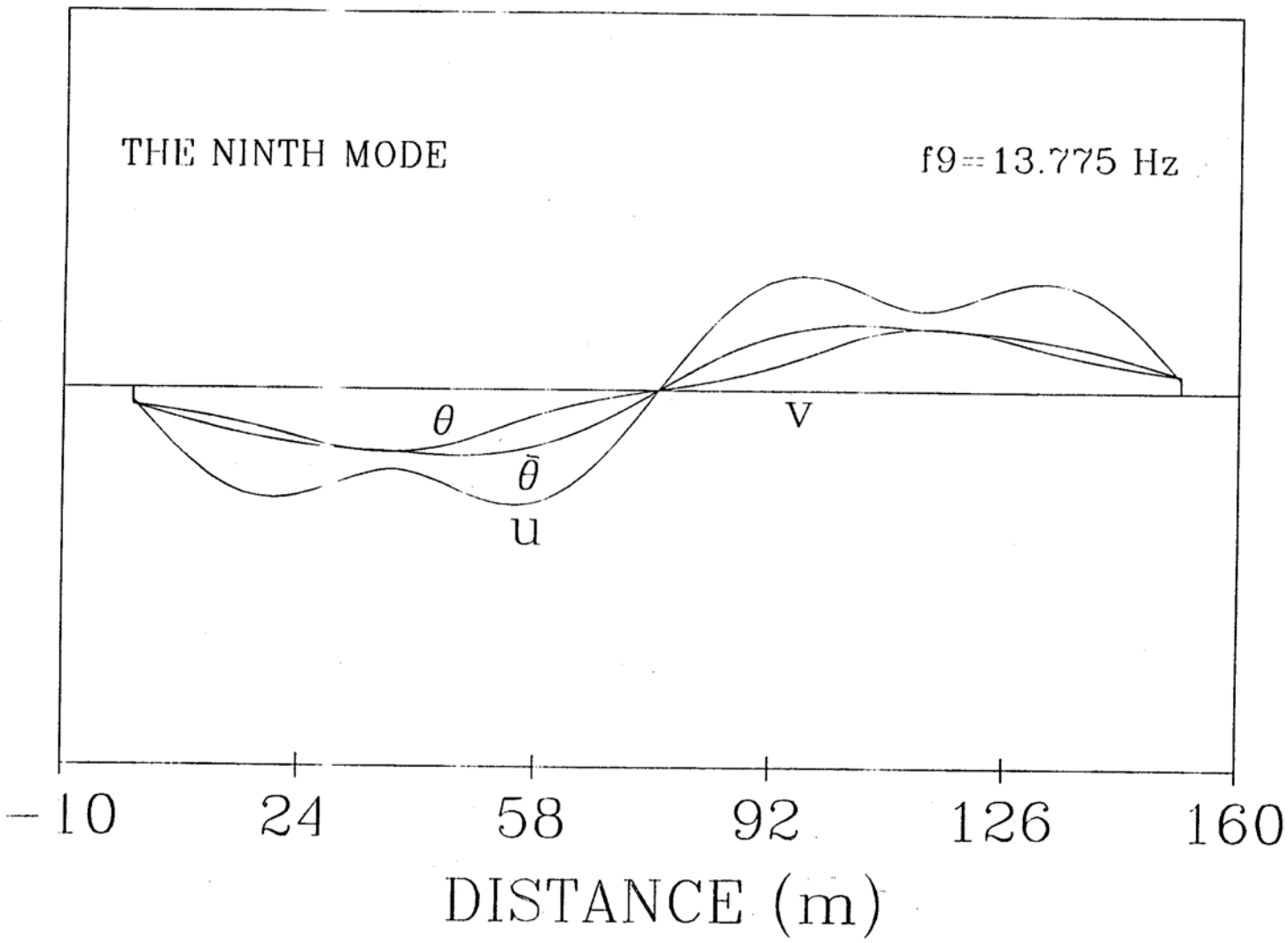

Fig. 4-33. The Ninth Vibration Mode of the Cantilever Bridge with One Hinge

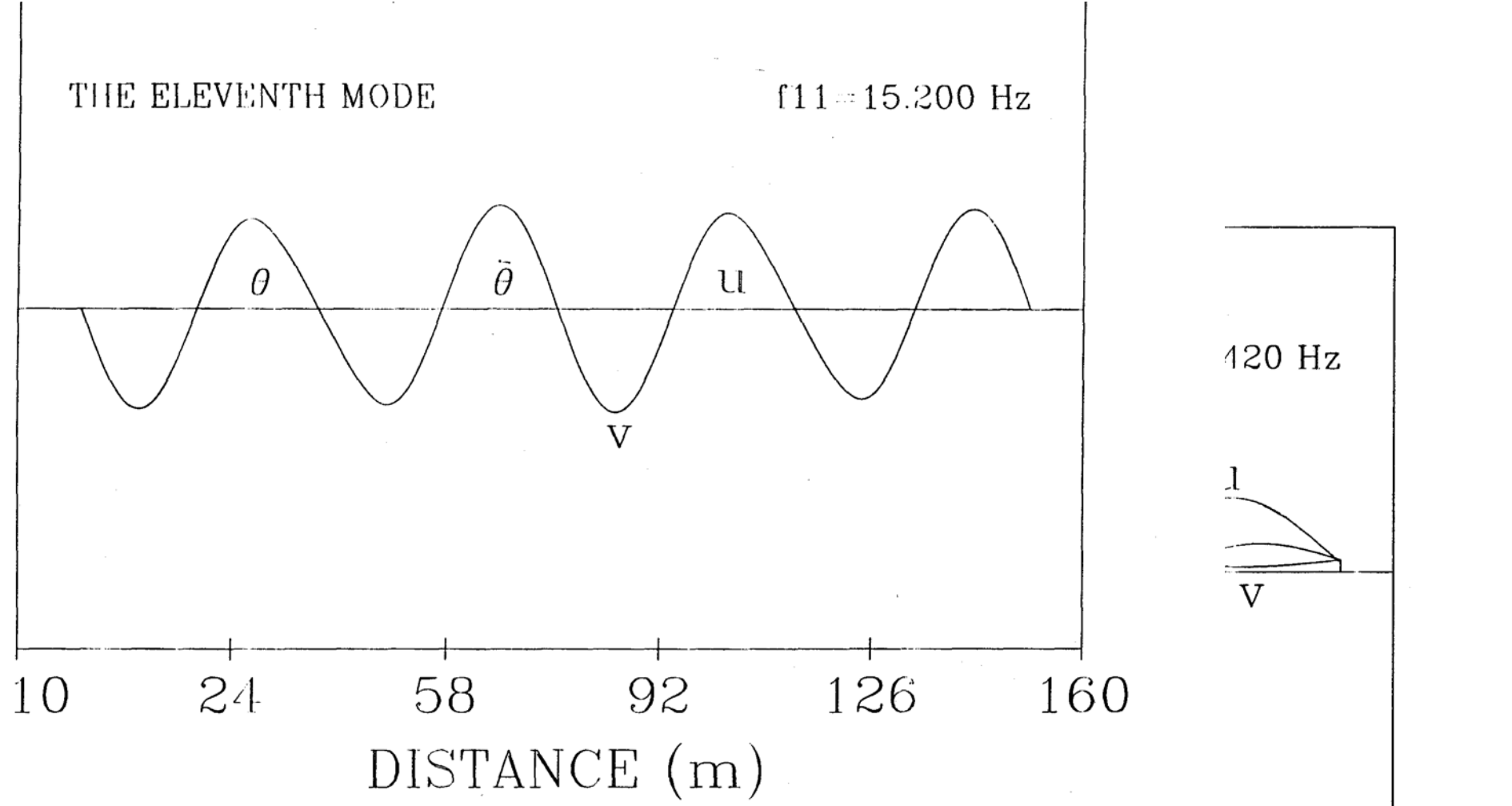

Fig. 4-35. The Eleventh Vibration Mode of the Cantilever Bridge with One Hinge

Fig. 4-34. The Tenth Vibration Mode of the Cantilever Bridge with One Hinge

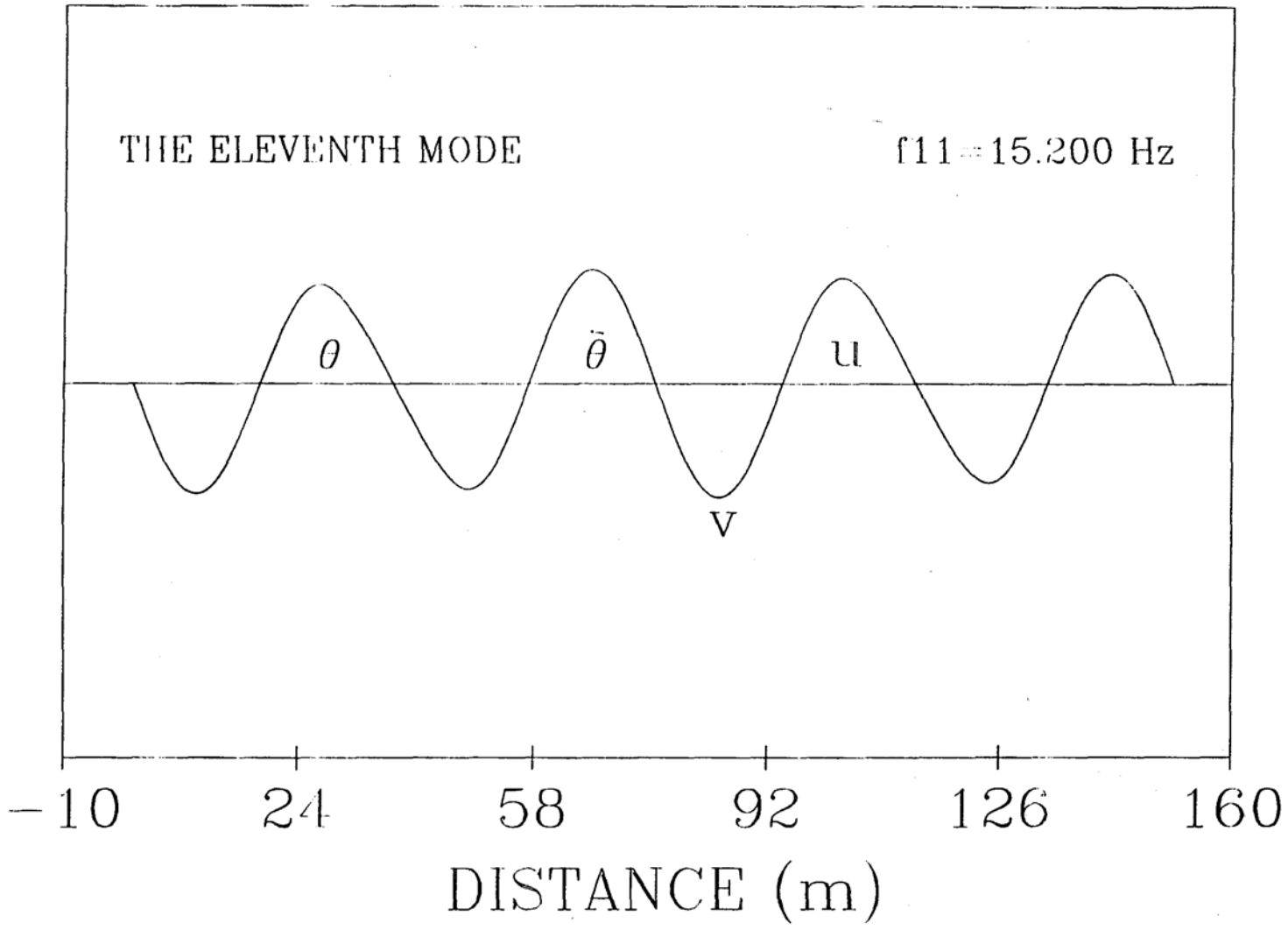

Fig. 4-35. The Eleventh Vibration Mode of the Cantilever Bridge with One Hinge

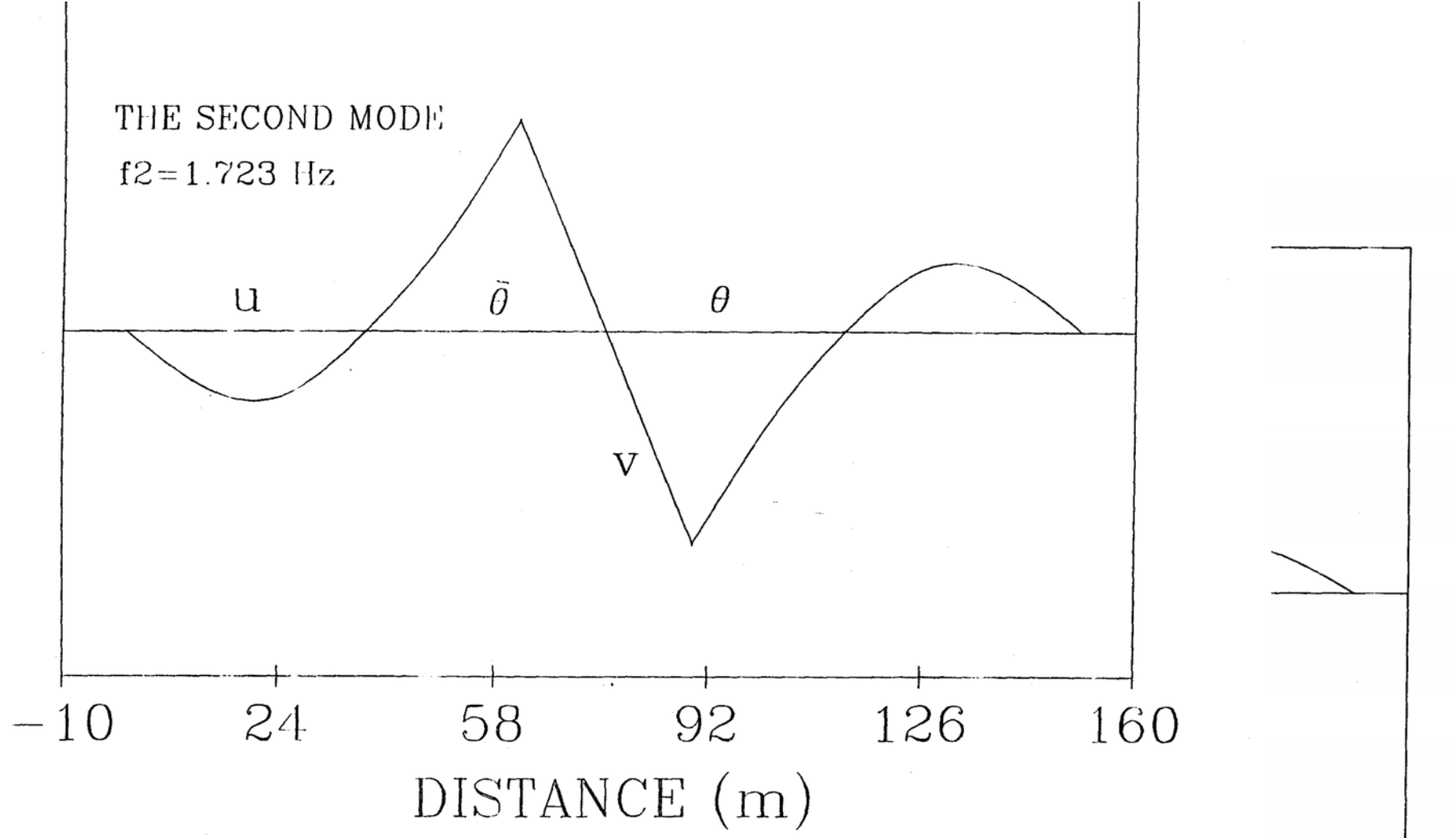

Fig. 4-37. The Second Vibration Mode of the Cantilever Bridge with Two Hinge

Fig. 4-36. The First Vibration Mode of the Cantilever Bridge with Two Hinge

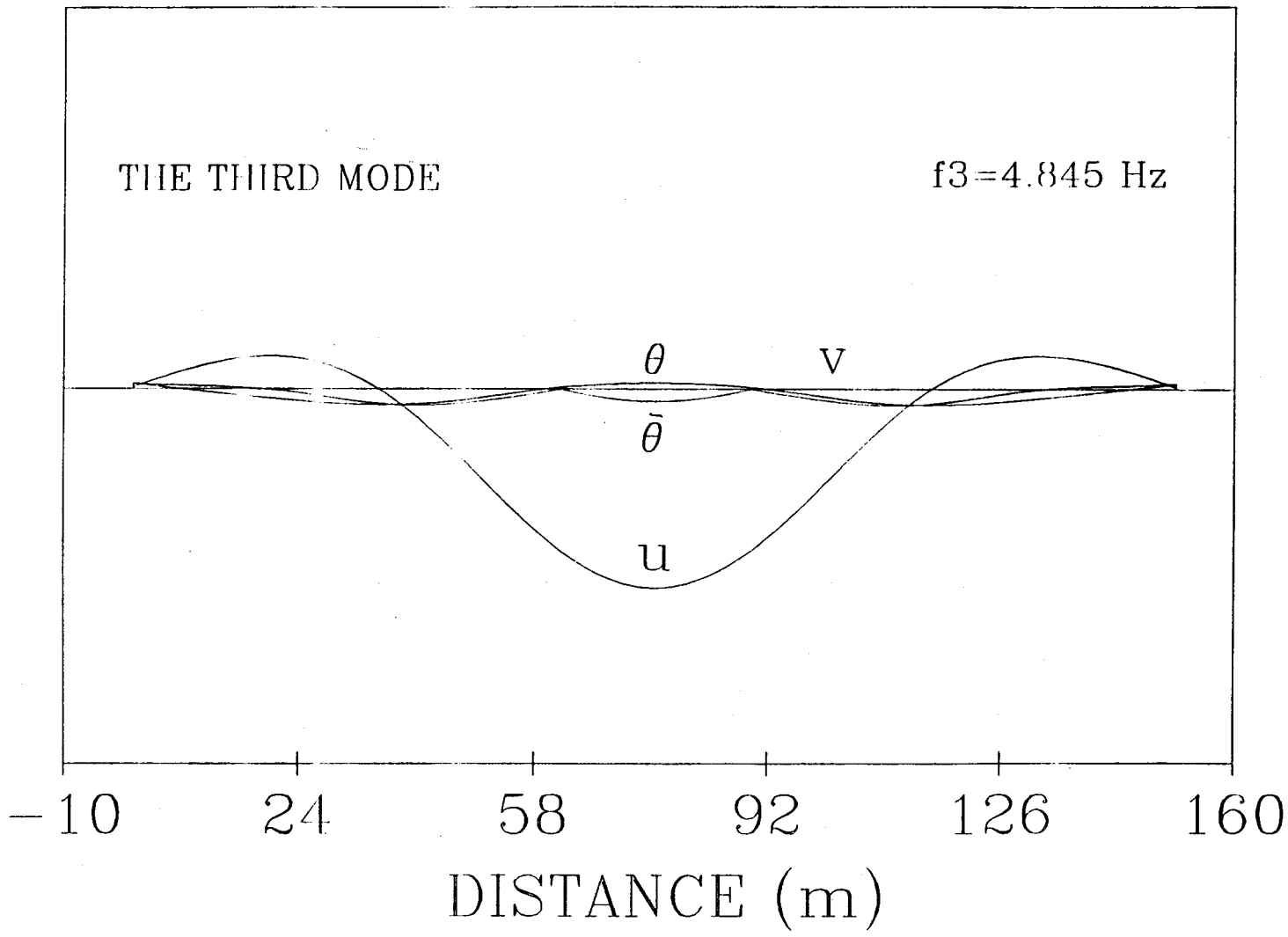

Fig. 4-38. The Third Vibration Mode of the Cantilever Bridge with Two Hinge

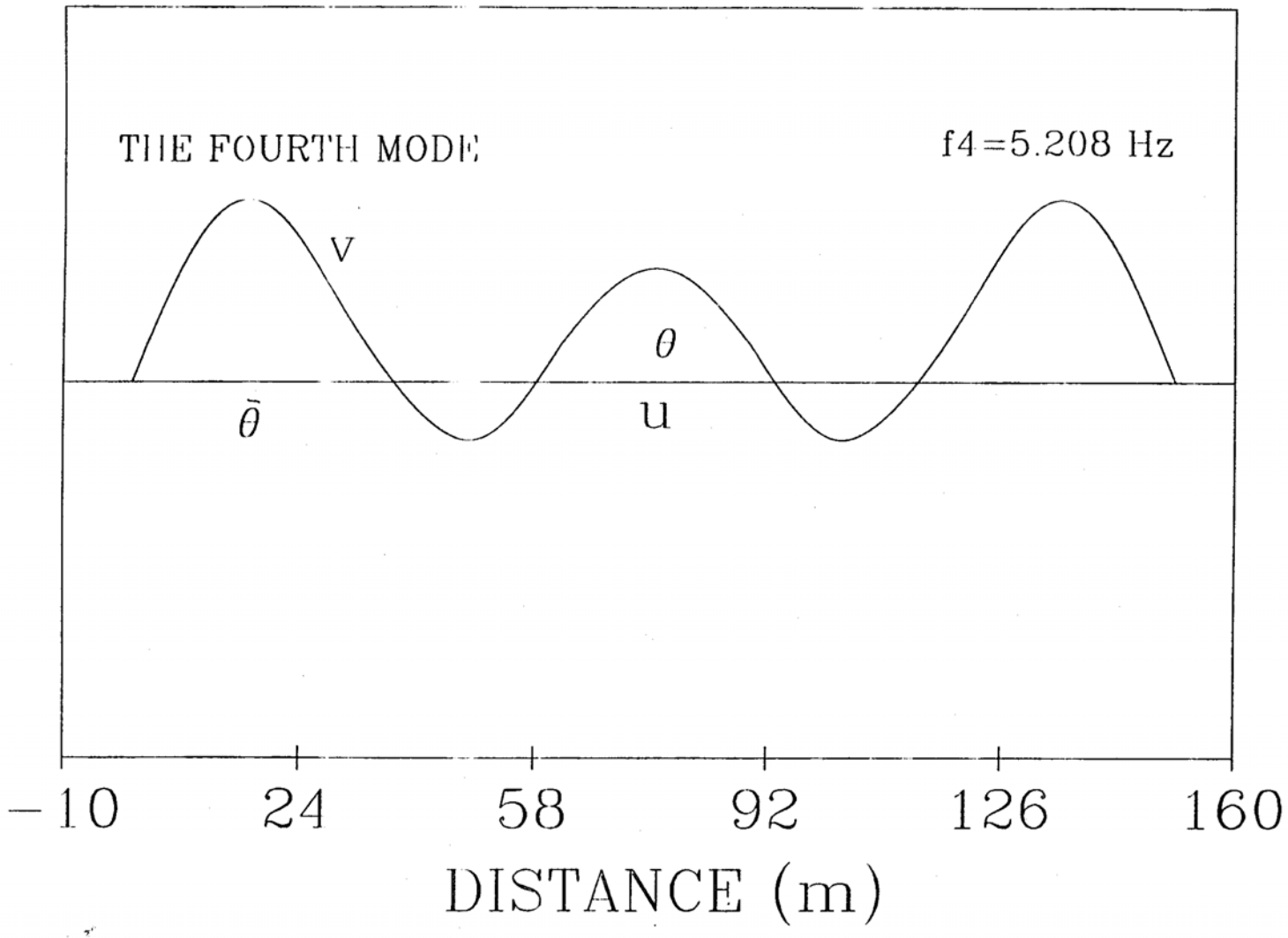

Fig. 4-39. The Fourth Vibration Mode of the Cantilever Bridge with Two Hinge

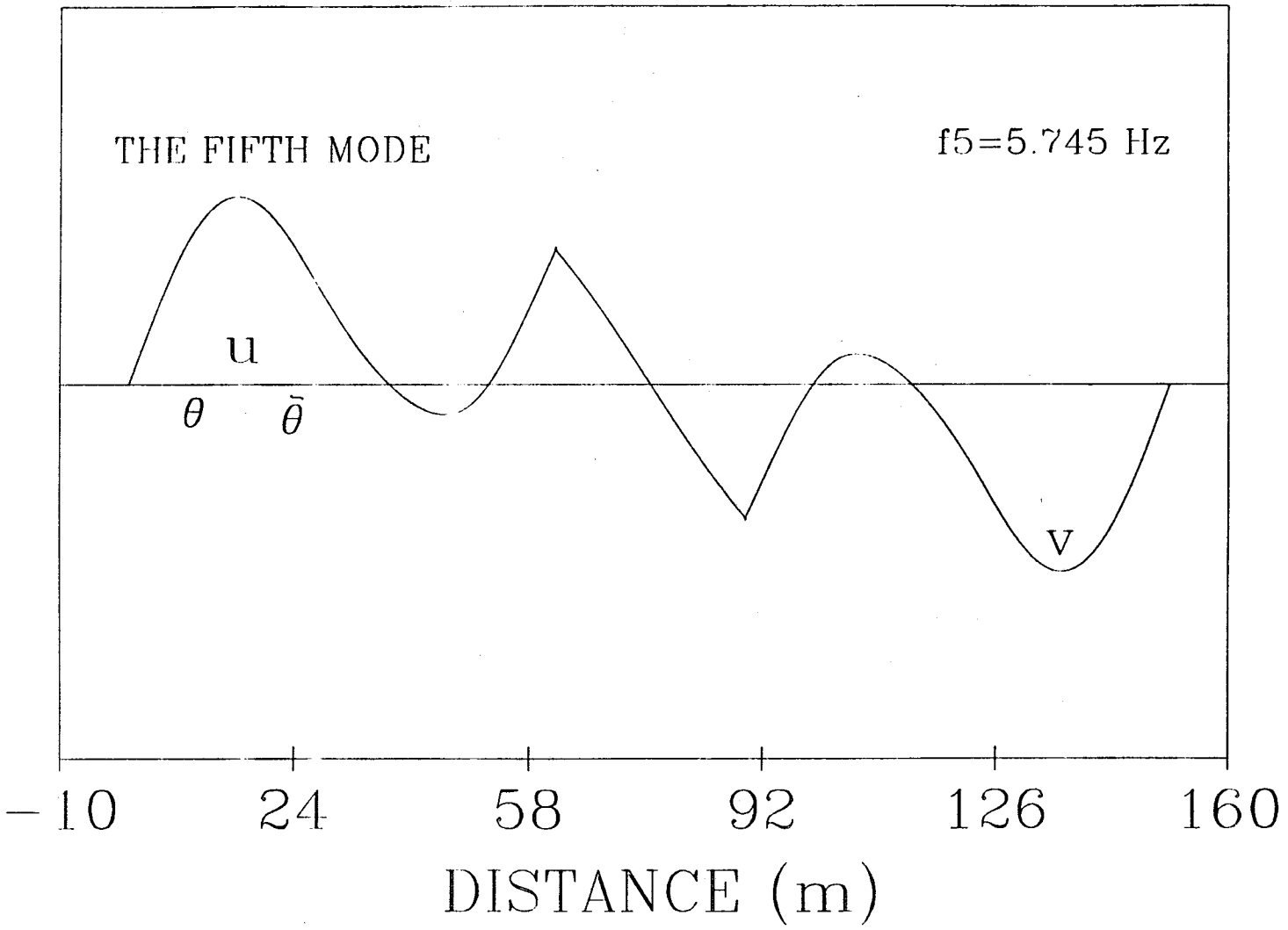

Fig. 4-40. The Fifth Vibration Mode of the Cantilever Bridge with Two Hinge

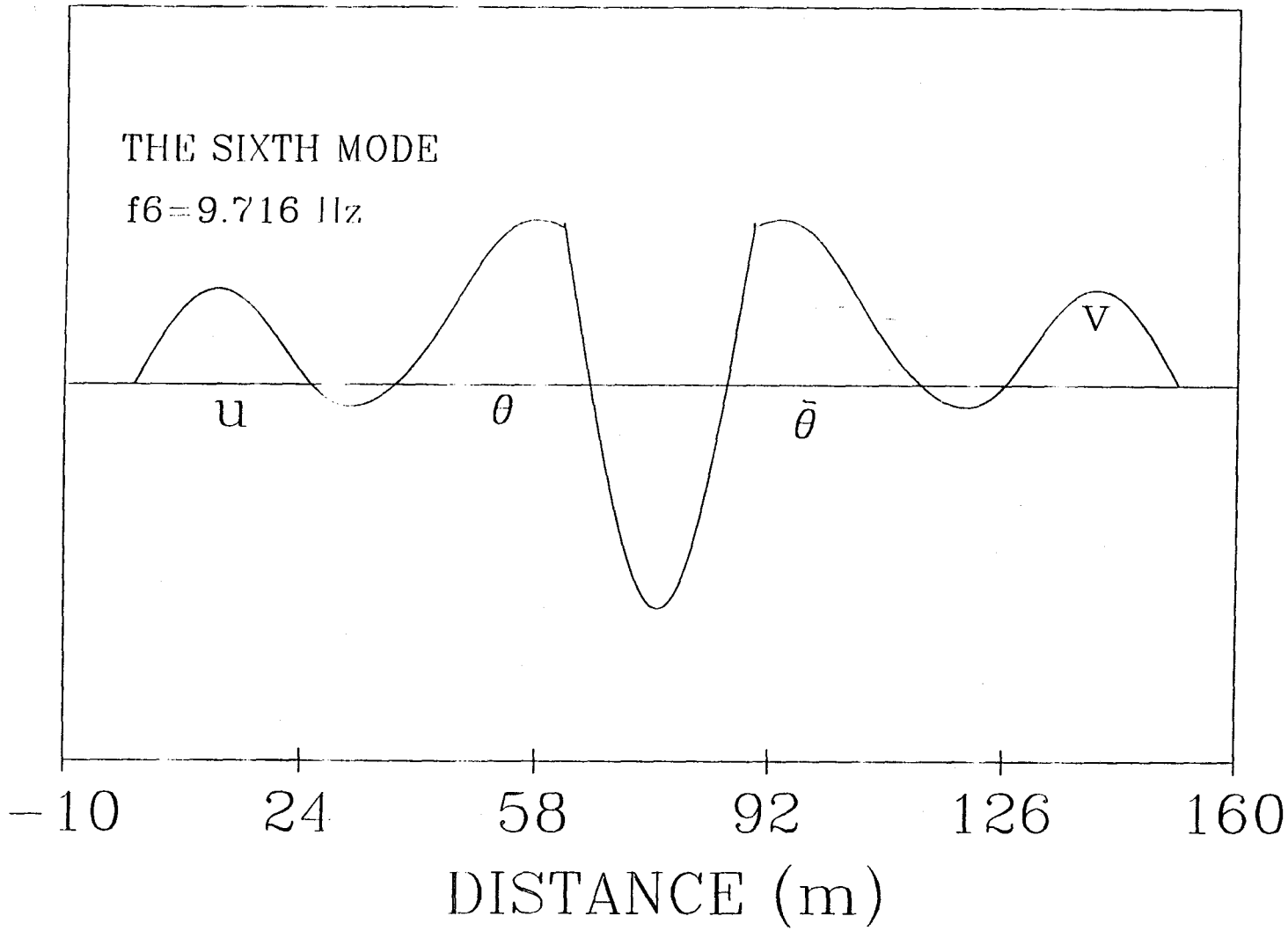

Fig. 4-41. The Sixth Vibration Mode of the Cantilever Bridge with Two Hinge

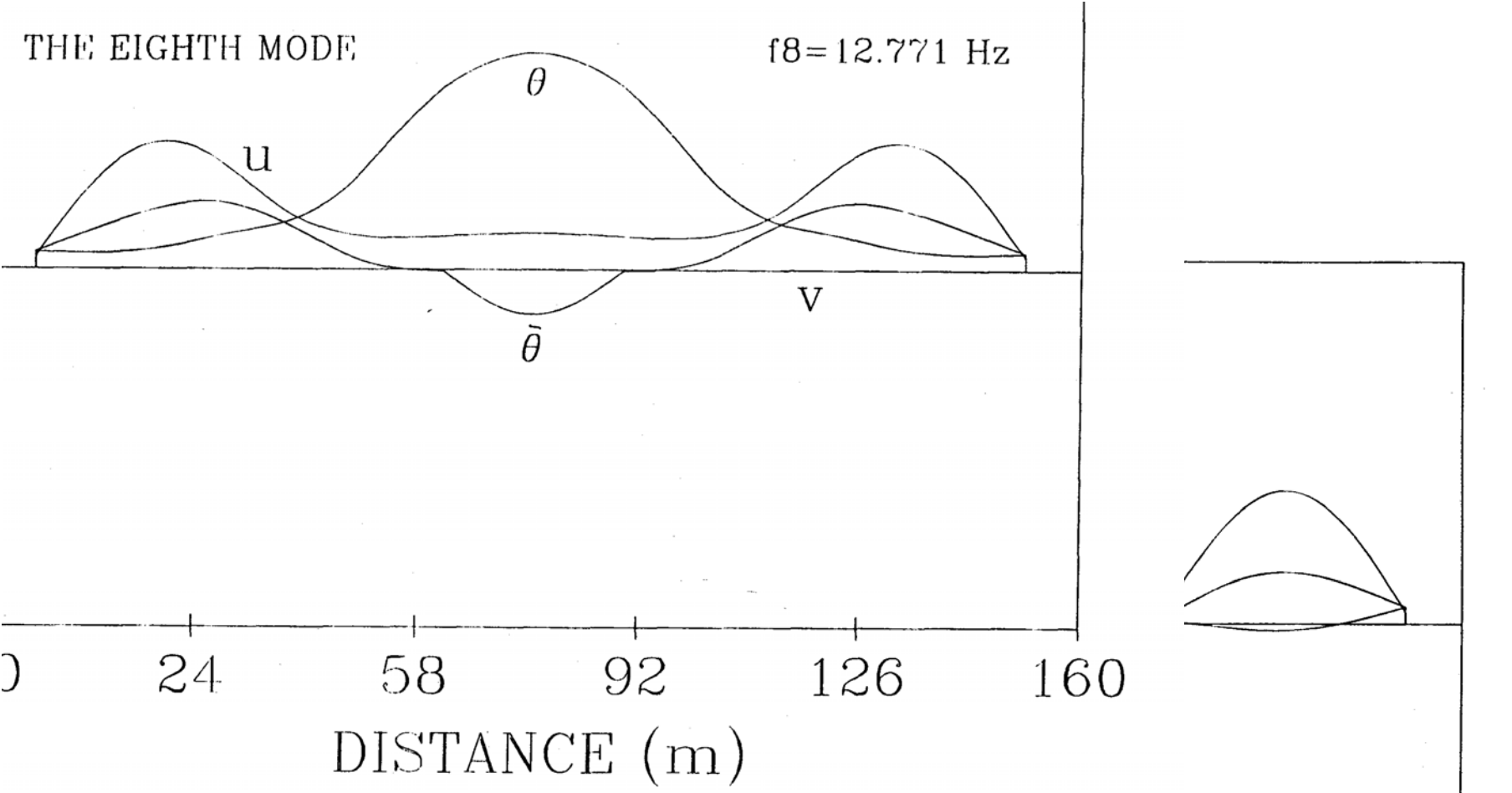

Fig. 4-43. The Eighth Vibration Mode of the Cantilever Bridge with Two Hinge

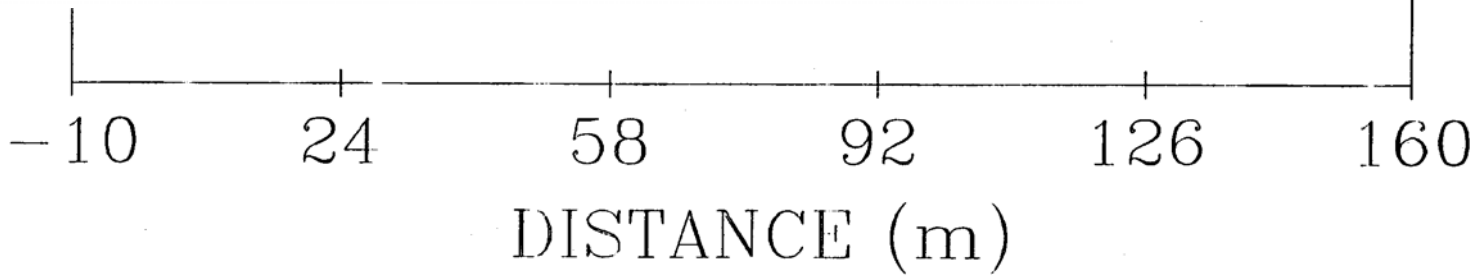

Fig. 4-42. The Seventh Vibration Mode of the Cantilever Bridge with Two Hinge

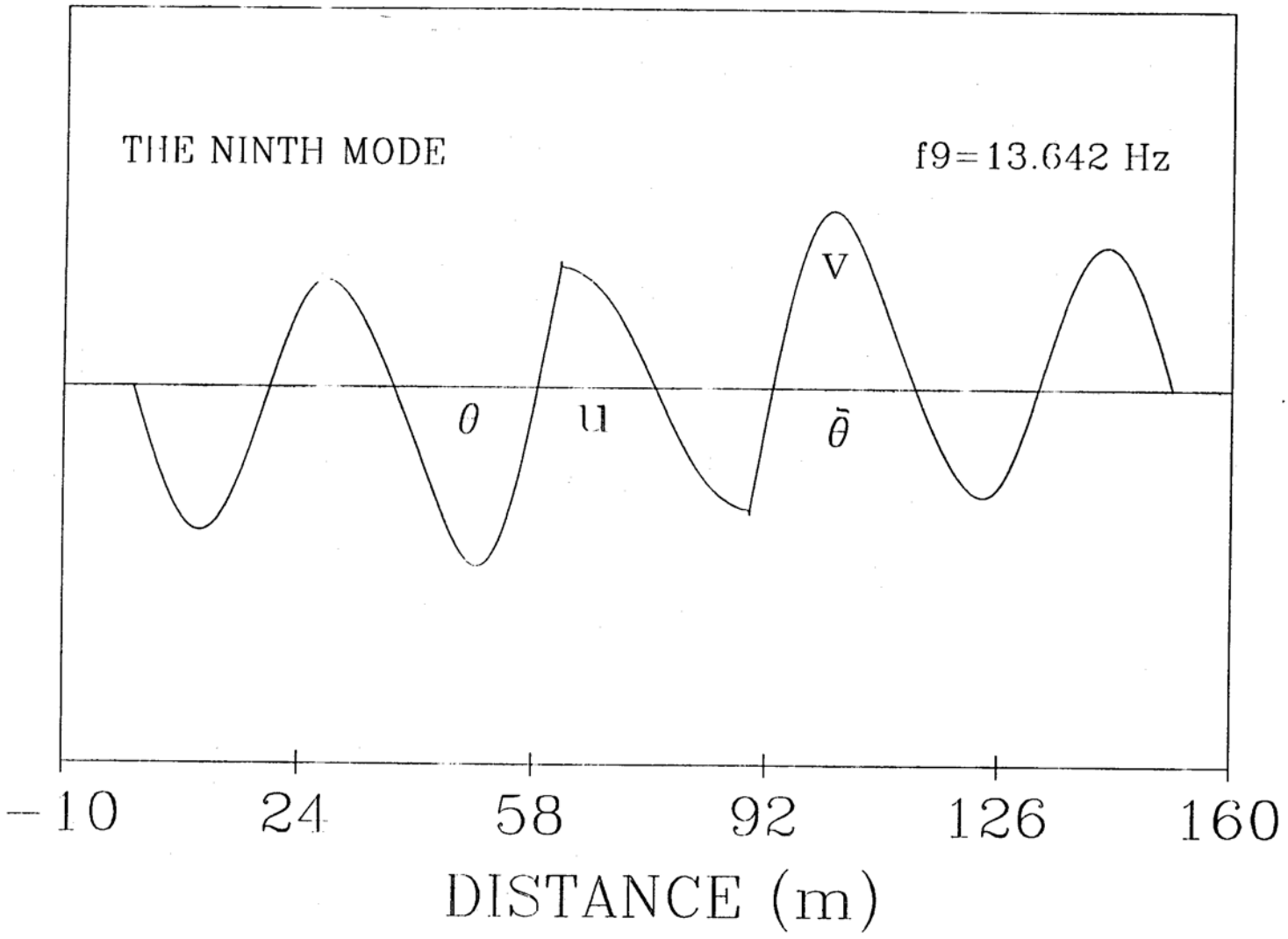

Fig. 4-44. The Ninth Vibration Mode of the Cantilever Bridge with Two Hinge

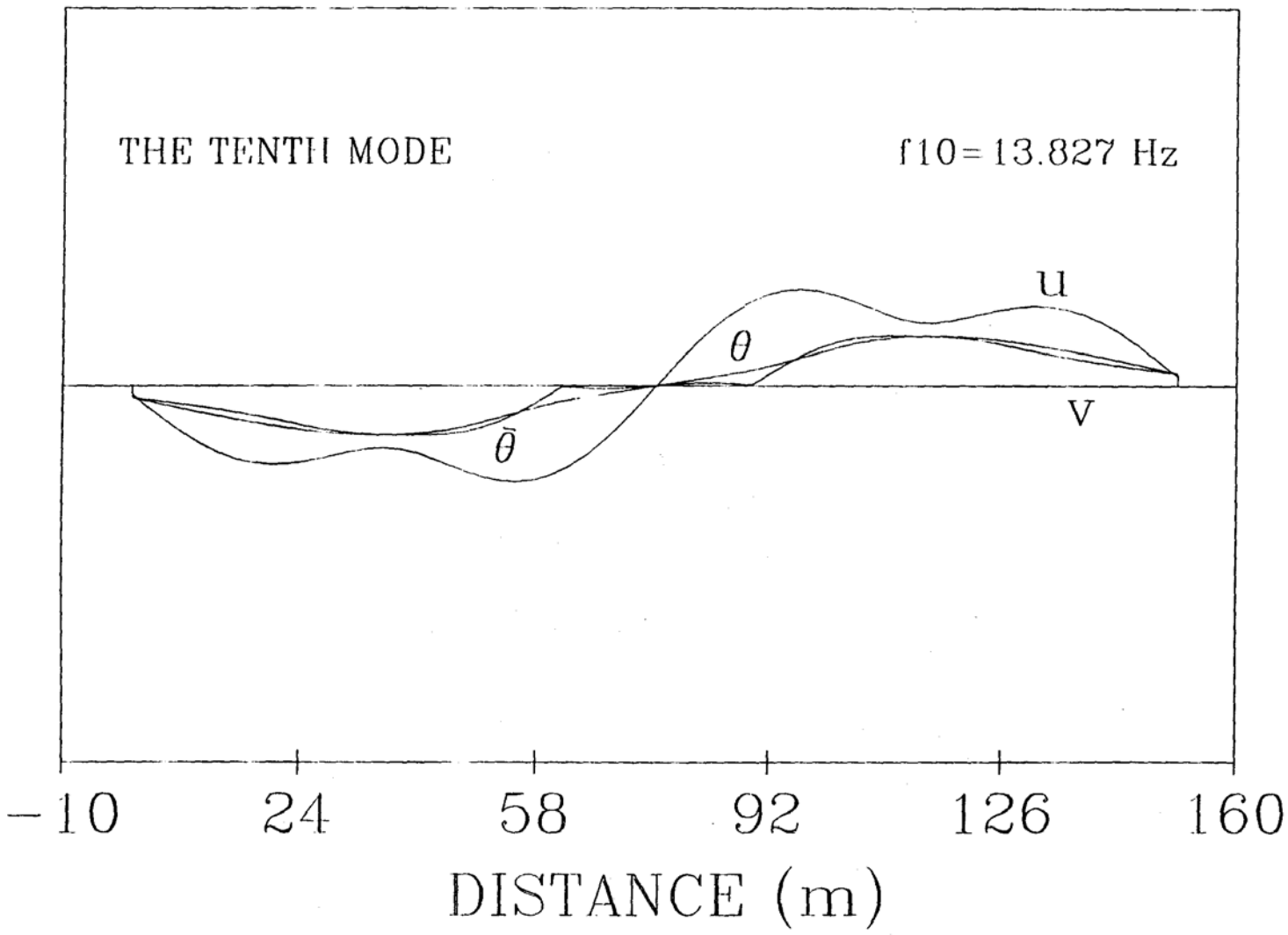

Fig. 4-45. The Tenth Vibration Mode of the Cantilever Bridge with Two Hinge

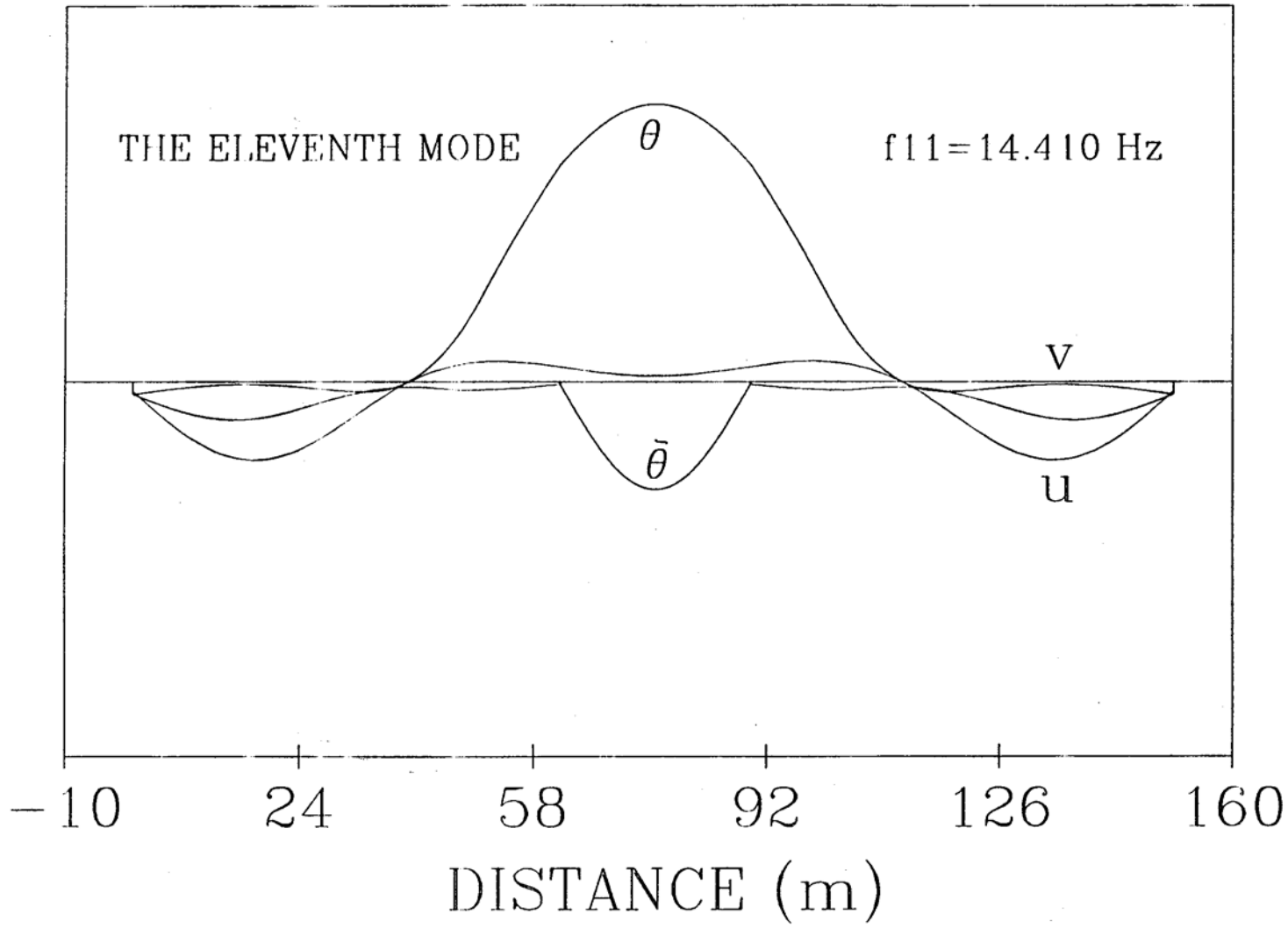

Fig. 4-46. The Eleventh Vibration Mode of the Cantilever Bridge with Two Hinge

at the hinges. Observing Figs 4-3 to 4-24, we can find that the diaphragms over supports greatly affect the torsional frequencies and their vibration modes, while no effect is taken place for the bending frequencies. It can be expected that more torsional vibration modes will influence the dynamic torsional response if external excited force is large enough.

4.4. Forced vibration analysis

Some assumptions have been made in the dynamic analysis. The bridges are hypothesized to have damping characteristics that can be modeled as viscous. The damping matrix is assumed to be proportional to mass and stiffness and be made up of the combination of these (5]. One percent of damping is supposed for the first and second modes according to Ruhl (45]. The solutions of Eq. 2-28 are obtained by the Newmark method (2]. It is found that the time step of 0.001 sec. can give very good accuracy for all kinds of dynamic responses. In order to get the initial displacements and velocities of vehicle DOF's when the vehicles entered the bridge, the vehicles were started the motion at a distance of 42.67 m (140 ft), (i.e. five-car length) away from the left end of the bridge and continued moving until the entire vehicles cleared the right end of the bridge. All trucks have the same left and right road surface roughnesses. The same class of road surface is assumed for both the approach roadways and bridge decks.

4.4.1. Time Histories

In order to illustrate the detailed responses of the bridges, the complete histories of

deflection, shear, bending moment, torque, and bi-moment for the three different types of box girder bridges are plotted, respectively in Figs. 4-47 to 4-100. The abscissa in these figures represents the distance between the left support and the position of the front axle of the vehicles on the bridge. Also shown in dotted lines in each figure is the static response. The dynamic responses are represented by solid lines. All history curves are calculated based on the loading model of three HS20-44 trucks side by side (see Fig. 4-101 (b)), good road surface, and vehicle speed of 88.5 km/hr.(55 mph). The histories of the continuous box girder bridge are demonstrated in Figs. 4-47 to 4-64; those of the cantilever bridges with one hinge are presented in Figs. 4-65 to 4-82; and Figs. 4-83 to 4-100 illustrate the histories of the cantilever bridge with two hinges. Eighteen figures of time histories are given for each type of bridges, corresponding to vertical shear (y-direction) Q_y, torque T_c and distortion torque $T_{\bar{\omega}}$. at left end support, deflection D_y. at mid-span, as well as lateral bending moment M_X, Q_y, T_c, bi-moment B_w, $T_{\bar{\omega}}$ distortion bi-moment $B_{\bar{\omega}}$, at Sections 4 and 5.

The following characteristics of the curves in Figs. 4-47 through 4-100 are particularly important. First, the periods of dominant waves in the various curves are different. The fundamental natural mode is the principal contributor to the response at the center of bridges. For the remaining effects, several of the higher natural modes also contribute significantly. The contribution of the second, third, or fourth modes are particularly pronounced for the response of vertical bending moment at Sections 4 and 5. The responses of bi-moment and torque at Section 4 are apparently dominated by the third/fourth and higher modes.

The second feature of importance in Figs. 4-47 to 4-100 is the critical dynamic response

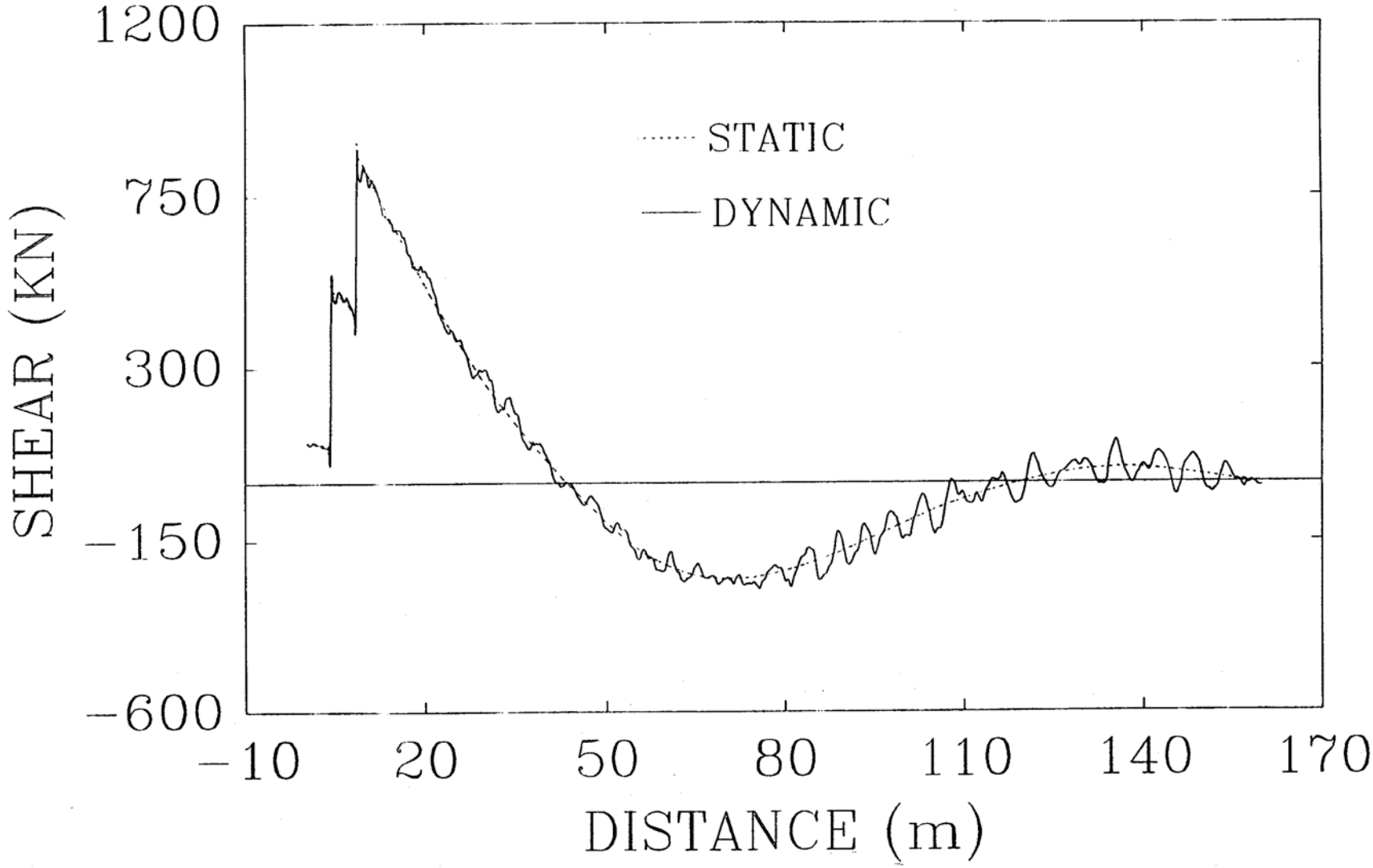

Fig. 4-47. Histories of Vertical Shear at Section 0 of Bridge Type I

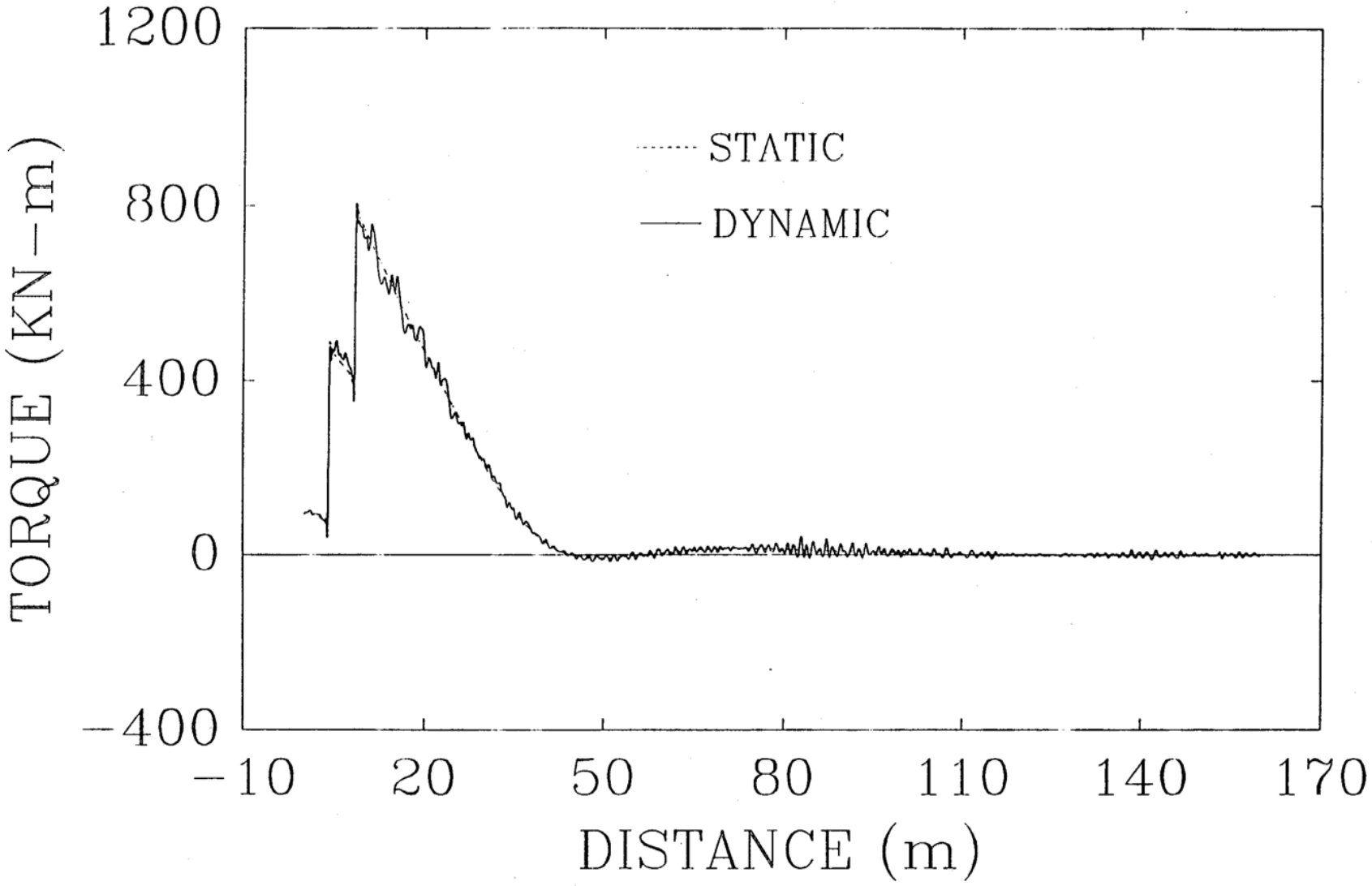

Fig. 4-48. Histories of Torque at Section 0 of Bridge Type I

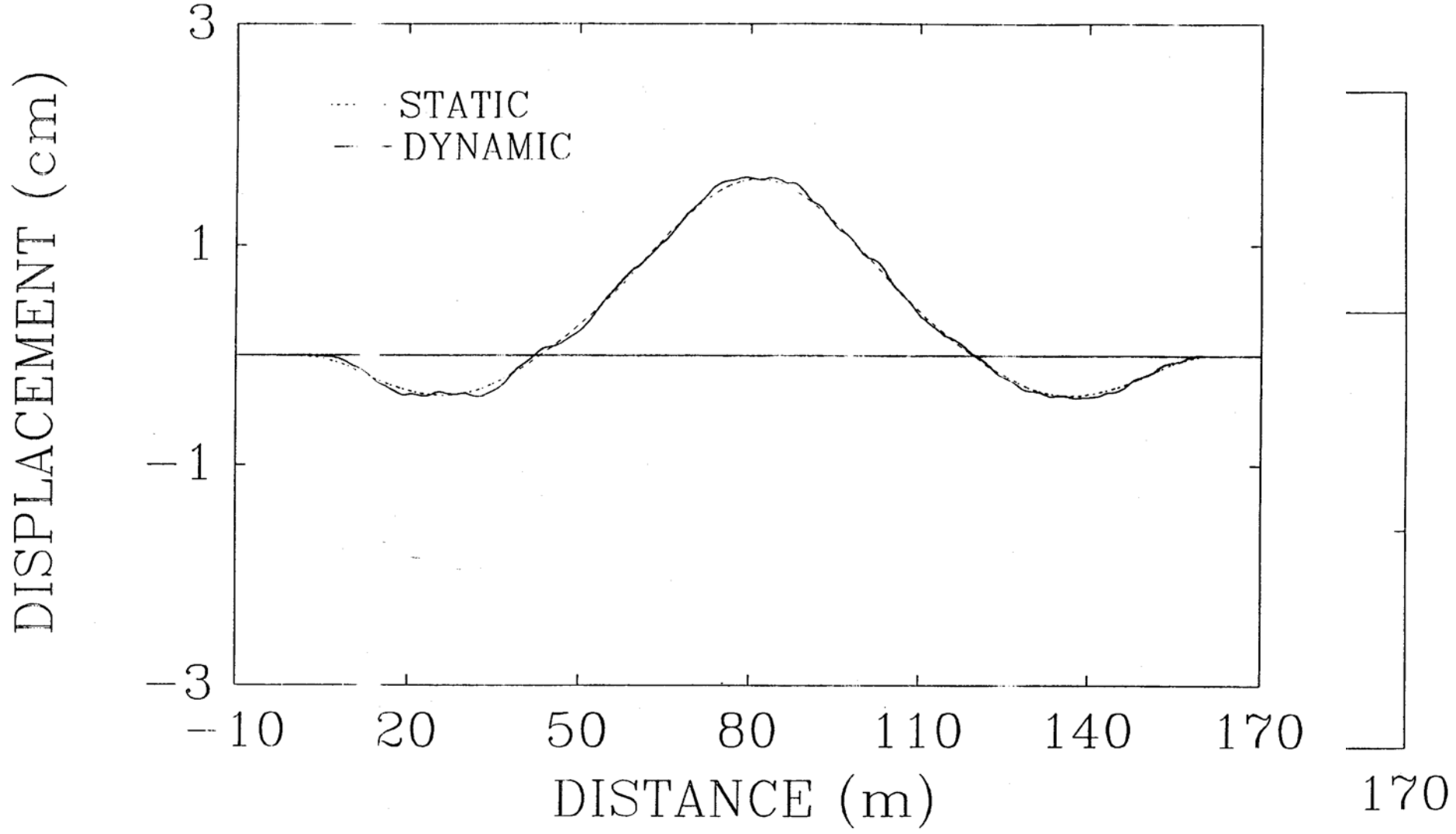

Fig. 4-50. Histories of Deflection at Mid-span of Bridge Type I

Fig. 4-49. Histories of Torque due to Distortion at Section 0 of Bridge Type I

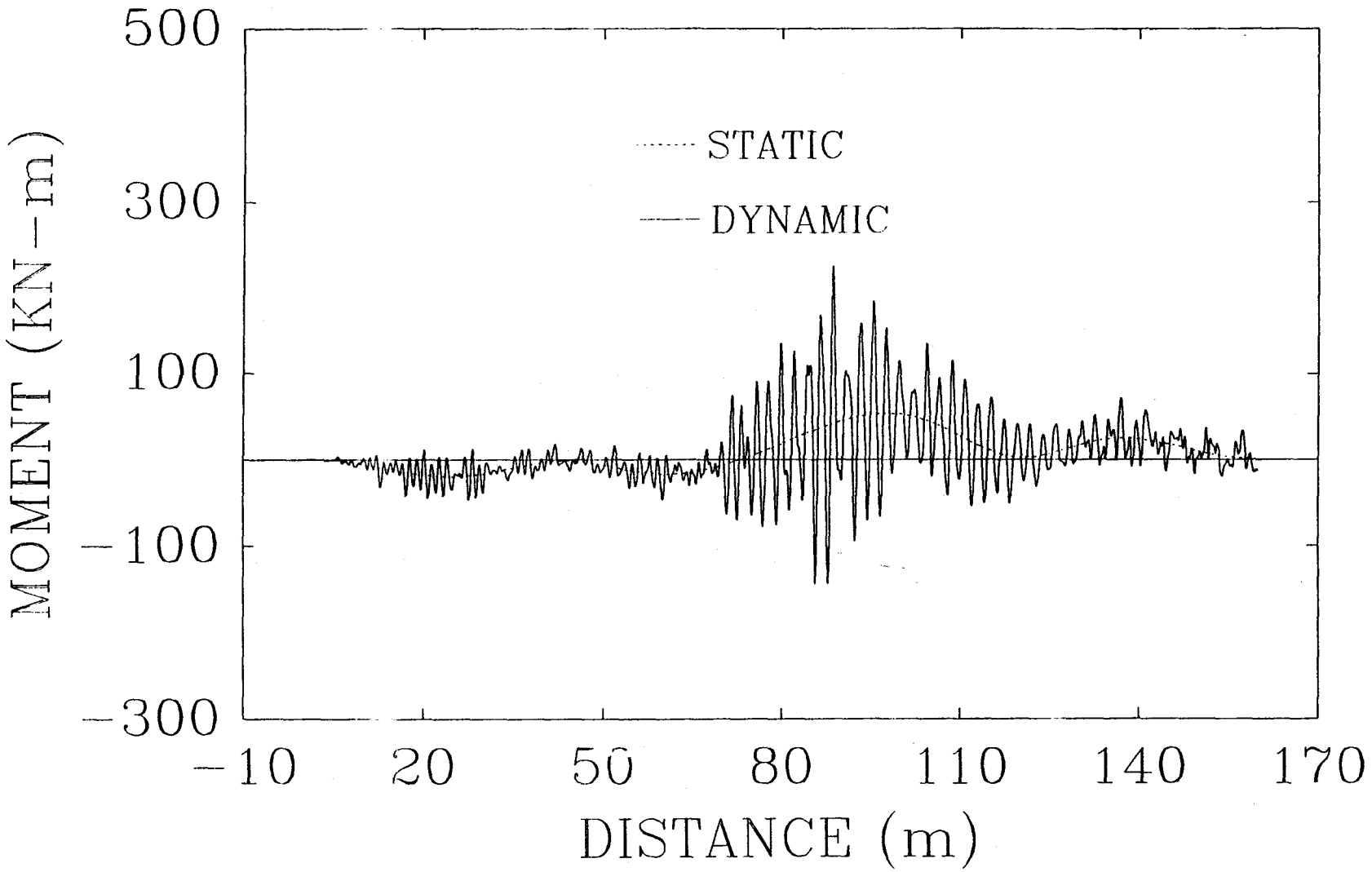

Fig. 4-51. Histories of Lateral Bending Moment at Section 4 of Bridge Type I

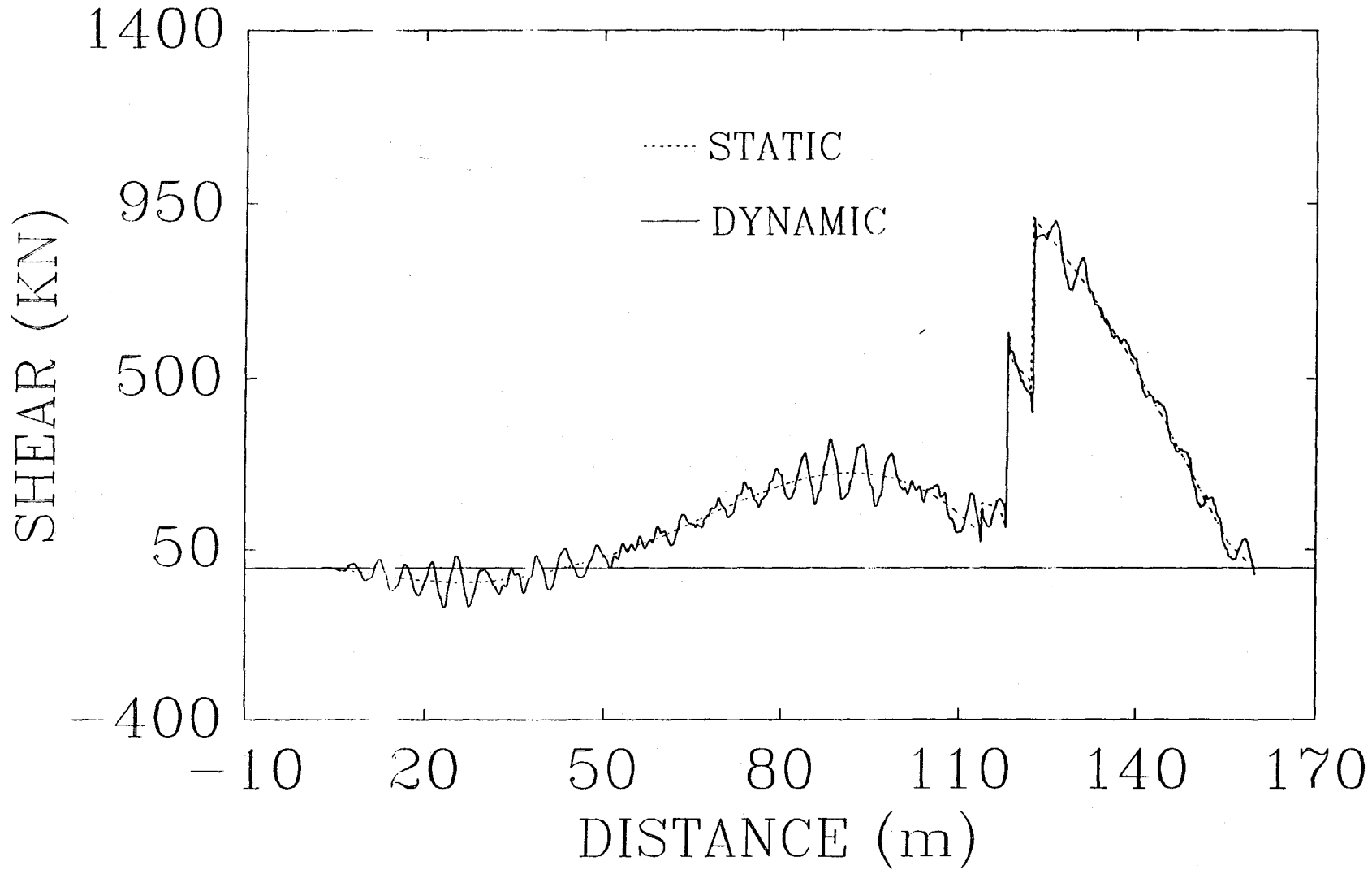

Fig. 4-52. Histories of Vertical Shear at Section 4 of Bridge Type I

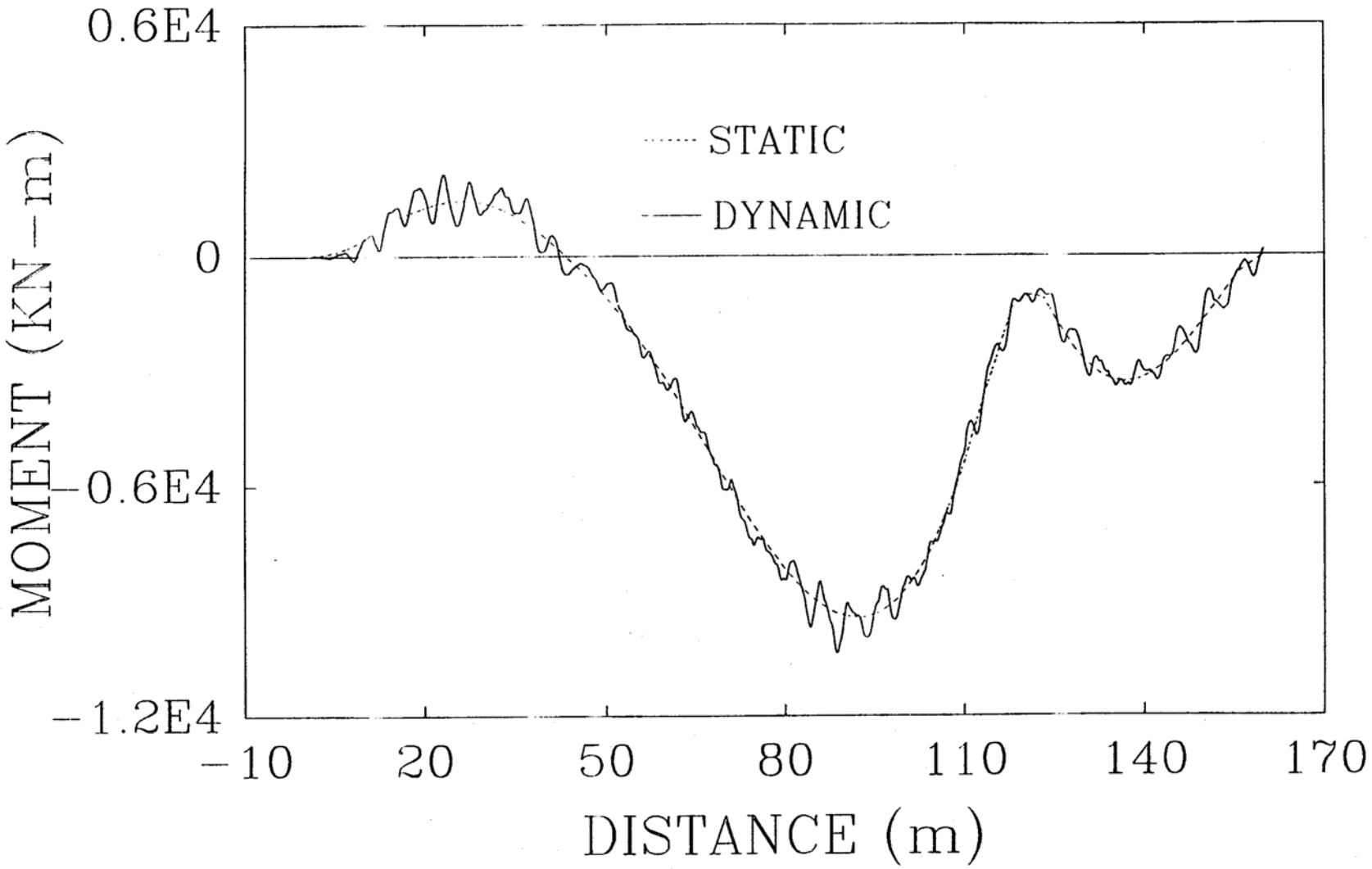

Fig. 4-53. Histories of Vertical Bending Moment at Section 4 of Bridge Type I

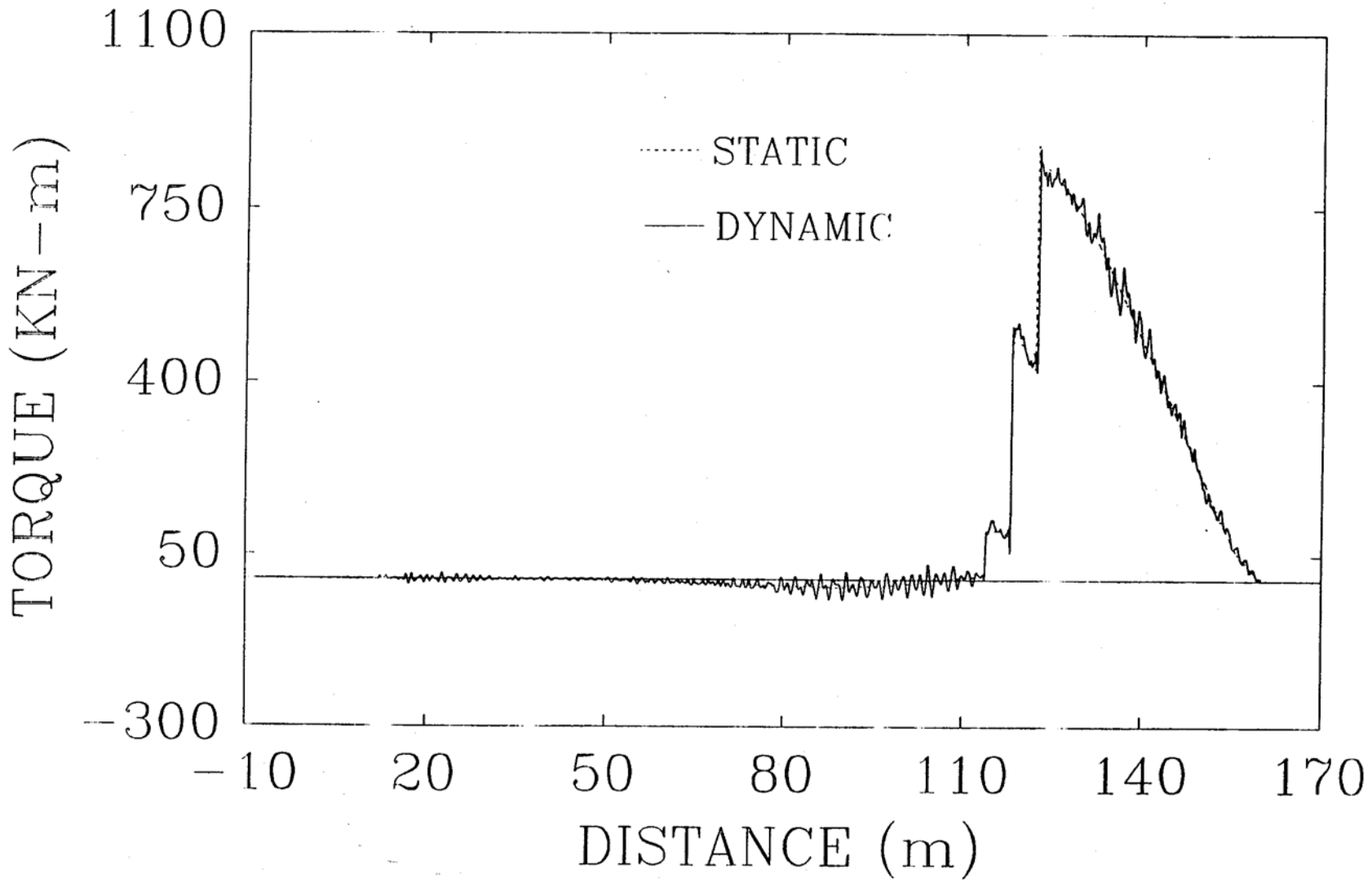

Fig. 4-54. Histories of Torque at Section 4 of Bridge Type I

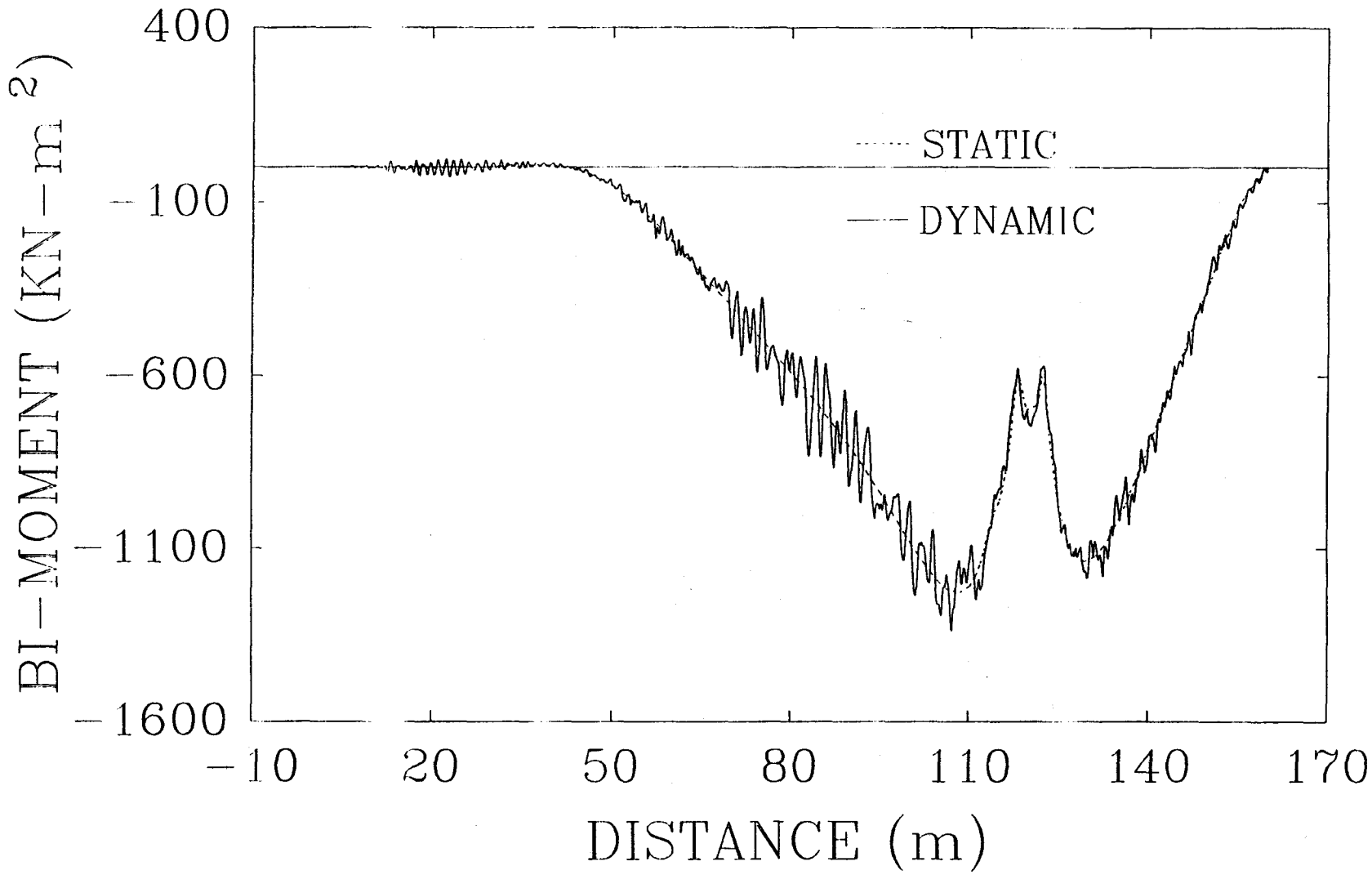

Fig. 4-55. Histories of Bi-moment at Section 4 of Bridge Type I

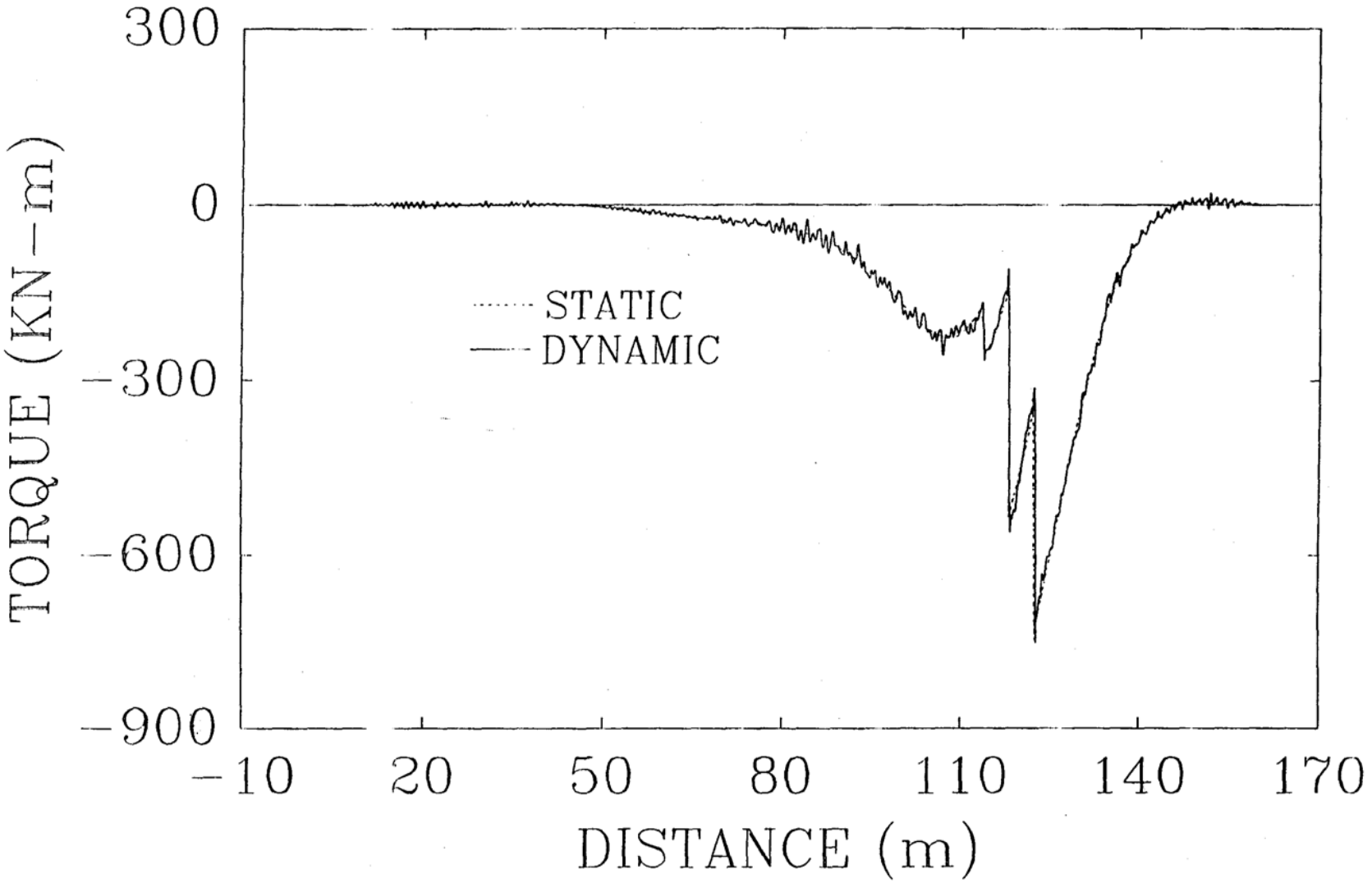

Fig. 4-56. Histories of Torque due to Distortion at Section 4 of Bridge Type I

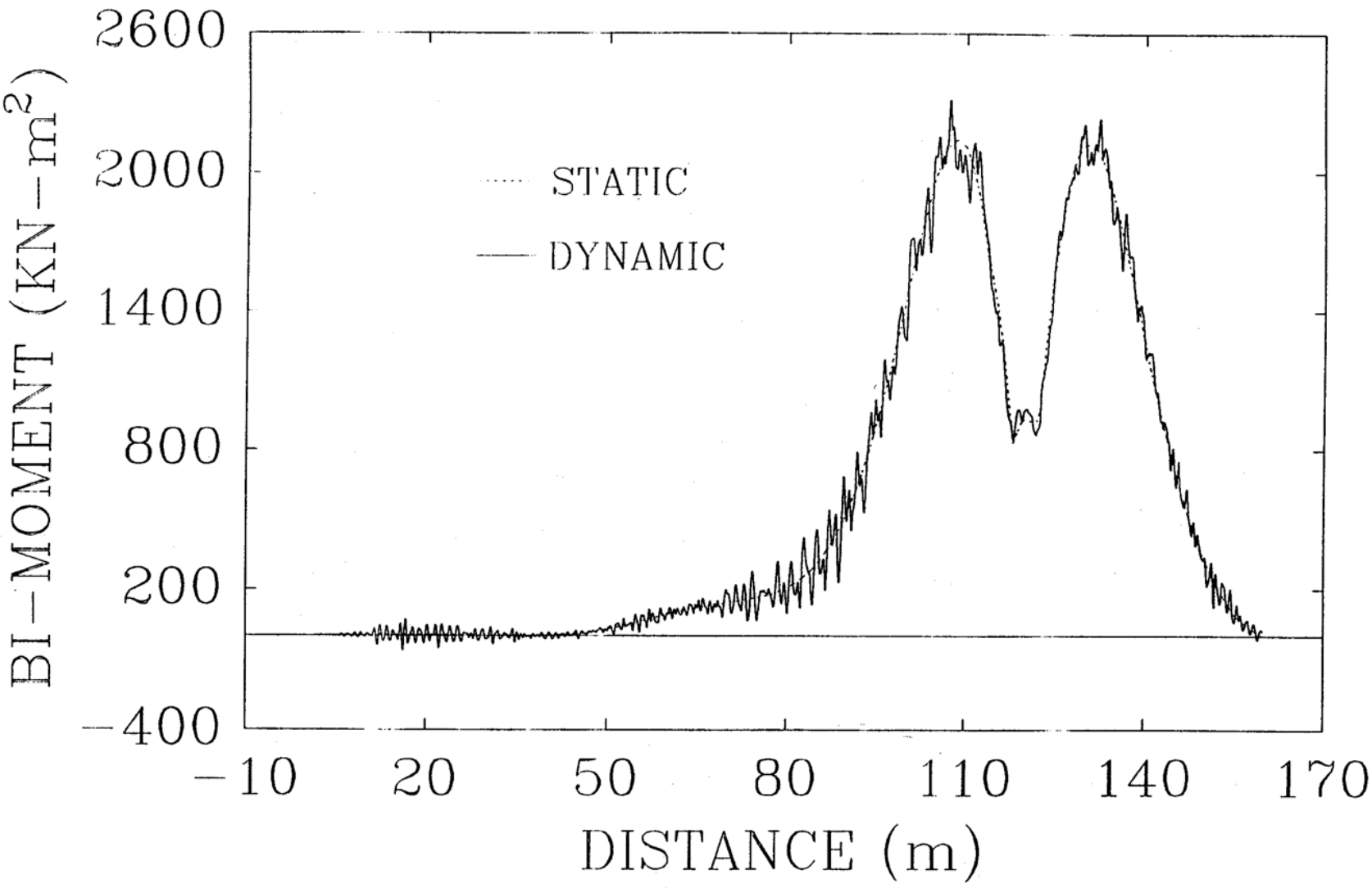

Fig. 4-57. Histories of Bi-moment due to Distortion at Section 4 of Bridge Type I

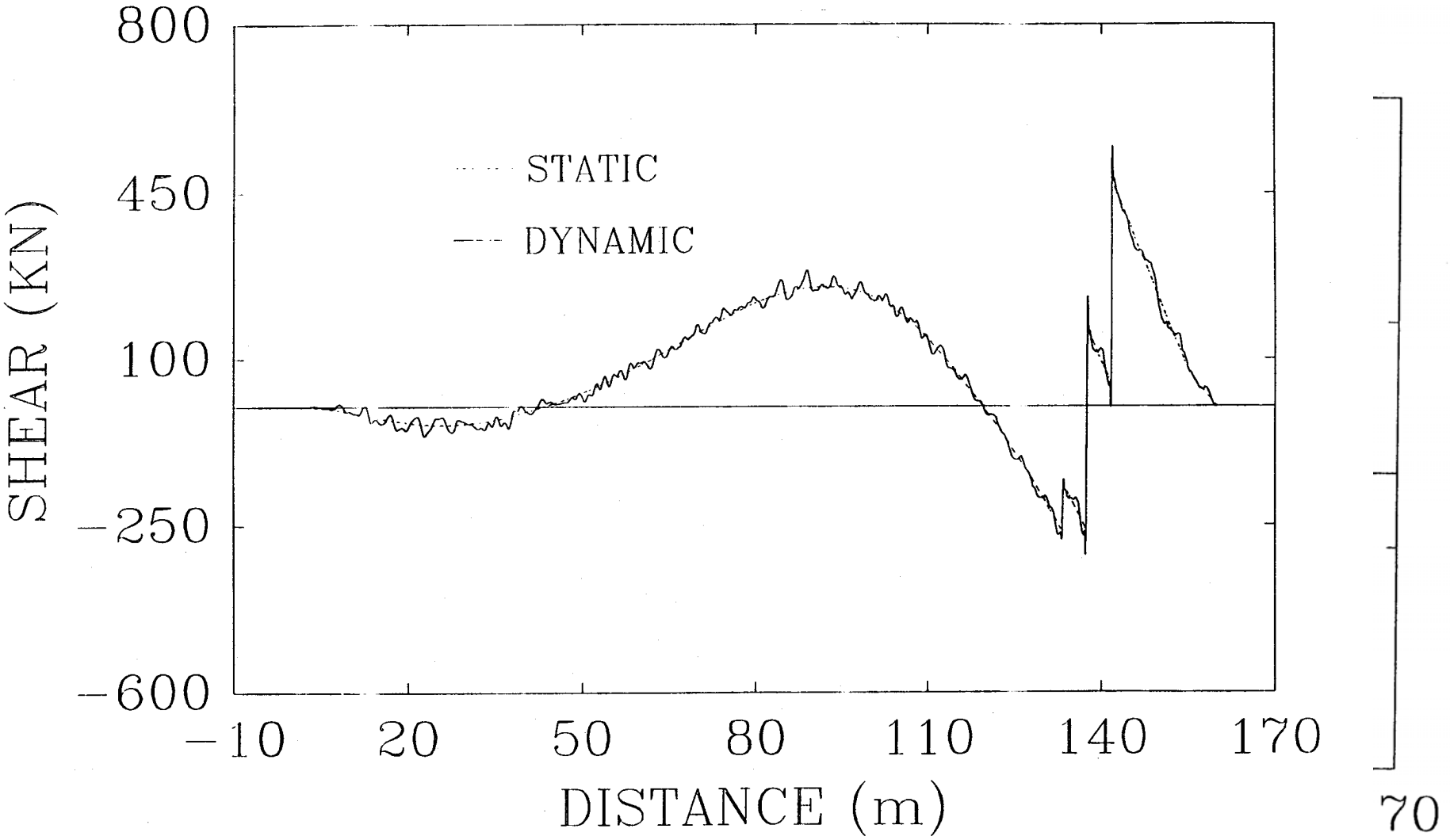

Fig. 4-59. Histories of Vertical Shear at Section 5 of Bridge Type I

Fig. 4-58. Histories of Lateral Bending Moment at Section 5 of Bridge Type I

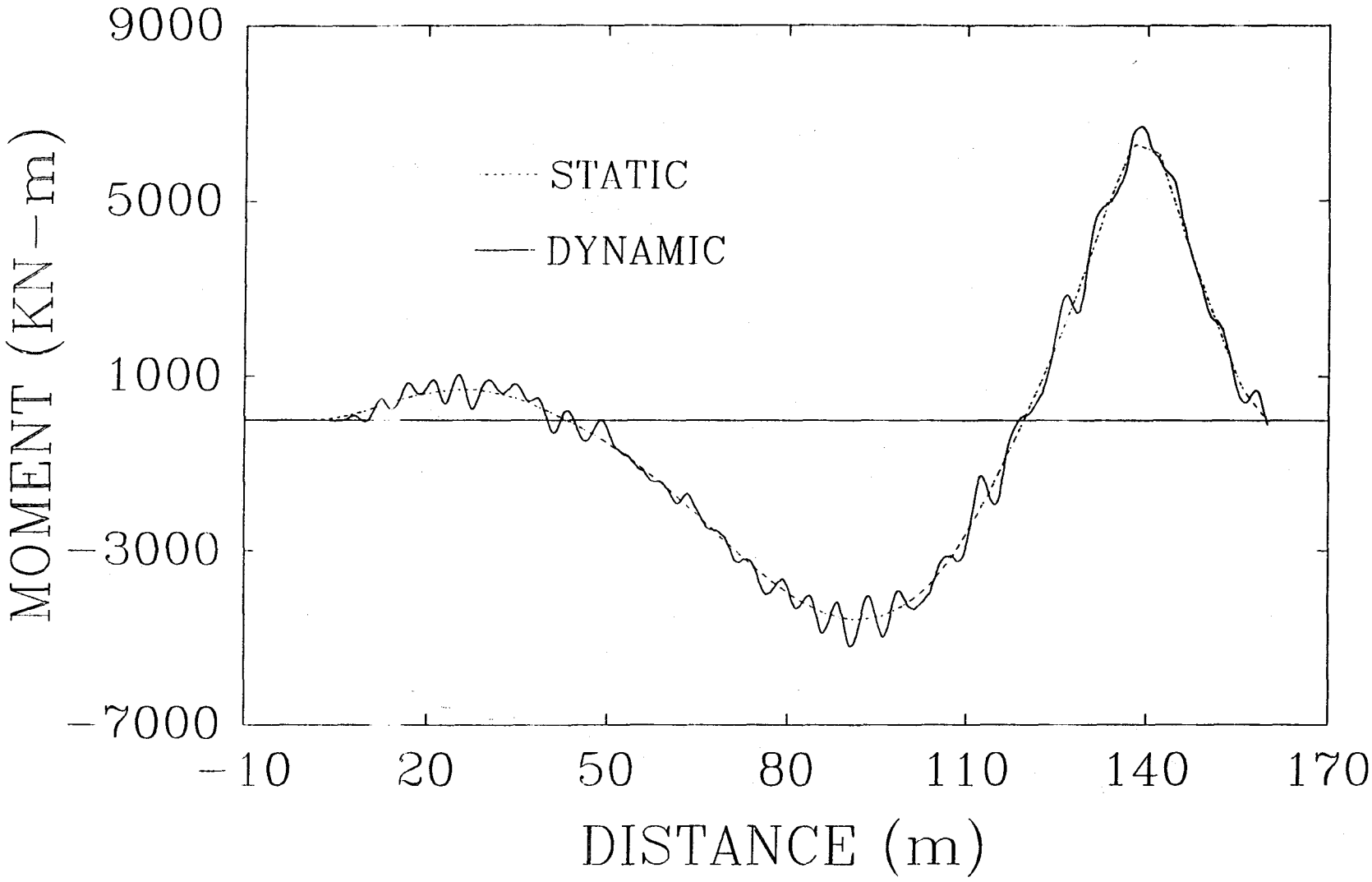

Fig. 4-60. Histories of Vertical Bending Moment at Section 5 of Bridge Type I

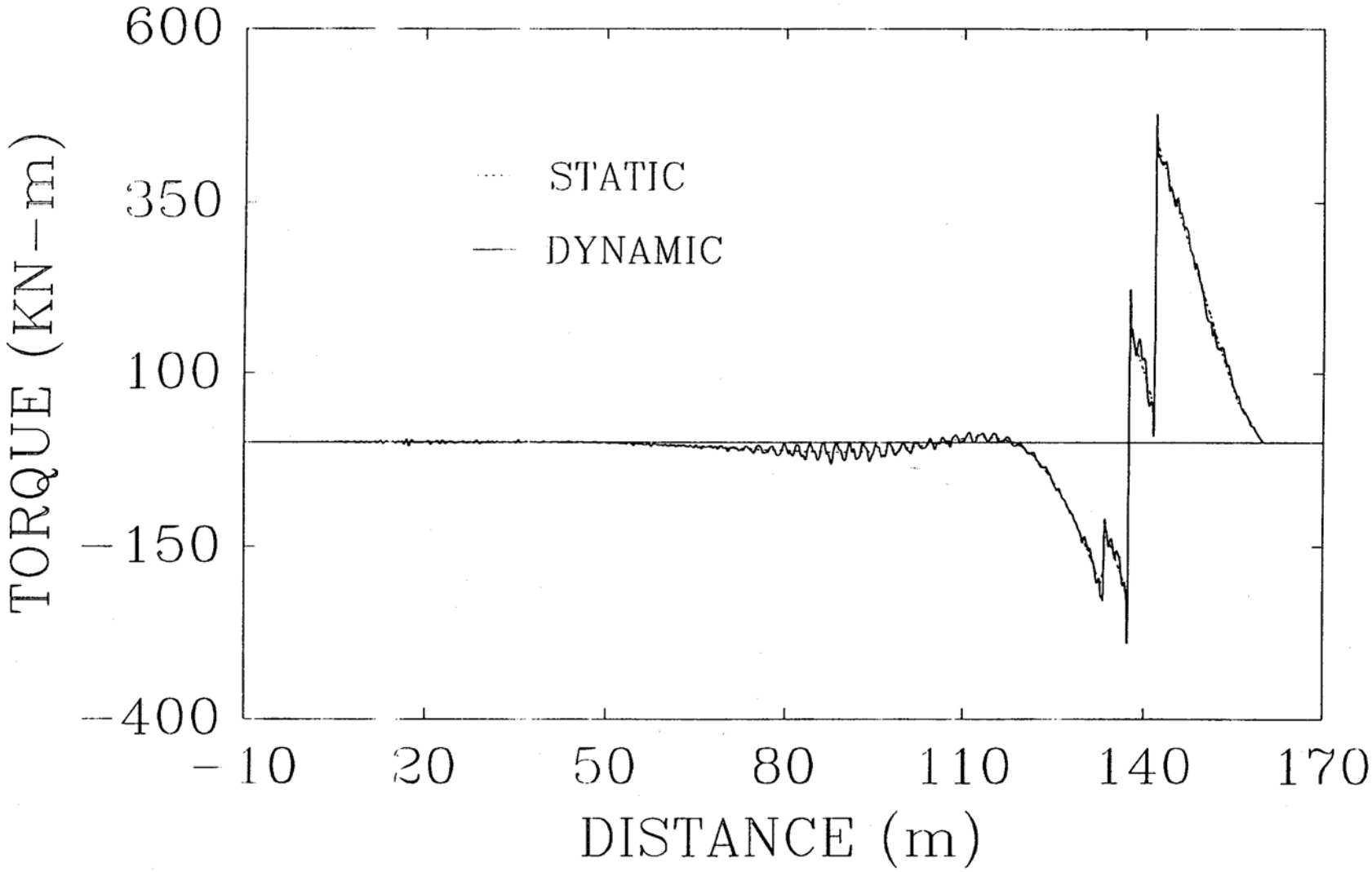

Fig. 4-61. Histories of Torque at Section 5 of Bridge Type I

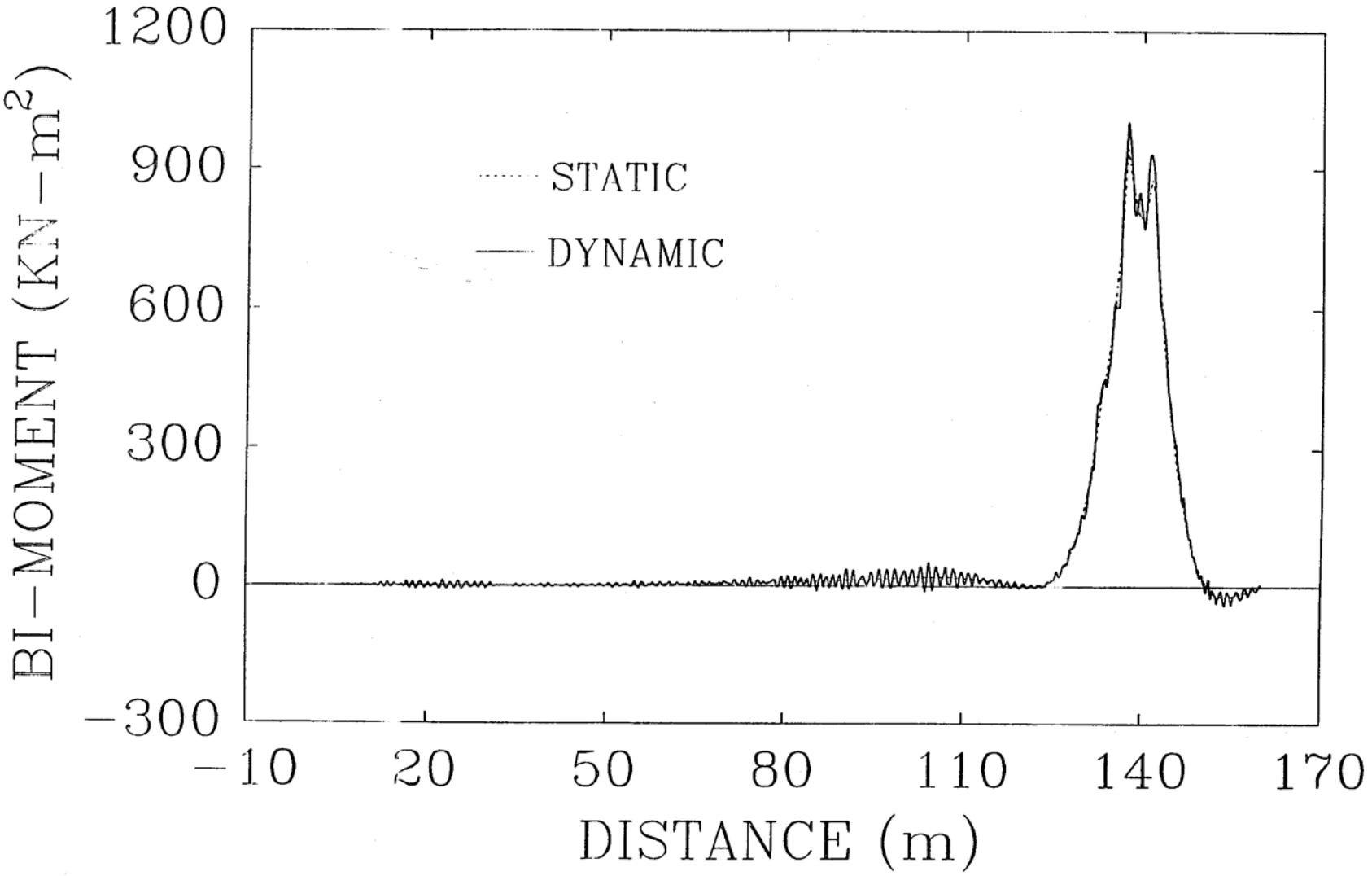

Fig. 4-62. Histories of Bi-moment at Section 5 of Bridge Type I

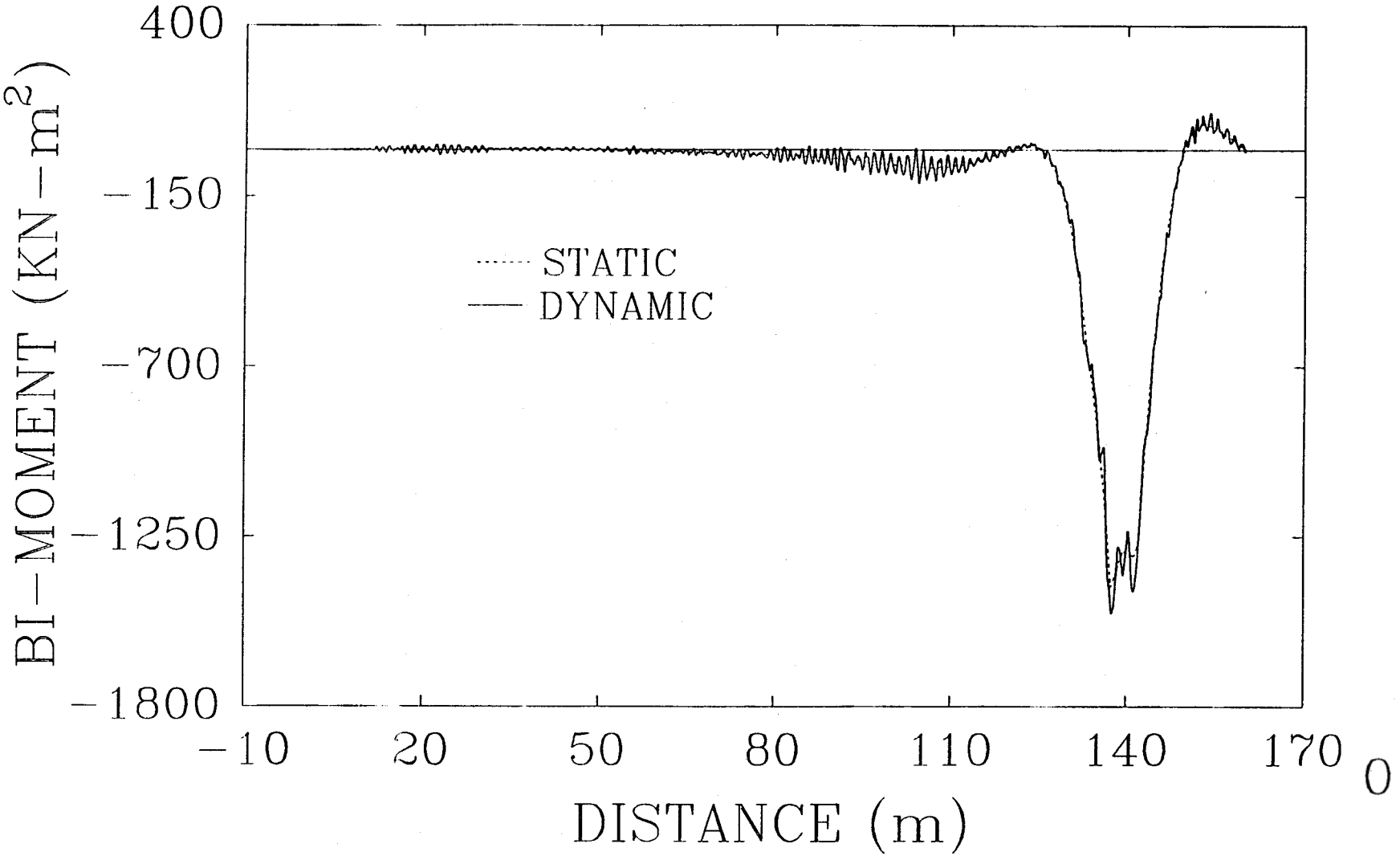

Fig. 4-64. Histories of Bi-moment due to Distortion at Section 5 of Bridge Type I

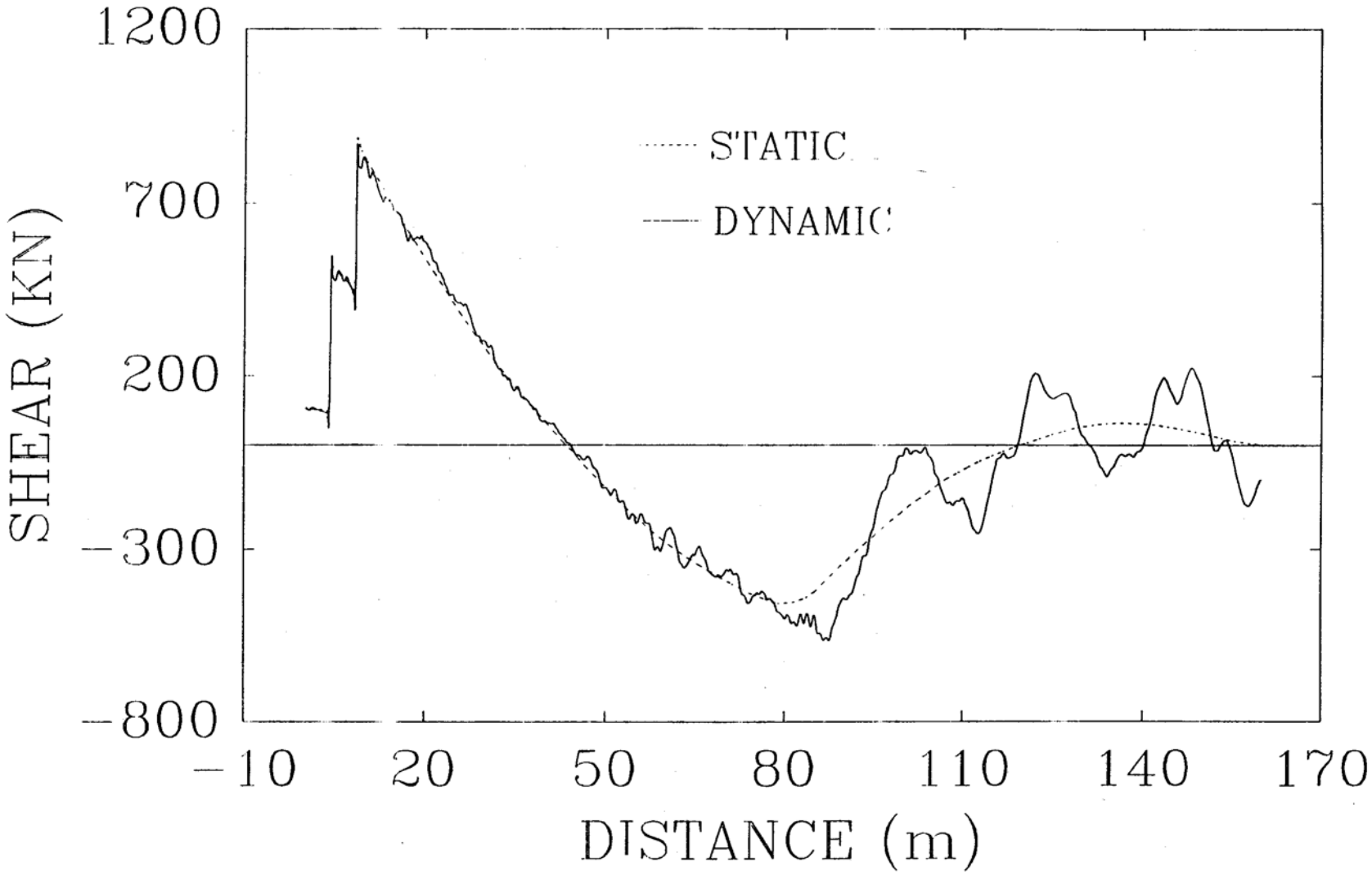

Fig. 4-65. Histories of Vertical Shear at Section 0 of Bridge Type II

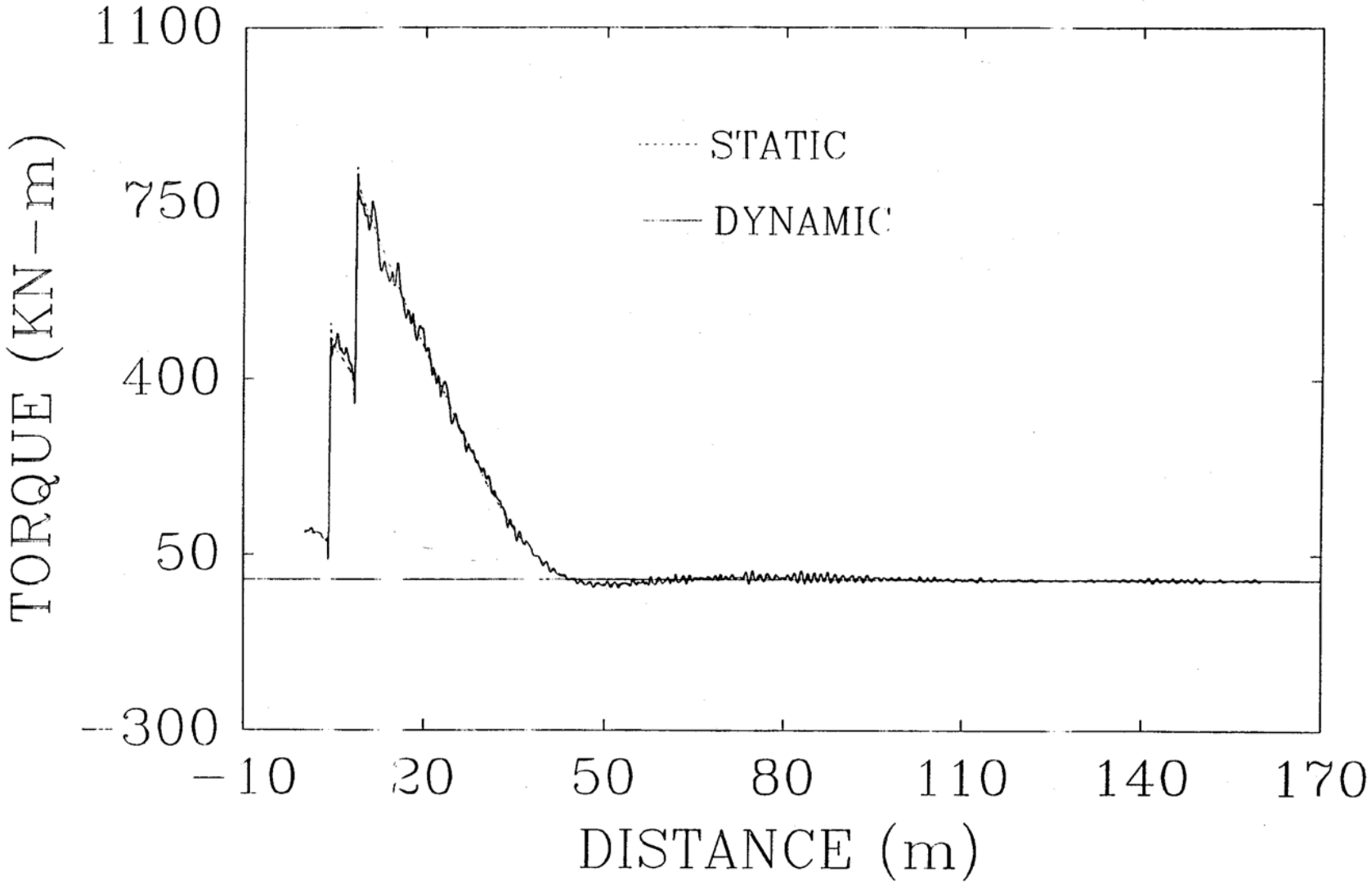

Fig. 4-66. Histories of Torque at Section 0 of Bridge Type II

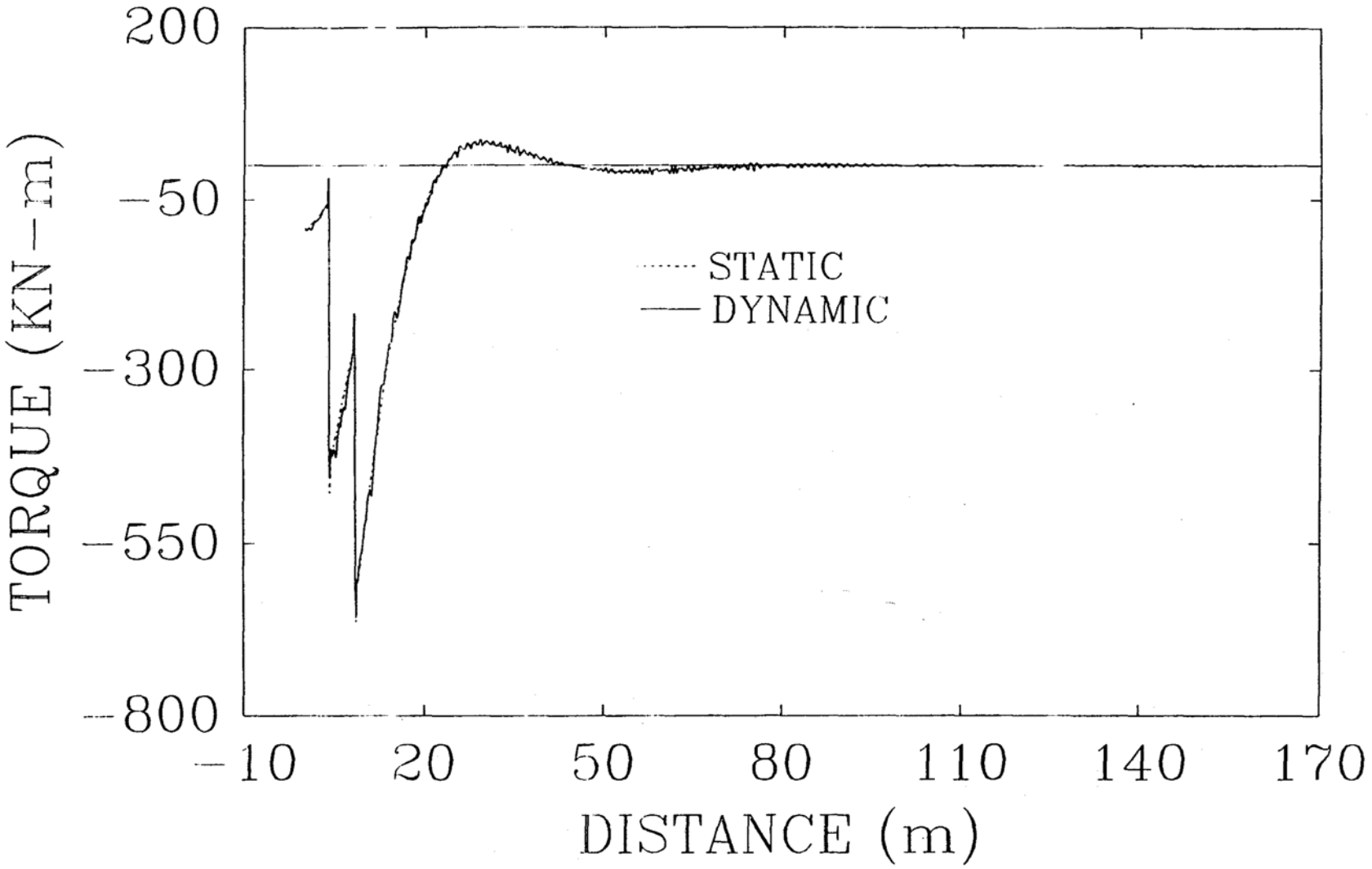

Fig. 4-67. Histories of Torque due to Distortion at Section 0 of Bridge Type II

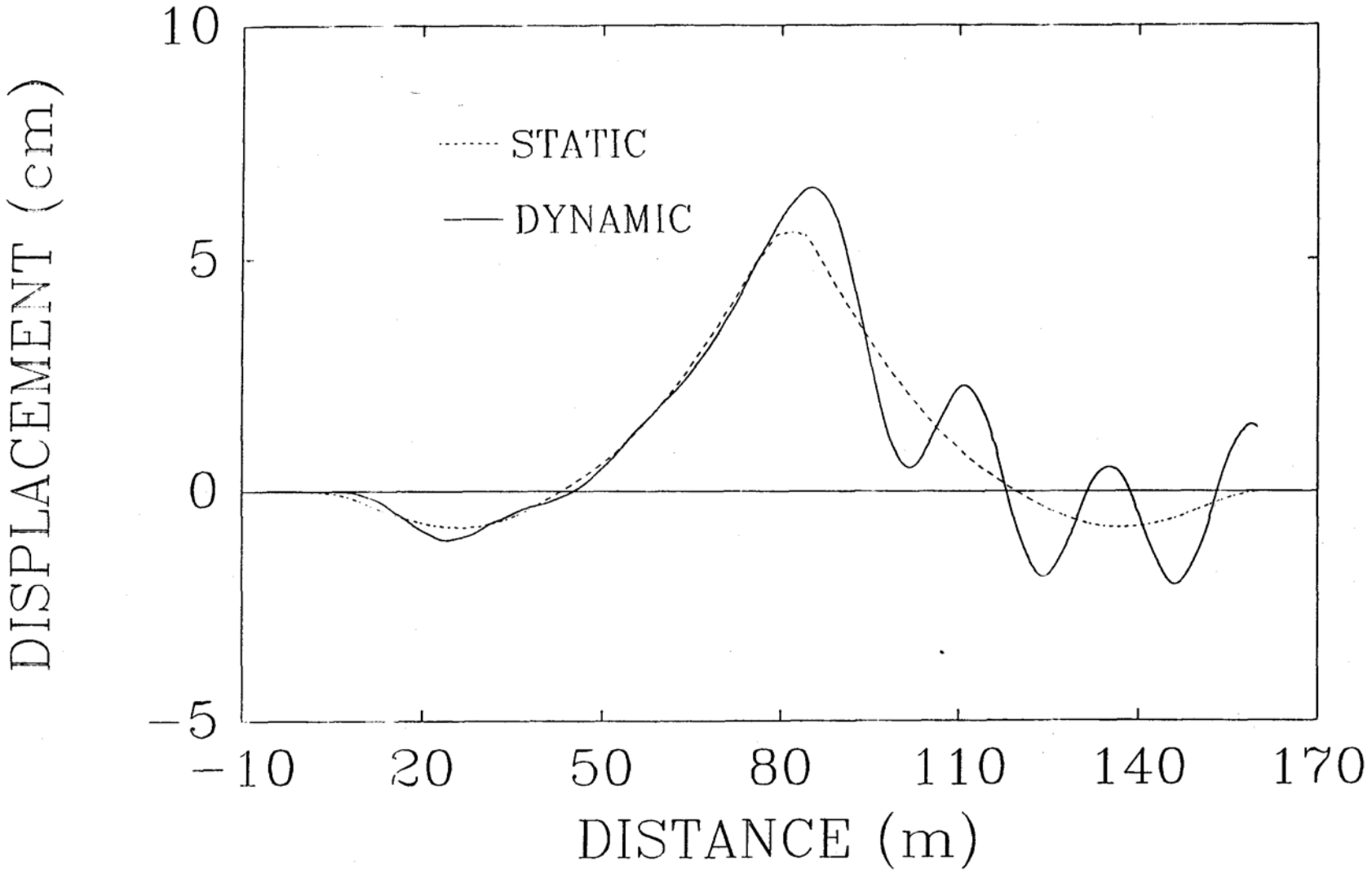

Fig. 4-68. Histories of Deflection at Mid-span of Bridge Type II

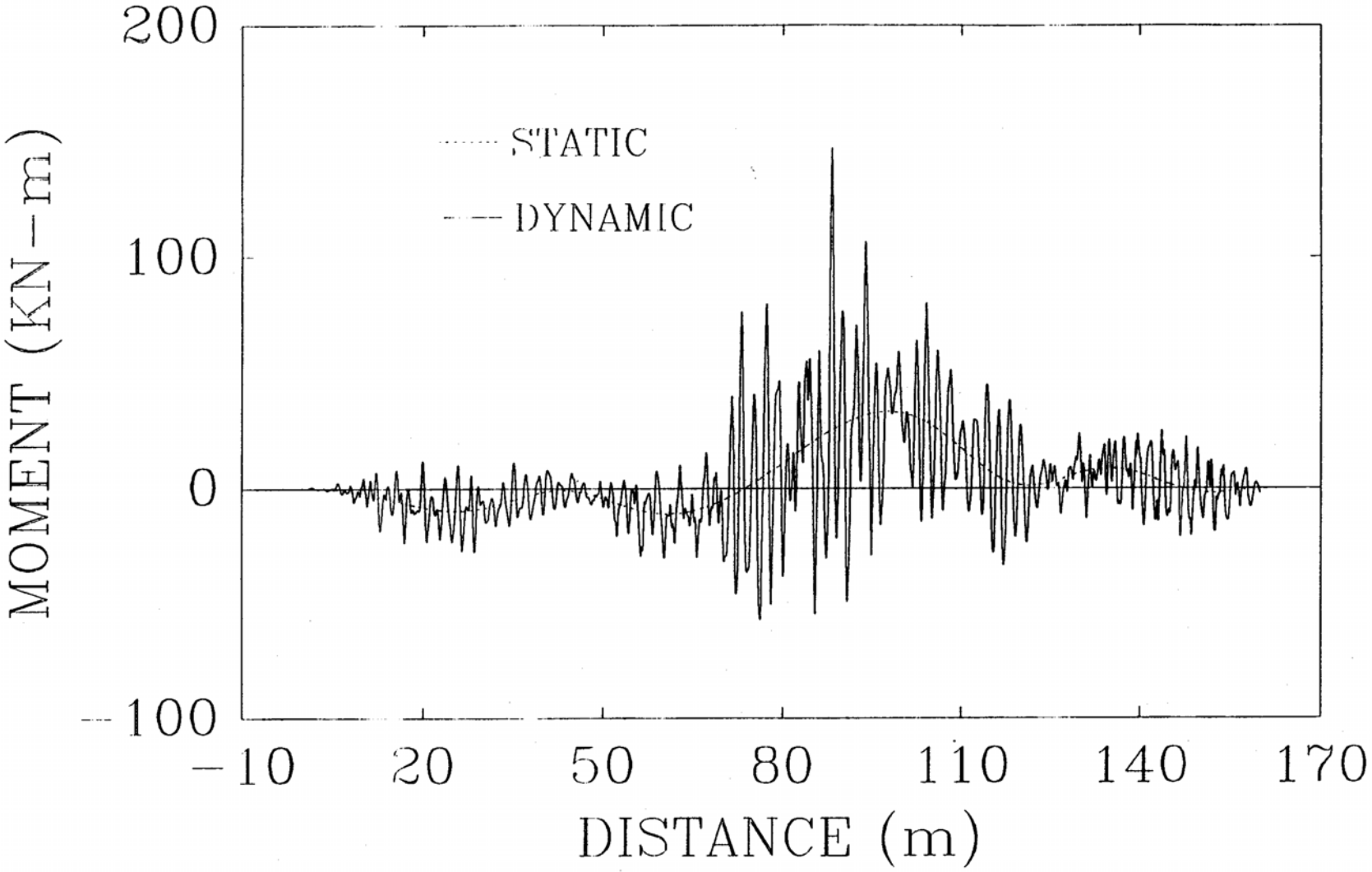

Fig. 4-69. Histories of Lateral Bending Moment at Section 4 of Bridge Type II

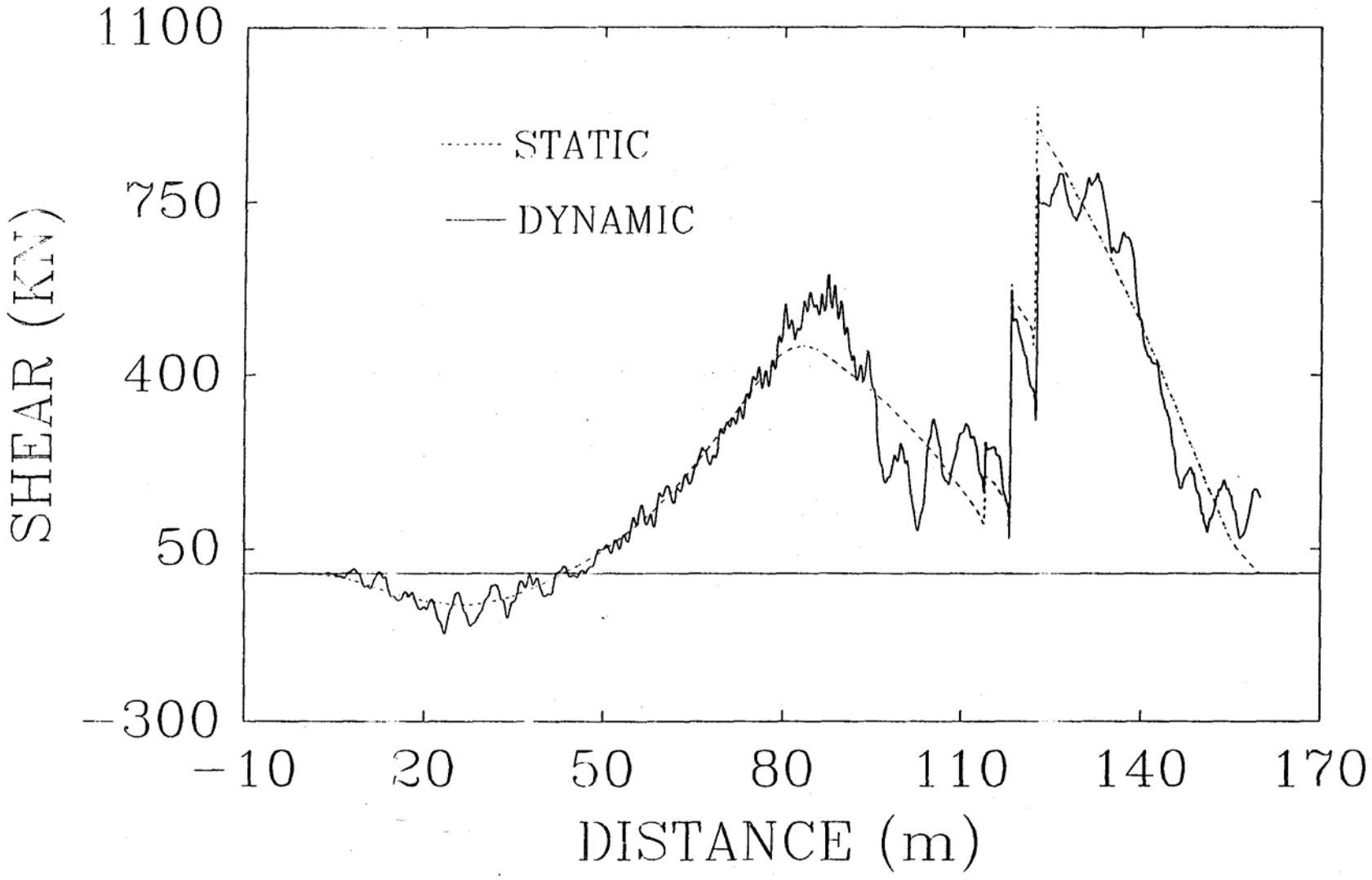

Fig. 4-70. Histories of Vertical Shear at Section 4 of Bridge Type II

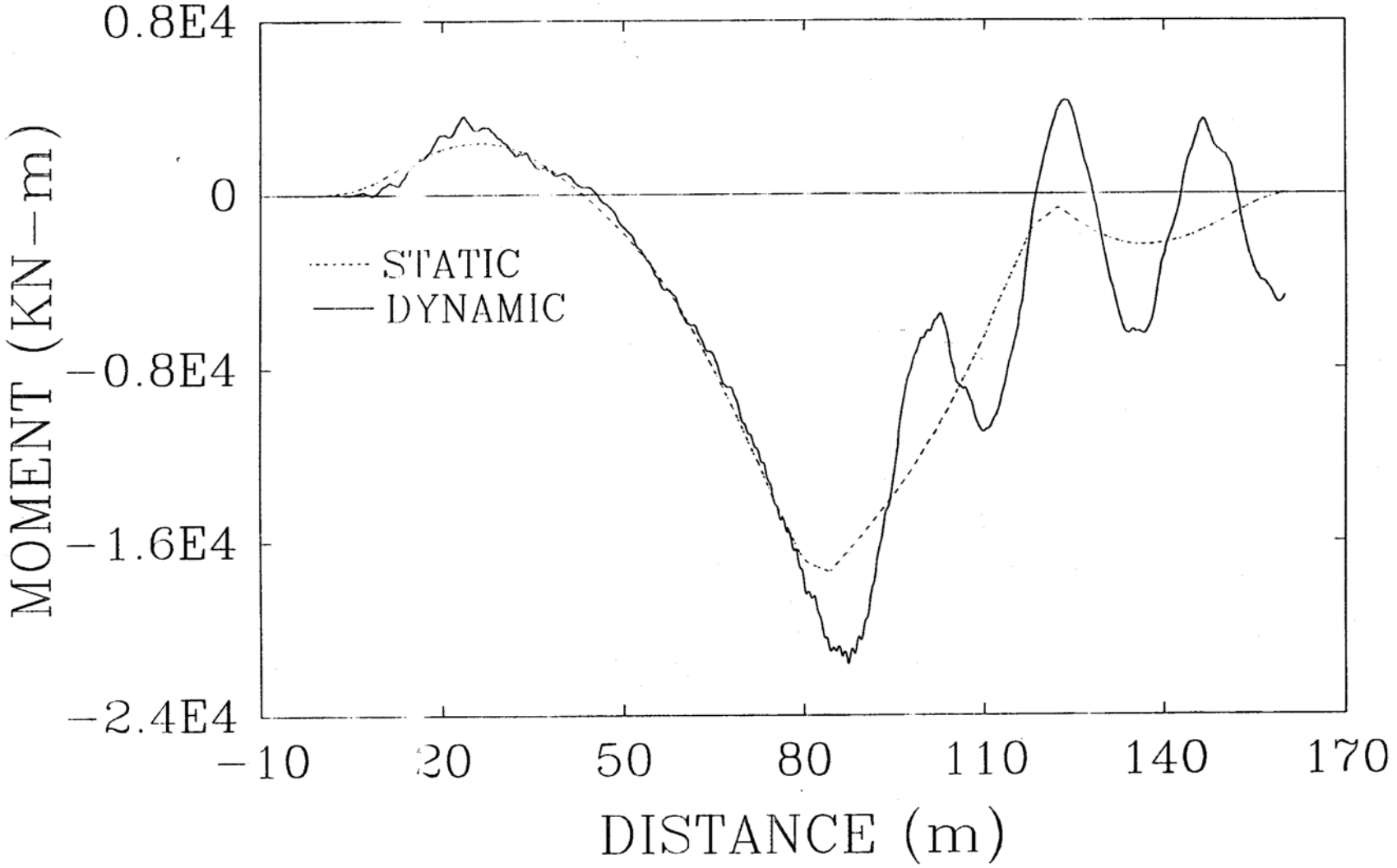

Fig. 4-71. Histories of Vertical Bending Moment at Section 4 of Bridge Type II

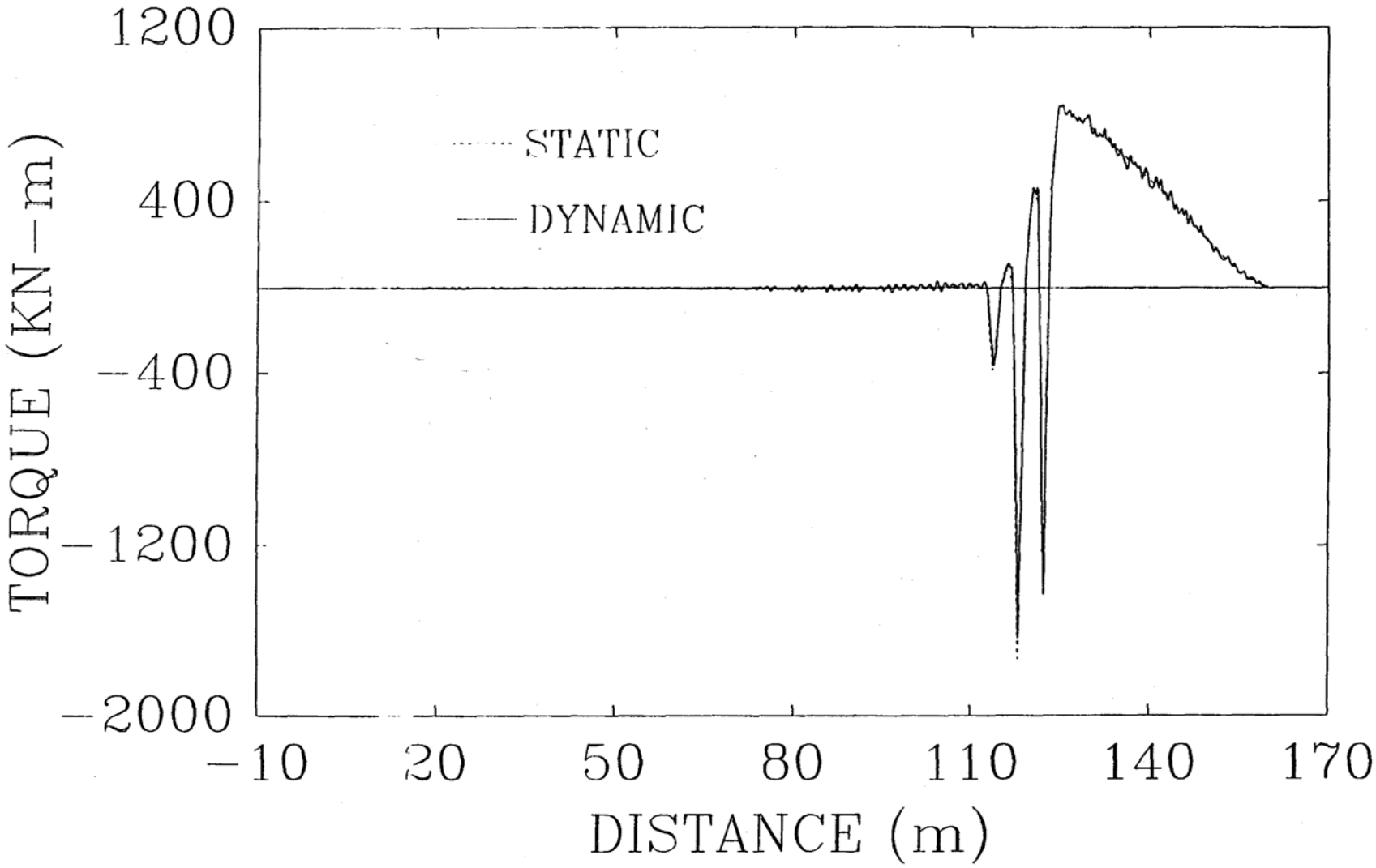

Fig. 4-72. Histories of Torque at Section 4 of Bridge Type II

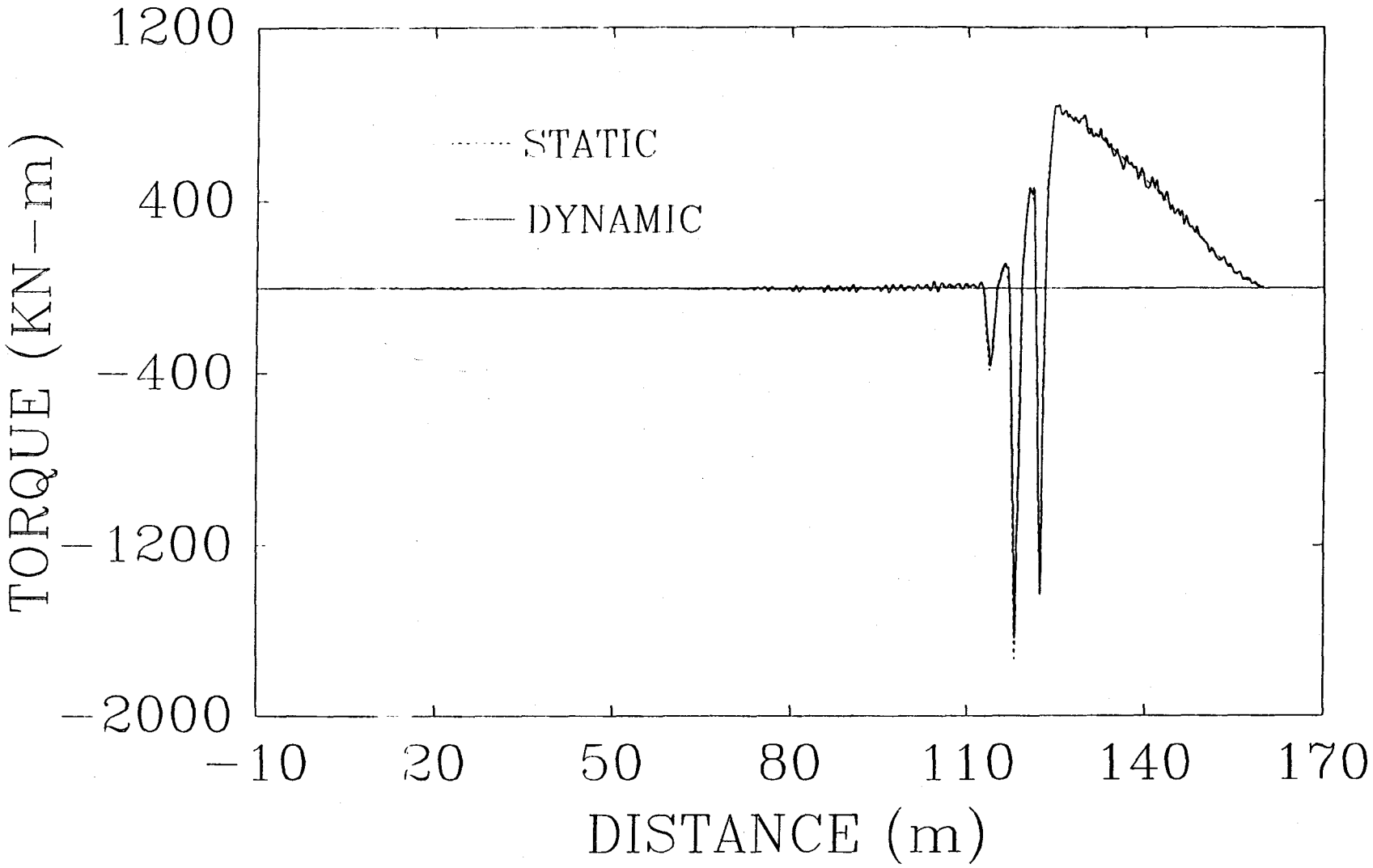

Fig. 4-72. Histories of Torque at Section 4 of Bridge Type II

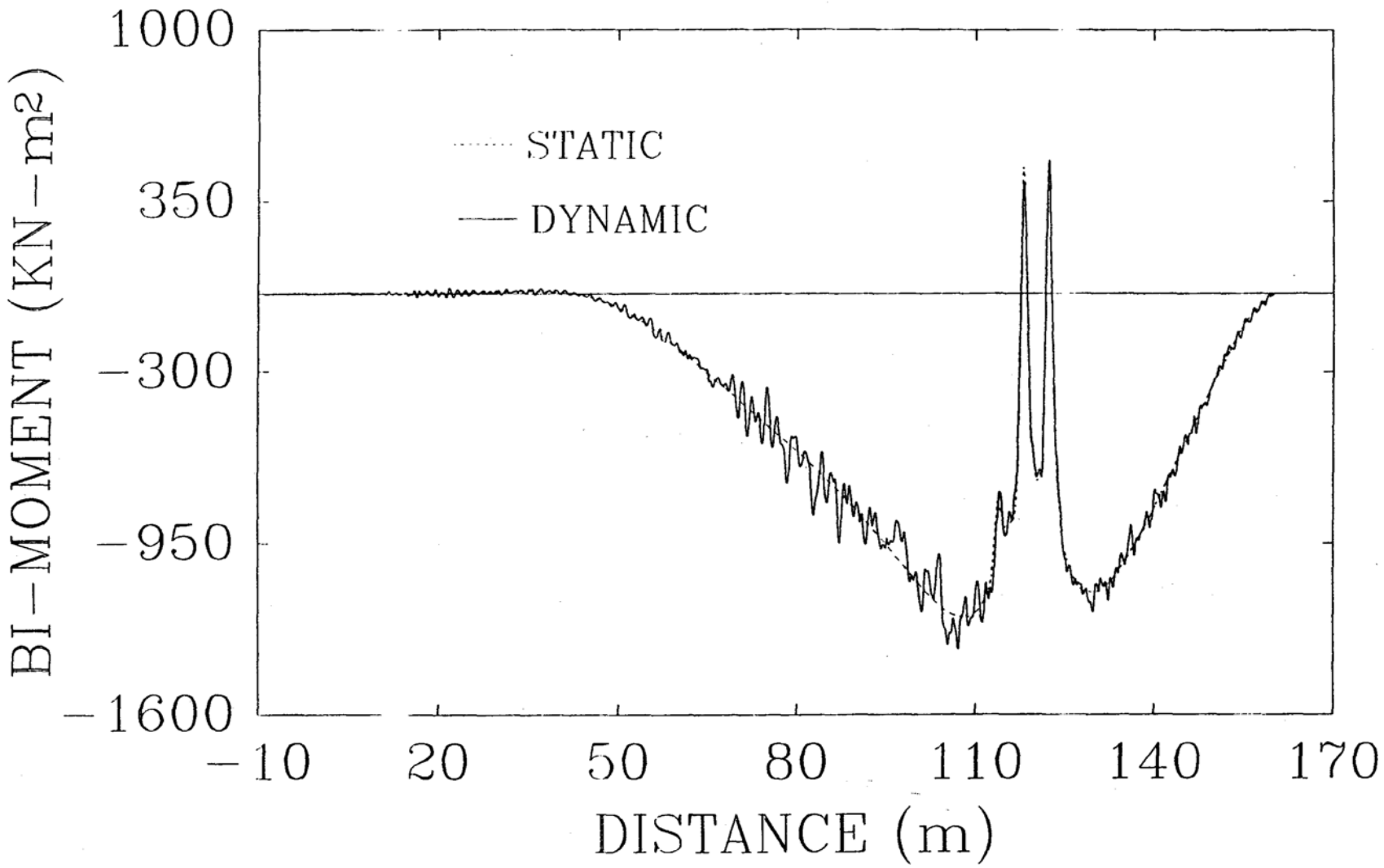

Fig. 4-73. Histories of Bi-moment at Section 4 of Bridge Type II

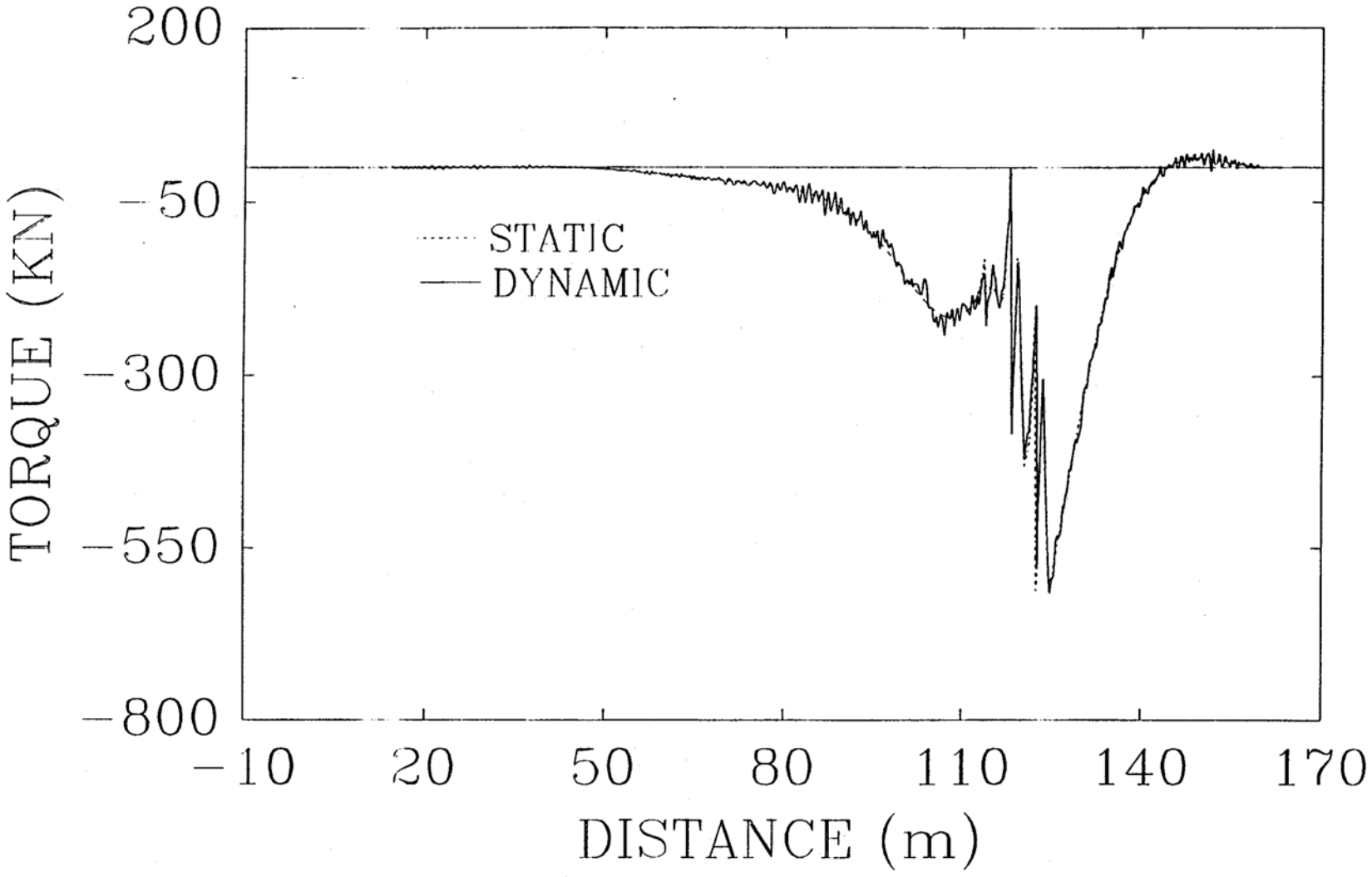

Fig. 4-74. Histories of Torque due to Distortion at Section 4 of Bridge Type II

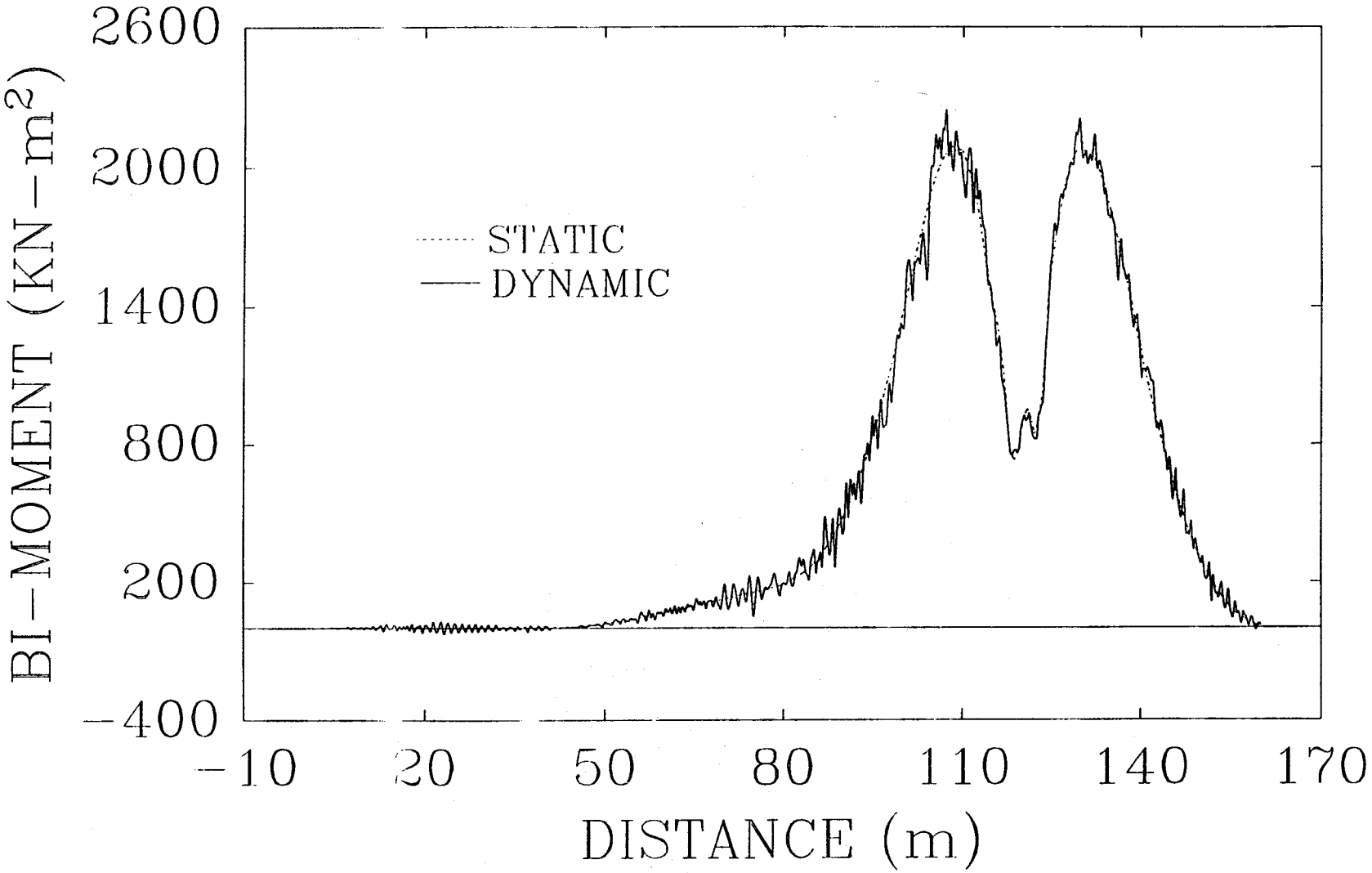

Fig. 4-75. Histories of Bi-moment due to Distortion at Section 4 of Bridge Type II

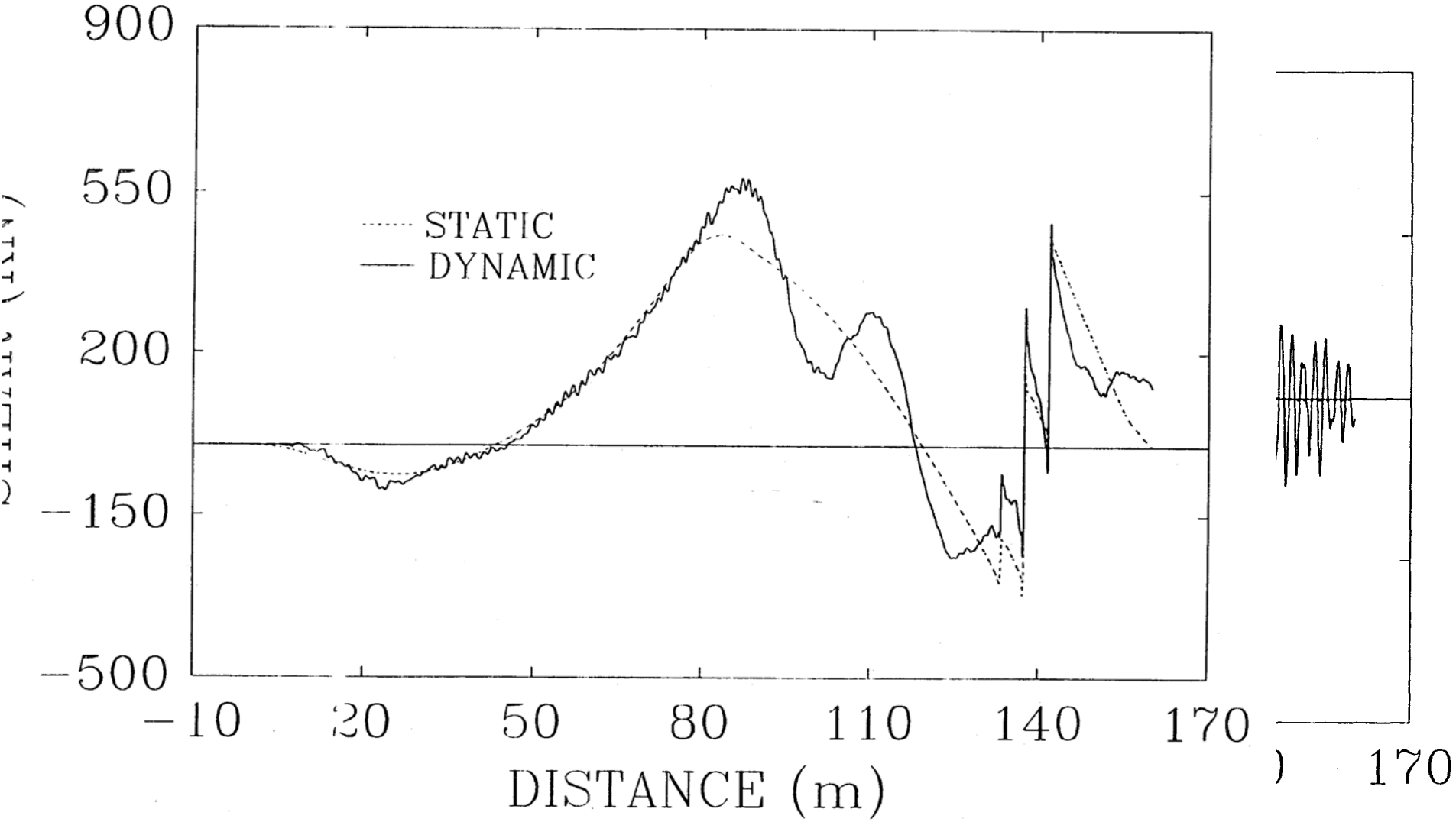

Fig. 4-77. Histories of Vertical Shear at Section 5 of Bridge Type II

Fig. 4-76. Histories of Lateral Bending Moment at Section 5 of Bridge Type II

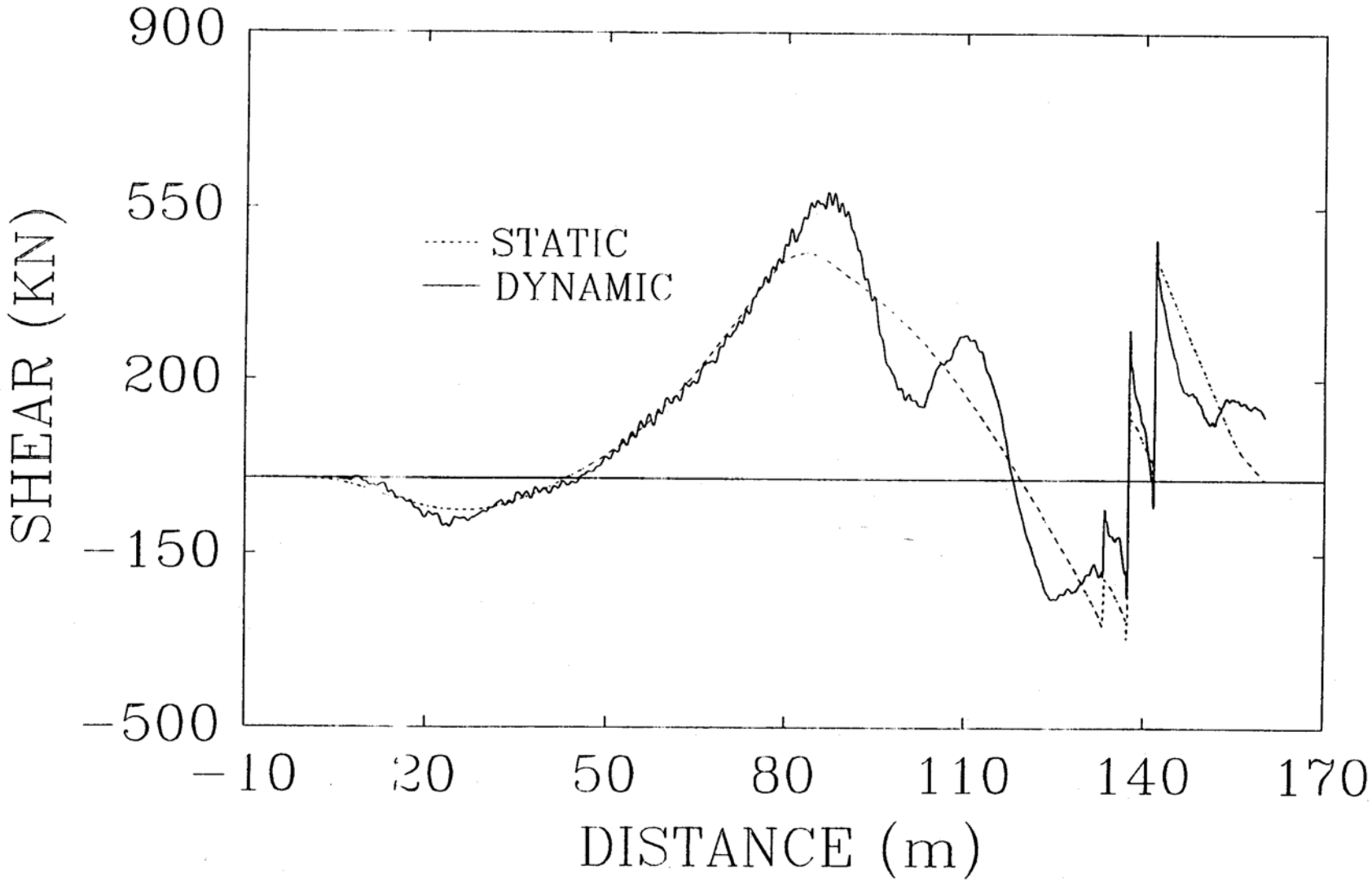

Fig. 4-77. Histories of Vertical Shear at Section 5 of Bridge Type II

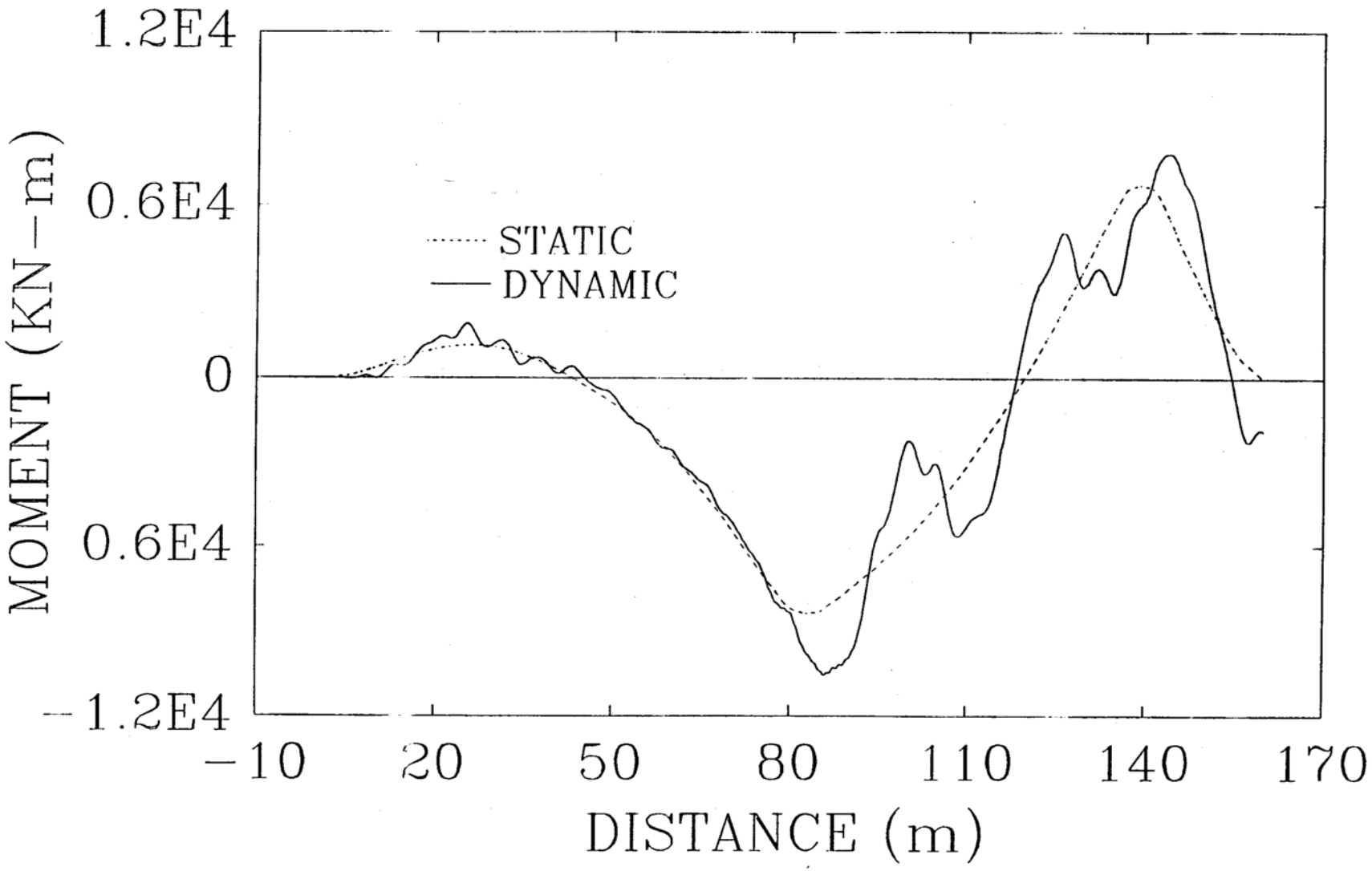

Fig. 4-78. Histories of Vertical Bending Moment at Section 5 of Bridge Type II

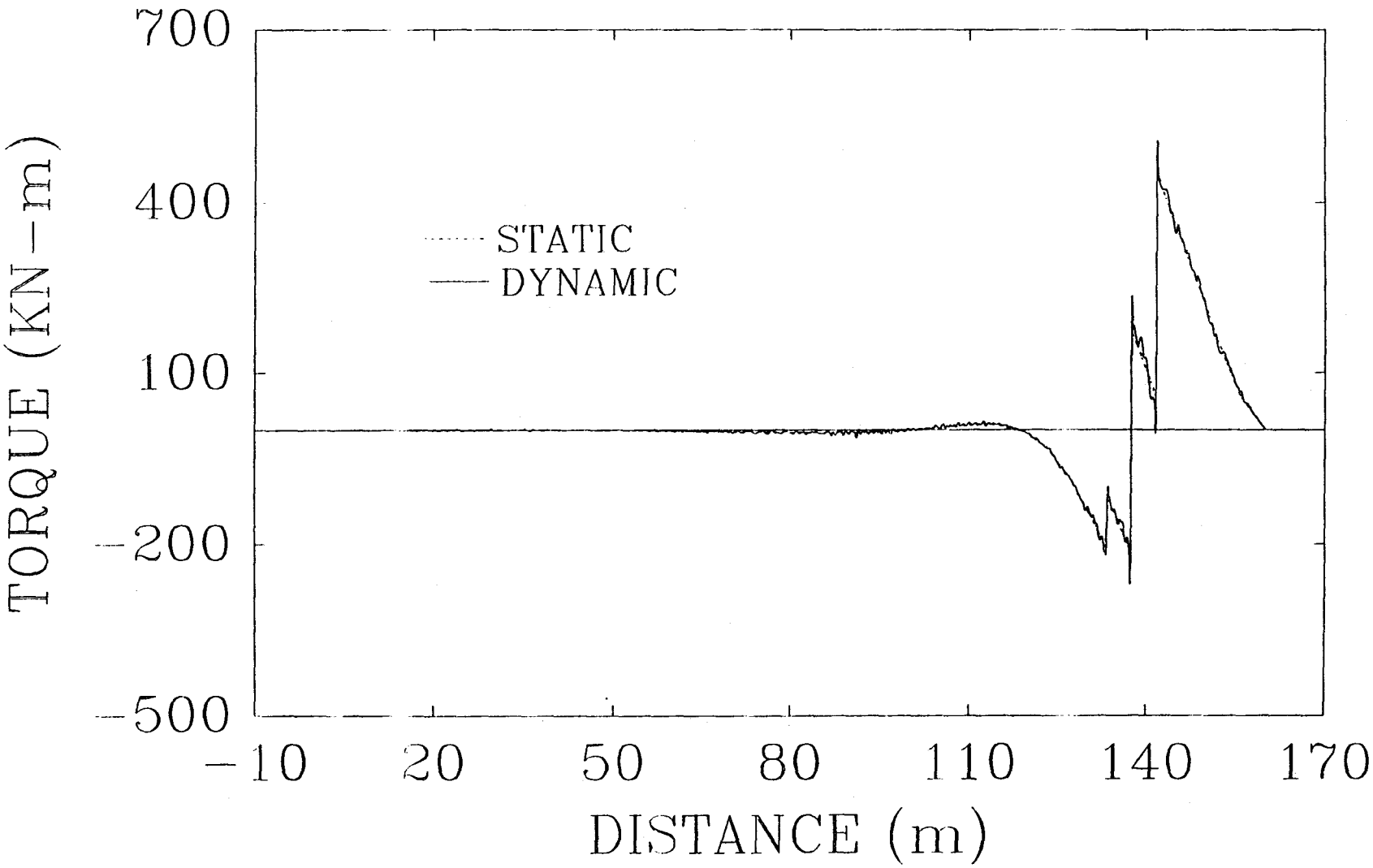

Fig. 4-79. Histories of Torque at Section 5 of Bridge Type II

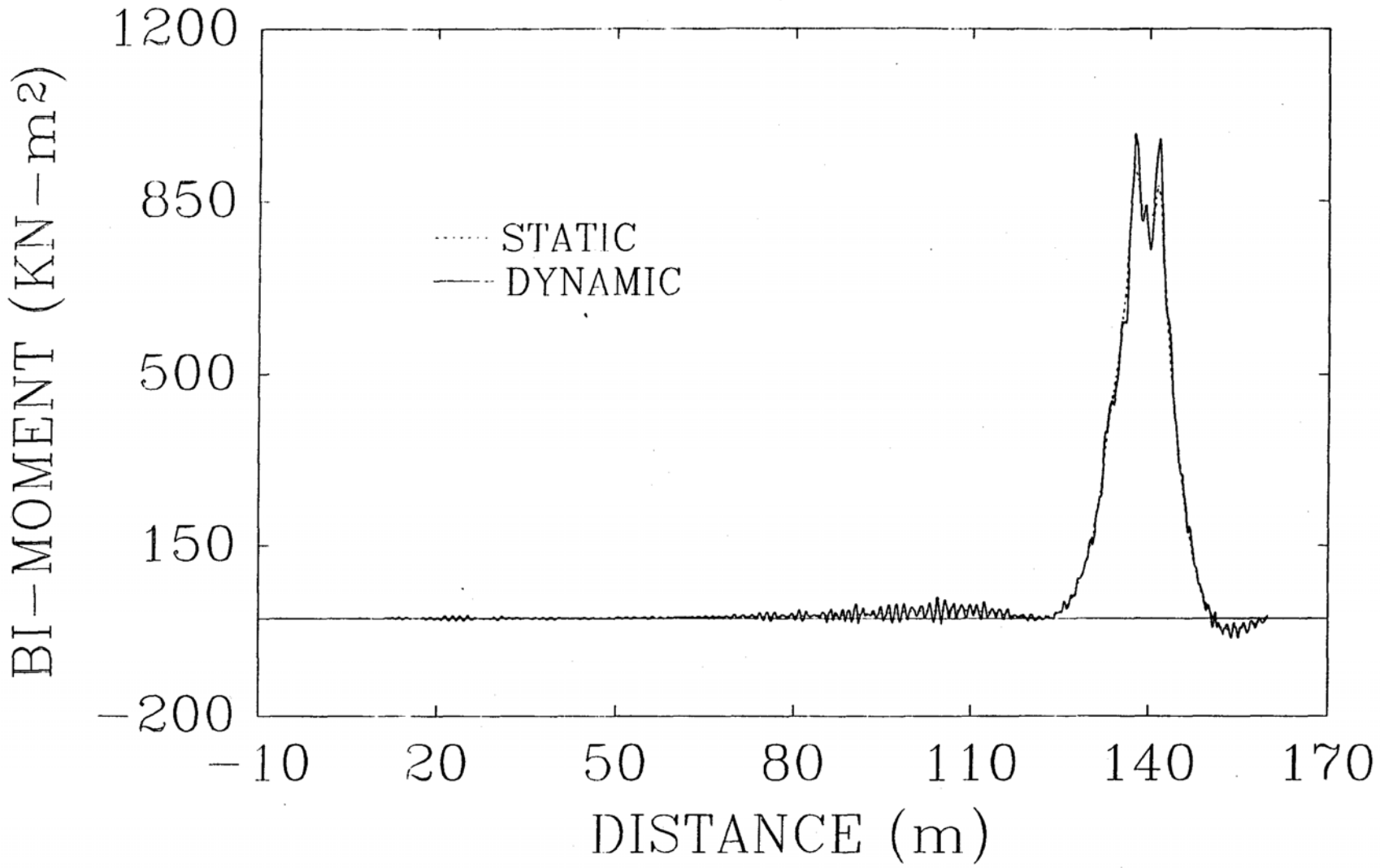

Fig. 4-80. Histories of Bi-moment at Section 5 of Bridge Type II

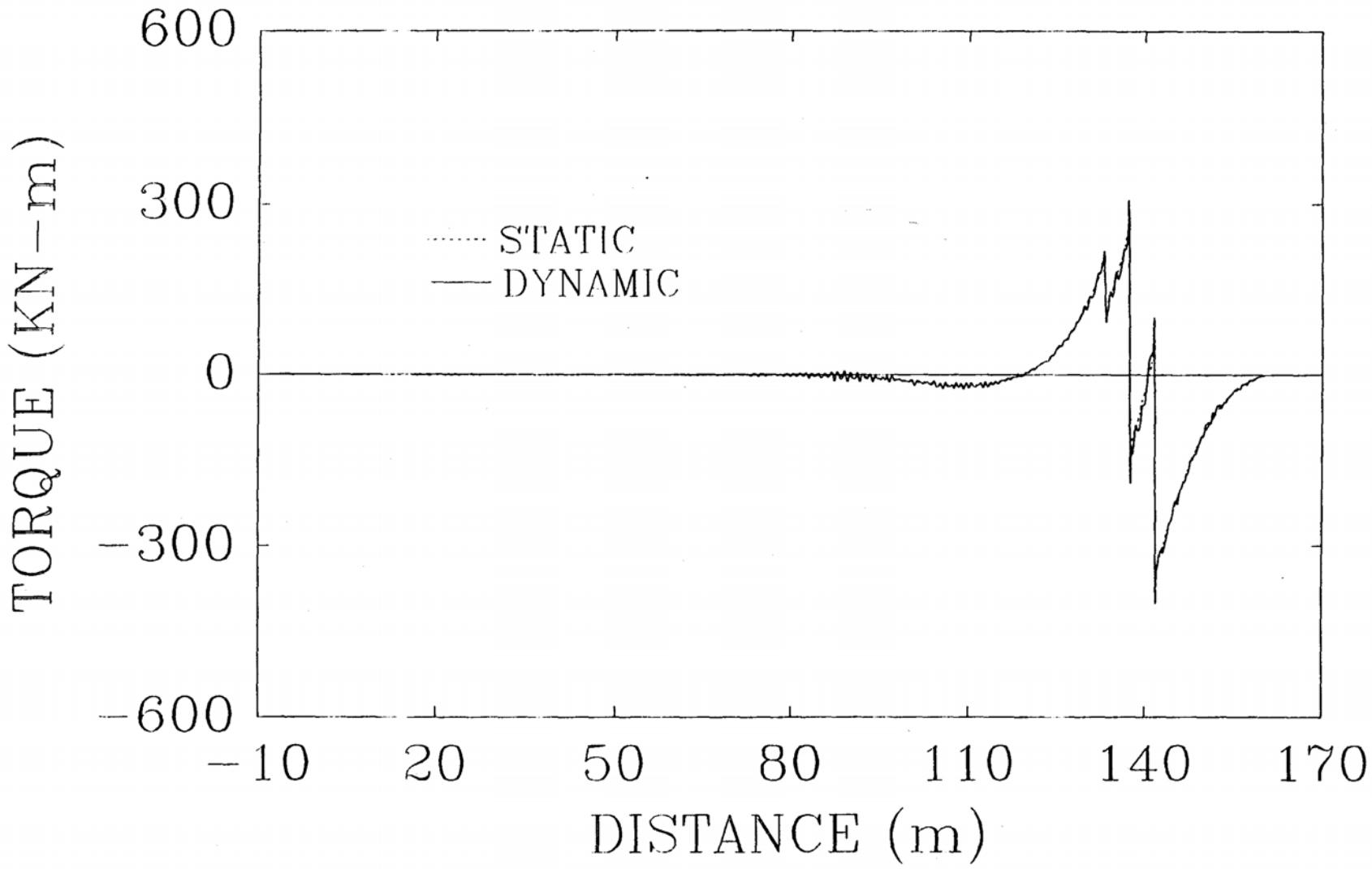

Fig. 4-81. Histories of Torque due to Distortion at Section 5 of Bridge Type II

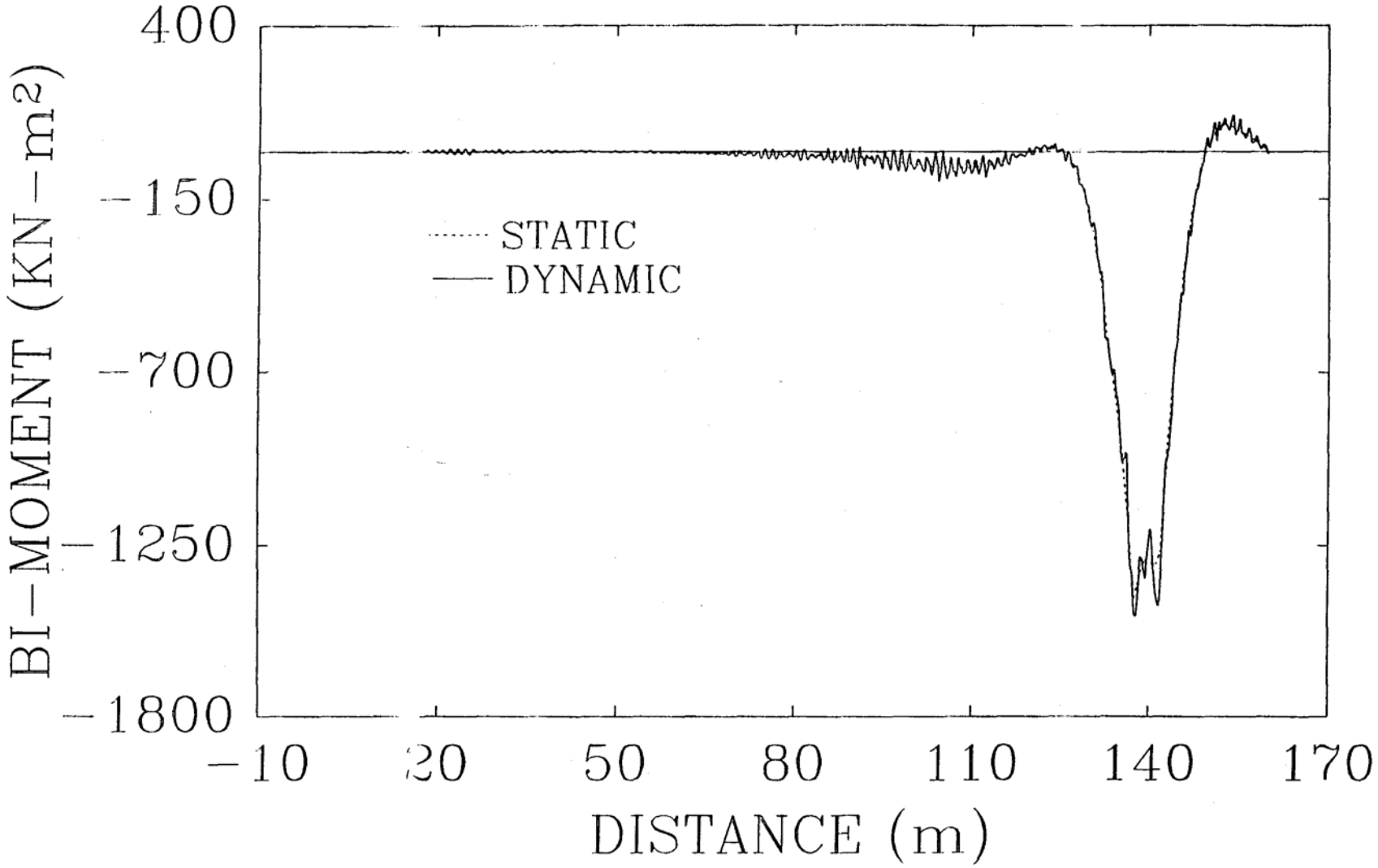

Fig. 4-82. Histories of Bi-moment due to Distortion at Section 5 of Bridge Type II

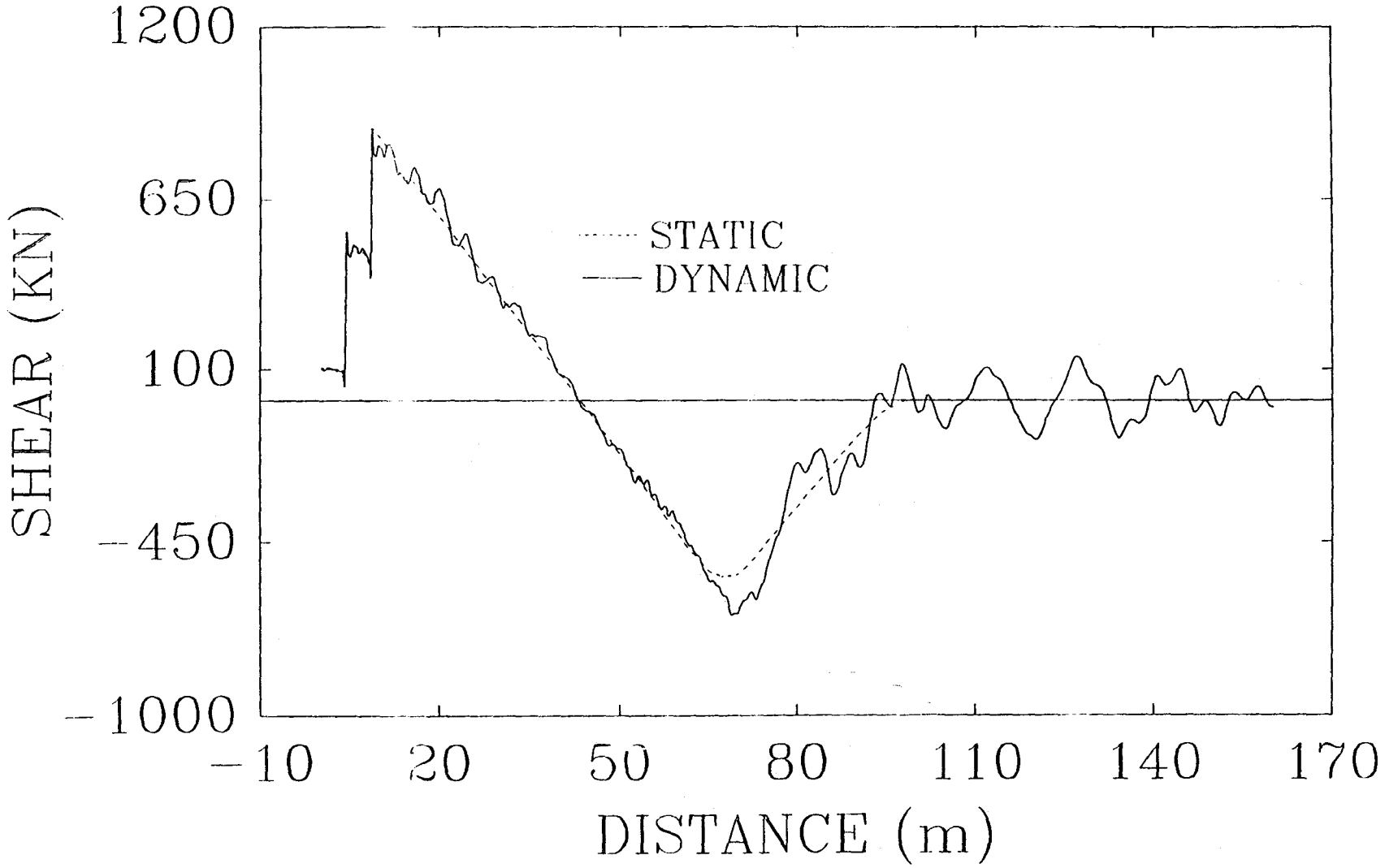

Fig. 4-83. Histories of Vertical Shear at Section 0 of Bridge Type III

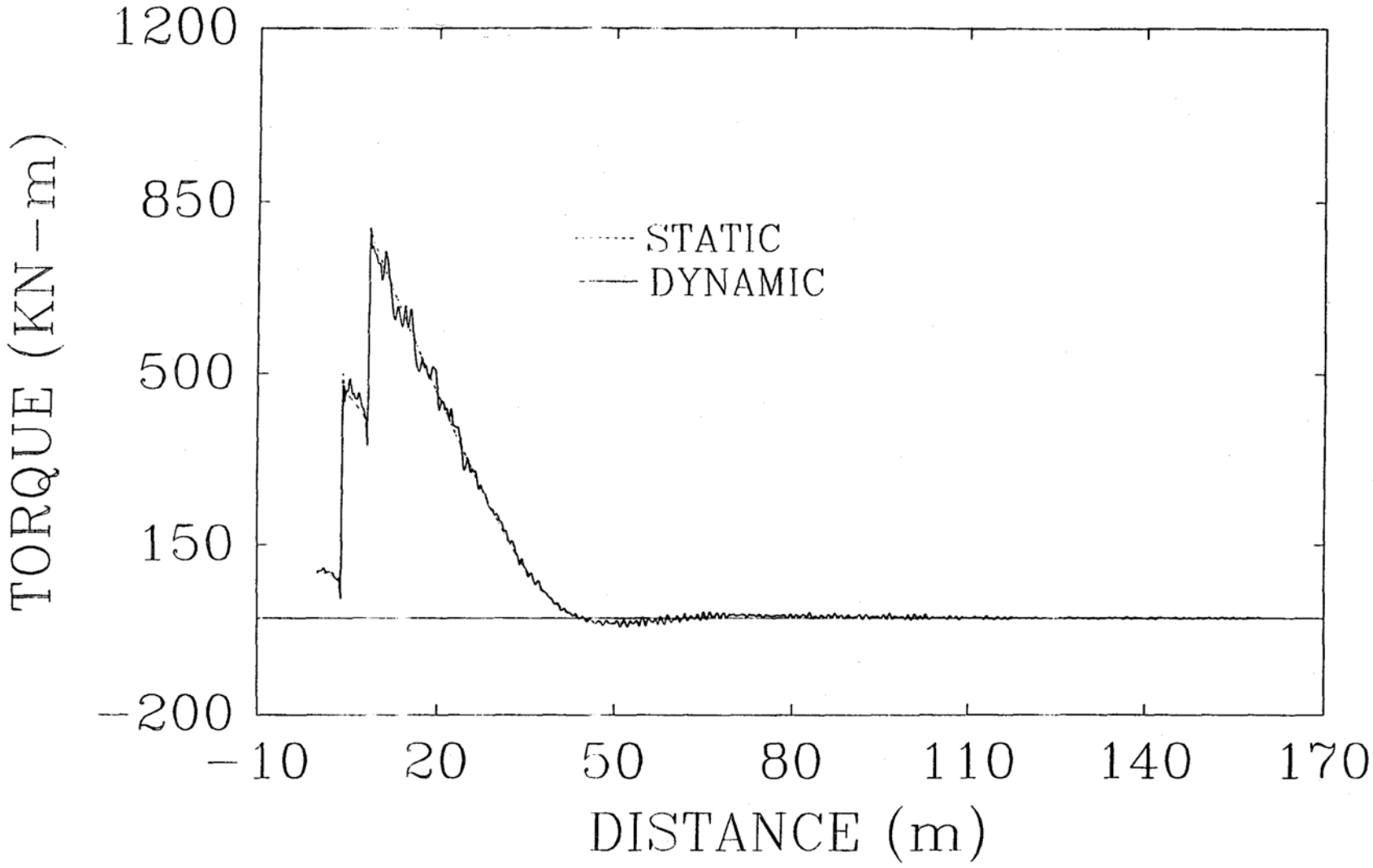

Fig. 4-84. Histories of Torque at Section 0 of Bridge Type III

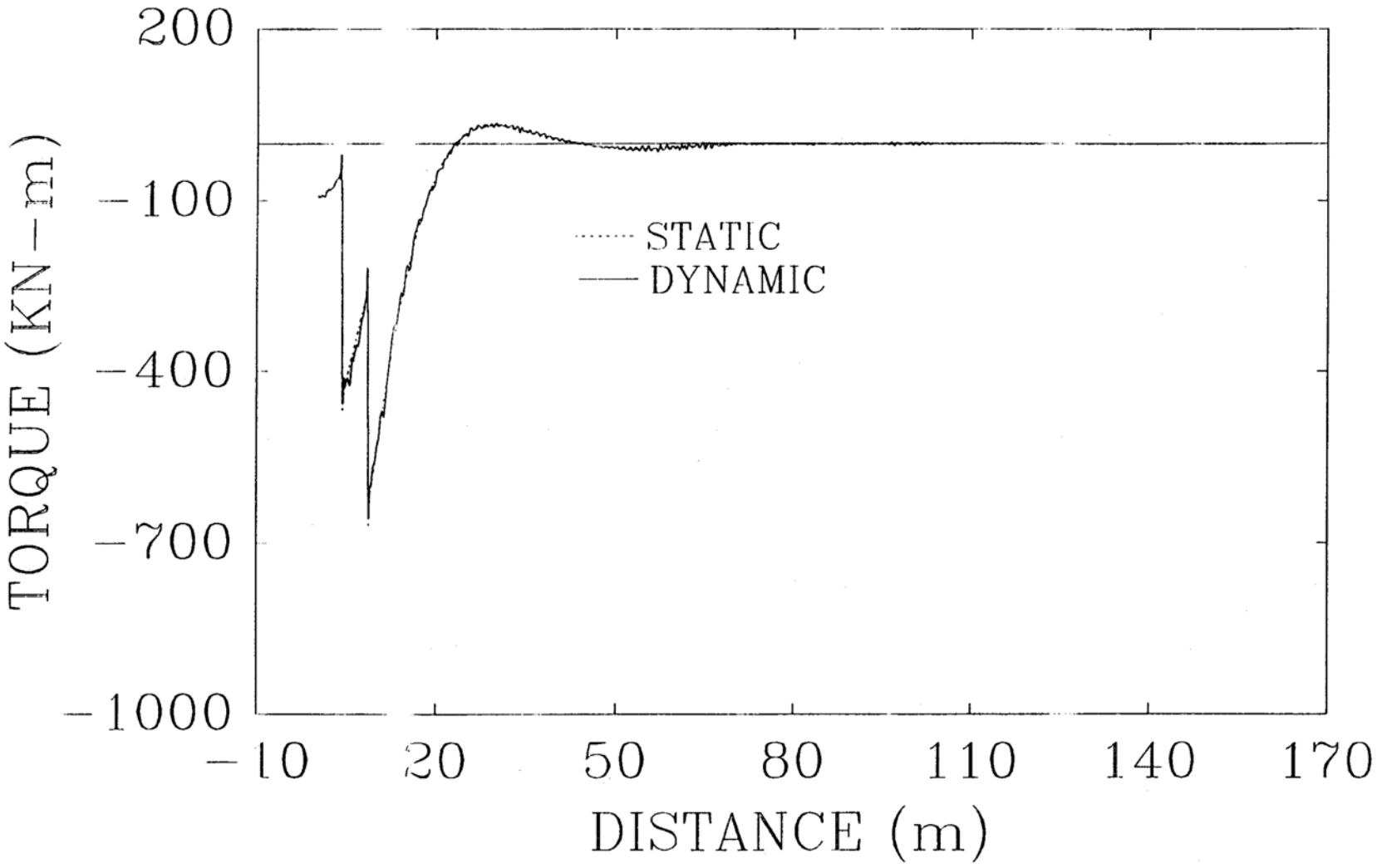

Fig. 4-85. Histories of Torque due to Distortion at Section 0 of Bridge Type III

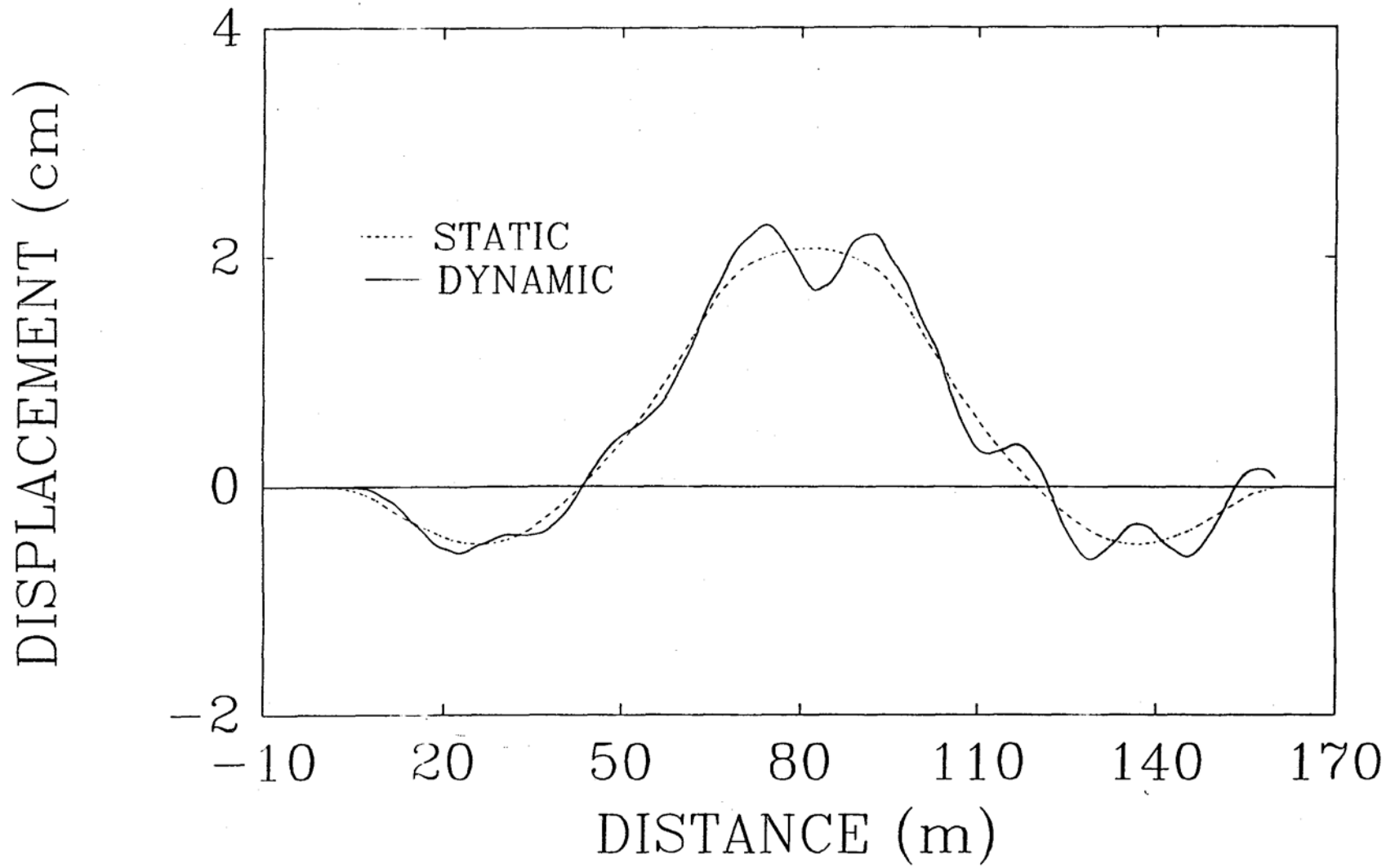

Fig. 4-86. Histories of Deflection at Mid-span of Bridge Type III

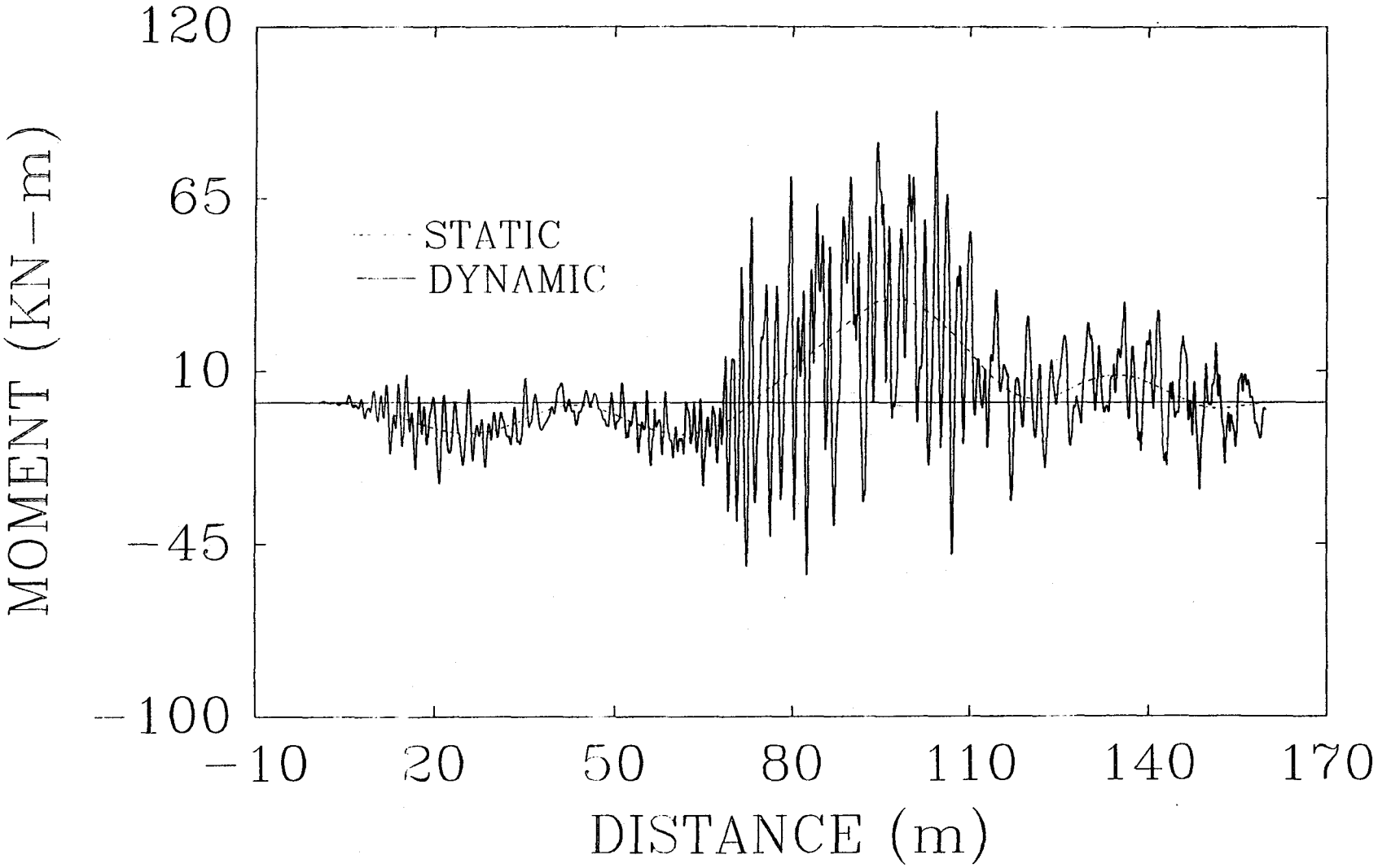

Fig. 4-87. Histories of Lateral Bending Moment at Section 4 of Bridge Type III

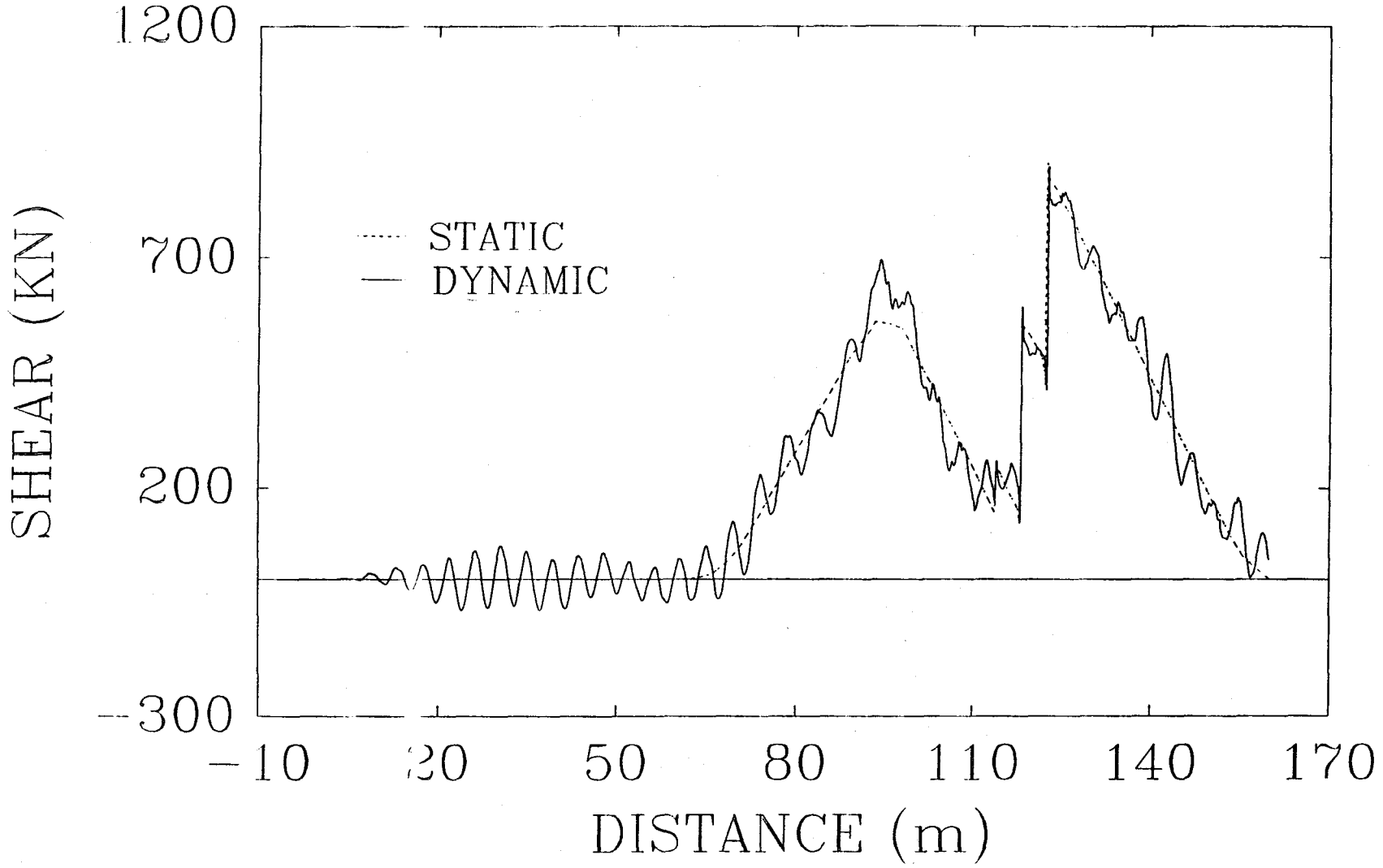

Fig. 4-88. Histories of Vertical Shear at Section 4 of Bridge Type III

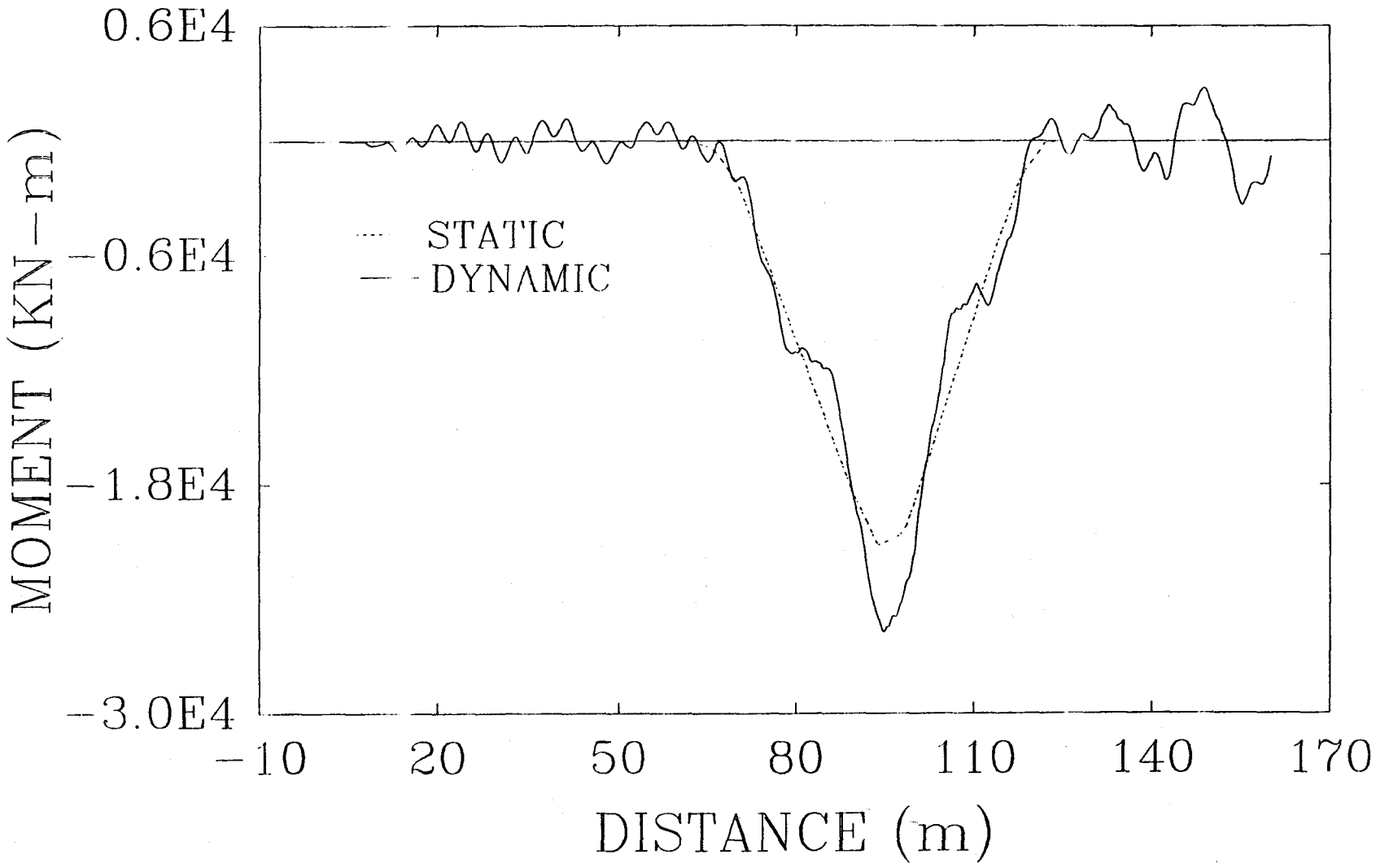

Fig. 4-89. Histories of Vertical Bending Moment at Section 4 of Bridge Type III

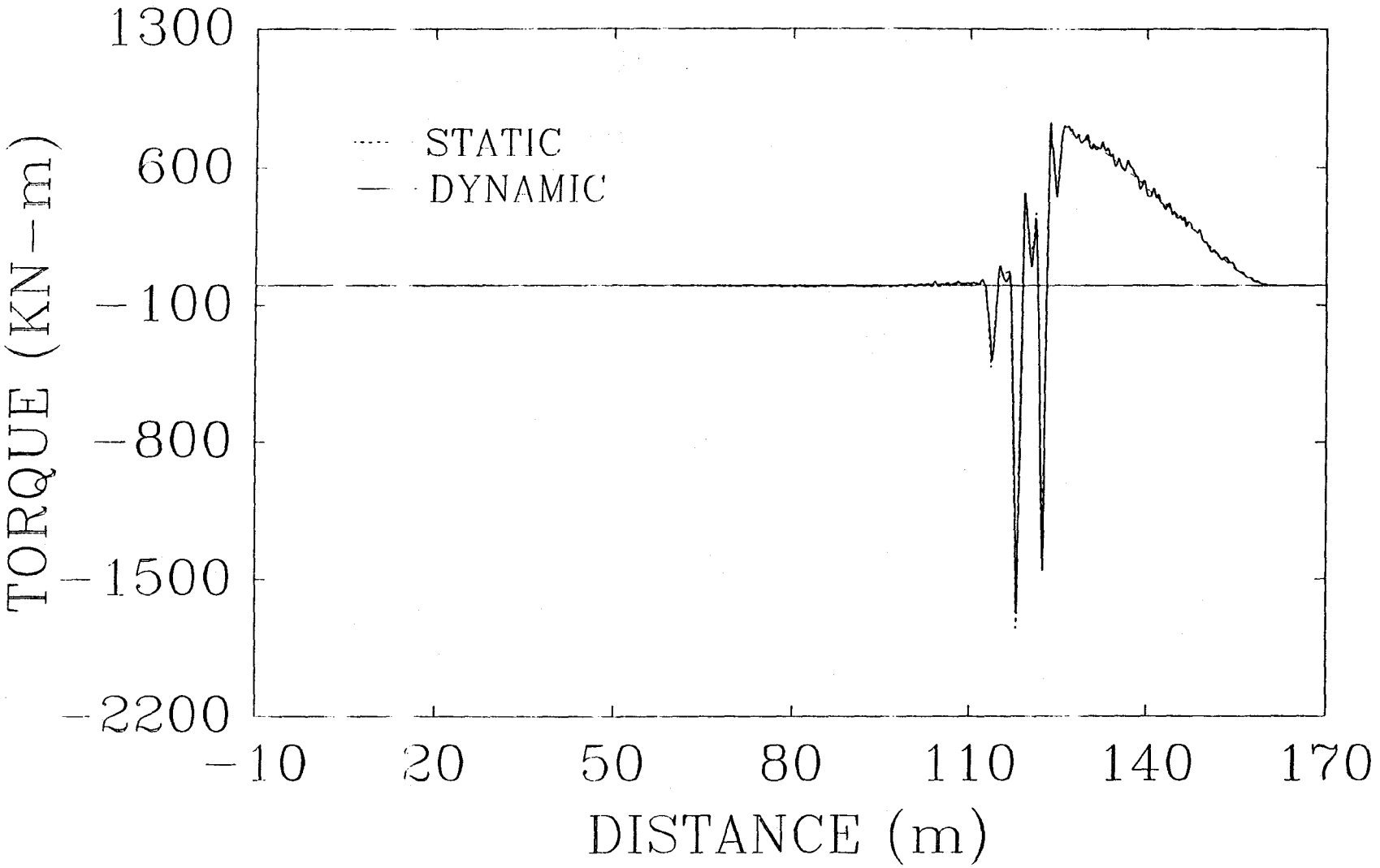

Fig. 4-90. Histories of Torque at Section 4 of Bridge Type III

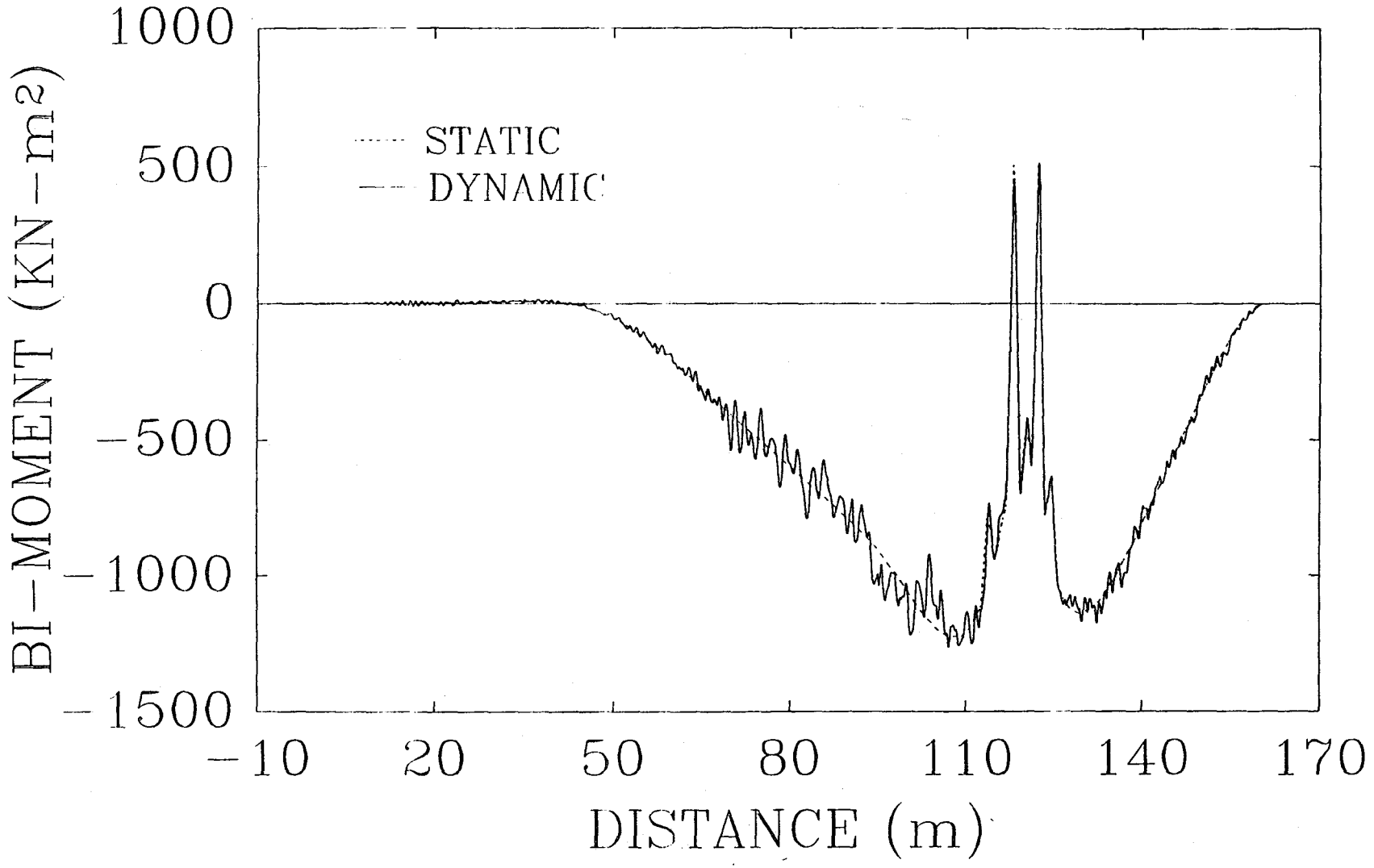

Fig. 4-91. Histories of Bi-moment at Section 4 of Bridge Type III

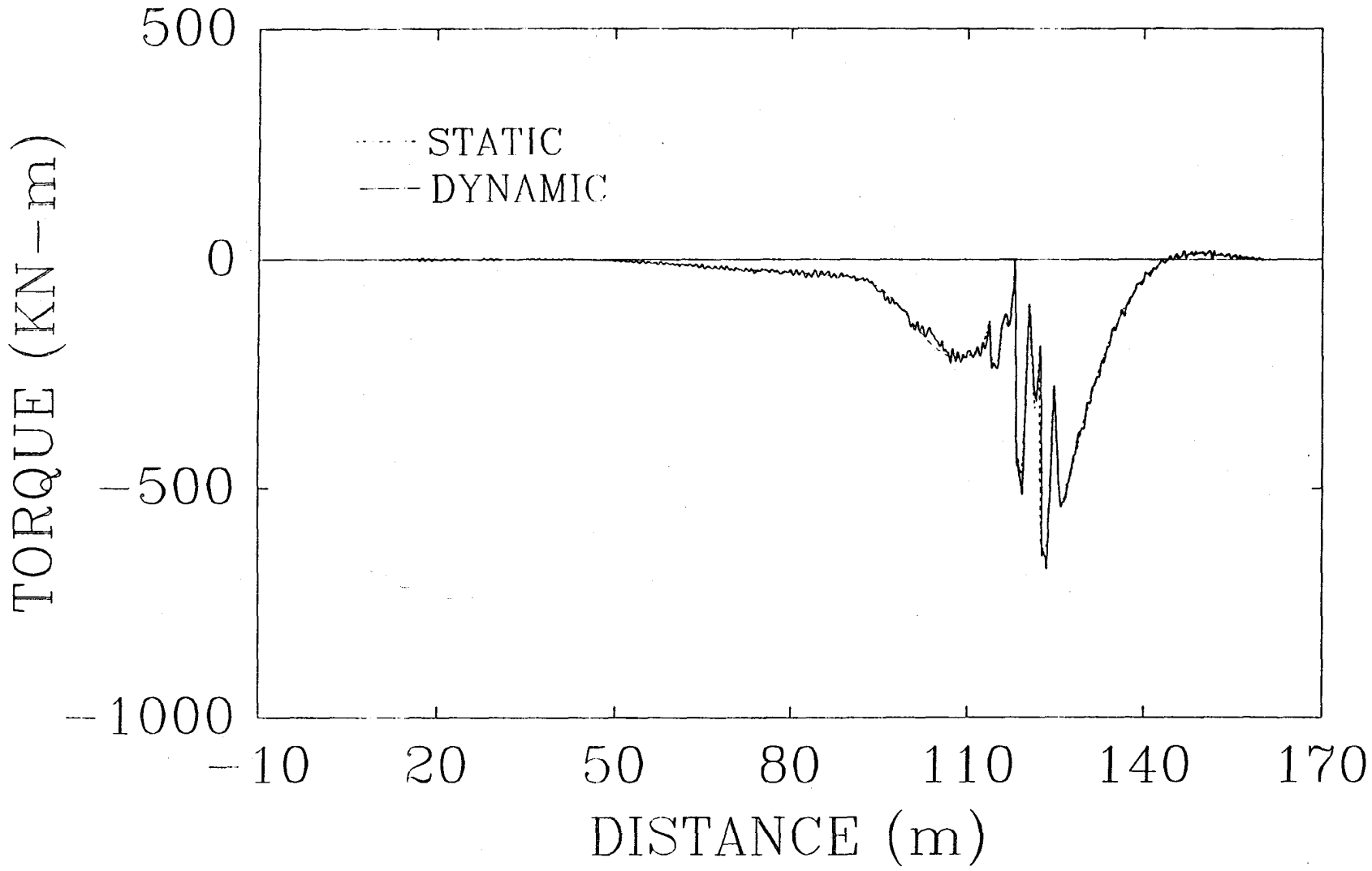

Fig. 4-92. Histories of Torque due to Distortion at Section 4 of Bridge Type III

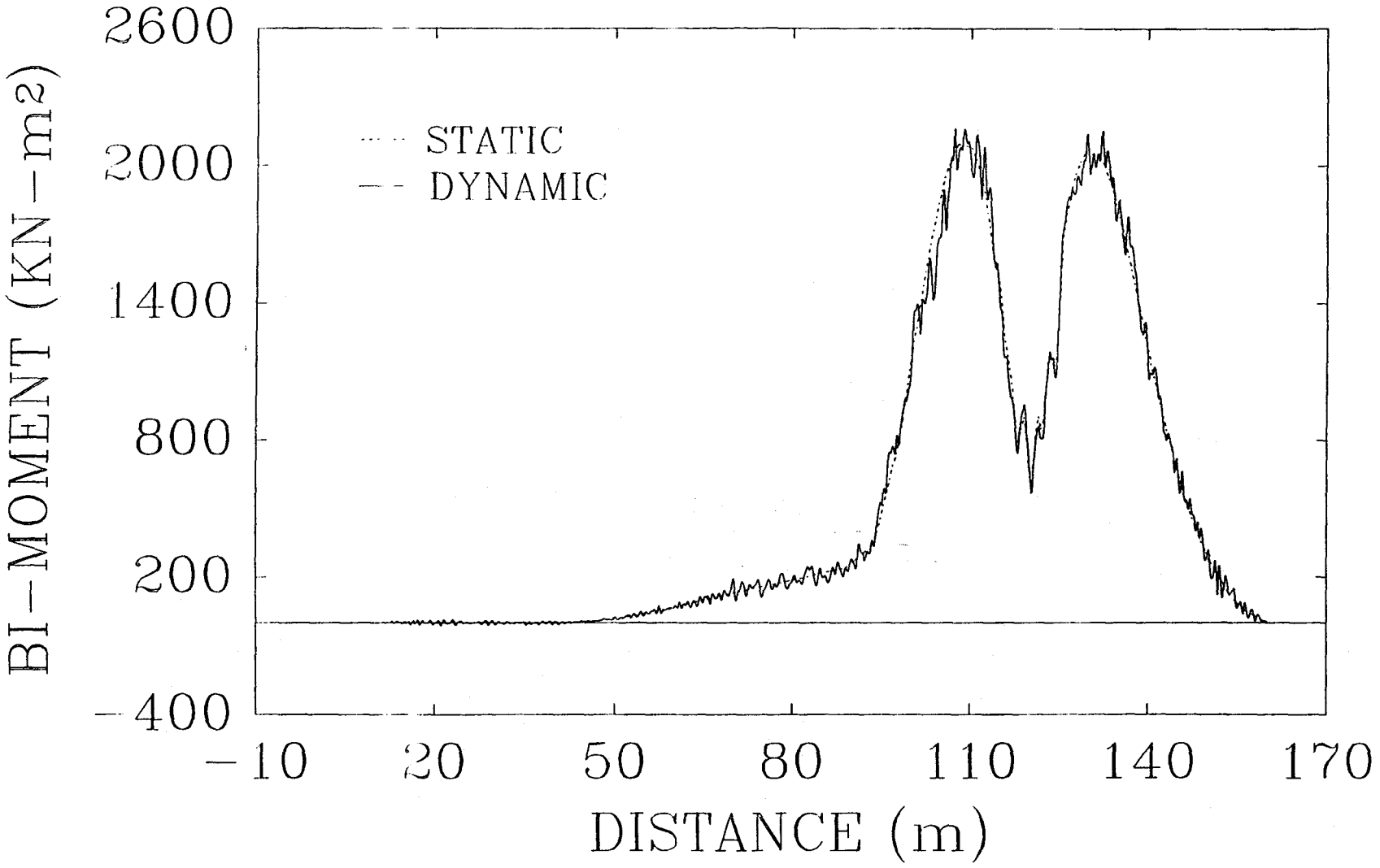

Fig. 4-93. Histories of Bi-moment due to Distortion at Section 4 of Bridge Type III

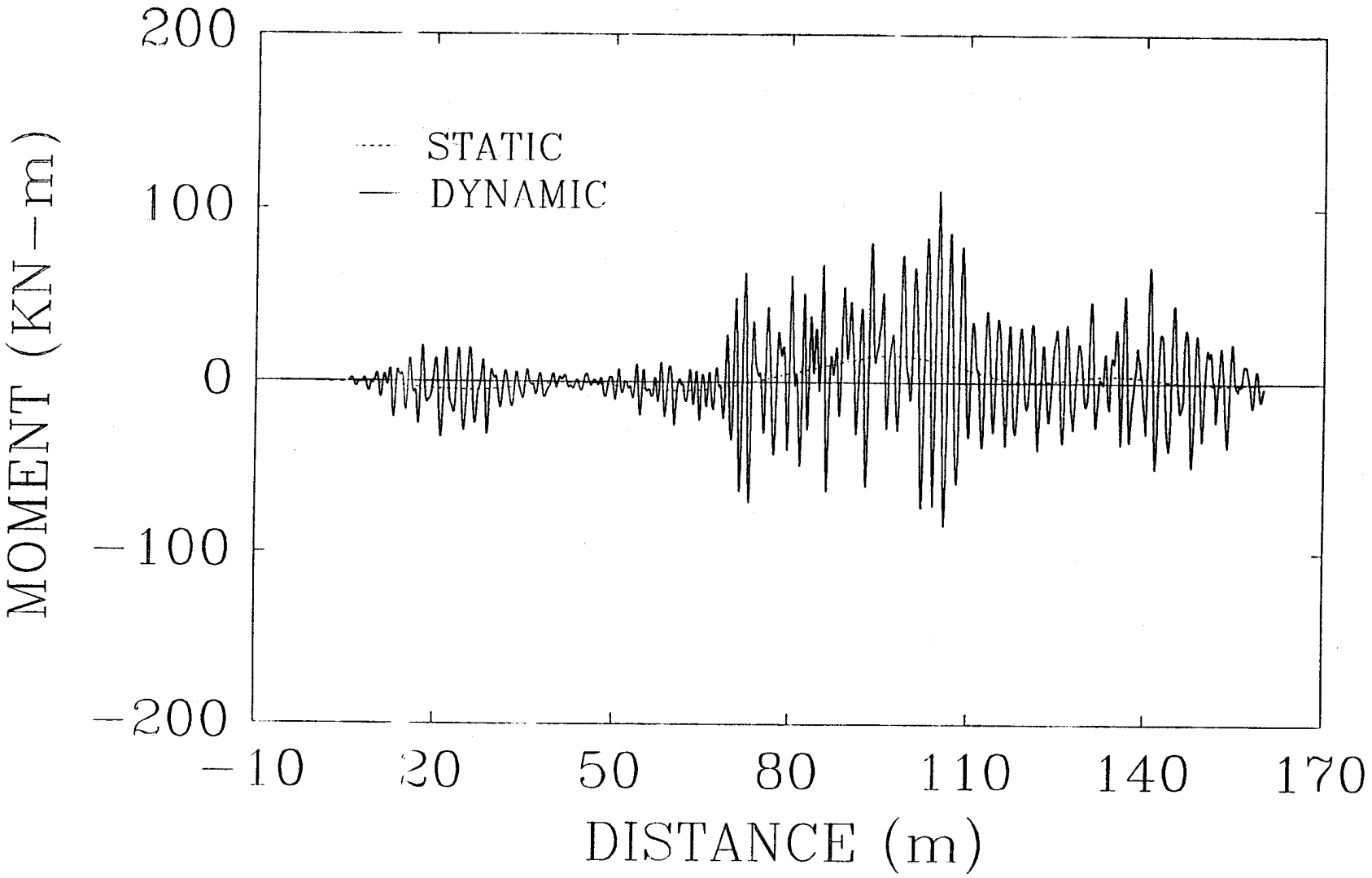

Fig. 4-94. Histories of Lateral Bending Moment at Section 5 of Bridge Type III

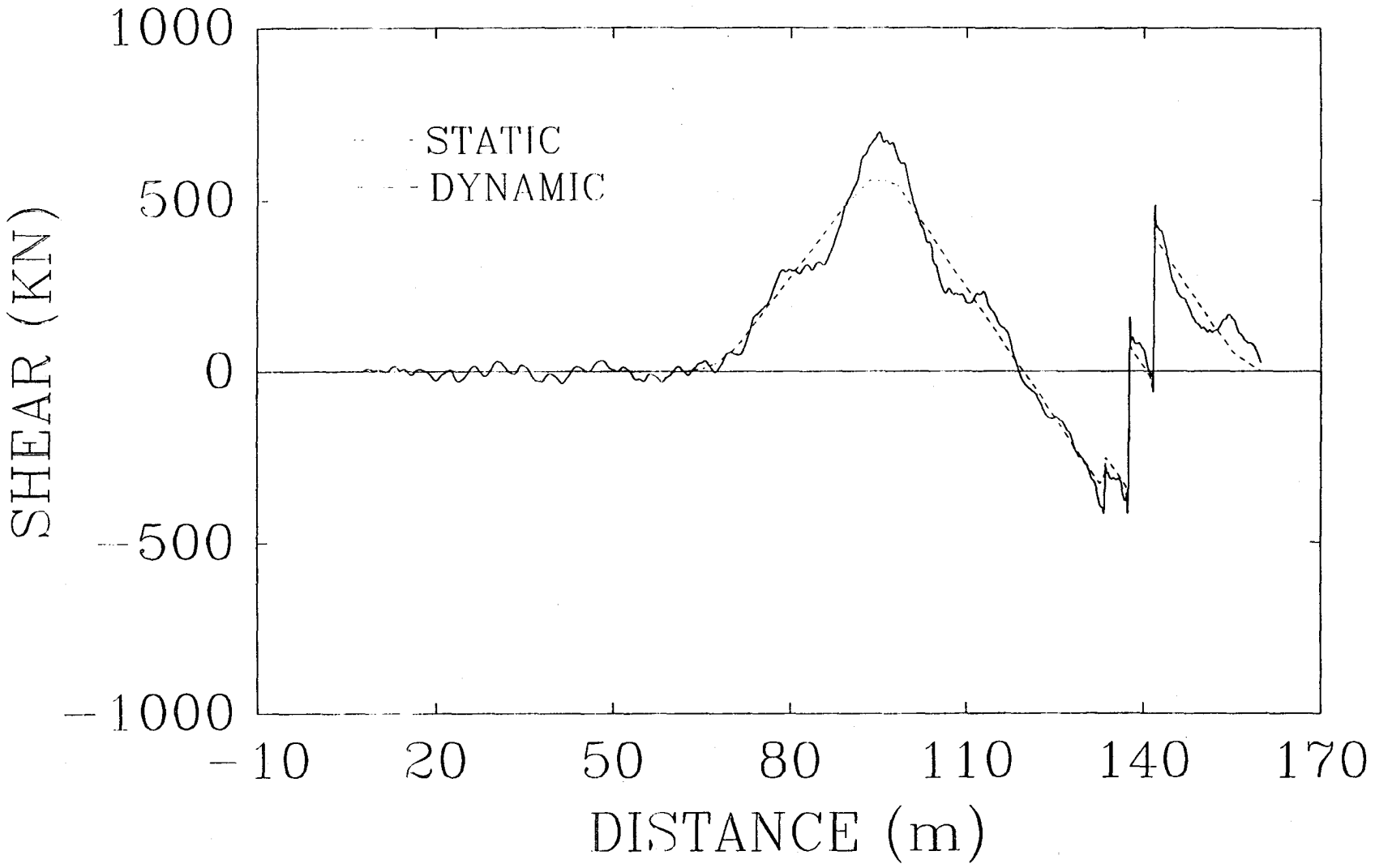

Fig. 4-95. Histories of Vertical Shear at Section 5 of Bridge Type III

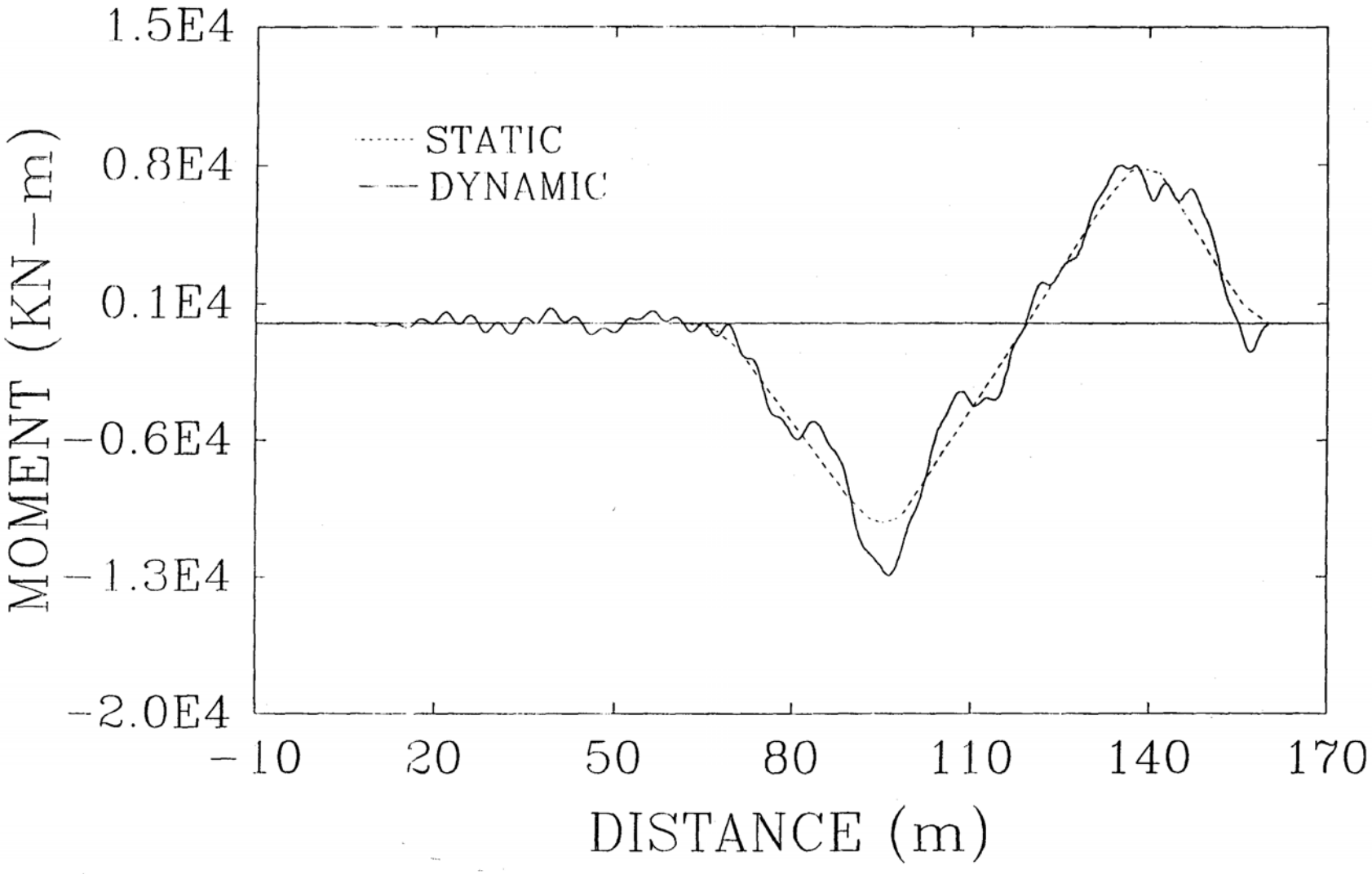

Fig. 4-96. Histories of Vertical Bending Moment at Section 5 of Bridge Type III

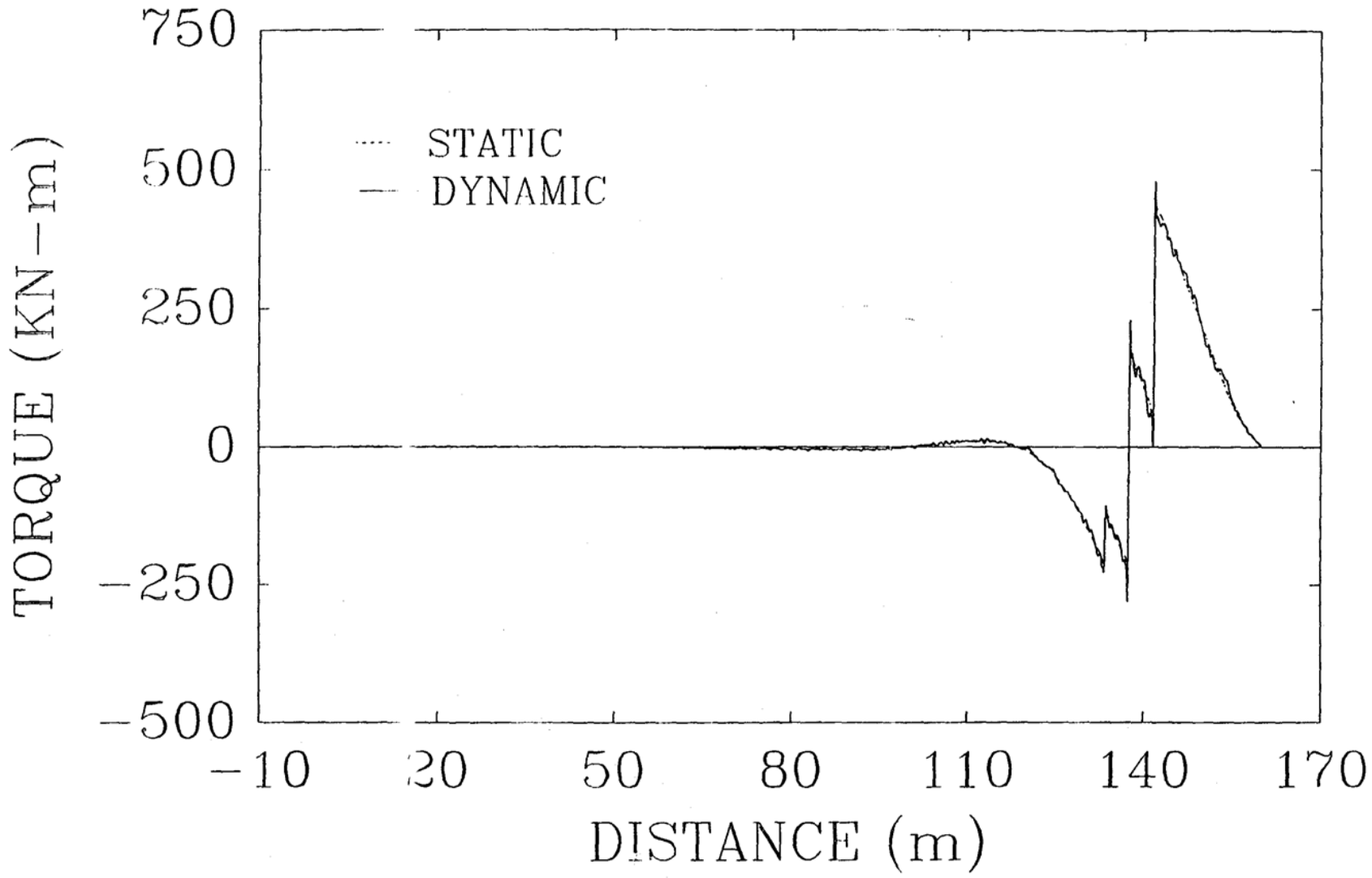

Fig. 4-97. Histories of Torque at Section 5 of Bridge Type III

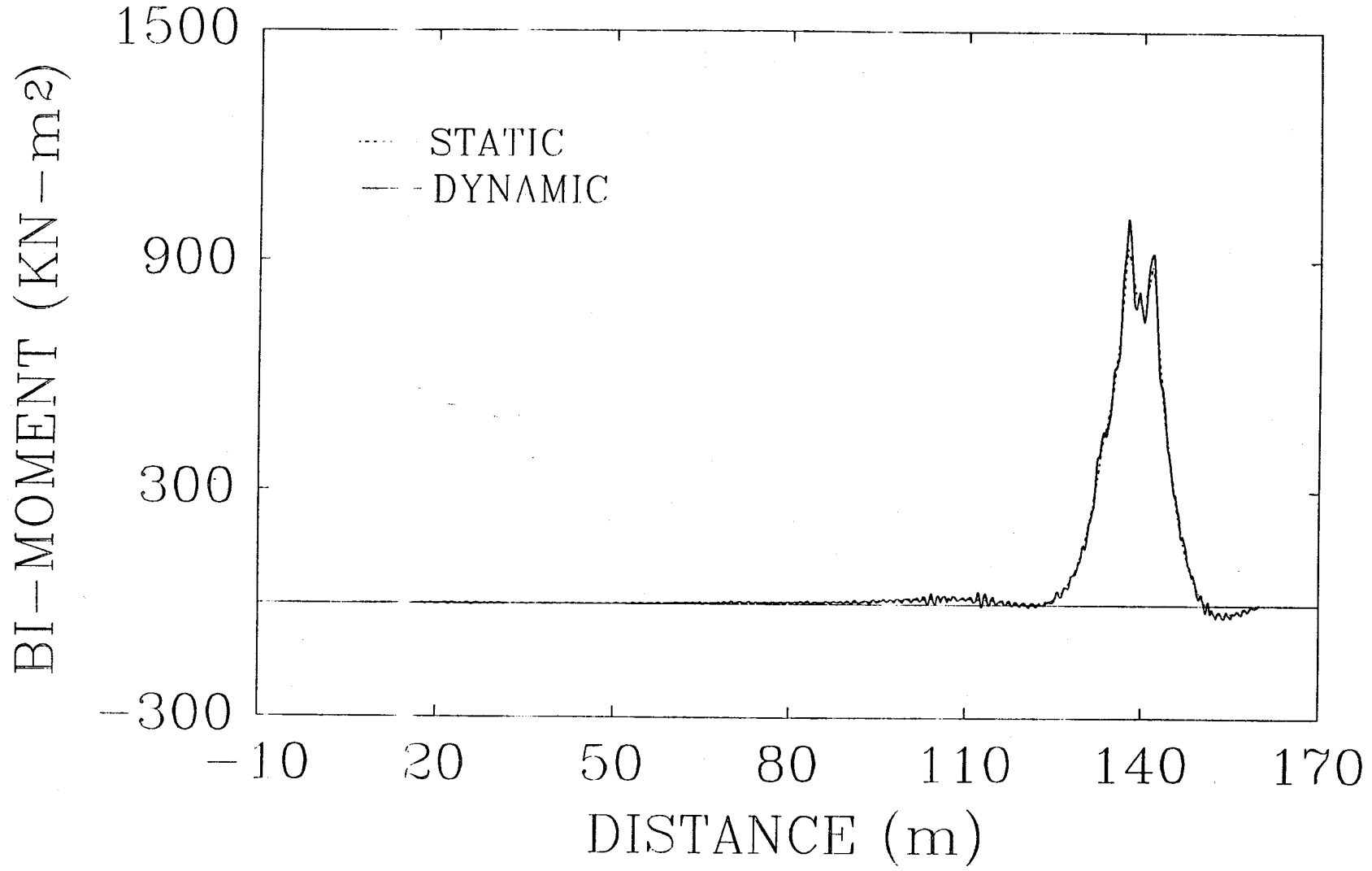

Fig. 4-98. Histories of Bi-moment at Section 5 of Bridge Type III

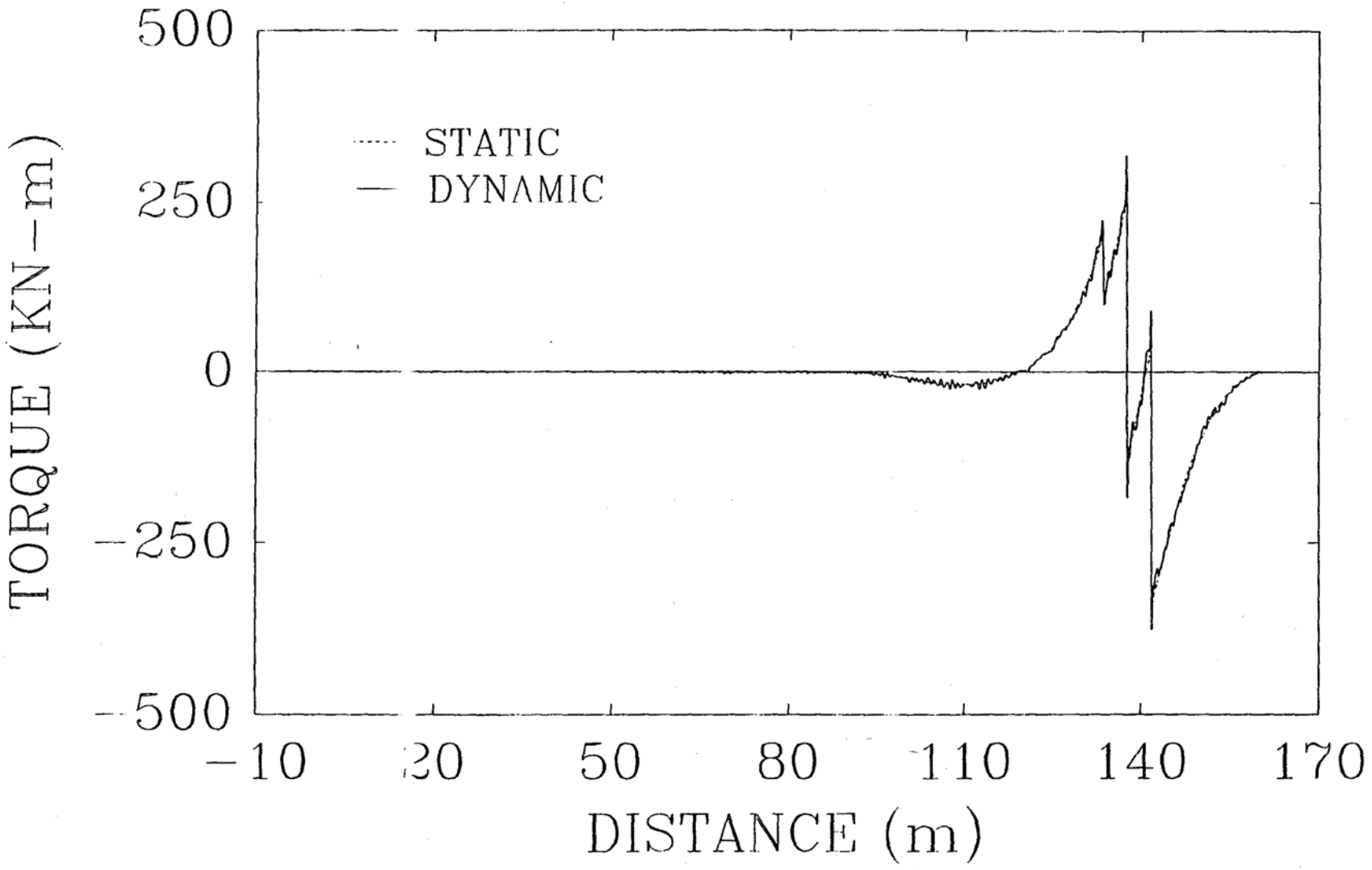

Fig. 4-99. Histories of Torque due to Distortion at Section 5 of Bridge Type III

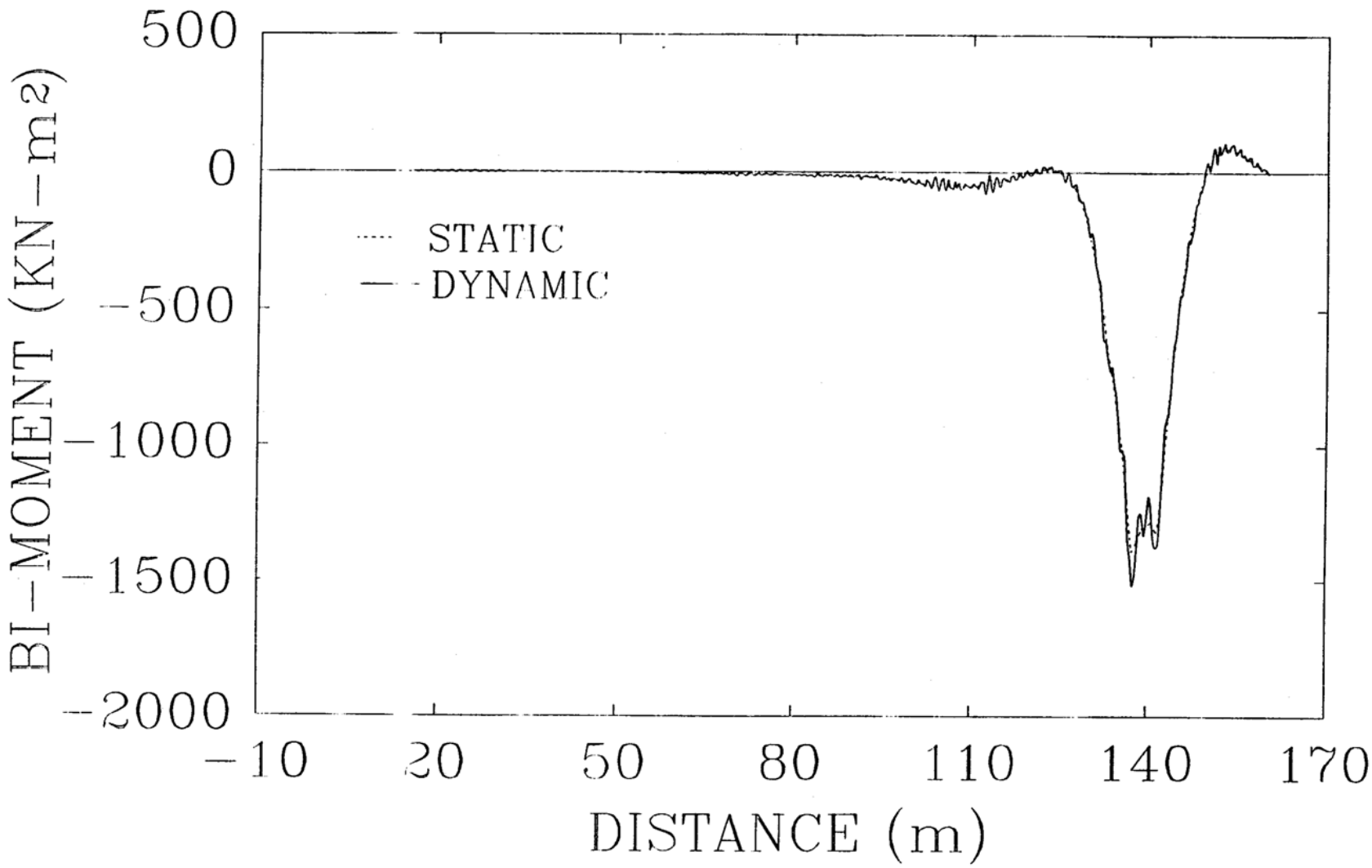

Fig. 4-100. Histories of Bi-moment due to Distortion at Section 5 of Bridge Type III

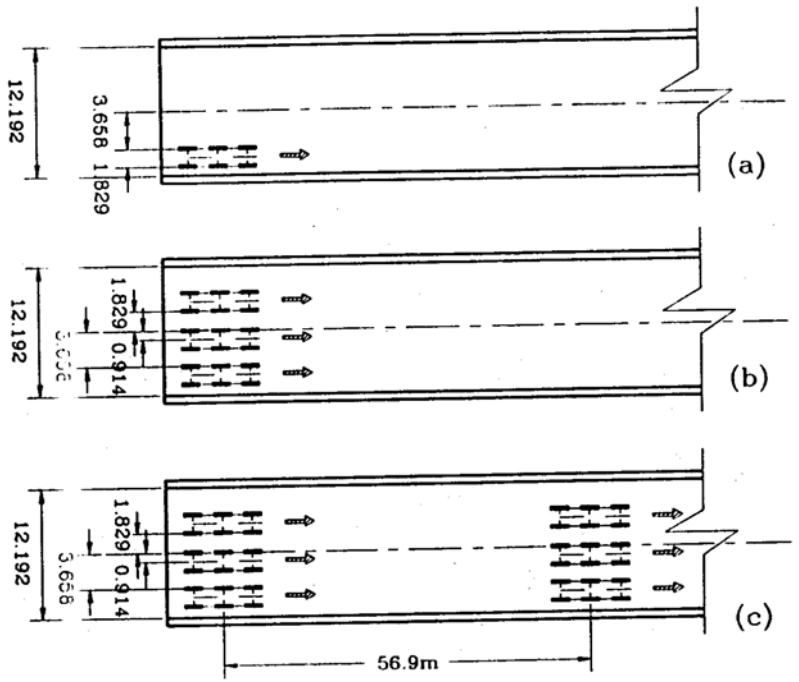

Fig. 4-101. Loading Cases: (a) Loading Model 1, (b) Loading Model 2, (c) Loading Model 3

for different types of bridges. From a practical design point of view, the most important information presented in these Figures is the magnitude of the critical dynamic increments for responses at Sections 3, 4, and 5, as well as the relationship of these values among different types of bridges. It can be observed from those figures that the absolute maximum dynamic increments of both moment and deflection for cantilever box girder bridges are several times larger than those for the continuous bridge. The factor most responsible for the increased susceptibility to vibration of the cantilever bridge is the hinge inserted at middle span. The deflected shapes of the bridges due to a concentrated static force applied at midspan or over the hinge are shown in Fig.4-102. Although the corresponding configurations for moving vehicles at the instant they cross that position are likely to be different, it can be expected to exhibit the same major discontinuity in slope directly under the load. As the loads cross the hinge, they are abruptly forced to change their direction of travel from downhill to uphill. This change causes a sudden increase in the rate of spring deformation, thus increases both the amplitude and periodicity of the interacting force as well as the response level of the bridges [18]. It can be seen from Figs. 4-65 to 4-100 that as soon as the vehicles cross the hinge, the fluctuations of vertical bending moment become larger and nearly periodic. By comparison, the effect of hinge on the dynamic responses of torque and bi-moment is small. This is because the torsional deformations at hinges are continuous and the excited force of vehicles is not large enough to develop higher torsional modes of bridges. The impact of lateral bending moment is extremely large. However, the ratio of lateral to vertical bending moment is comparatively small.

4.4.2. Effect of Loading Model

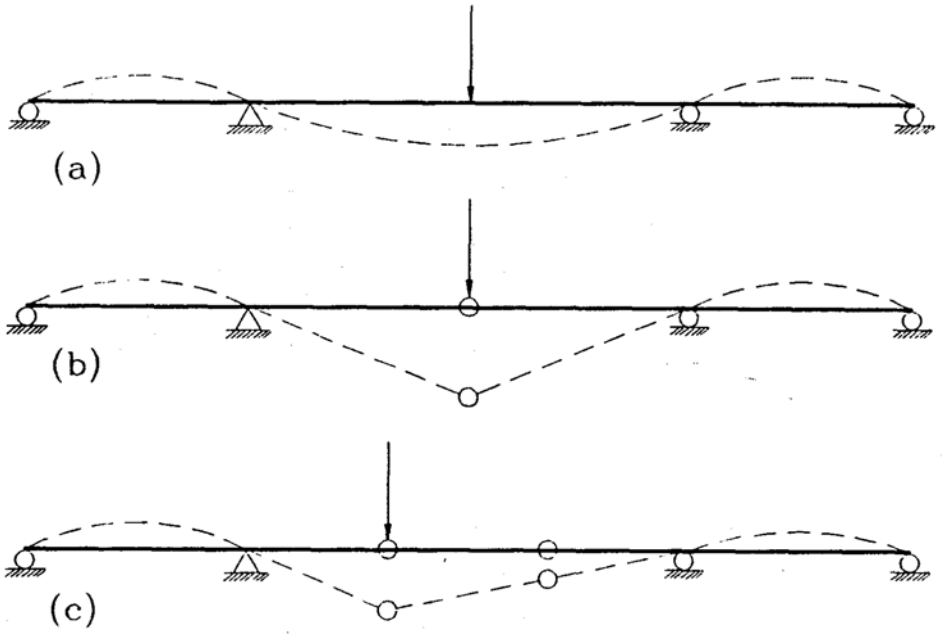

Fig. 4-102. Deflection Characteristics: (a) Bridge Type I, (b) Bridge Type II, (C) Bridge Type III

Most previous investigators used a single car to study the dynamic response of highway bridges [12, 22]. Recently, a loading model of multi-truck (side by side) was used to study the impact of multi-girder bridges [19, 20, 54, 56, 57]. To further understand the influence of loading modes on the dynamic response of box girder bridges, herein three loading cases (see Fig.4-101) will be considered. Loading model 1 shown in Fig.4-101 (a) is a single truck of asymmetric loading. Loading model 2 illustrated in Fig 4-101 (b) is a three-truck asymmetric loading positioned transversely (side by side). Loading model 2 will induce the maximum positive bending moment for both side span and middle span. Fig.4-101 (c) demonstrates loading model 3 which contains 6 trucks positioned three transversely and two in longitudinal direction. The distance between two longitudinal trucks is determined according to the fact that it will cause the absolute maximum bending moment over sections at inner supports. However, it is also found that loading model 3 can approximately produce both maximum positive and negative bending moment for Sections 1, 3, and 5.

Table 4-1 gives the maximum impact factors of different types of response at sections over inner supports and midspan for different loading models. The impact factor is defined as Eq. 3-2.

The maximum impact factors are obtained based on vehicle speeds changing from 24.14 km/hr (15 mph) to 120.68 km/hr (75 mph). The results shown in Table 4-1 are determined according to average road surface. As the sections 2 and 4 (see Fig. 4-1) are symmetrical about midspan, only one of the maximum impact factors related to the larger dynamic response of these two sections has been listed in Table 4-1. Notations Pos. and Neg. in the table indicate

Table 4-1. Effect of Loading Models - Maximum Impact Factors (%)

Bridge Type	Loading Model	Over Inner Supports								At Midspan
		Q_y	M_x		T_c		B_ω	$T_{\bar{\omega}}$	$B_{\bar{\omega}}$	D_y
		Pos.	Pos.	Neg.	Pos.	Neg.	Pos.	Neg.	Pos.	Pos.
I	1	7.48	143.0	21.5	10.4	216.0	14.8	4.29	16.1	20.5
	2	9.40	102.0	13.5	14.5	318.0	27.2	5.17	19.2	15.2
	3	12.10	82.3	19.1	19.0	491.0	30.9	9.15	23.2	18.9
II	1	8.19	278.0	38.4	9.81	8.91	14.3	3.60	15.9	25.2
	2	9.66	368.0	40.5	14.6	6.53	22.3	3.62	19.8	27.2
	3	11.10	458.0	66.5	14.7	18.2	31.3	5.88	21.1	30.4
III	1	15.10	N/A	21.2	9.77	9.56	15.1	4.42	16.9	8.42
	2	11.40	N/A	26.1	15.1	9.94	21.8	5.35	16.4	18.0
	3	13.30	N/A	47.6	15.9	17.7	35.4	7.60	15.0	31.7

that the maximum (positive and negative) responses respectively. Notations Q_r, M_x, T., B.,, T_a,, B. and D,, have the same meaning as those defined before. In order to demonstrate some relations between impact and static response, Table 4-2 gives the maximum (positive and negative) static inner forces for different loading case and bridge types. From Tables 4-1 and 4-2, the following information can be gained. The effects of loading models for different types of bridges are quite different. For continuous box gird r bridge, one-truck loading will produce the maximum impact factors of moment and deflection, as well as the minimum impact factors of torsional response. It seems that there is a tendency that smaller static responses are related to larger impact factors, though this situation is not always true because other factors may influence the impact as well. For cantilever bridges, he impact factors of almost all kinds of responses increase greatly with increasing the number of loading trucks. This behavior is due to the hinges existed at middle span. As more trucks cross the hinge, the heavier the excited of vehicle force will be. The maximum impact factors moment and deflection of cantilever those bridge with one hinge at midspan are much large than with two hinges.

4.4.3. Effect of Diaphragm

Diaphragms are the important component of box girder bridges. In order to discern the influence of diaphragms, Tables 4-3 and 4-4 give the static and dynamic responses of three types of the bridges with and without diaphragms respectively. The results presented in Tables 4-3 and 4-4 are computed under the same conditions as those illustrated in Tables 4-1 and 4-2, except that only loading case 2 is considered in this analysis. Table 4-3 indicates that most

Table 4-2. Effect of Loading Models - Maximum Static Response

Bridge Type	Loading Model	Over Inner Supports								At Midspan
		Q_y KN x10^2	M_x KN-m x10^3		T_c KN-m x10^3		B_ω KN-m^2 x10^3	$T_{\bar{\omega}}$ KN-m x 10^3	$B_{\bar{\omega}}$ KN-m^2 x10^3	D_y cm
		Pos.	Pos.	Neg.	Pos.	Neg.	Pos.	Neg.	Pos.	Pos.
I	1	3.139	0.482	-3.152	1.446	-0.024	-2.049	-1.231	3.587	0.533
	2	9.430	1.446	-9.456	0.854	-0.014	-1.228	-0.737	2.155	1.600
	3	9.964	1.446	-10.63	0.914	-0.015	-1.435	-0.741	2.232	1.402
II	1	3.139	0.791	-5.807	1.446	-0.311	-2.069	-1.220	3.501	1.872
	2	9.430	2.373	-17.40	0.864	-1.887	-1.240	-0.734	2.106	5.613
	3	10.186	2.373	-18.76	0.913	-1.966	-1.446	-0.737	2.172	5.131
III	1	3.203	N/A	-7.084	1.446	-0.314	-2.052	-1.231	3.644	0.691
	2	9.608	N/A	-21.12	0.864	-1.887	-1.231	-0.738	2.121	2.075
	3	9.830	N/A	-21.12	0.913	-1.977	-1.446	-0.759	2.155	2.075

Table 4-3. Effect of Diaphragm - Maximum Static Response

Bridge Type	Case of Diaphr.	Over Inner Supports							At Midspan
		Q_y KN x10^2	M_x KN-m x10^3	T_c KN-m x10^3		B_ω KN-m^2 x10^3	$T_{\bar{\omega}}$ KN-m x 10^3	$B_{\bar{\omega}}$ KN-m^2 x10^3	D_y cm
		Pos.	Neg.	Pos.	Neg.	Pos.	Neg.	Pos.	Pos.
I	With	9.430	-9.456	0.854	-0.014	-1.228	-0.735	2.155	1.600
	Without	9.430	-9.456	0.870	-0.049	-1.283	-0.756	3.013	1.600
II	With	9.430	-17.399	0.864	-1.887	-1.240	-0.734	2.106	5.610
	Without	9.430	-17.399	0.862	-1.887	-1.280	-0.663	2.927	5.610
III	With	9.608	-21.124	0.864	-1.887	-1.231	-0.738	2.121	2.075
	Without	9.608	-21.124	0.865	-1.888	-1.280	-0.751	3.071	2.075

Table 4-4. Effect of Diaphragm - Maximum Impact Factors (%)

Bridge Type	Case of Diaphr.	Over Inner Supports							At Midspan
		Q_y	M_x	T_c		B_ω	$T_{\bar{\omega}}$	$B_{\bar{\omega}}$	D_y
		Pos.	Neg.	Pos.	Neg.	Pos.	Neg.	Pos.	Pos.
I	With	9.40	13.5	14.5	N/A	27.2	6.00	19.2	15.2
	Without	9.10	14.1	20.6	N/A	26.2	9.19	14.7	15.1
II	With	9.66	40.5	14.6	6.53	22.3	3.62	19.8	27.2
	Without	9.68	40.6	30.0	15.0	35.6	5.53	23.9	27.2
III	With	11.4	26.1	15.1	9.94	21.8	5.35	16.4	18.0
	Without	11.3	26.2	23.6	7.43	32.0	6.21	18.9	18.0

maximum (positive and negative) torsional static responses of the bridges without diaphragms are larger than those with diaphragms, while the other responses are not affected by the diaphragms. It can be observed from Table 4-4 that: (1) Diaphragms have little influence on the maximum impact factors of vertical bending responses, such as moment, deflection, as well as shear; (2) Most maximum impact factors of torsional responses of the bridges without diaphragm are distinctly larger than those with diaphragms, because more torsional vibration modes of the bridges without diaphragm will contribute to their dynamic response(see Figs.4-3 to 4-24). Therefore, the diaphragms over support will apparently benefit both static and dynamic behavior of box girder bridges.

4.4.4 Effect of Vehicle Speed and Road Surface Roughness

Vehicle speed and road surface roughness are two important parameters which affect the impact of bridges. Figs. 4-103 to 4-110 show the variation of impact factors with vehicle speeds and road surface roughness. Figs 4-103, 4-105, and 4-107 illustrate the impact of moment at Section 4 for Bridge Type I, II, and III, respectively. Figs 4-104, 4-106, and 4-108 demonstrate the impact of bi-moment at Section 2 for Bridge Type I, II, and III, separately. The relations of impact to vehicle speeds at Section 5 for moment of Bridge Types II and III are shown in Figs. 4-109 and 4-110 individually. It can be observe from those figures that the relations of impact factor of moment to vehicle speeds and road surface roughness for continuous and cantilever box girder bridges are dramatically different. The impact of moment for the continuous bridge is distinctly affected by road surface roughness, especially when vehicle speed is greater than 88.5 km/hr (55 mph). Velocity of vehicle is main factor which influence the

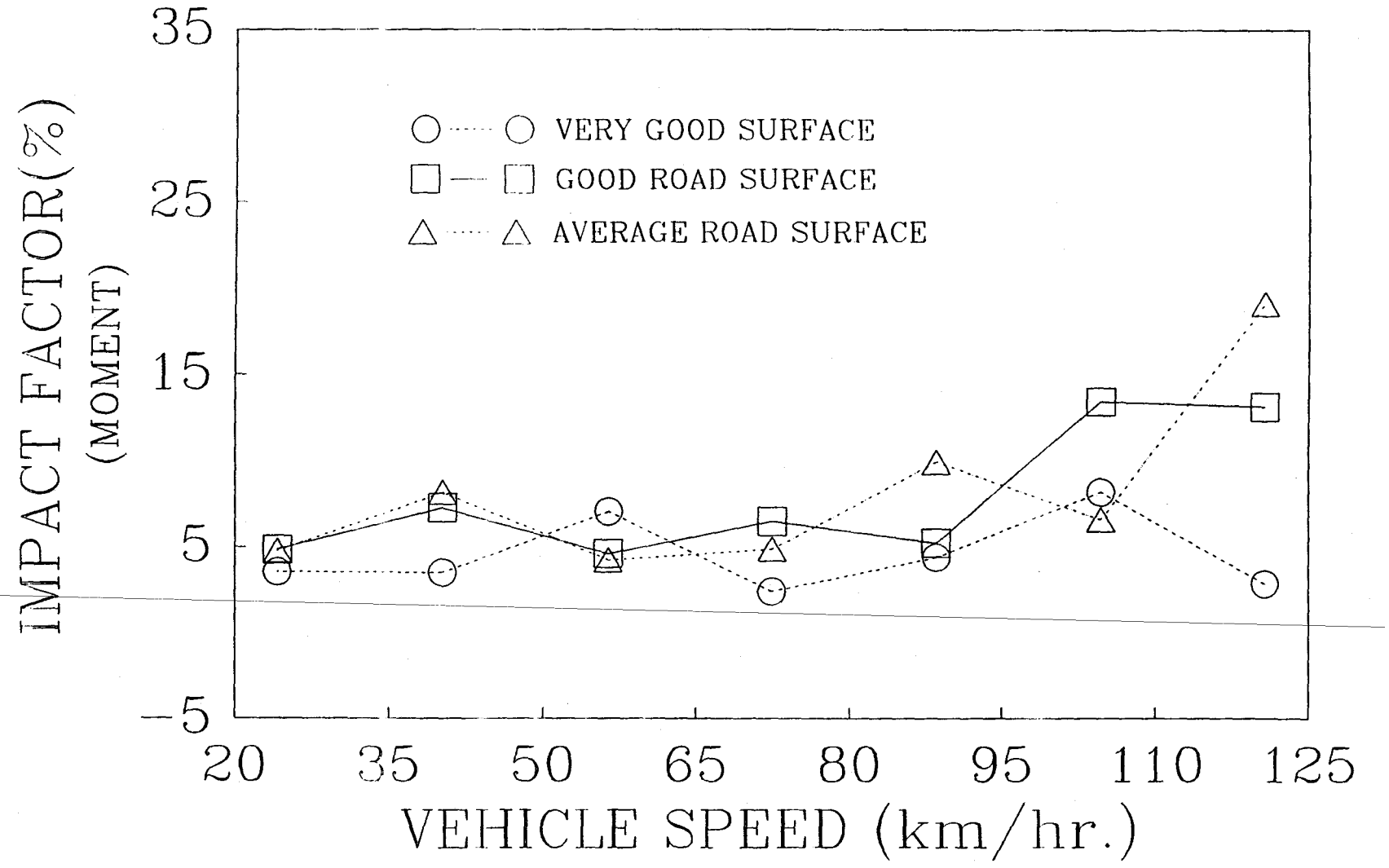

Fig. 4-103. Variation of Impact Factors of Vertical Moment at Section 4 of Bridge Type I with Vehicle Speeds

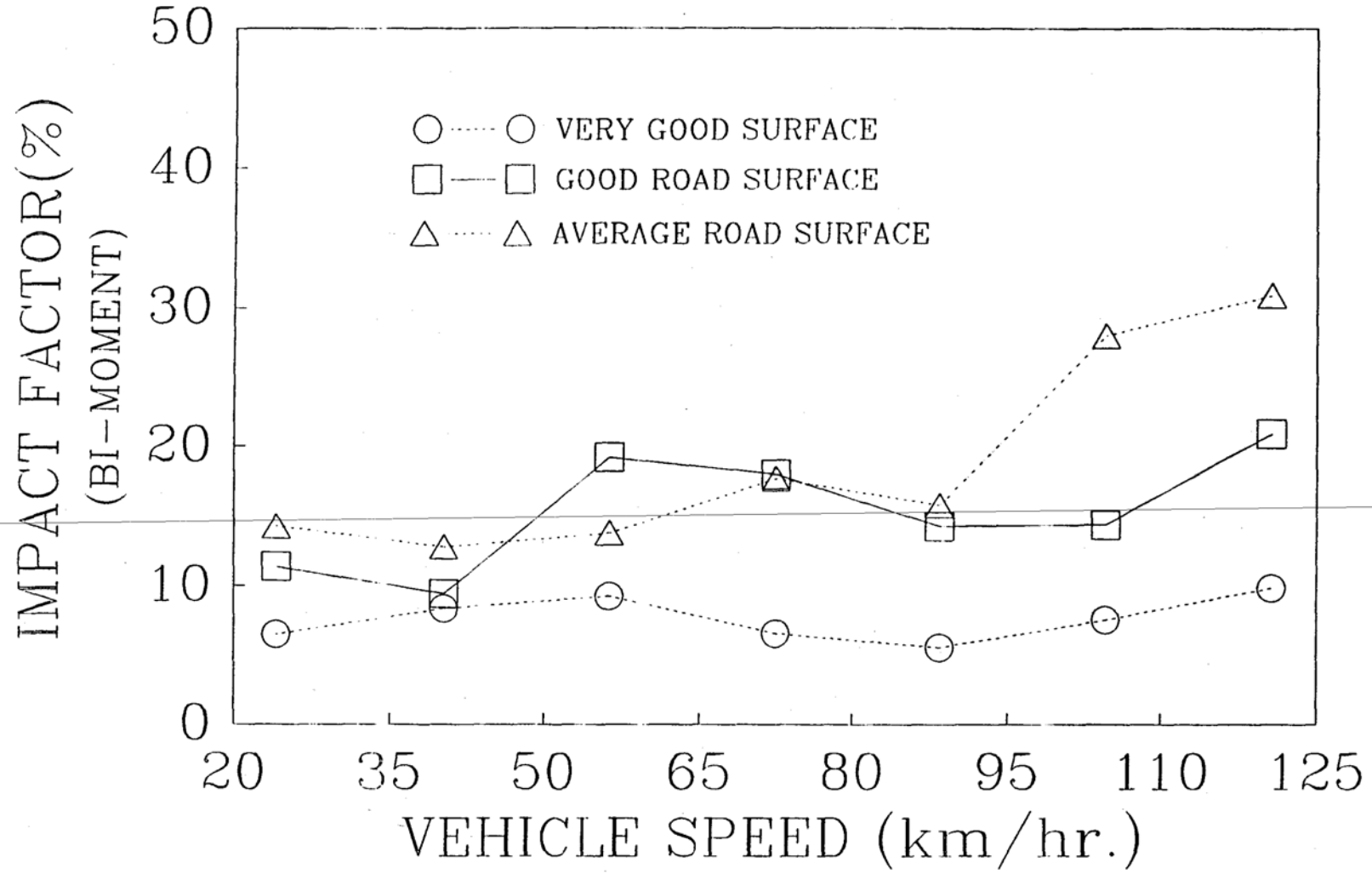

Fig. 4-104. Variation of Impact Factors of Bi-moment at Section 4 of Bridge Type I with Vehicle Speeds

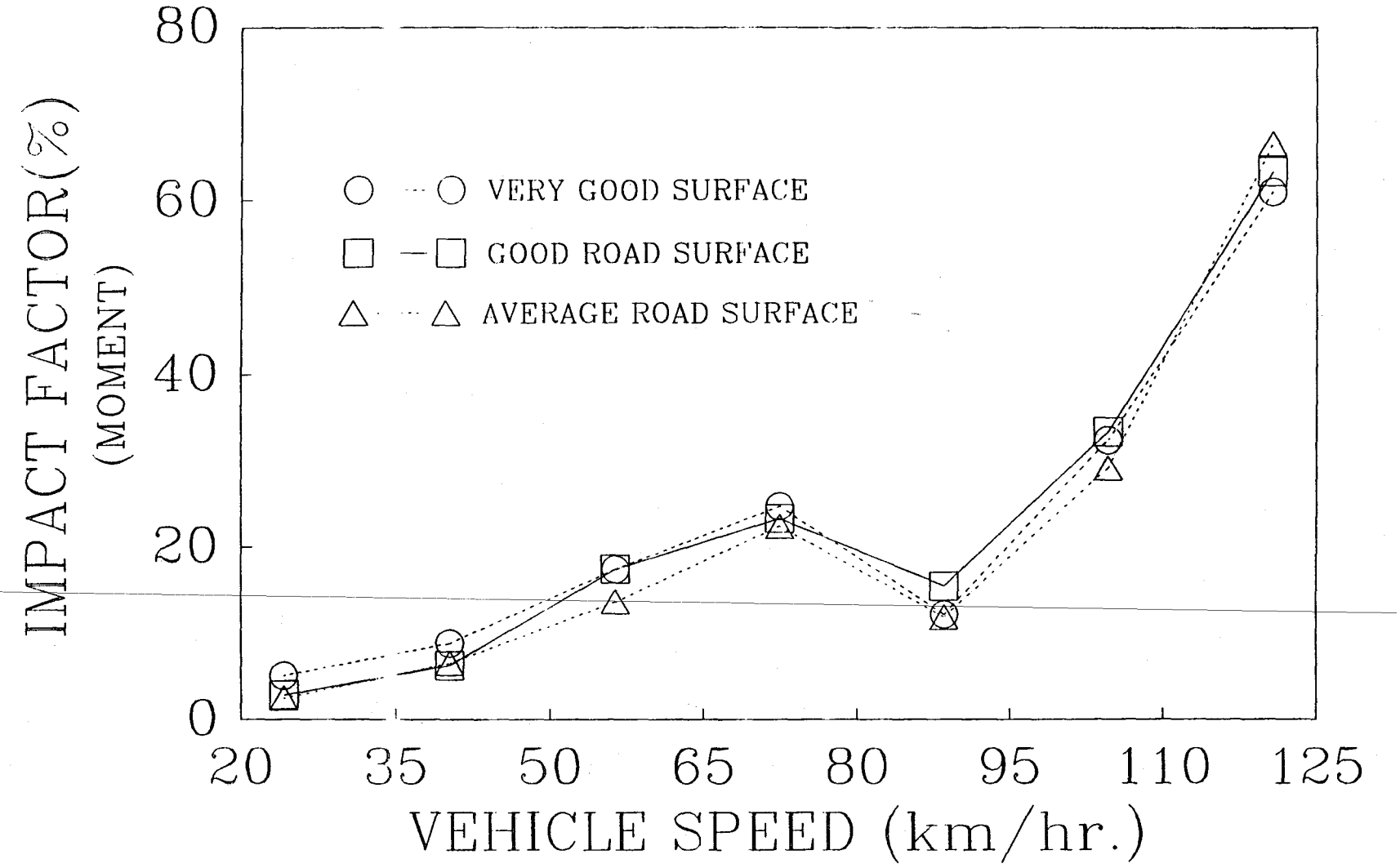

Fig. 4-105. Variation of Impact Factors of Vertical Moment at Section 4 of Bridge Type II with Vehicle Speeds

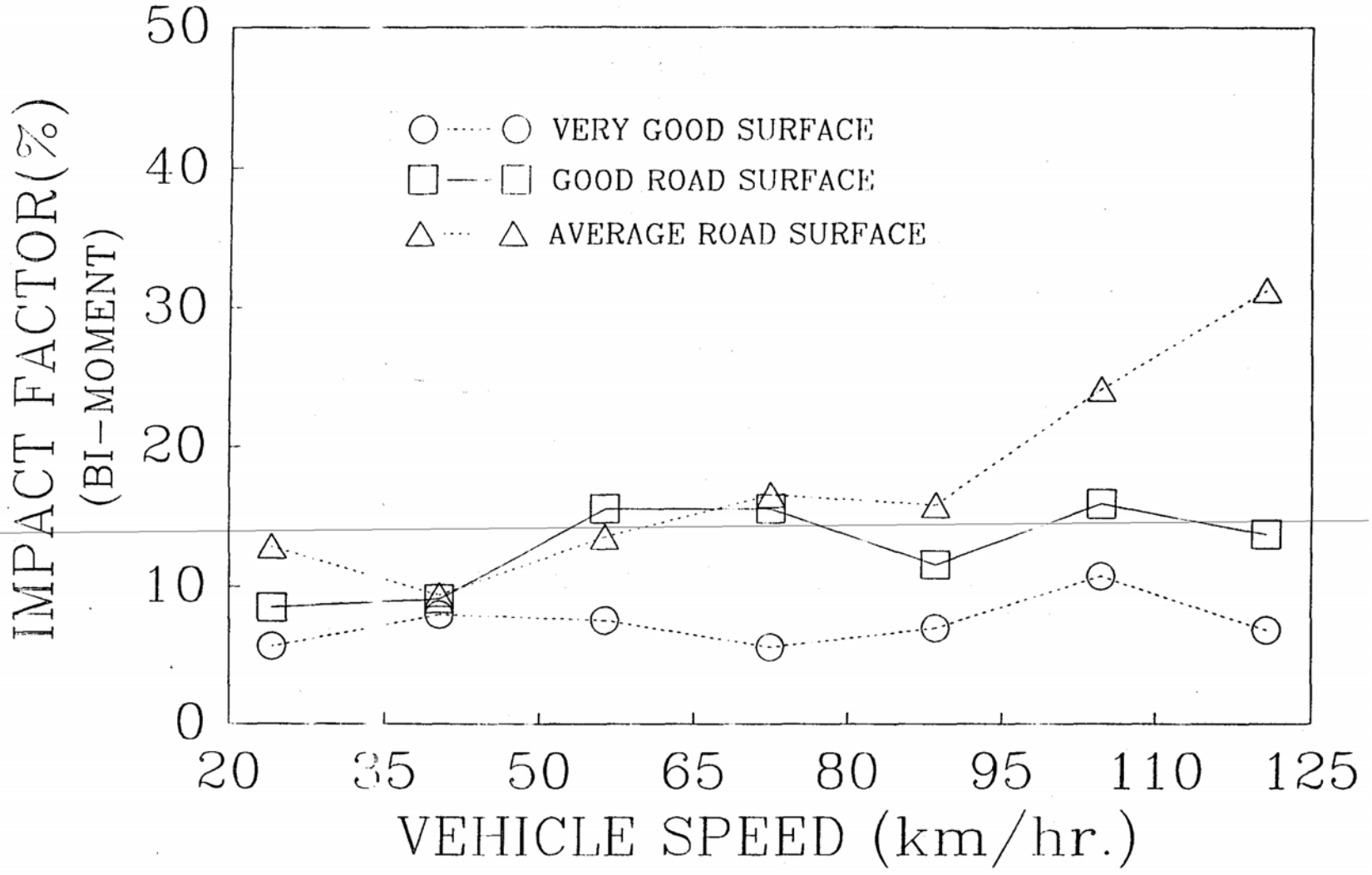

Fig. 4-106. Variation of Impact Factors of Bi-moment at Section 4 of Bridge Type II with Vehicle Speeds

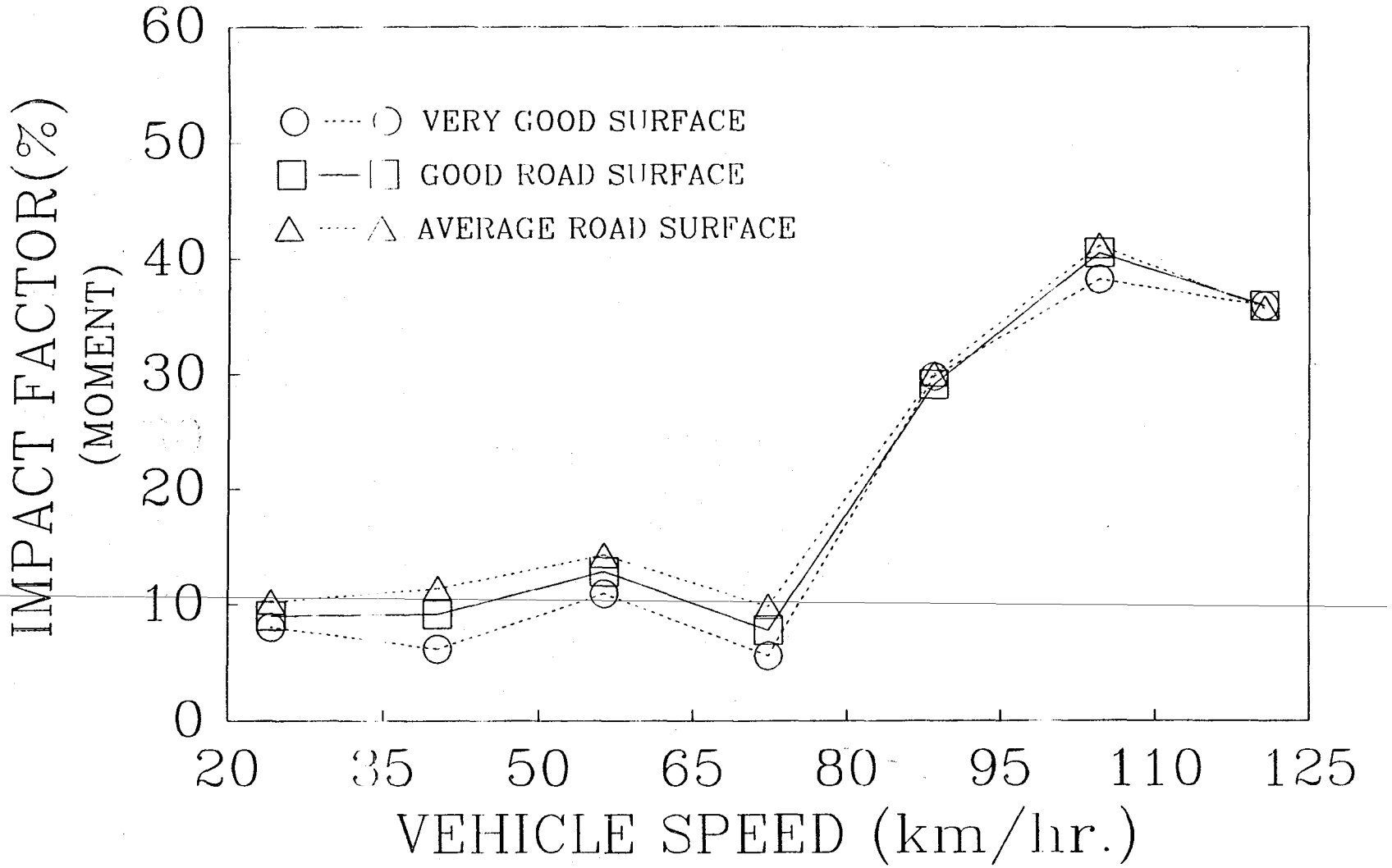

Fig. 4-107. Variation of Impact Factors of Vertical Moment at Section 4 of Bridge Type III with Vehicle Speeds

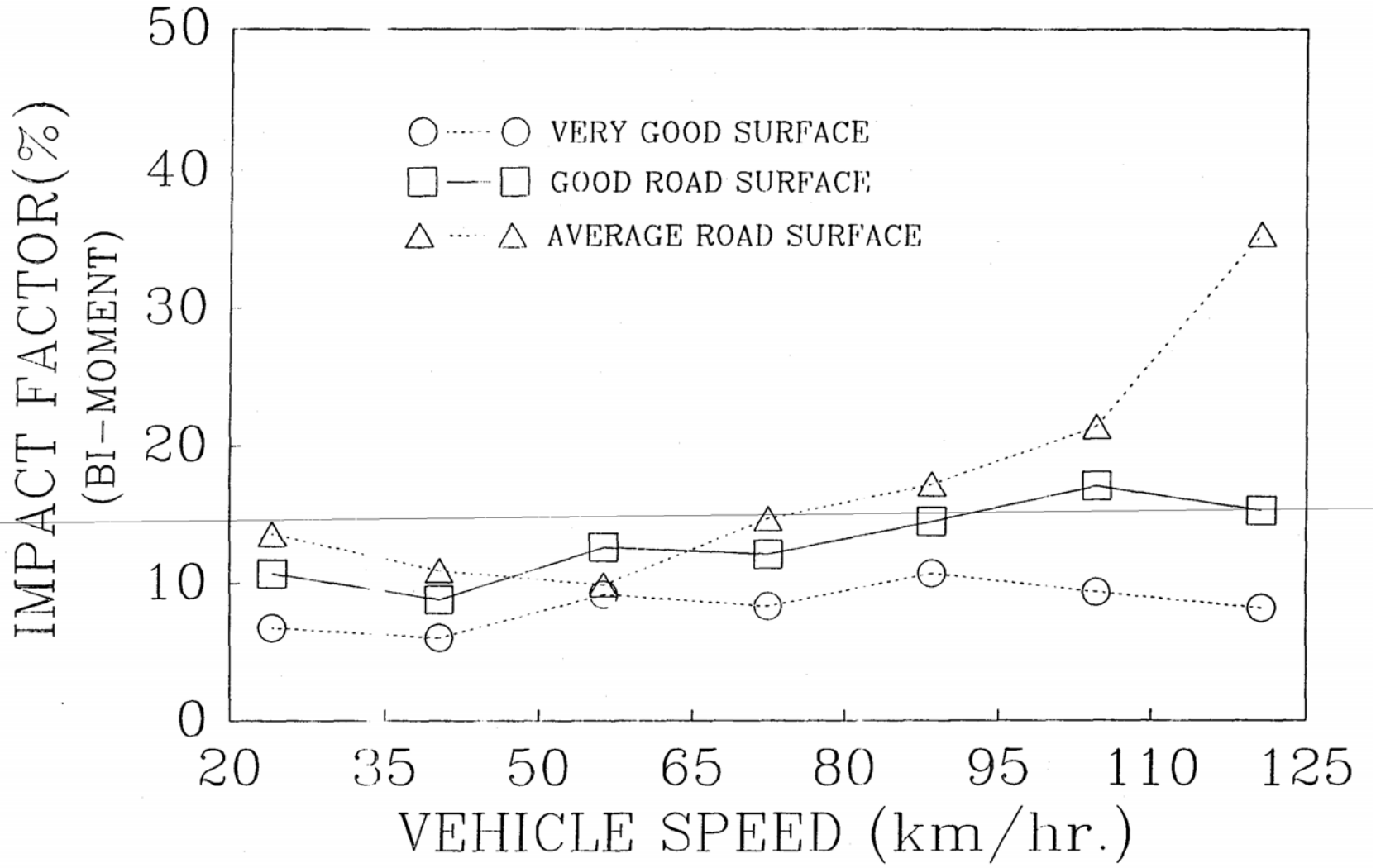

Fig. 4-108. Variation of Impact Factors of Bi-moment at Section 4 of Bridge Type III with Vehicle Speeds

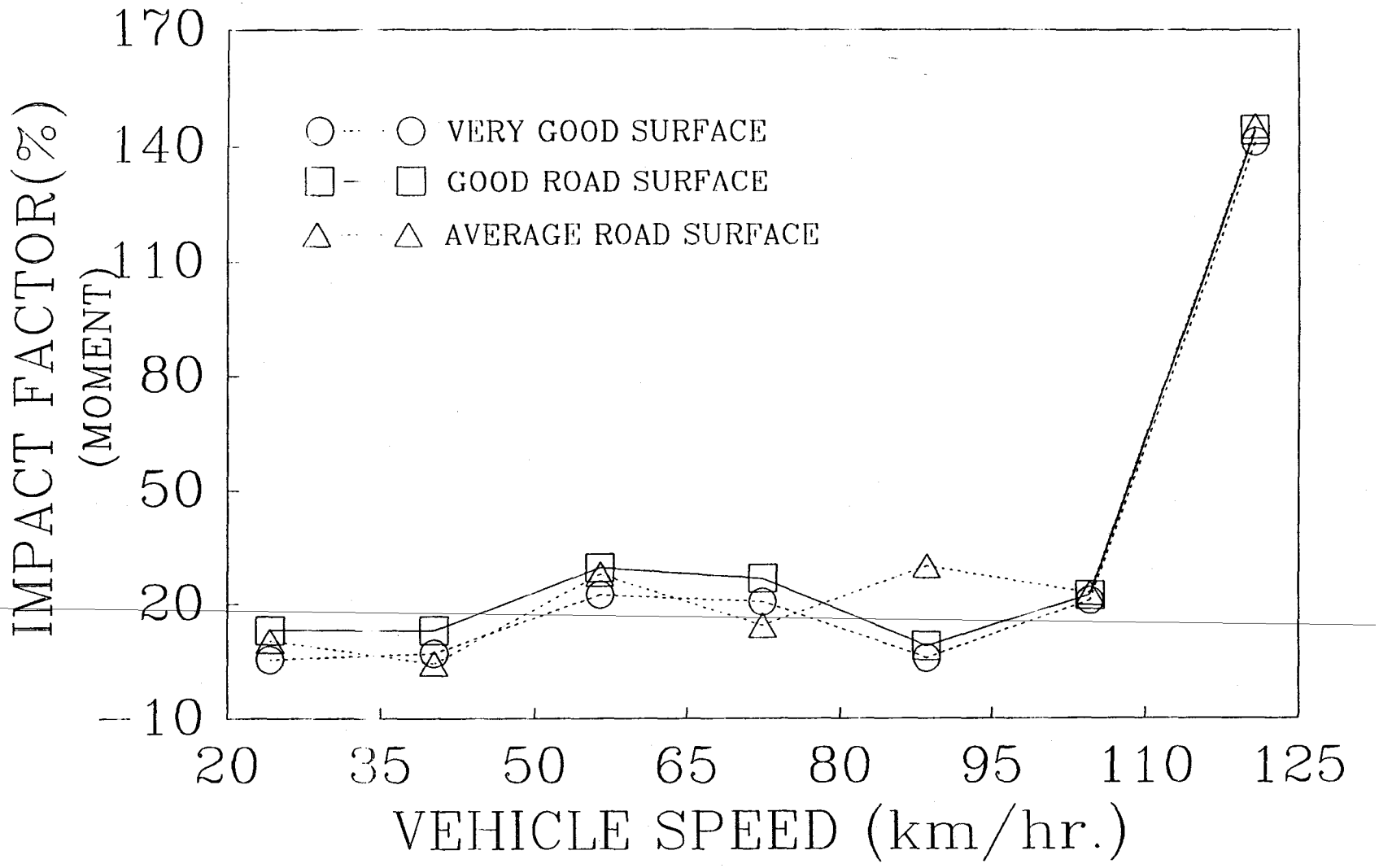

Fig. 4-109. Variation of Impact Factors of Vertical Moment at Section 5 of Bridge Type II with Vehicle Speeds

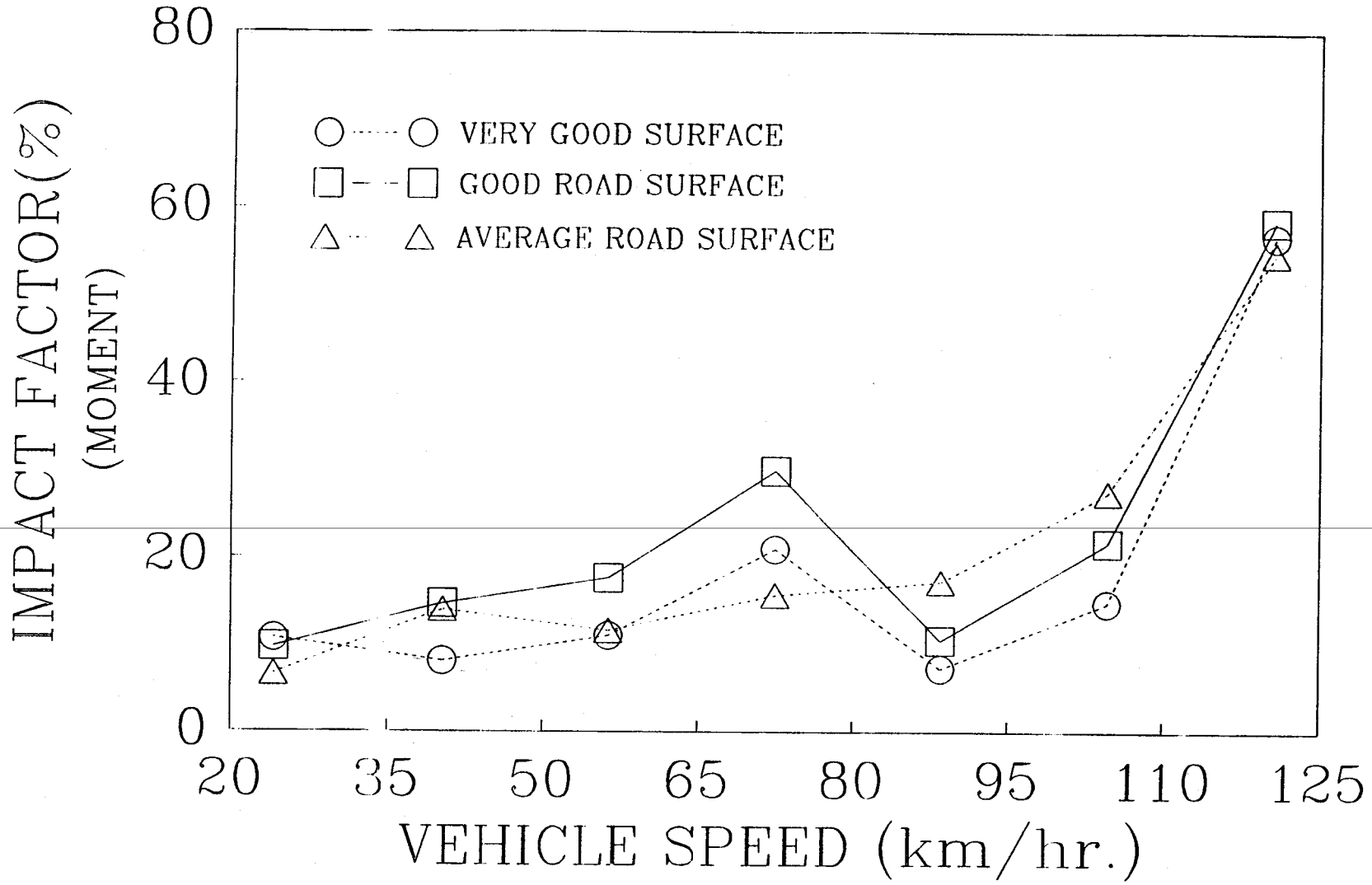

Fig. 4-110. Variation of Impact Factors of Vertical Moment at Section 5 of Bridge Type II with Vehicle Speeds

impact of cantilever bridges, particularly when vehicle speed exceeds 88.5 km/hr (55 mph), while road surface roughness is the secondary factor. It seems hat as the vehicle speed reaches 120.675 km/hr (75 mph), very high impact factor of moment ay occur, especially at Section 5. In order to reduce the impact of moment for cantilever bridges, the most effective method is to limit the vehicle speed. With good road surface and vehicle speed less than 88.5 km/hr (55 mph), the maximum impact factors of moment at most sections for cantilever bridges will not be greater than 25 %. Figs 4-104, 4-106, and 4-108 infer that the hinges in middle span have little influence on the impact of bi-moment. The same situation has been found for the other torsional responses.

4.4.5. Maximum Impact Factors

Table 4-5 presents the maximum impact factors of the three types of bridges shown m Fig.4-1 for different road surface roughness. The results listed in Table 4-5 are evaluated according to the vehicle speeds changing from 24.14 km/hr (15 mph) to 120.68 km/hr (75 mph) and loading model 3 (see Fig. 4-101). From the engineering standpoint, only the impact factors corresponding to larger dynamic responses of two symmetrical sections about midspan are given in Table 4-5. The notations in Table 4-5 have the same meaning as defined in Table 4-1. For comparison, the impact factors determined according to AAS TO specifications are also listed in Table 4-5. From this table, some important information can be obtained. With very good surface roughness, the impact factors of all types of responses for the continuous bridge are less than those predicted by AASHTO specifications. This is also true for the torsional responses of the cantilever bridges. The maximum impact factors of moment and deflection for the

Table 4-5. Maximum Impact Factors (%)

Bridge Type	Road Surface	Sections 1 and 5		Sections 2 and 4							Section 3
		M_x		Q_y	M_x		T_c	B_ω	$T_{\bar{\omega}}$	$B_{\bar{\omega}}$	D_y
		Pos.	Neg.	Pos.	Pos.	Neg.	Pos.	Pos.	Neg.	Pos.	Pos.
I	Very Good	12.3	19.4	4.02	36.1	8.2	5.98	9.8	5.72	10.5	2.78
	Good	16.0	23.1	9.31	74.7	13.4	13.3	20.9	7.36	20.1	12.8
	Average	19.5	24.4	12.1	82.3	19.1	19.0	30.9	9.15	23.2	18.9
II	Very Good	141.0	92.5	5.93	427.0	61.0	3.91	10.8	3.96	12.4	62.2
	Good	144.0	94.5	9.57	448.0	63.3	12.7	16.0	5.06	18.3	62.6
	Average	145.0	96.4	11.1	458.0	66.5	14.7	31.3	5.88	21.1	62.9
III	Very Good	56.7	46.7	4.58	N/A	38.2	5.22	10.7	5.36	13.1	30.7
	Good	58.5	49.0	7.57	N/A	40.5	13.9	17.1	6.44	14.8	30.3
	Average	54.8	46.0	13.3	N/A	41.7	15.9	35.4	7.60	15.0	31.7
AASHTO Spec.		20.12		16.06							13.34

cantilever bridges are much larger than those for the continuous bridge and those evaluated by AASHTO specifications, no matter which class of road surface roughness is. It is interesting to note that the impact factors of moment and deflection of the cantilever bridge with a suspension span are much less than those with one hinge at midspan. The information reveals that the cantilever bridge is much more susceptible to vibration than the continuous one, particularly the cantilever bridge with only one hinge at midspan. The elimination of hinges at midspan whenever possible is beneficial to the structural dynamic behavior of the bridge. It also can be noted from Table 4-5 that the impact factors related to maximum positive and negative static responses are different. Generally, the larger the absolute static response is, the smaller the impact factor will be.

CHAPTER V

CONCLUSIONS AND RECOMMNDATIONS

In this study, a procedure for predicating the dynamic response to moving vehicles is developed and validated. Both the vehicle and bridge re treated as space mathematical models. Moreover, the distortional deformation is considered. The results obtained by the presented method agree very well with those calculated by fold plate method [26]. It is easy to obtain not only the impact factors of different types of stresses, but also those of different kinds of inner forces, such as bending moments, torques, an bi-moments. It can be used for space dynamic analysis of either in the simply supported b x girder bridges with deformable cross sections, or in the continuous and cantilever box gird r bridges.

The dynamic characteristics of simply support thin-walled box girder bridges with and without diaphragms are studied first. Then, the dynamic behaviors of continuous and cantilever bridges are investigated. The effect of road surface roughness, vehicle speeds, damping ratio, and loading cases are analyzed. Also, the influence of hinges of cantilever bridges on the dynamic response is discussed. The conclusions of the research for simply supported box girder bridges are summarized as follows:

End diaphragms are like lateral supports which greatly affect the lateral bending and torsional dynamic characteristics of box girder bridges. Generally, with decreasing distortional rigidity of end diaphragms, the static responses of torsi n and distortion increase, while impact

factors decease. The effect of mid-span diaphragm is relatively smaller.

The dynamic response of vertical bending moment is caused mainly by first several low vibration modes, while that of bi-moment is greatly affected by higher modes when bridges have average and poor road surface roughnesses. For this reason, the effect of damping ratio on bi-moment is significant, while the influence on vertical bending 's comparatively small.

The impact factors vary with different transverse load positions and number of loading trucks. The meaningful impact factors used in bridge design are related to the loading model which can induce maximum static responses.

Under the conditions of very good and good road surface roughnesses, the impact factors of the analytic bridge for all responses are less than 10% a d vary slightly with increasing vehicle speeds. However, with average and poor road surface roughnesses, the impact factors increase significantly and very high values of impact factors or bi-moments can be reached. Fortunately, the proportion of the normal stress produced by warping to that induced by vertical bending moment is not high for the analytical bridge.

The conclusions of the investigation for continuous an cantilever bridges are:

Diaphragms over supports greatly affect the torsion frequencies and their vibration modes, while no apparent effect is taken place on the vertical ending frequencies. The hinges in meddle span only affect the vertical bending vibration, with little influence of torsional

vibration.

The forced vibration characteristics of continuous and cantilever box girder bridges are quite different. For cantilever bridges, the most important factor which affect the impact factors of vertical bending moment is the vehicle speed. At he speed exceeding 88.5 km/hr (55 mph), the maximum impact factor increases dramatically. By comparison, the road profile becomes the secondary factor. The most effective method of reducing bending moment impact factor for cantilever bridges is to limit the vehicle speed. For continuous bridges, both vehicle speed and road profile are important, concerning the impact magnitude. However, continuous and cantilever box girder bridges have similar torsional behaviors.

The influences of loading cases on the dynamic responses for different bridge types and kinds of responses are variable. For continuous box girder bridges, generally, one truck loading will produce the maximum impact factors of vertical ending moment and deflection as well as the minimum impact factors of torsional responses. For cantilever bridges, the maximum impact factors of almost all kinds of responses increase greatly with increasing the number of loading trucks. For this reason. the significant loading mode for predicating bridge impact in the field and theoretical study should be corresponding to the maximum static design inner force.

The installation of diaphragms over supports benefits not only the static behavior of box girder bridges, but also the dynamic behavior, especially for cantilever box girder bridges. Elimination of diaphragms over supports will greatly in crease the dynamic bi-moment over inner supports of cantilever box girder bridges.

With very good surface roughness, the maximum impact factors of all types of the responses for the continuous bridge are less than those predicated by AASHTO specifications. This is also true for the torsional responses of the cantilever bridges. The maximum impact factors of vertical bending moment and deflection for the cantilever bridges are much larger than those for the continuous bridge and those evaluated by AASHTO specifications, no matter which class of road surface roughness is. This situation can be changed by limiting the vehicle speed. The cantilever bridge with only one hinge at midspan is much more susceptible to vibration than that with middle suspension span.

14. Heins, C. P., and Firmage, D. A., Design of Modern Steel Highway Bridges, John Wiley & Sons, New York, 1979.

15. Heins, C. P., and Lawrie, R. A., Design of Modern Concrete Highway Bridges, John Wiley & Sons, New York, 1983.

16. Heins, C. P., and Oleinik, J. C., "Curved Box Beam Bridge Analysis," J. of Structures and Computers, Vol. 6, June, 1976, pp 65-73.

17. Hsu, Y. Z., "The Development and Behavior of Vlasov Elements for the Modeling of Horizontally Curved Composite Box Girder Bridge Superstructures," thesis presented to the University of Maryland in partial fulfillment of the requirements for the degree of doctor of Philosophy, 1989.

18. Huang, D. Z. and Wang, T. L., "Impact Analysis of Cable-stayed Bridges," Computers and Structures, Vol. 43, No.5, 1992, pp. 897-908.

19. Huang, D. Z., Wang, T. L. and Shahawy, M., "Impact Analysis of Continuous Multigirder Bridges due to Vehicle Moving," J. of Structural Engineering, 118, No. 12, Dec., 1992, 3427-3443.

20. Huang, D.Z., Wang, T.L. and Shahaway, M., "Impact studies of multigirder Concrete bridges," J. of Struct. Engrg., ASCE, 119(8), 1993, PP.2387-2402.

21. Huang, D.Z., and Li, G. H., "Elasto-plastic lateral stability of truss bridges." Selected Papers of Tongji University, Tongji University Press, Shanghai China. (in English), pp.23-35.

22. Huang, T., "Dynamic response of three-span continuous highway bridges," Ph.D. Dissertation, University of Illinois, Urbana, IL., 1960.

23. Hutton, S. G. and Cheung, Y. K., "Dynamic Response of Single Span Highway Bridges", Earthquake Engineering and Structural Dynamics, Vol. 7, 1979, pp. 543-553.

24. Inbanathan, M. and Wieland, M., "Bridge Vibration due to Vehicle Moving Over Rough Surface", J. of Structural Eng., ASCE, Vol. 113, No. 9, September, 1987, pp. 1994-2008.

25. Ishac, I. I. and Smith, T.R.G., "Approximations for moments in box girder," J. of Struc. Engrg., ASCE, Vol.111, No. 11, 1985, pp.2333-2341.

26. Jones, M. A., "Dynamic analysis of box girder bridges," Ph. D. Dissertation, Illinois Institute of Technology, Chicago, Illinois, 1972.

27. Jones, M., and Chu, K. H., "Dynamic Analysis of Box Girder Bridge," I.A.B.S.E. Me'morires, 36, No. 2, 1976, pp.121-131.

28. Kissane, R. J., and Beal, D. B., "Field Testing of Horizontally Curved Steel Girder Bridges: Fourth Interim Report," Report NY DOT-ERD-75-RR-27, New York State Department of Transportation, May, 1975.

29. Komatsu, S., and Nakai, H., "Study on Free Vibration of Curved Girder Bridges," Transaction of the Japanese Society of Civil Engineers, No. 136, Dec. 1966, pp.35-60 (in Japanese).

30. Komatsu, S., and Nakai, H., "Application of the Analogue Computer to the Analysis of Dynamical Response of Curved Girder Bridges,' Transaction of the Japanese Society of Civil Engineers, Vol. 2, Part 1, 1970, pp.143-149.

31. Komatsu, S., and Nakai, H., "Fundamental Study on Force Vibration of Curved Girder Bridges," Transaction of the Japanese Society o Civil Engineers, Vol. 2, Part 1, 1970, pp.37-42.

32. Komatsu, S., Nakai, H., and Kotoguchi, H., "Study of Dynamic response and Impact of Horizontally Curved Girder Bridges under Moving Vehicles," Transaction of the Japanese Society of Civil Engineers, Vol. 3, Part 2, 1971, pp. 132-133.

33. Kou, C. H., Benzley, S. E., Huang, J. Y., and Firmage, D. A., "Free Vibration Analysis of Curved Thin-walled Girder Bridges," J. of Structural Engineering, ASCE, Vol. 118, No. 10, 1990, pp.2890-2910.

34. Li, H. G., and Razaqpur, G., "Thin-walled Multicell Box Girder Finite Element," J. of Structural Engineering, ASCE, Vol. 117, No. 10 1991, pp.2953-2971.

35. Li, G. H., Analysis of Box Girder and Truss Bridges, Springger-Verlag, Berlin, Germany, 1987.

36. Lim, P. T. K., Kilford, J. K., and Moffatt, H. R., "Finite Element Analysis of Curved Box Girder Bridges," Development in Bridge Design d Construction, Crosby, Lockwood and Son. Ltd., University College, Cardiff, Wales, A r., 1971.

37. Mikkola, M. J., and Raavola, J., "Finite Elemen Analysis of Box Girder Bridges," J. of Structural Engineering, ASCE, Vol. 104, No. ST , 1978, pp.453-463.

38. Mozer,J. D., and Culver, C. G., "Stability of Curved Box Girders," Consortium of University Research Team Report No. B3, Carne ie-Mellon University, Pittsburgh, PA., dEC., 1971.

39. Nakai, H. and Yoo, C. H., Analysis and Design of Curved Steel Brides, McGraw-Hill Book Company, New, York, 1988.

40. Paavola, J., and Mikkola, M. J., "Finite Element analysis of Box Girders," J. of Structural Engineering, ASCE, Vol. 106, No. ST6, 1980, p . 1343-1557.

41. Podolny, W. and Muller, J. M., Construction and design of prestressed concrete segmental bridges, John Wiley & Sons, Inc. New York, N.Y., 1982.

42. Rabizadeh, R. O., and Shore, S., " Dynamic Analysis of Curved Box-girder Bridges," J. of Structural Engineering, ASCE, Vol. 101 (9), 1975, pp. 1899-1912.

43. Roik, K. and Sedlacek, G., "Theory of warping torsion considering secondary shear deformation analogy with analysis of the transversely loaded beam in torsion," Der Stahlban, Germany, 35(2), 1966, pp.43-52 (in German).

44. Roik, K. and Sedlacek, G., "Extension of engineer's theory of bending and torsion, considering shear deformation," Die Bautechnik, Germany, 147(1), 1970, pp.20-32. (in German).

45. Ruhl, J., "Stress histories for highway bridges subjected to traffic loading," Ph. D. Dissertation, Illinois, Urbana, Ill., 1974.

46. Schelling, D. R., Galdos, N. H., and Sahin, M. A., " Evaluation of Impact Factors for Horizontally Curved Steel Box BridgeS," J. of Structural Engineering, ASCE, Vol. 118, No.11, 1992, pp. 3203-3221.

47. Scordelis, A. C., and Larsen, D. K., " Structural Response of Curved RC Box-Girder Bridge," J. of Structural Engineering, ASCE, Vol. 103, No. ST8, 1975, pp. 1507-1525.

48. Sisodiya, R. G., and Ghali, A., " Analysis of Box Girder Bridges of Arbitrary Shapes," Publications International Association for Bridge and Structural Engineering, Vol. 33-1, 1973, pp. 203-218.

49. Standard Specifications for Highway Bridges. 14th Ed., American Association of State Highway and Transportation Officials, Washington, D.C., 1989

50. The Task Committee on Curved Box Girders of the ASCE-AASHTO Committee on Flexural Members of the Committee on Metals of the ASCE Structural Division, " Curved Steel Box-Girder Bridges: State-of-the-Art," J. of Structural Engineering, ASCE, Vol. 104, No. ST11, 1978, pp. 1719-1739.

51. Turktra, C. J., and Fam, A. R. M., "Behavior Study of Curved Box Bridges," J. of the Structural Engineering, ASCE, Vol. 104, No ST3, 1978, pp. 453-463.

52. Veletsos, A. S. and Huang, T., "Analysis of dynamic Response of Highway Bridges," J. of the Eng. Mechanics Division, ASCE, Vol. 90, No. EM5, October, 1970, pp. 593-620.

53. Wang, T. L. and Haung, D. Z., "Computer Modeling Analysis in Bridge Evaluation," Research Report No. FL/DOT/RMC/0542-3394, Florida Dept. of Transp., Tallahassee, Fla., 1992.

54. Wang, T. L. and Huang, D. Z., "Computer Modeling Analysis in Bridge Evaluation: Phase II," Research Report No. FL/DOT/RMC/0542-4108, Florida Dept. of Transp., Tallahassee, Fla., 1992.

55. Wang, T. L. and Huang, D. Z., "Cable-stayed Bridge Vibration due to Road Surface Roughness," Journal of Structural Engineering, ASCE, 118 (5), 1992, pp. 1354-1374.

56. Wang, T. L., Huang, D. Z. and Shahawy, M. "Dynamic Response of Multigirder Bridges," J. of Structural Engineering, ASCE, Vol. 118, August, 1992, pp. 2222-2238.

57. Wang, T. L., Huang, D. Z. and Shahaway, M., "Dynamic behavior of slant-lagged rigid frame highway bridge," J. of Struct. Engrg., ASCE, 120(3), 1994, pp.885-902.

58. Wang, T. L., Shahawy, M. and Huang, D. Z. "Numerical and Analytical Description of Highway Surface Roughness," Proceeding, ASCE Eighth Conference on Computing in Civil Engineering, Dallas, Texas, June 7-9, 1992, pp. 309-316.

59. Weaver, W. and Johnston, P. R., Structural dynamics by finite elements, Prentice-Hall, Inc., Englewood Cliff, New Jersey, 1987..

60. Wen, R. K. and Toridis, T., "Dynamic Behavior of Cantilever Bridges", J. of the Engineering Mechanics Division, ASCE, August, 1962, pp. 27-42.

61. Wright, R.N., Abdel-samad, S. R., and Robinson, A. R., "BEF analogy for analysis of box girders," Journal of the Struc. Div., ASCE, 94(7), 1968, pp. 1719-1743.

62. Wu, J. S. and Dai, C. W., "Dynamic responses of Multispan nonuniform beam due to moving loads," J. of Struct. Engrg., ASCE, Vol. 113, No.3, 1988, pp.458-474.

63. Vlasov, V.Z.(1961), "Thin-walled elastic beams," National Science Foundation, Washington, D. C.